US Army Corps of Engineers

TECHNICAL REPORT GL-91-22

(2)

SEISMIC STABILITY EVALUATION OF RIRIE DAM AND RESERVOIR PROJECT

Report 2
STABILITY CALCULATIONS, ANALYSIS, AND EVALUATIONS

Volume I: Main Text

by

D. W. Sykora, J. P. Koester, M. E. Hynes

Geotechnical Laboratory

DEPARTMENT OF THE ARMY
Waterways Experiment Station, Corps of Engineers
3909 Halls Ferry Road, Vicksburg, Mississippi 39180-3199

September 1991
Report 2 of a Series

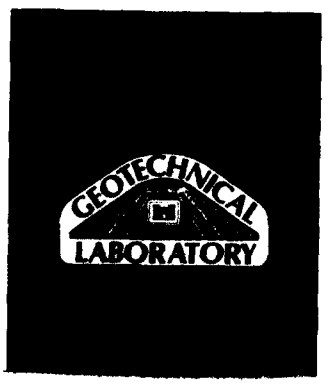

Prepared for US Army Engineer District, Walla Walla
Walla Walla, Washington 99362-9265

Destroy this report when no longer needed. Do not return it to the originator.

The findings in this report are not to be construed as an official Department of the Army position unless so designated by other authorized documents.

The contents of this report are not to be used for advertising, publication, or promotional purposes. Citation of trade names does not constitute an official endorsement or approval of the use of such commercial products.

Unclassified

SECURITY CLASSIFICATION OF THIS PAGE

REPORT DOCUMENTATION PAGE

Form Approved OMB No. 0704-0188

1a. REPORT SECURITY CLASSIFICATION Unclassified	1b. RESTRICTIVE MARKINGS
2a. SECURITY CLASSIFICATION AUTHORITY	3. DISTRIBUTION/AVAILABILITY OF REPORT Approved for public release; distribution unlimited.
2b. DECLASSIFICATION/DOWNGRADING SCHEDULE	
4. PERFORMING ORGANIZATION REPORT NUMBER(S) Technical Report GL-91-22	5. MONITORING ORGANIZATION REPORT NUMBER(S)
6a. NAME OF PERFORMING ORGANIZATION USAEWES Geotechnical Laboratory 6b. OFFICE SYMBOL (If applicable) CEWES-GG-H	7a. NAME OF MONITORING ORGANIZATION
6c. ADDRESS (City, State, and ZIP Code) 3909 Halls Ferry Road Vicksburg, MS 39180-3199	7b. ADDRESS (City, State, and ZIP Code)
8a. NAME OF FUNDING/SPONSORING ORGANIZATION US Army Engineer District, Walla Walla 8b. OFFICE SYMBOL (If applicable) NPW-EN-GB	9. PROCUREMENT INSTRUMENT IDENTIFICATION NUMBER
8c. ADDRESS (City, State, and ZIP Code) Bldg. 602, City-County Airport Walla Walla, WA 99362-9265	10. SOURCE OF FUNDING NUMBERS PROGRAM ELEMENT NO. / PROJECT NO. / TASK NO. / WORK UNIT ACCESSION NO
11. TITLE (Include Security Classification) Seismic Stability Evaluation of Ririe Dam and Reservoir Project; Report 2, Stability Calculations, Analysis, and Evaluation; Vol I: Main Text; Vol II: Appendixes A-E.	
12. PERSONAL AUTHOR(S) Sykora, David W., Koester, Joseph P., Hynes, Mary E.	
13a. TYPE OF REPORT Report 2 of a Series 13b. TIME COVERED FROM _____ TO _____ 14. DATE OF REPORT (Year, Month, Day) September 1991 15. PAGE COUNT See reverse.	
16. SUPPLEMENTARY NOTATION Available from National Technical Information Service, 5285 Port Royal Road, Springfield, VA 22161.	
17. COSATI CODES FIELD / GROUP / SUB-GROUP	18. SUBJECT TERMS (Continue on reverse if necessary and identify by block number) Dam safety Earthquakes and hydraulic structures Ririe Dam (Idaho)

19. ABSTRACT (Continue on reverse if necessary and identify by block number)

The man-made water retaining structure at the Ririe Dam and Reservoir Project, located on Willow Creek about 20 miles upstream of the City of Idaho Falls, Idaho, has been evaluated for seismic safety in the event of a Magnitude 7.5 earthquake occurring at the Grand Valley Graben, about 5 miles from the site. The construction history and the results of recent field and laboratory studies are documented in Report 1 of this series. This report, representing the second phase, documents the numerical analyses and engineering evaluation used to assess seismic stability. In general, it was concluded that Ririe Dam will be marginally safe if subjected to the design earthquake. Significant damage is expected to occur, however.

(Continued)

20. DISTRIBUTION/AVAILABILITY OF ABSTRACT ☒ UNCLASSIFIED/UNLIMITED ☐ SAME AS RPT ☐ DTIC USERS	21. ABSTRACT SECURITY CLASSIFICATION Unclassified
22a. NAME OF RESPONSIBLE INDIVIDUAL	22b. TELEPHONE (Include Area Code) / 22c. OFFICE SYMBOL

DD Form 1473, JUN 86 Previous editions are obsolete. SECURITY CLASSIFICATION OF THIS PAGE

Unclassified

(A)

15. PAGE COUNT.

(Vol I, 189; Vol II, 392)

19. ABSTRACT (Continued).

(cont)

Nearly all of the upstream random fill and upper portions of the gravel alluvium will liquefy as a consequence of the design earthquake. Slope stability calculations indicate, however, that the dam will remain stable because the magnitude of residual strengths for liquefied materials is significant.

Best estimates of permanent displacements are quite large (up to 6 ft) for the upstream side of the dam. The estimated displaced shape indicates that the crest will move vertically about 6 ft leaving a freeboard of 10 ft for the design pool (el 5,112 ft).

(8)

PREFACE

The US Army Engineer Waterways Experiment Station (WES) was authorized to conduct this study by the US Army Engineer District, Walla Walla (NPW), by Intra-Army Orders for Reimbursable Services Nos. NPW E86830106, E86840062, E86840095, E86850074, E86850090, E86860001, E86870013, E86870081, and E86890008. This report is one of two reports that document the seismic stability evaluations of the man-made water retaining structure of the Ririe Dam and Reservoir Project, located on Willow Creek, in eastern Idaho. The two reports are as follows:

Report 1: Construction History and Field and Laboratory Studies

Report 2: Stability Calculations, Analysis, and Evaluation

Both reports contain two volumes: Volume I includes the main body of the report; Volume II contains the appendixes.

The work on these two reports was a joint endeavor between NPW and WES. Messrs. Grady W. Williams and Wendell L. Greenwald, of the Soils Section, Foundations Branch, Engineering Division (NPW-EN-GB-SC), were the project coordinators at NPW. Mr. Fred Miklancic, Chief, NPE-EN-GB, was the overall Project Manager.

The WES Principal Investigator and Research Team Leader was Dr. Mary Ellen Hynes, Chief, Earthquake Engineering and Seismology Branch (EESB), Earthquake Engineering and Geosciences Division (EEGD), Geotechnical Laboratory (GL), WES. Primary Engineers on the WES team were Messrs. Joseph P. Koester and David W. Sykora, EESB. Additional engineering support was provided by Mr. Ronald E. Wahl, EESB, and Mr. Michael K. Sharp, EEGD. Messrs. Harley Alderson, Daniel Habeeb, Willie McGeeHee, and Melvin Seid, EEGD, assisted in the preparation of figures.

Professor H. Bolton Seed served as a Consultant to WES and provided valuable guidance during the course of the study.

Overall direction at WES was provided by Dr. A. G. Franklin, Chief, EEGD, and Dr. William F. Marcuson III, Chief, GL.

COL Larry B. Fulton, EN, is Commander and Director of WES. Dr. Robert W. Whalin is Technical Director.

CONTENTS

LIST OF TABLES

LIST OF FIGURES

LIST OF FIGURES (cont'd)

LIST OF FIGURES (cont'd)

LIST OF FIGURES (cont'd)

CONVERSION FACTORS, NON-SI TO SI (METRIC) UNITS OF MEASUREMENT

Non-SI units of measurement used in this report can be converted to SI (metric) units as follows:

Multiply	Abbreviation	By	To Obtain
acres	--	4,046.873	square metres
acre-feet	acre-ft	1,233.489	cubic metres
cubic yards	cu yd	0.7645549	cubic metres
feet	ft	0.3048	metres
gallons per minute	gpm	0.0038	cubic metres per minute
inches	in.	2.54	centimetres
inches	in.	25.4	millimetres
kips (force) per square foot	ksf	47.88026	kilopascals
miles (US statute)	mi	1.609347	kilometres
pounds (force)	lb	4.448222	newtons
pounds (force) per square foot	psf	47.88026	pascals
square miles	--	2.589998	square kilometres
tons per square foot	tsf	95.76052	kilopascals

SEISMIC STABILITY EVALUATION OF RIRIE DAM AND RESERVOIR PROJECT

Report 2: STABILITY CALCULATIONS, ANALYSIS, AND EVALUATION

PART I: INTRODUCTION

General

1. This report is the second of two reports that document the investigations and results of a seismic stability evaluation of the man-made water retaining structure at Ririe Dam and Reservoir, Bonneville County, Idaho, about 15 air-miles* east-northeast of the City of Idaho Falls and 4 miles southeast of the small community of Ririe. A photograph of the dam taken in June of 1976, shortly after first reservoir filling, and a location map of the project area are shown in Figures 1 and 2, respectively. The scope of the overall seismic stability study includes quantitative evaluation of the seismic stability of the embankment and its foundation and a qualitative evaluation of the stability of the abutments. The seismic stability of the concrete structures is not within the scope of this study. This seismic safety evaluation was performed as a cooperative effort between the US Army Engineer (USAE) Waterways Experiment Station (WES), Vicksburg, Mississippi and the US Army Engineer District, Walla Walla (NPW), Walla Walla, Washington. The late Professor H. Bolton Seed of the University of California at Berkeley, served as a Consultant for the study.

2. The seismic stability of Ririe Dam and Reservoir was required to be analyzed under a dam safety program instituted by the Office of the Chief of Engineers (OCE), USAE following the near-catastrophic failure of the Lower San Fernando Dam, California, as a consequence of the San Fernando Valley earthquake that occurred on 9 February 1971. (For comprehensive reviews of this failure and consequent analyses, see Seed et al. 1973, Seed et al. 1989, Castro, Keller, and Boynton 1989, and Vasquez-Herera and Dobry 1989.) Seismic design and analysis methods to evaluate the effects of strong ground motions available at the time when Ririe Dam was in the design phase (1964 to 1972)

---

* A table of factors for converting US customary units of measurement to metric (SI) units is presented on page 9.

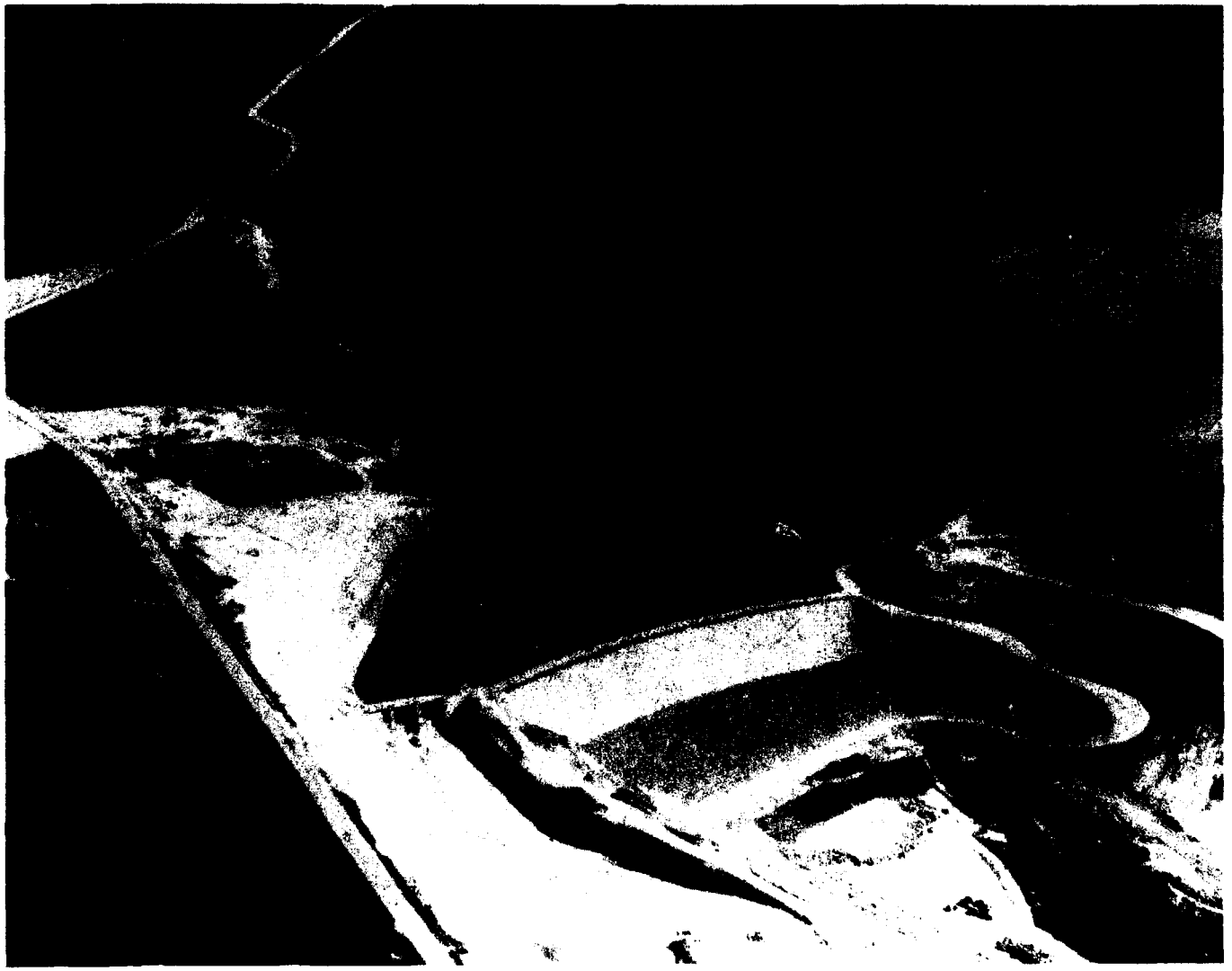

Figure 1. Ririe Dam and Reservoir Project shortly after first reservoir filling (7 June 1976)

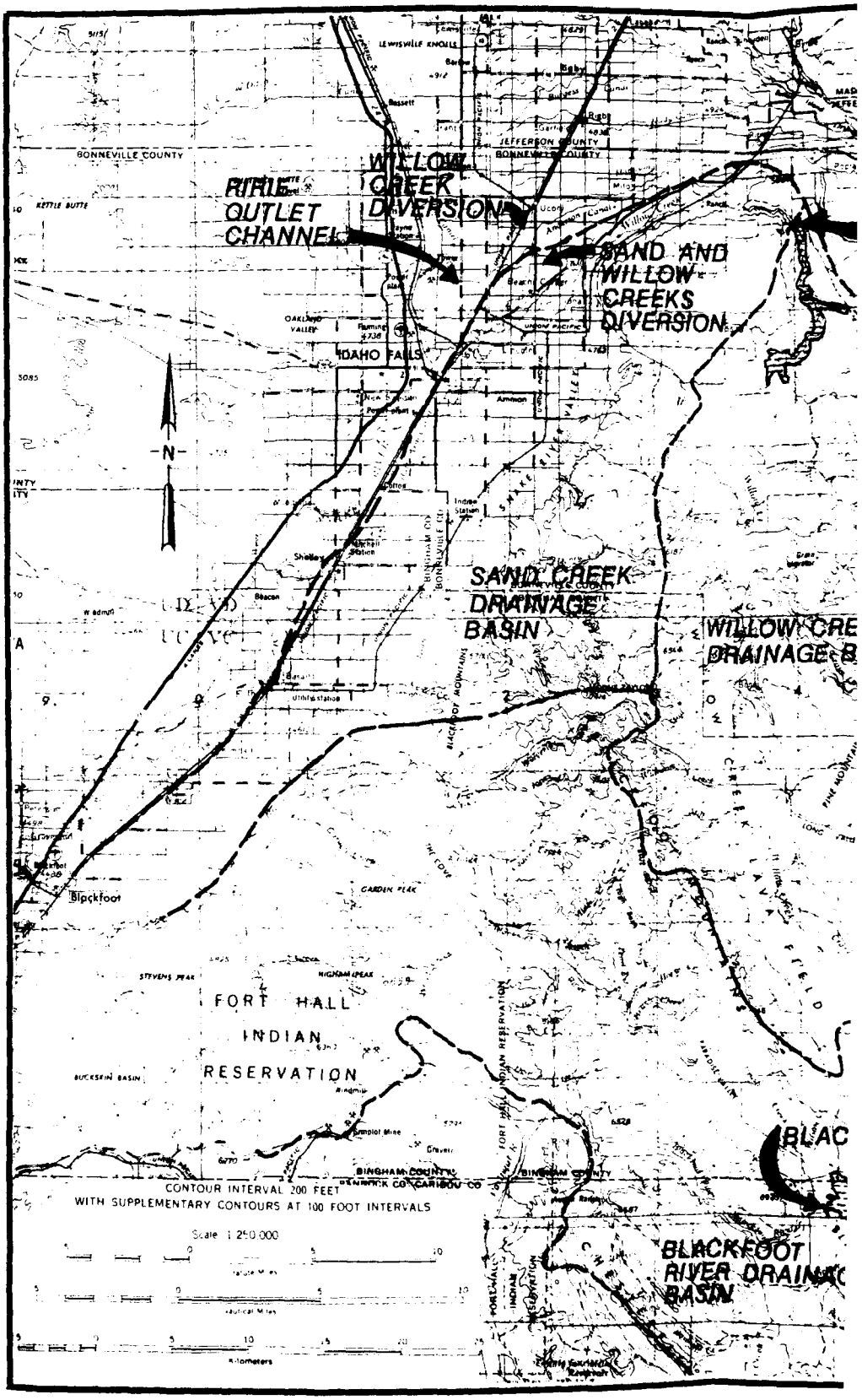

Figure 2. Regional map of eastern Idaho showing

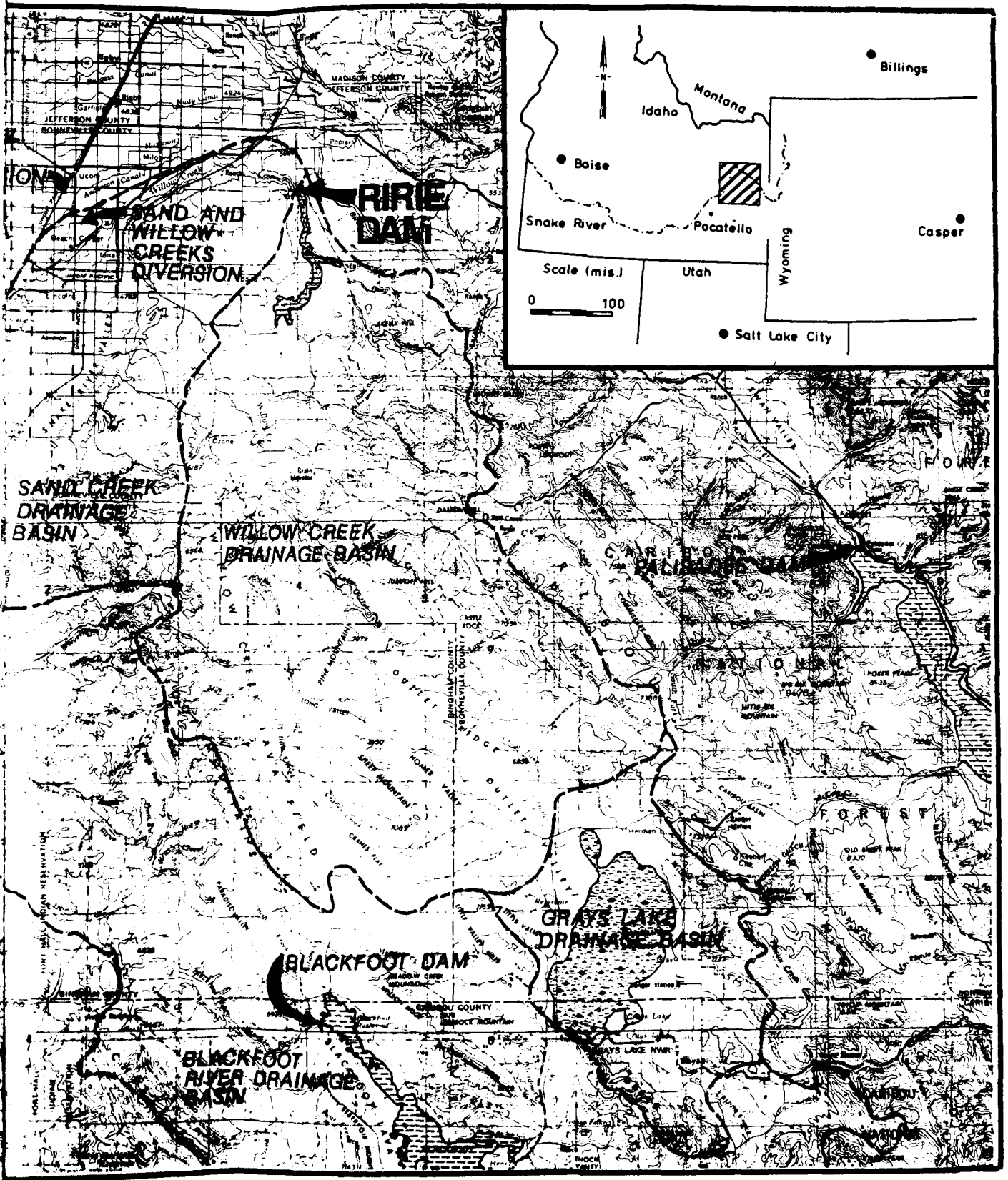

l map of eastern Idaho showing location of the Ririe Dam and Reservoir Project

were much less developed than at the present. A recent Engineering Regulation ER 1110-2-1806 (Department of the Army 1983) requires that dams that could be subjected to large earthquake motions be analyzed using state-of-the-art dynamic response techniques and seismic stability methodologies that have become available since the design of Ririe Dam.

3. The evaluation of seismic stability of Ririe Dam is difficult because of the technical complexities involved. Two factors make significant contributions to the overall complexity: the recently recognized capability for relatively loose, saturated gravel to liquefy when subjected to sufficiently large earthquake ground motions (Finn 1982, Ishihara 1985, Youd et al. 1985, and Harder 1988) and the results of a recent geologic and seismologic study specific to Ririe Dam (Krinitzsky and Dunbar 1991) that demonstrated that very strong ground motions were possible at Ririe Dam from movements in nearby faults. Other factors contributing to the complexity of the analysis include: the three-dimensional geometric effects produced by the narrow and curved valley, the diversity and variability of geologic strata in the abutments and foundation, and the small freeboard (16 ft) associated with the analysis pool. One valuable circumstance at Ririe Dam was the recording of low-level accelerations (less than 0.05 g) from the 1983 Mt. Borah Peak earthquake at the dam using accelerometers installed by NPW during construction. The calculated response of the dam for that event was found to be in good agreement with the measured response. Thus, it was concluded that the model used for analysis provides an adequate means for evaluating the dynamic response of the dam.

4. This report summarizes the results of numerical analyses and the evaluation of seismic stability. Various input parameters were derived from the examination of construction records, evaluation of recent field and laboratory investigations, and selection of an idealized system and material properties presented in Report 1. A brief synopsis of Report 1 is presented in Part II of this report for convenience.

Methodology

5. Seed (1979) suggests that there are nine possible ways in which an earthquake may cause failure of an earth dam:

a. Disruption of dam by major fault movement in foundation.

b. Loss of freeboard due to differential tectonic ground movements.

c. Slope failures induced by ground motions.

d. Loss of freeboard due to slope failures or soil compaction.

e. Sliding of dam on weakened foundation materials.

f. Piping failure through cracks induced by ground motions.

g. Overtopping of dam due to seiches in reservoir.

h. Overtopping of dam due to slides or rockfalls into reservoir.

i. Failure of spillway or outlet works.

Each of these potential modes of failure was addressed to some extent for the seismic stability study of Ririe Dam except modes (g) and (i), which are beyond the scope of this study. The information presented in Report 1 and by Krinitzsky and Dunbar (1991) can be used to conclude that modes listed as: (a), (b), (f), and (h) above are not applicable to the seismic stability concerns at Ririe Dam. More specifically, Krinitzsky and Dunbar (1991) concluded that no faults exist in the foundation and differential tectonic movements would not occur in the valley. Piping is unlikely because of the adequate filter design of the structure as reviewed in Report 1. Even if cracks were to develop, internal erosion should be adequately controlled by the existing filter zones. Finally, a qualitative analysis of the seismic stability of canyon walls suggests that overtopping due to slides or rockfalls is not likely. Three potential modes of failure remain from the original list: (c) slope failures induced by ground motion, (d) loss of freebroad due to slope failures or soil compaction, and (e) sliding of dam on weakened foundation materials. For USAE projects subjected to a Maximum Credible Earthquake (MCE), as considered for this study, failure is defined as an uncontrollable loss or reservoir. Therefore, the ultimate potential failure mode of concern from Professor Seed's list for this project is the loss of freebroad. The seismic stability evaluation for Ririe Dam focused on the means and likelihood of slope failures or sliding of the dam producing an uncontrollable loss of reservoir (loss of freebroad). Slope failures induced by ground motion are presumed to be caused by inertial forces acting on potential failure wedges. The evaluation of this type of failure focuses on the Newmark sliding block analysis. Sliding of the dam on weakened foundation materials may occur as a consequence of a buildup of pore water pressures.

This includes liquefaction of materials wherein these materials exhibit a residual strength. The ultimate evaluation for this type of failure involved traditional slope stability calculations, although the distribution of pore pressures was calculated by a complicated means.

6. A methodology for seismic stability evaluation was selected that thoroughly examined the potential for the three identified potential modes of failure. This methodology involves an interactive sequence of activities that may best be thought of in three separate phases: "Characterization Studies," "Numerical Analyses," and "Earthquake Engineering Evaluation". A schematic diagram of basic components of the interactive sequence within and between each phase is shown in Figure 3. For each activity shown in Figure 3, the results of the most recent engineering research and field studies were incorporated. Some uncommon techniques were used, primarily in the characterization studies, to obtain the most accurate information necessary and most information readily available to conduct the overall seismic stability study.

7. The "Characterization Studies" were described in detail in Report 1 of this series and by Krinitzsky and Dunbar (1991) and comprise the collection of information necessary and useful to conduct the computations necessary to evaluate seismic stability. They involve the examination of construction records and performance of field and laboratory investigations. The final products of this phase included: the determination of the design earthquake, development of idealized cross sections, and material properties for each material represented.

8. The "Numerical Analyses" phase consists of the static effective stress and dynamic response calculations. The results of these computations are used primarily for the evaluation of liquefaction potential. The static stress analysis is used to determine stresses acting within the embankment prior to the earthquake. The dynamic response analysis is used to determine dynamic stresses that are induced by the earthquake. The potential for liquefaction is evaluated on the basis of comparisons between the static and dynamic stresses, along with the cyclic strength and characteristics of pore pressure generation of the materials. Dynamic response calculations also provide useful information regarding dynamic characteristics of the dam including the fundamental frequency and acceleration-time records. The finite element method was used for both the static and dynamic stress analyses using

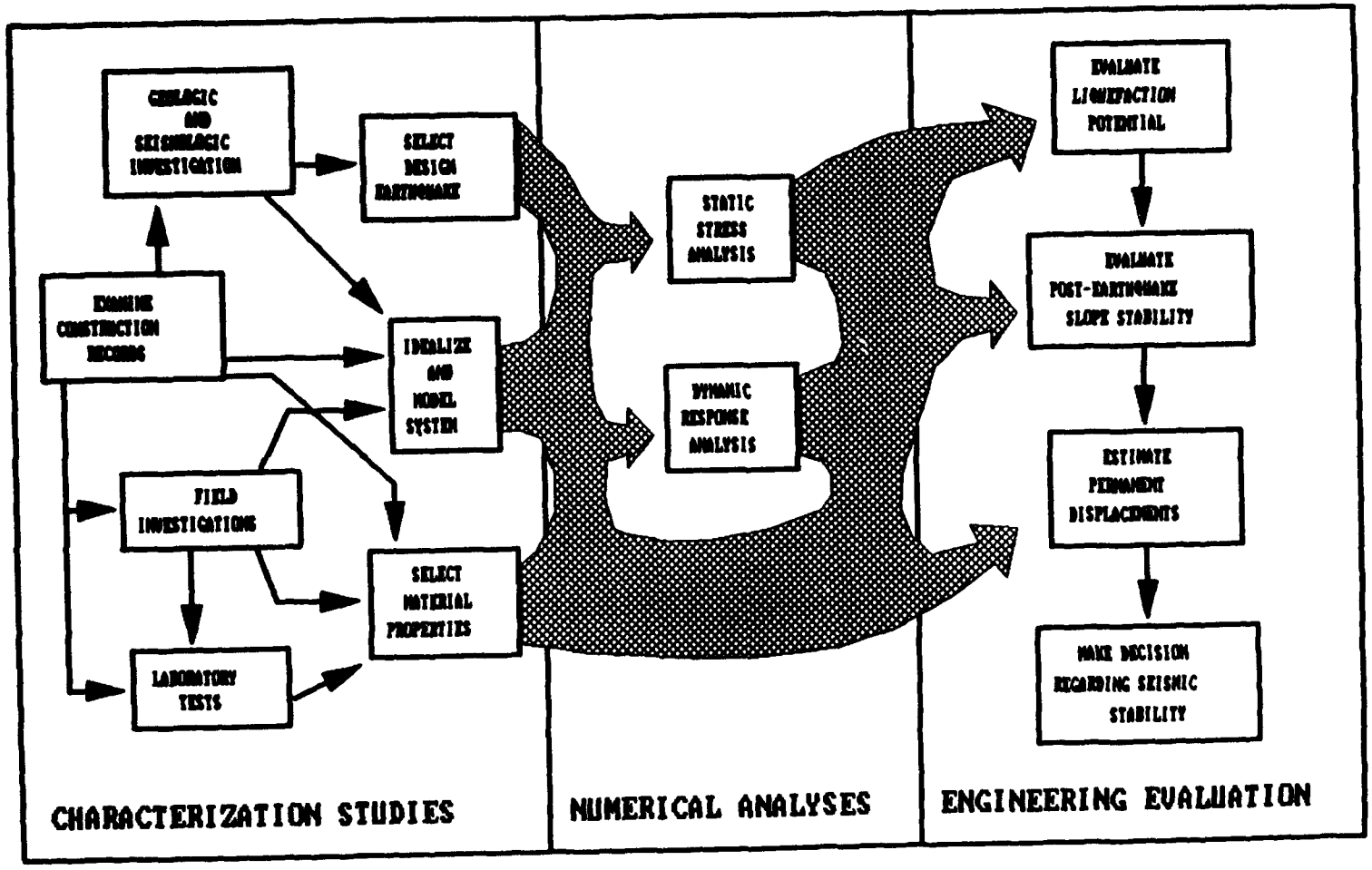

Figure 3. Schematic diagram indicating the simplified interaction between activities associated with the seismic stability analysis of Ririe Dam

two-dimensional, plane strain computer codes that have been used and verified extensively by the geotechnical engineering profession.

9. Assumptions of plane strain were made to calculate the static and dynamic stresses and dynamic response. Plane strain implies that the strains in the principal direction along the axis of the dam (perpendicular to the cross section) are zero. Very long structures, such as dams in flat, wide valleys, generally exist under static plane strain conditions. The adequacy of assumptions of plane strain was not clear for cross sections of Ririe Dam because of the small length-to-height ratio (3.4), the curved centerline and abutments, in plan, and possible epicenters of earthquakes off the upstream-downstream axis.

10. State-of-the-art procedures for evaluating the three-dimensional seismic response of earth dams in narrow canyons were used for this study. Although a complete three-dimensional finite element response analysis was not performed for Ririe Dam, the implications of three-dimensional geometry for dynamic response were evaluated through a careful analysis of two idealized cross sections, site geotechnical data, and comparison with two-dimensional and three-dimensional calculated and observed response of similar dams in narrow canyons.

11. The "Earthquake Engineering Evaluation" phase involves evaluating the potential for modes of failure (slope failure or sliding of dam causing a loss of freebroard) to occur. Much of the seismic stability analysis focuses on evaluating the potential for granular soils to liquefy which could cause slope failure and a consequent loss of freeboard (mode (d)). Liquefaction, in general, refers to excessive deformations or movements as a result of transient or repeated disturbance of saturated cohesionless soil (National Research Council 1985). The onset of liquefaction was defined for this study as the instaantin time when the excess pore water pressure at a point in a soil deposit equals the vertical effective stress at that same point.

12. The performance-based approach pioneered at the University of California at Berkeley by Seed, Lee, and Idriss (e.g., Seed and Lee 1966; Idriss and Seed 1968; Seed and Idriss 1971; and Seed, Idriss, and Arango 1983) was used to accomplish the evaluation of liquefaction potential. The various facets of the performance-based approach were itemized by Seed (1985):

a. The acquisition of a comprehensive background concerning field case histories of soil liquefaction during earthquakes and all

proposed methods for evaluating the liquefaction potential of soil deposits.

b. The development and use of methods of evaluating the liquefaction potential based on field observations and case studies.

c. The conduct of laboratory studies on soil samples to throw light on the physical mechanisms by which liquefaction occurs under idealized conditions in the laboratory and to evaluate the possible effects of earthquake shaking on representative samples taken from the field.

d. The conduct of analytical studies to explore the mechanisms leading to the generation and dissipation of pore pressures in idealized models of soil deposits, including where appropriate consideration of soil softening and surface layer isolation.

e. The development of simplified procedures for evaluating the liquefaction potential in practice, based on a knowledge of all aspects of the problem listed but with special emphasis on the use of engineering judgment based on field performance data: where analysis procedures are used they are checked against field performance data for applicability.

This approach is valuable because it uses measured data from sites that have liquefied during earthquakes and involves common geotechnical engineering parameters. The effects of pore pressure dissipation are not included which make the analysis conservative.

13. The performance-based approach evolves around the comparison of shear stresses induced by an earthquake with shear stresses required to cause liquefaction (called cyclic strength). The stresses caused by the design earthquake are estimated using the results of a dynamic response analysis. The cyclic strength for each material is estimated using the Standard Penetration Test (SPT) resistance. It is this latter determination that is derived from correlations of soils that have and have not liquefied during previous earthquakes. For this study, the Becker Hammer Penetration Test (BPT) resistance was used to evaluate cyclic strength by means of a correlation between BPT and SPT values.

14. Other aspects of seismic performance are more difficult to assess using the performance-based approach. Strains and deformations of zones that have undergone plastic deformation or have liquefied may not be determined using the performance-based approach. Shear strains are calculated as part of the dynamic response analysis using an equivalent-linear soil model. However, the evaluation of liquefaction involves a simple comparison of stresses, not a coupled system of induced stresses, stress-strain curves, and consequent

deformations. It is possible to estimate the distribution of excess pore water pressure throughout the embankment using the ratio of the induced stress to the stress causing liquefaction (defined as the factor of safety against liquefactions, FS_L) with the results of cyclic triaxial tests performed on representative samples. The distribution of excess pore water pressures are then used to evaluate the postearthquake slope stability using traditional means of analysis.

15. Other analyses were used to confirm the results of the dynamic response analysis calculations. These included one-dimensional wave amplification calculations and nonlinear shear beam analogies. These methods were used to compare the variation of stress and acceleration with time at select points in the cross section.

16. The potential for slope failures induced by ground motion was evaluated using simplified procedures and comparisons with empirical studies. This method of analysis is called a permanent displacement analysis. Simplified procedures have been derived from a sliding block analogy that considers the forces acting on a mass resting on a slope. The empirical studies considered the performance of rock-fill dams during small earthquakes and the range of calculated permanent displacements for a number of other dams.

General Results of Analyses

17. The results of the liquefaction analysis conducted by WES indicate that the upstream random fill and a large portion of the upper alluvial gravel (loose and medium-dense) strata both upstream and downstream of the core will liquefy as a consequence of the design earthquake motions. Postearthquake stability calculations using residual strengths for liquefied zones indicate that the upstream and downstream slopes are stable (the lowest calculated factor of safety against sliding was 1.33 for the downstream slope of the dam). In our judgment, the dam will not fail from a loss of freeboard or overtopping as a consequence of slope failure resulting from liquefaction of foundation and embankment materials.

18. The results of permanent displacement analyses along potential slip surfaces using five different simplified methods and an empirical relation indicate that Ririe Dam may undergo significant displacements along the downstream and upstream slopes. The best-estimates for permanent

displacements are 0.6 and 6 ft, respectively. If these magnitudes of displacements were to occur along the likely slip surfaces the dam is not expected to fail but a safety hazard could be created requiring immediate draining of the reservoir. The methods of analysis used, however, provide only general estimates of the magnitudes of displacement. Moderate damage to the dam is expected in the event of the MCE.

19. A best estimate of the crest settlement was obtained assuming that slip surfaces corresponding to best-estimates of maximum permanent displacement are activated. The displacements caused by shear straining expected to occur in liquefied zones (15 percent) were also superimposed onto best-estimates of maximum permanent displacements. The crest of the dam above the slip surface was assumed to remain as a single body as it displaces. The vertical displacement of the crest will be about 6 ft leaving a freeboard of 10 ft above the analysis pool level. The top of the impervious core will also drop about 6 ft leaving about 4 ft above the phreatic surface. The impervious gravel cap atop the impervious core should remain in place relative to the underlying core.

PART II: BACKGROUND

20. Details of "Characterization Studies" shown in Figure 3 are contained in Report 1. A very limited amount of this information is reproduced in this chapter for convenience. It is intended to provide a brief background of information to allow readers of this report to basically understand the conditions present at Ririe Dam.

Project Description and History

21. The Ririe Dam and Reservoir Project is a federal, multipurpose, water resource development project authorized by Public Law 87-874: "Flood Control Act of 1962." This Act specified that the project be constructed by USACE and operated by the US Department of the Interior (USDI), Bureau of Reclamation (BOR). Events leading up to the passage of this bill are documented in US Army Engineer District, Walla Walla (1978). The primary purpose of the project was flood control, but recreation facilities and public and irrigation water supply were also factors.

22. The major impact of the project is the reduction of flooding in areas downstream. Seventeen floods produced from rain and snowmelt caused damage to the farmlands and urban areas, particularly the city of Idaho Falls, Idaho, during the period of the years 1911 to 1976 (when the project was completed). A flood occurring in 1962 inundated 69,400 acres of land for up to 3 days. Ririe Dam now protects 100,000 acres valued in 1972 at $300 million for land and improvements (US Army Engineer District, Walla Walla 1972).

23. Water collected and stored by Ririe Dam typically is used for irrigation and recreation in the summer months. The total reservoir storage is 100,000 acre-ft (at maximum pool elevation of 5,119) providing 70,000 acre-ft for irrigation purposes, 1,560 acres of lake for boating, and creating a lake 12 miles long with 25 miles of lake shore. Much of the shore is inaccessible except by boat. A plan view of the Ririe Project is shown in Figure 4.

24. The stability of Ririe Dam affects eastern Idaho. According to a dam break scenario conducted by the USDI, Bureau of Reclamation (1982), a sudden release of the reservoir behind Ririe Dam would flood over 200 square miles of farmland and communities and directly affect over 75,000 persons.

The initial flood wave would reach the first community in less than 30 min and would ultimately inundate most of the City of Idaho Falls

25. The NPW designed and monitored construction of the Ririe Dam and Reservoir Project. Construction was initiated in July 1967; the main embankment was essentially complete on 26 November 1975. A Project Transfer Agreement with the Water and Power Resources Service, BOR, was signed on 14 October 1976. The responsibility for this safety evaluation was directed to USACE because of their involvement in the design and construction of the project.

26. The dam is a zoned earth- and rock-fill embankment containing approximately 2.9 million cu yd of material and incorporates a narrow impervious central core. The axis of the dam (in plan) is arched with a radius of curvature of 1,432 ft. The center of the arc is located in the valley downstream. The maximum height of the embankment is about 250 ft, 184 ft above the preexisting ground surface, and the length of the dam at the crest is 840 ft. The length-to-height ratio of the dam at the crest elevation is about 3.4. Dams with a length-to-height ratio of 3.0 or less are considered to be narrow for analytical studies which signifies that dynamic stability is generally affected by the three-dimensional geometry of the embankment (e.g., Mejia and Seed 1983).

27. The core is bordered by three distinct filter zones, each designed to protect the core material and adjacent filter zones from erosion and migration of sand and fines. Rock and gravel fill flanks the core and filter zones on the upstream and downstream sides. Random fill, a collection of rock, gravel, sand, and silt, was used to buttress the dam. A rock-fill cofferdam was constructed to divert water during excavation of the core trench. This cofferdam was incorporated into the dam and serves as the upstream toe. An as-built, maximum-height cross section of Ririe Dam is also shown in Figure 4.

28. The crest of the dam is at el 5128* and is 34 ft in width. Downstream slopes vary in segments from 2:1 (horizontal : vertical) near the crest to 5:1. A portion of the downstream face is horizontal for 100 ft of transverse extent and supports an access road which enters from the left abutment. Upstream slopes vary from 2:1 near the crest to 7:1 with a 59-ft

---

* Elevation in this report refers to feet, NGVD.

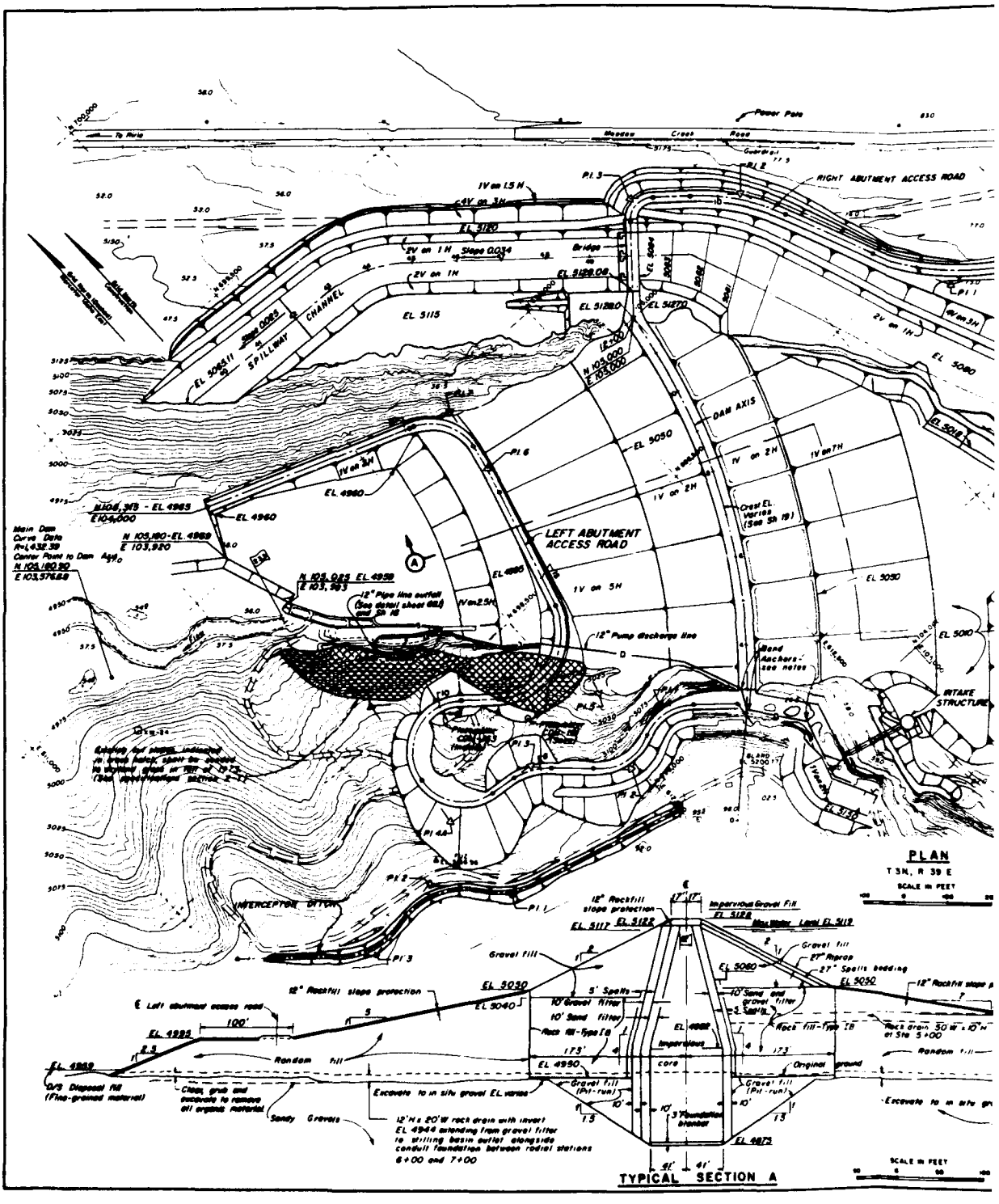

Figure 4. Plan view and typical as-built maximum section of

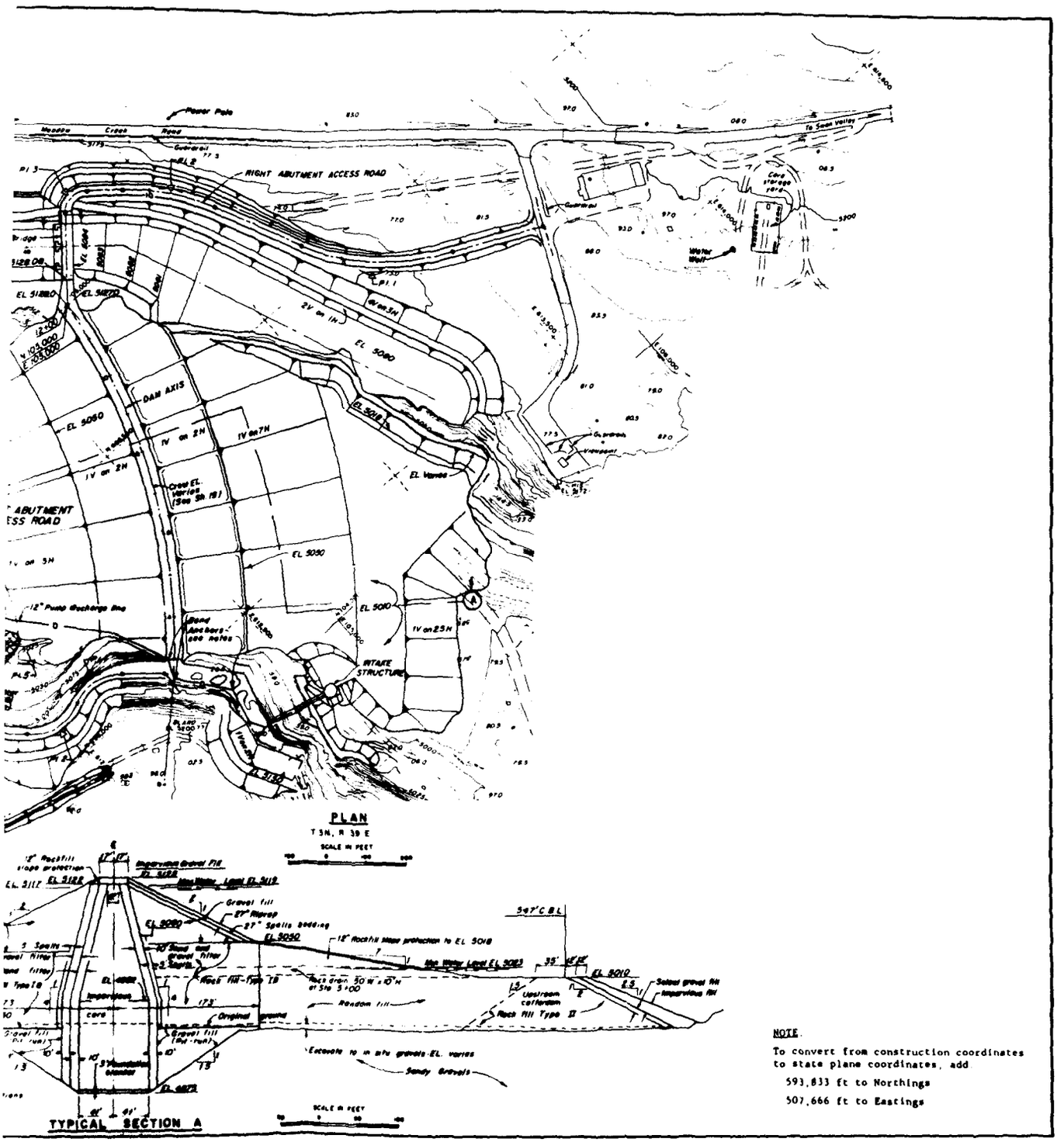

typical as-built maximum section of Ririe Dam and Reservoir Project

horizontal section which is the crest of the cofferdam integrated into the dam.

29. Seventeen types of materials were used to construct Ririe Dam. The impervious core was constructed using silt indigenous to the region. Materials for successive filter zones downstream of the core are: sand, gravel, and "spalls" (clean basalt gravel). A sand and gravel filter and a transition layer of spalls were used upstream of the core. Rock fill, gravel fill, pit-run gravel, and random fill were used in specific zones located both upstream and downstream of the filtered core. Random fill is essentially rock material which did not meet gradational requirements for rock fill (generally having too great a percentage of finer materials), but it also contains pit-run gravel and silt. Gradation curves corresponding to the ranges for the embankment materials and the specification limits are shown in Figures 5-8

30. The embankment is founded directly on alluvium or basalt. The core extends through alluvium to basalt to provide a positive cutoff to seepage. Filter zones, gravel fill, rock fill and random fill overlie silty gravel with a maximum determined thickness of 90 ft. Rock drains exist through random fill on the upstream and downstream sides of the embankment to provide adequate drainage of the filter zones. Tuffaceous sediments, the product of regional volcanic activity, underlie basalt but are in contact with alluvium in a particular region beneath the dam where the basalt does not exist. The extent of this region estimated by US Army Engineer District, Walla Walla (1977) is indicated in Figure 9. Also indicated in Figure 9 are the locations of rock drains through the downstream and upstream shells and random fill zones of the dam.

31. The reservoir is controlled by an outlet works consisting of a concrete intake structure with concrete conduit through the embankment and founded on and against the left abutment and a concrete emergency spillway cut through the right abutment. Flow through the emergency spillway is controlled by two tainter gates. The elevation at the top of the overflow section (the base of the tainter gates) is 5,093 ft, 9 ft above the emergency spillway section. The capacities of the outlet works and spillway are 1,900 and 40,000 cfs, respectively. The design maximum pool elevation is 5,119 ft, yielding a freeboard of 9 ft and a height of water of 26 ft at the tainter gates. The relative locations of these elevations are shown in Figure 10.

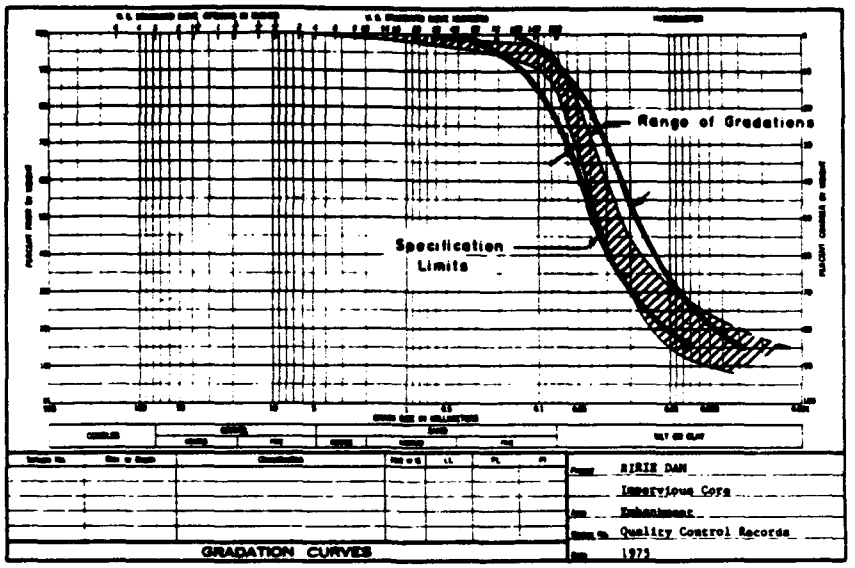

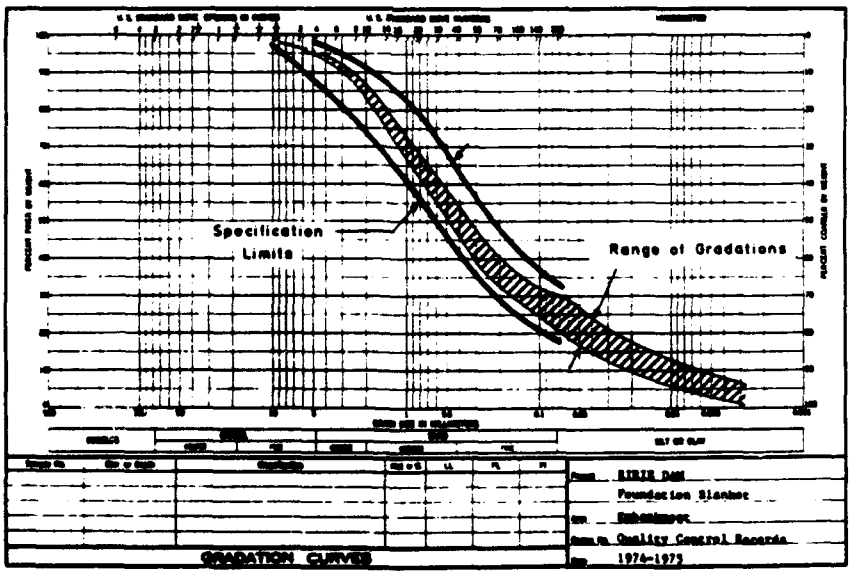

Figure 5. Range in gradations and criteria for core material and foundation blanket

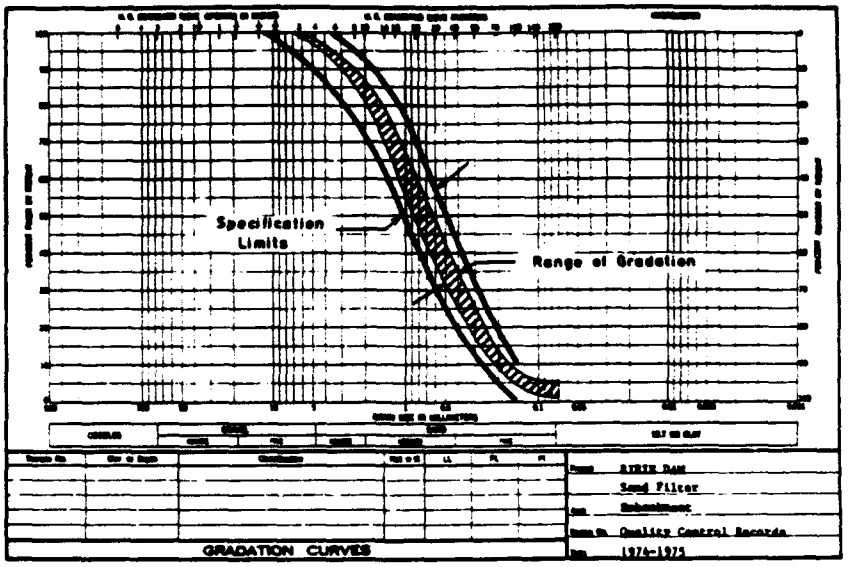

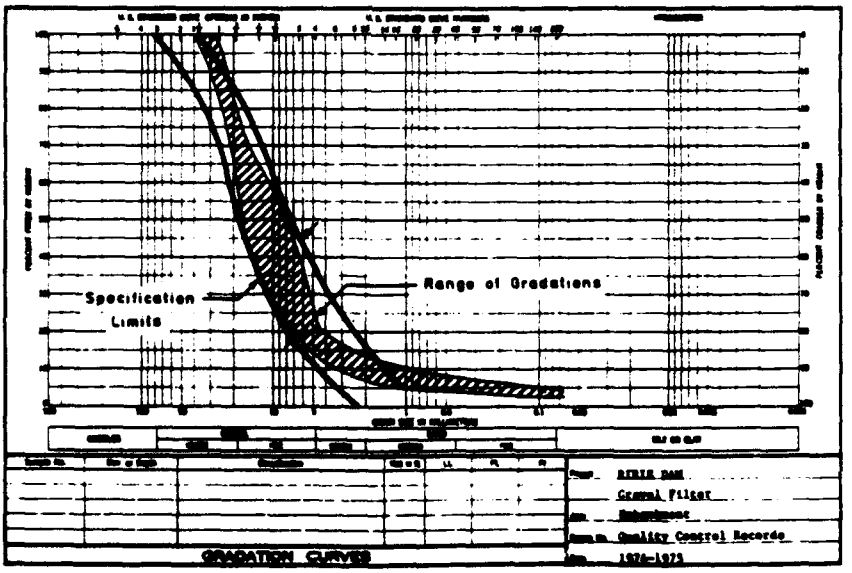

Figure 6. Range in gradations and criteria for sand filter and gravel filter

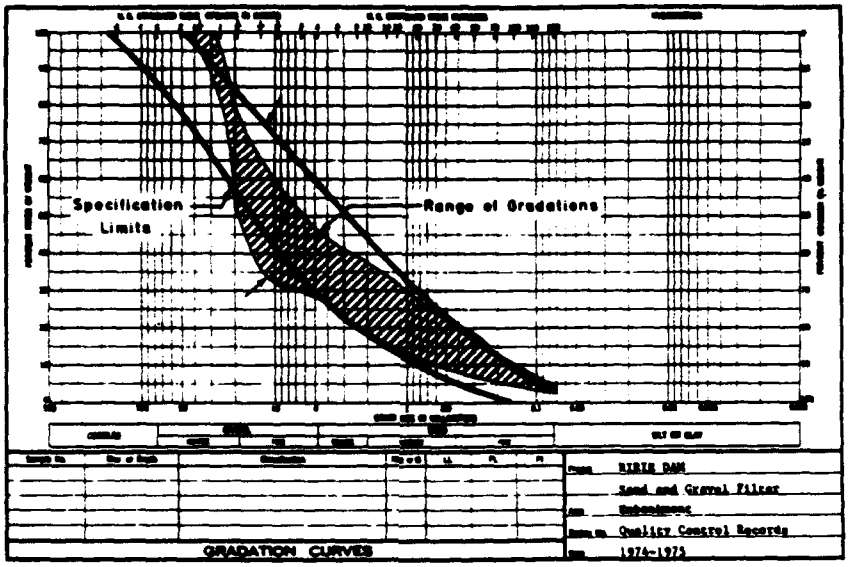

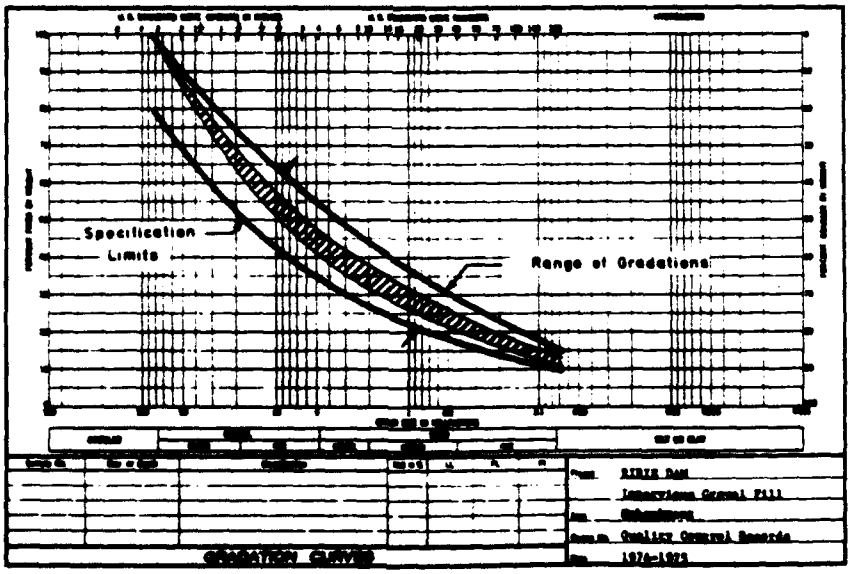

Figure 7. Range in gradations and criteria for sand and gravel filter and impervious gravel

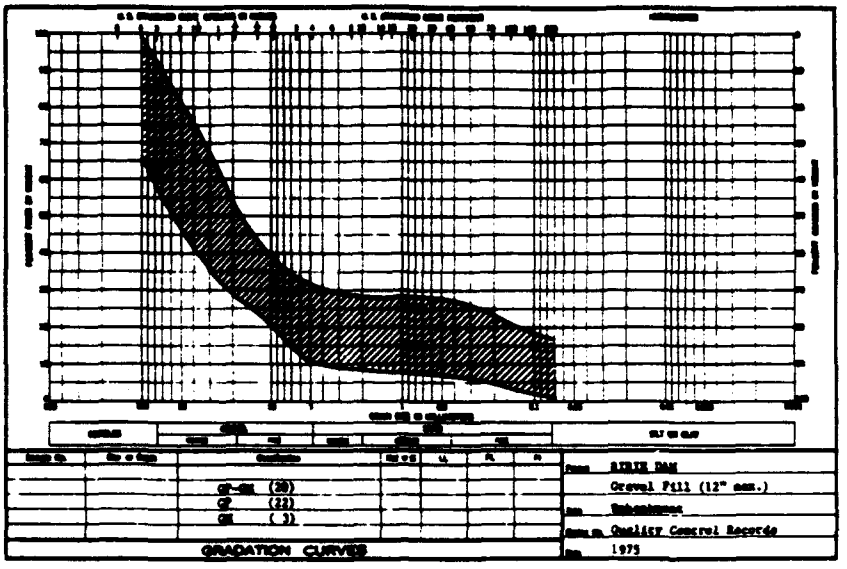

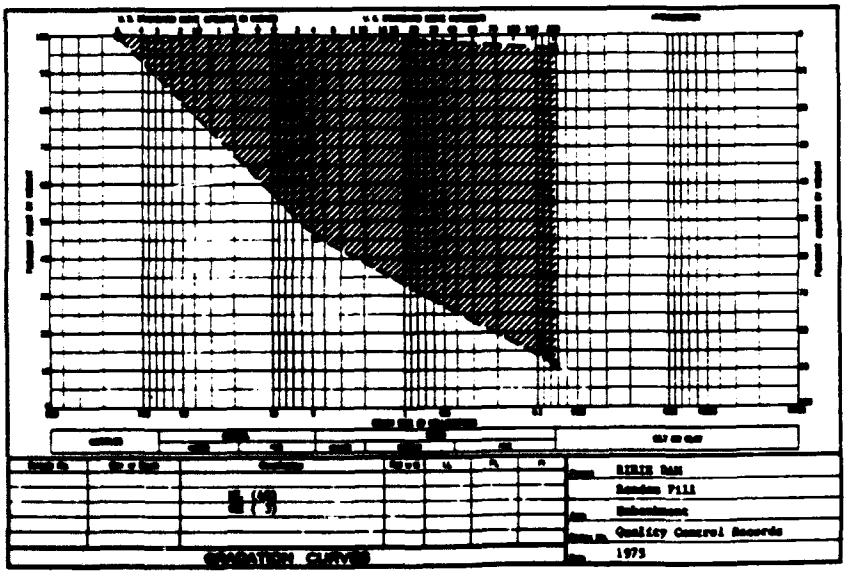

Figure 8. Range in gradations for gravel fill and random fill

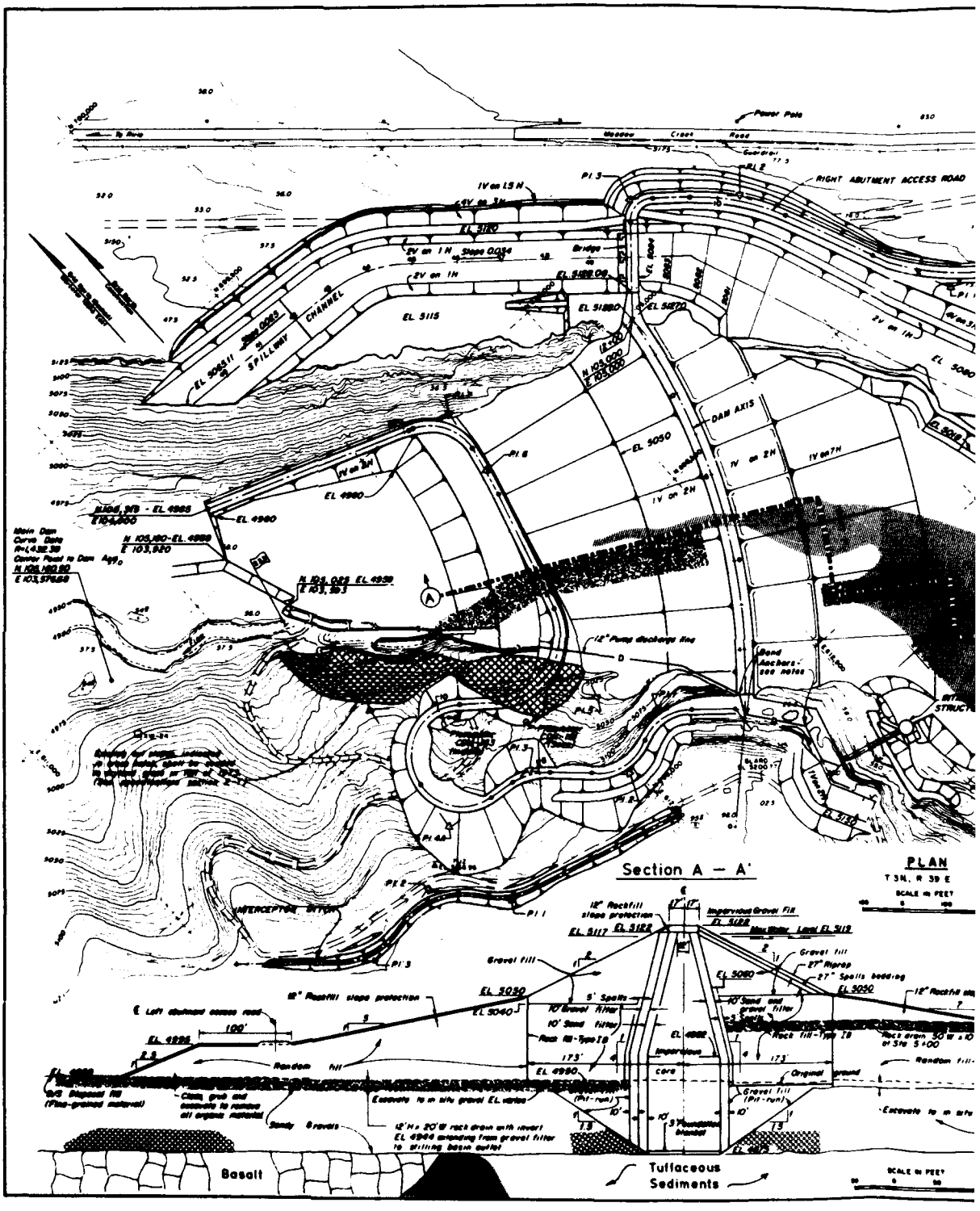

Figure 9. Locations of unique zones in the emb

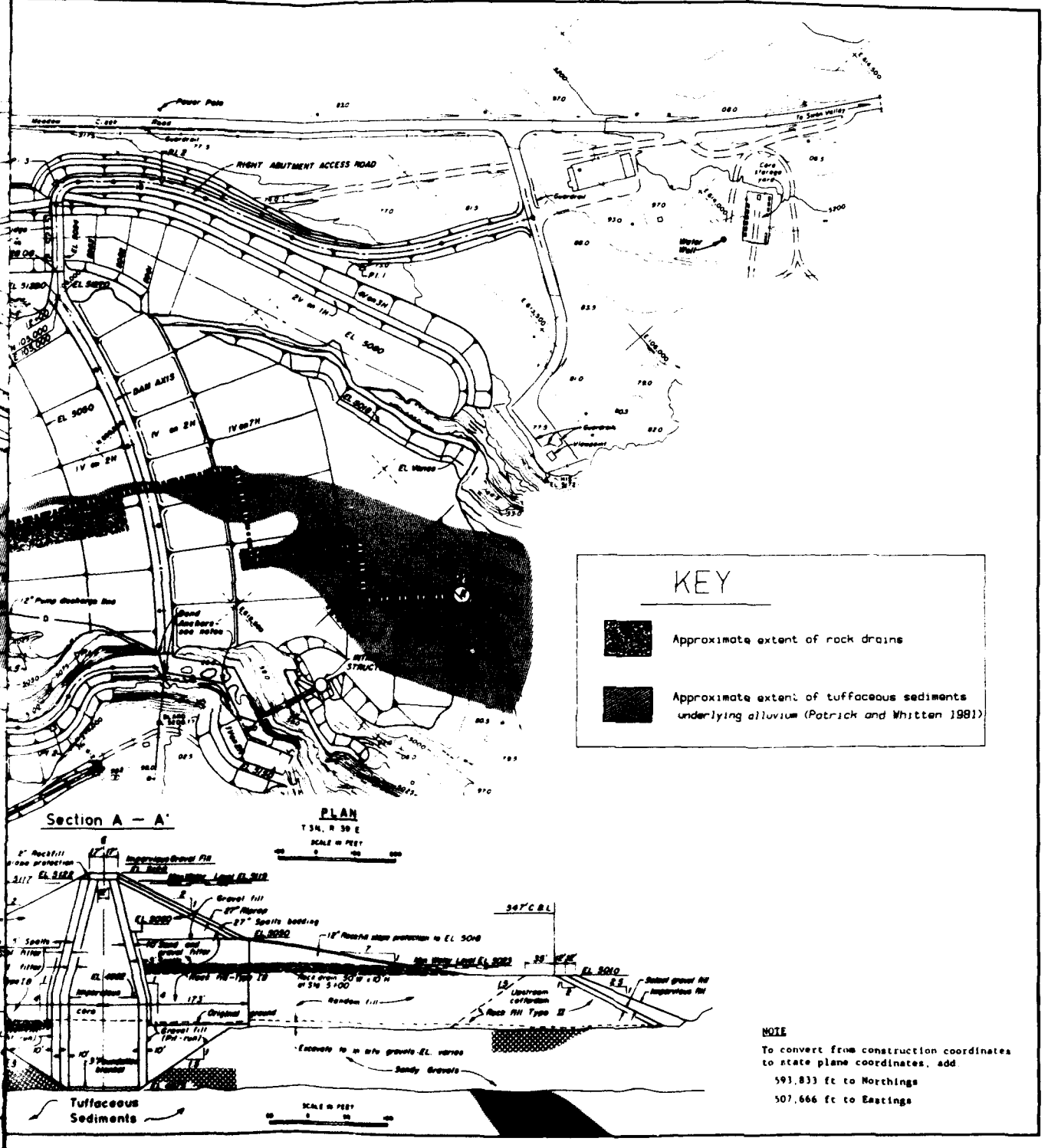

cations of unique zones in the embankment and foundation

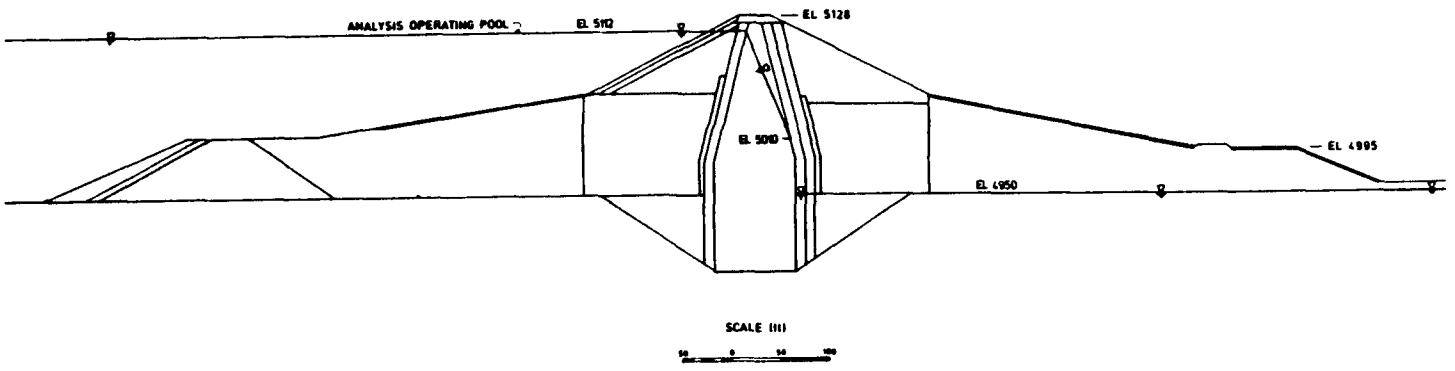

Figure 10. Phreatic surface selected for seismic stability analyses

32. An idealized phreatic surface was selected for seismic and post-earthquake stability analyses based on US Army Engineer District, Walla Walla (1979), pool levels and piezometric data collected by the USDI, Bureau of Reclamation (1989), and well soundings made by field geologists during recent investigations and is shown in Figure 11. This surface is assumed to vary in two directions only (vertically and perpendicular to the embankment), that is:

$$\frac{\partial h}{\partial y} = 0 \tag{1}$$

where

h = total (hydraulic) head

y = horizontal direction tangent to the axis of the dam at the point of interest

The idealized phreatic surface used for analysis consists of multiple segments beginning with a pool level at el 5,112, extending to the upstream side of the core at el 5,112 and continuing to a point on the downstream side of the core at el 5,010. Beyond that point downstream, the phreatic surface is assumed to coincide with the downstream side of the core. At el 4,950, the phreatic surface is assumed to be horizontal through the random fill and exit downstream as the tailwater.

Canyon Geology

33. Three major geologic regions meet in the vicinity of the Ririe Dam and Reservoir Project. These regions are: the Basin and Range Province, the Rocky Mountain Orogenic Belt, and the Snake River Plain. Ririe Dam is situated on the northern margin of the Basin and Range Province, 3 miles to the south and 2 miles to the east of the Snake River Plain, and about 35 miles west of the Rocky Mountains. These geologic regions have been greatly affected locally by volcanic activity during the Cenozoic Era (65 million years to the present). Most volcanic activity has occurred in the Snake River Plain.

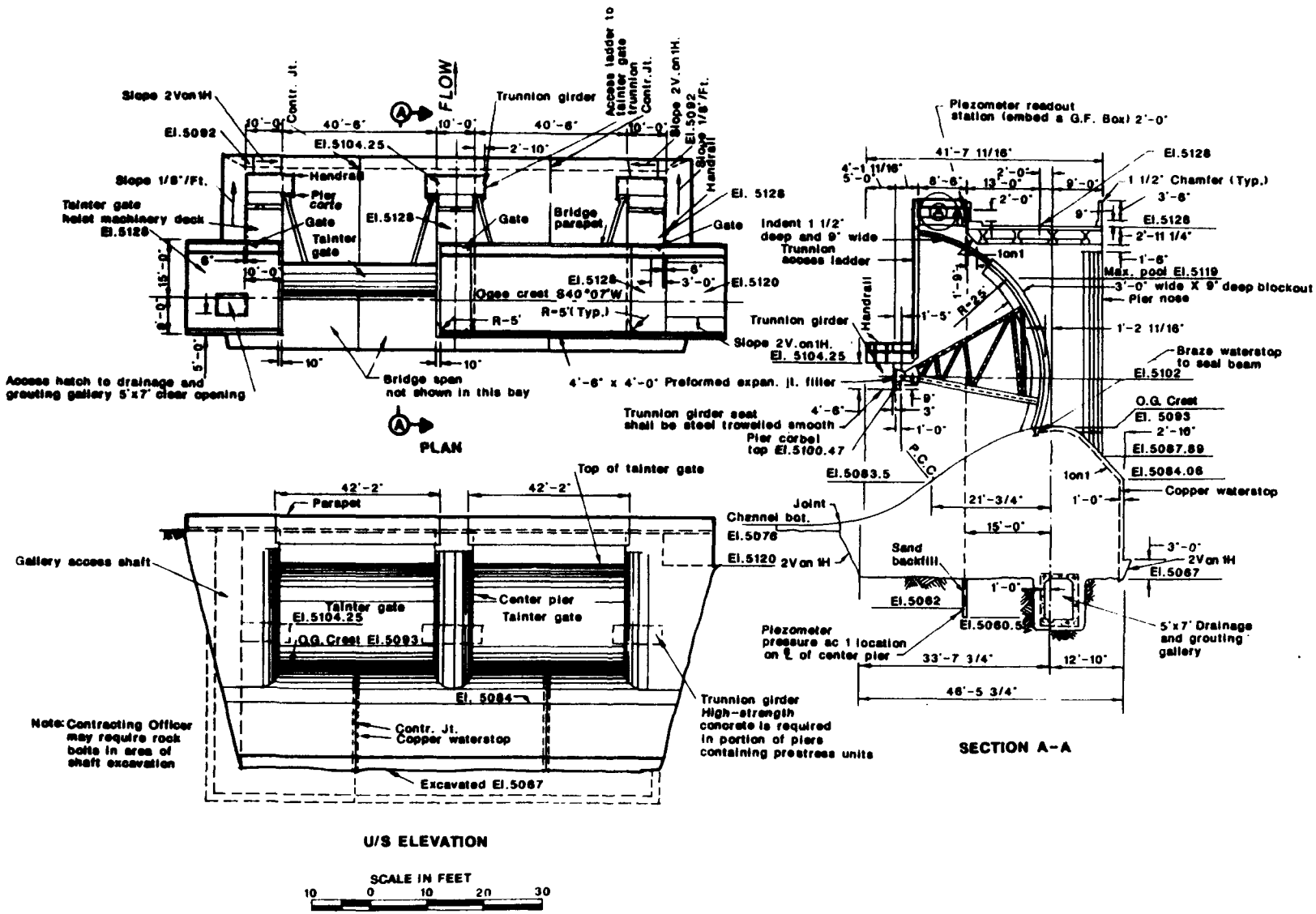

Figure 11. Details of emergency spillway (US Army Engineer District, Walla Walla 1972b)

34. The region around Ririe Dam is comprised of a complex series of flow units. A number of stratigraphic units exist in abutments and foundation, typically separated by soil-like breccia zones. These units generally dip about 5 to 10 deg striking toward the left abutment. A revised stratigraphic column was presented in Report 1 and is shown in Figure 12. A cross section of the valley showing the profiles in the abutments and in the foundation are shown in Figure 13.

35. A thick deposit (estimated to be about 100 to 300 ft) of tuffaceous sediments lies beneath Ririe Dam. The top of this unit was found to be fairly flat but dip considerably to the north. The upper part of the tuffaceous sediments are soft and are appropriately described and characterized using soil engineering terminology. The lower parts of the tuffaceous sediments are stiffer as measured using seismic geophysical techniques. A similar unit located deeper in the foundation, below a layer of very competent rhyolite, is named the "Tuff of Wolverine Creek."

36. Alluvial gravel exists in the valley upstream and downstream of the core and beneath rock and random fill. The presence of an unstable material in these locations, such as liquefied gravel, could have a pronounced impact on the overall stability of the structure. Pierce and Scott (1982) concluded that the alluvial gravels in alluvial fans and main streams in the region of Ririe Dam are of late Pleistocene Age (between 25,000 and 11,000 years old). In general, Youd and Perkins (1978) found on the basis of soils known to liquefy during earthquakes that Pleistocene soils have a low susceptibility to liquefy. However, Pleistocene gravels were found to liquefy in the Thousand Springs Valley, Idaho, during the Mt. Borah, Idaho, earthquake of 1983 (Youd et al. 1985 and Andrus 1986).

Seismic Hazard Assessment

37. A site-specific geologic and seismologic study was conducted by Krinitzsky and Dunbar (1991) to estimate the components of earthquake motions required for the dynamic response analysis of Ririe Dam. Earthquake motions originating at nearby faults were found to control the seismic threat to Ririe Dam. The faults identified near Ririe Dam are shown in Figure 14. One fault very near Ririe Dam was interpreted to be capable of producing an earthquake of magnitude M_s = 7.0. The entire near-field region (4 to 10 km),

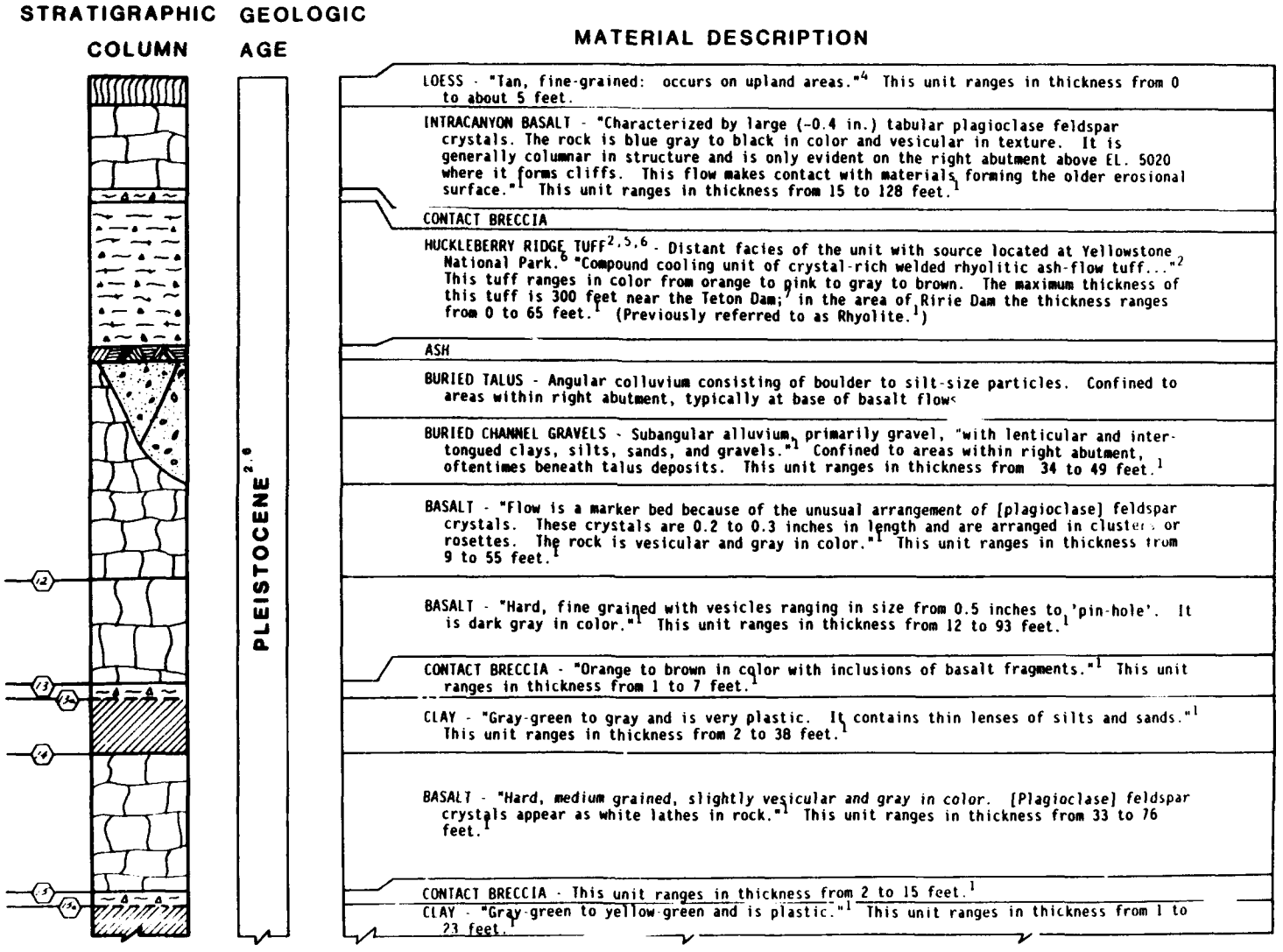

Figure 12a. Stratigraphic column and material descriptions for abutment and foundation materials

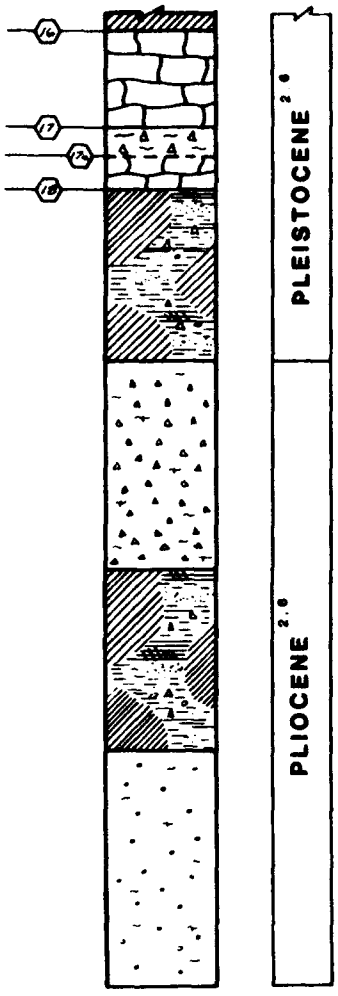

PLEISTOCENE 2.6

PLIOCENE 2.6

BASALT - "Hard, fine grained, slightly vesicular and dark gray in color."[1] This unit ranges in thickness from 13 to 41 feet.[1]

FLOW BRECCIA - This unit ranges in thickness from 2 to 15 feet.[1]

BASALT - "Similar to flow 16-17."[1] This unit ranges in thickness from 9 to 52 feet.[1]

TUFFACEOUS SEDIMENTS (UNNAMED) - Formerly referred to as "Basal Sediments." This unit consists of various and numerous layers of nonwelded and partially-welded ash-flow and air-fall tuffs.[6] Layers of bentonitic material may exist within these sediments.[6] The upper part of these sediments generally is a reddish-brown, has low plasticity, and can be classified as a silty or clayey material. This unit is estimated to be about 100 to 300 feet thick beneath Ririe Dam.[6] These sediments are assumed to be similar to the Tuff of Wolverine Creek which are exposed in the Call Dugway upstream of Ririe Dam.[6]

TUFF OF KILGORE - "A compound cooling unit consisting of at least four sheets of rhyolitic welded ash-flow tuff, each containing different percentages of flattened pumice and phenocrysts."[2] "At the Call Dugway near Ririe Dam, the layers are due to welding and devitrification, not flow units. There the base of the unit consists of a few inches of poorly welded tan-colored vitric tuff which grades upward into a dark brown densely welded vitrophyre which is generally 3-5 feet thick. Above the vitrophyre is a resistant cliff forming lithophysal (swiss cheese like) zone with 1/2" diameter white lithophysae in a black glassy matrix. This zone is overlain by a gray to purple densely welded, devitrified tuff with scattered lithophysae. The top of the sheet consists of orange to red moderately welded vitric tuff."[7]

TUFF OF WOLVERINE CREEK - This tuff is "poorly-resistant, mostly light to dark gray and yellowish-gray, nonwelded, and partially welded, crystal poor rhyolitic ash-flow and airfall tuffs containing light-gray, non-flattened pumic fragments and black obsidian chips. Upper part of unit...is partially welded ash-flow tuff, commonly stained bright shades of red, orange, and purple. Middle part of unit is a thick single ash-flow cooling unit, light-gray in color...Lower part of unit is non-welded, bedded air-fall tuff."[2] Total thickness of the unit ranges from 0 to 180 feet.[2] Exposed along Call Dugway about 4 miles upstream of Ririe Dam in the Meadow Creek Valley and was previously considered to be the same unit which exists directly beneath Ririe Dam.[4]

TUFF OF BLACKTAIL - "Brown, orange, pink, and purple, mostly devitrified densely welded ash-flow tuff containing about 10-20 percent small phenocrysts and abundant, small, very flattened pumices. Perlitic basal vitrophyre generally present as well as several discontinuous lithophysal zones."[2] The thickness of this unit ranges from 3 to 650 feet.

References
1. U.S. Army Engineers (1972b)
2. Prostka and Embree (1978)
3. Embree et al. (1982)
4. Patrick and Whitten (1981)
5. Christiansen (1982)
6. Embree (1986)
7. Embree (1989)

Figure 12b. Stratigraphic column and material descriptions for abutment and foundation materials

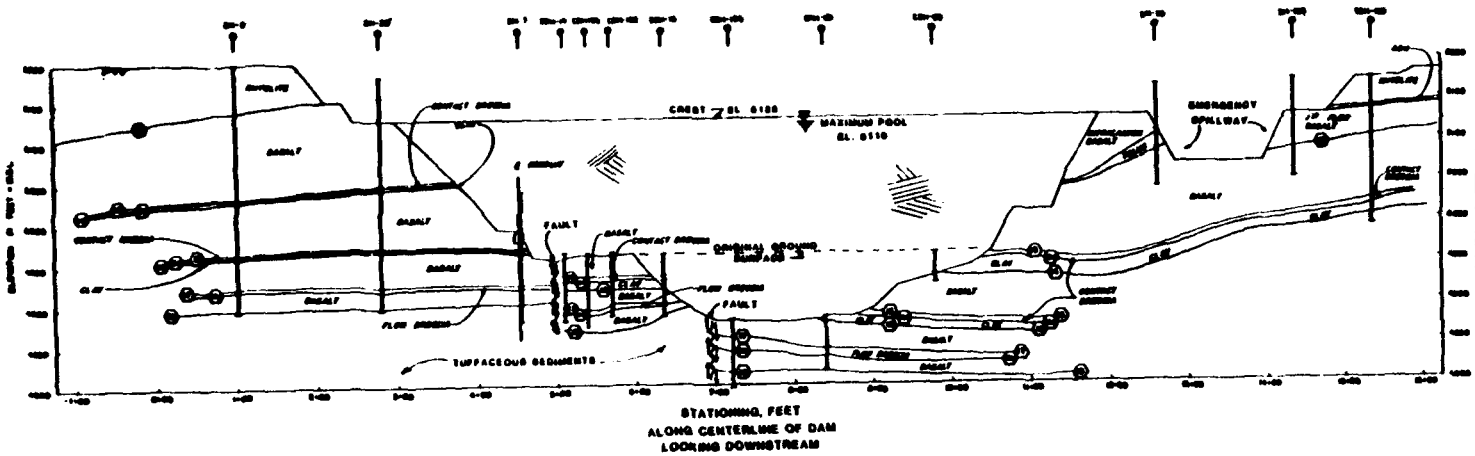

Figure 13. Profile of valley geometry and geology of abutments along the centerline of the dam looking downstream (US Army Engineer District, Walla Walla 1978)

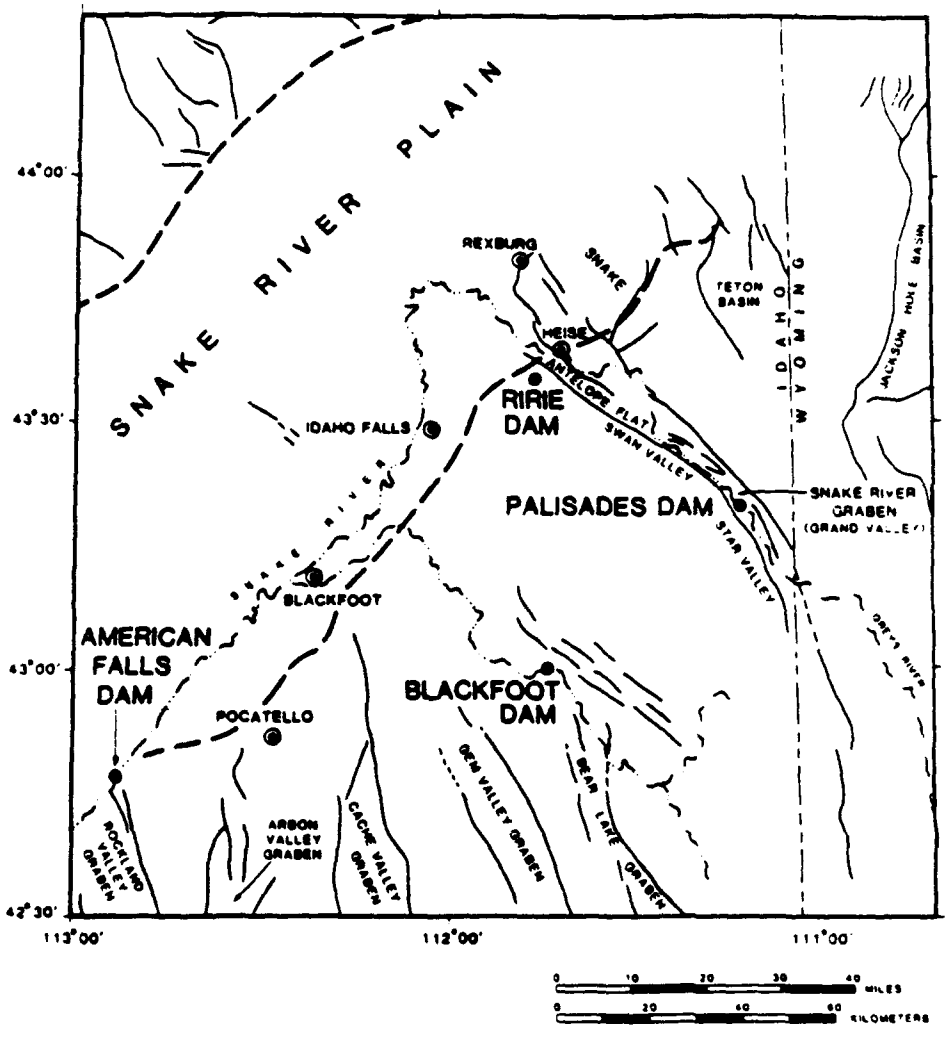

Figure 14. Nomenclature of major structural features in the area of Ririe Dam (from Krinitzsky and Dunbar 1991)

specifically the Grand Valley graben, was interpreted as active and capable of producing earthquakes with magnitude M_s = 7.5. The nearest segment of the graben is the Heise-Rexburg fault which is located about 5 miles from the site.

38. Parameters for the Operating Basis Earthquake (OBE--expected to occur over the life of the structure) and the Maximum Credible Earthquake (MCE--largest that is reasonably expected to every occur) were proposed by Krinitzsky and Dunbar (1991). The OBE corresponds to a far field event resulting in a MM intensity VIII at the site with values for peak acceleration of 280 cm/sec^2 (0.29 g), peak velocity of 25 cm/sec, and a duration of strong motion (greater than 0.05 g) of 65 sec. The MCE is described as a near-field event having a site intensity of MM X, and resulting in a peak acceleration of 1,200 cm/sec^2 (1.22 g), a peak velocity of 120 cm/sec, and a duration of strong motion 33 sec at the site.

39. Hypothetical earthquake motions representing the MCE were synthesized by Professor H. Bolton Seed, University of California, Berkeley, using the S 19° E component of an accelerogram recorded on rock at Pacoima Dam during the 1971 San Fernando Earthquake and a portion of the N 21° E component of the 1952 Taft record. The recorded motions were sealed to obtain about a maximum acceleration of 1.2 g and lengthened the duration of strong motion (accelerations larger than 0.05 g). This accelerogram is shown in Figure 15. The variation of velocity with time corresponding to this accelerogram is shown in Figure 16. The (pseudo) spectral acceleration as a function of period is shown in Figure 17 for a damping ratio of 5 percent. Parameters for these records and the OBE and MCE are summarized in Table 1.

Construction Records

40. The Ririe Dam embankment is shown by the historical record to have been constructed with great care using widely accepted practices for dam construction. The collection of documents available indicates that the personnel of NPW were keenly aware of day-to-day construction activities, specifications, and design recommendations and made appropriate decisions when unexpected situations arose. The embankment was designed to account for the foundation conditions present and the types of borrow materials available (e.g., extensive use of filter zones to protect the silt core). Modifications

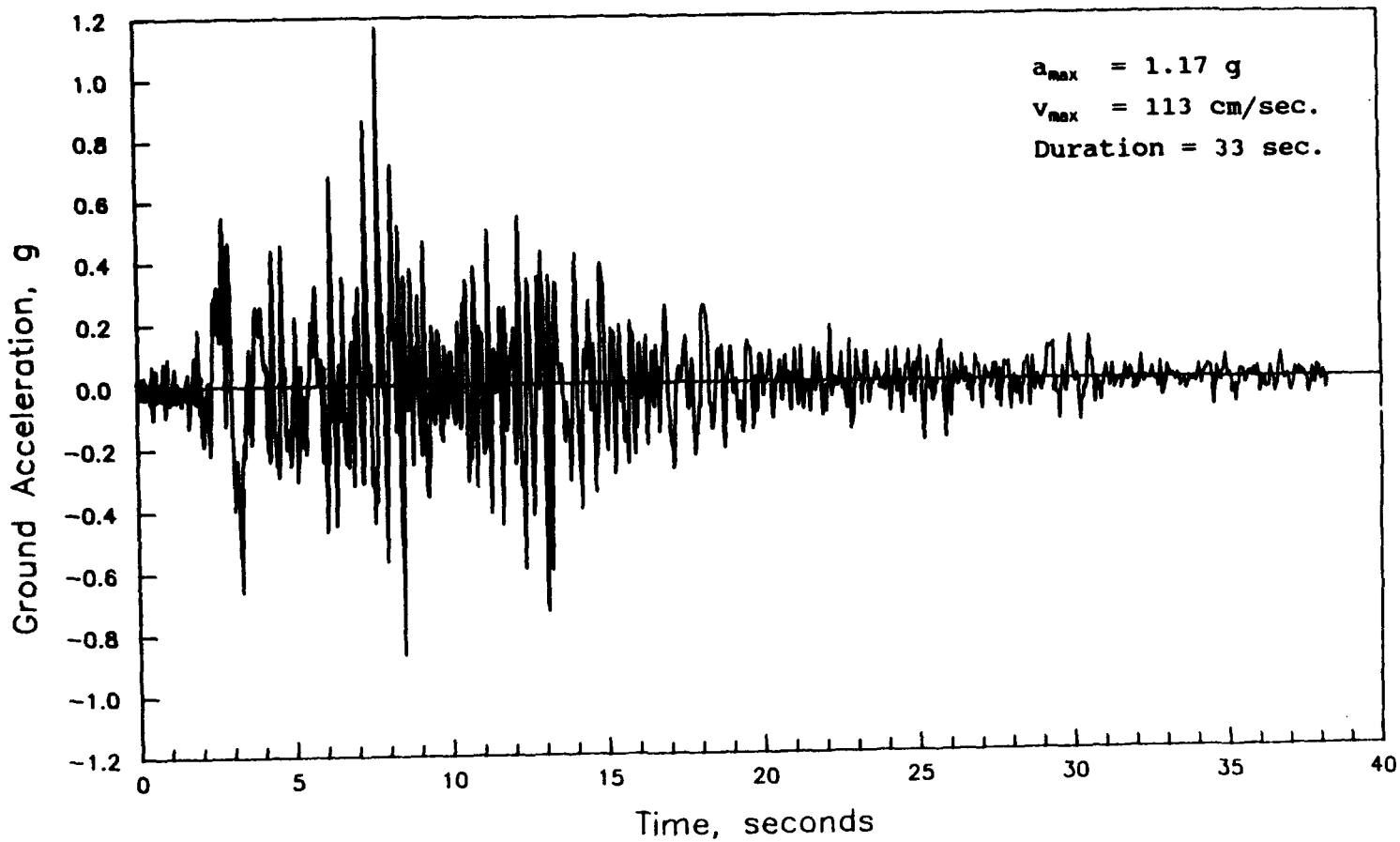

Figure 15. Acceleration record adopted for analysis (Seed 1987)

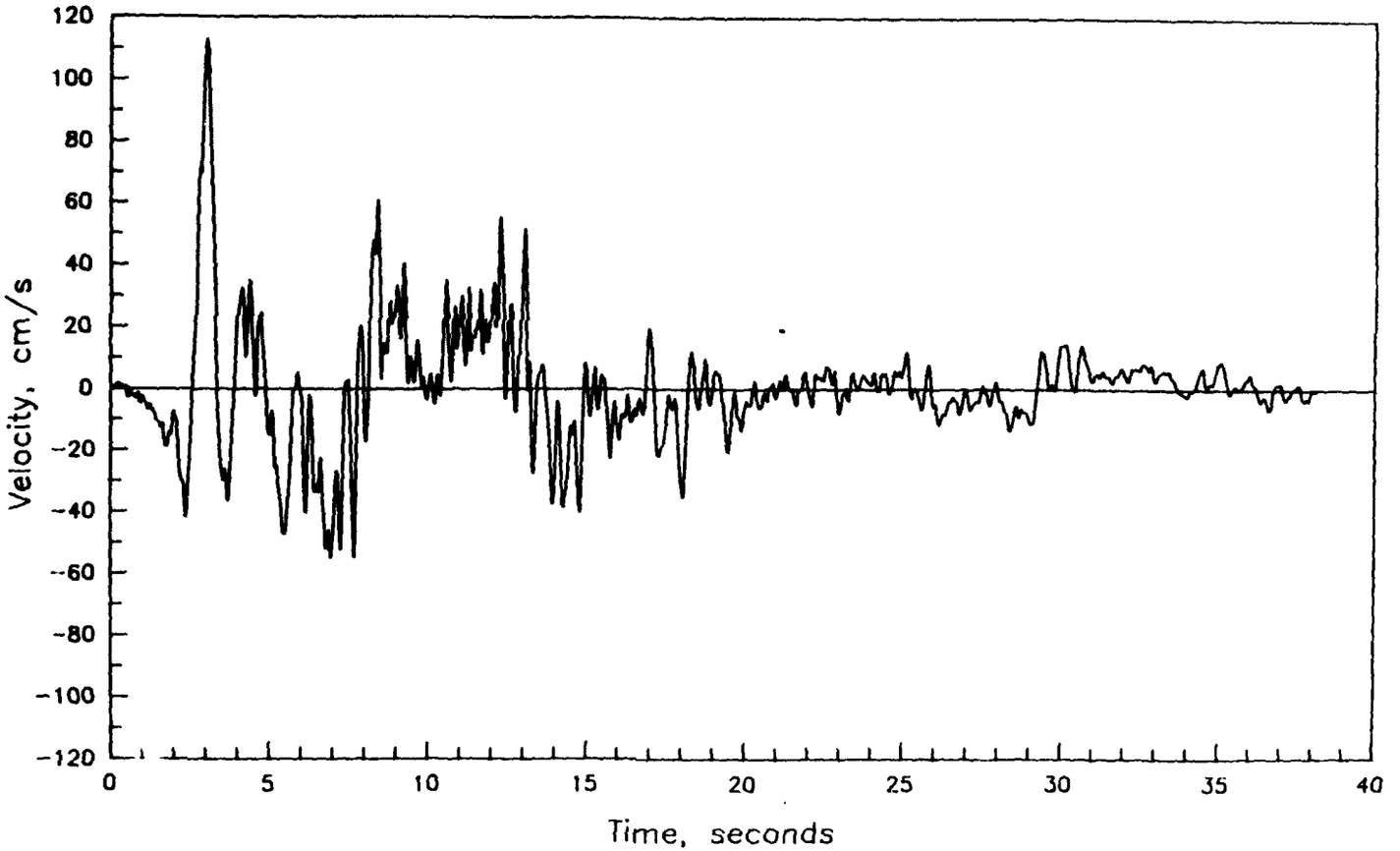

Figure 16. Velocity record corresponding to the accelerogram adopted for analysis (Seed 1987)

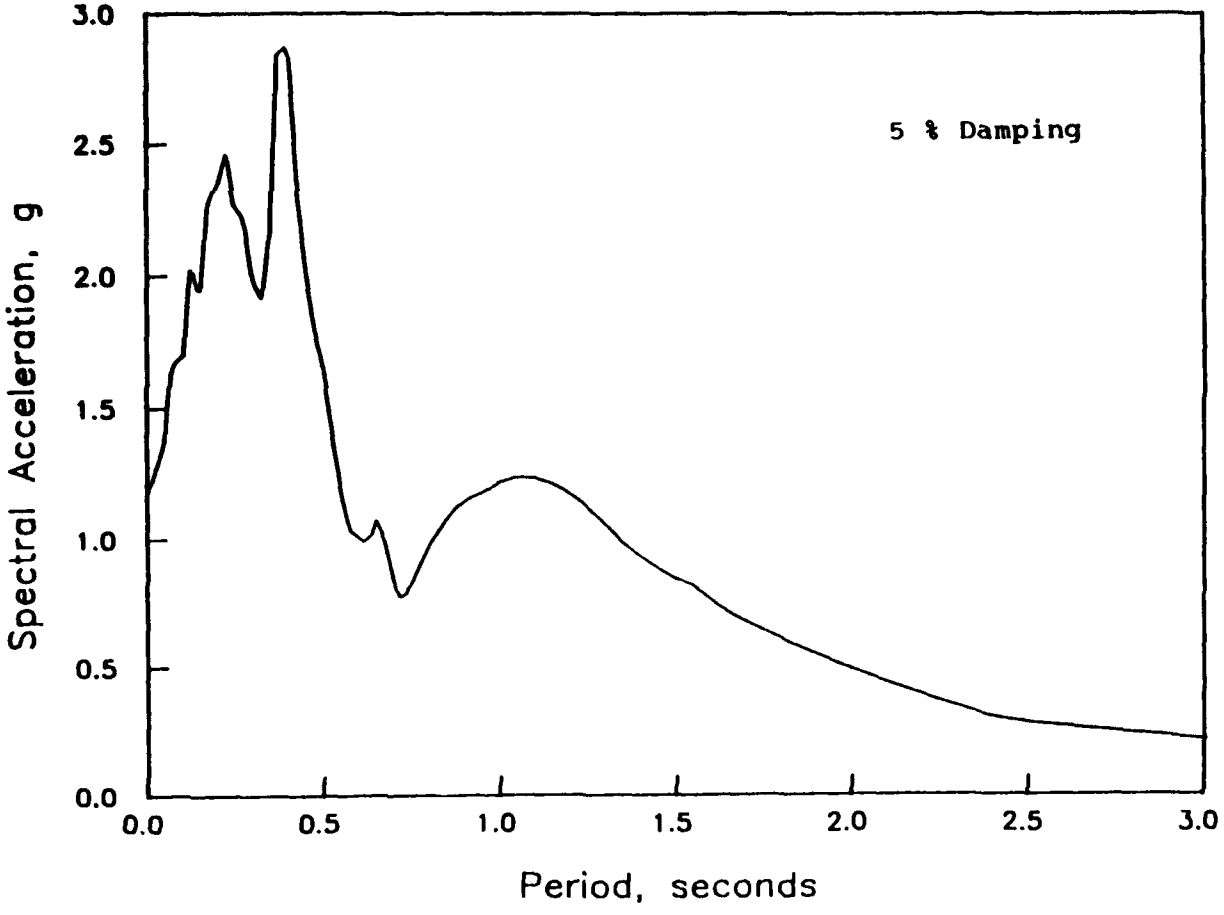

Figure 17. Response period spectra of accelerogram adopted for analysis (Seed 1987)

Table 1

Characteristic Parameters of Maximum Potential Earthquakes at Ririe Dam

Source	Peak Acceleration	Peak Velocity cm/sec	Duration sec	Spectral Acceleration
OBE	0.29 g	25	65	--
MCE	1.22 g	120	33	2.7 g
Seismic Analysis (Seed 1987)	1.17 g	113	33	2.8 g

to the design were devised to mitigate conditions revealed during excavation and construction (e.g., creation of fillet walls).

Recent Geotechnical Investigations

41. Geotechnical engineering investigations in the field and laboratory were selected to provide soil parameters necessary to perform seismic stability evaluations. The different investigations conducted included:

a. Excavation of a 8-ft diam test shaft.

b. Cone Penetration Tests (CPT).

c. Standard Penetration Tests (SPT).

d. Becker Hammer Penetration Tests (BPT).

e. Seismic geophysical measurements.

f. Laboratory triaxial shear testing of gravels.

g. Laboratory cyclic triaxial shear testing of gravels.

Seismic geophysical investigations consisted of: surface vibratory, surface refraction, crosshole, and downhole measurements. The locations of tests and explorations for recent engineering field and seismic geophysical studies are presented in Figures 18 and 19, respectively.

42. The results of geotechnical engineering investigations show that the embankment was well constructed, confirming the conclusions drawn from a review of construction records. In general, the foundation alluvium is dense to very dense as indicated by Becker Hammer resistance although weaker zones were found. The foundation rock consists of hard basalt underlain by softer

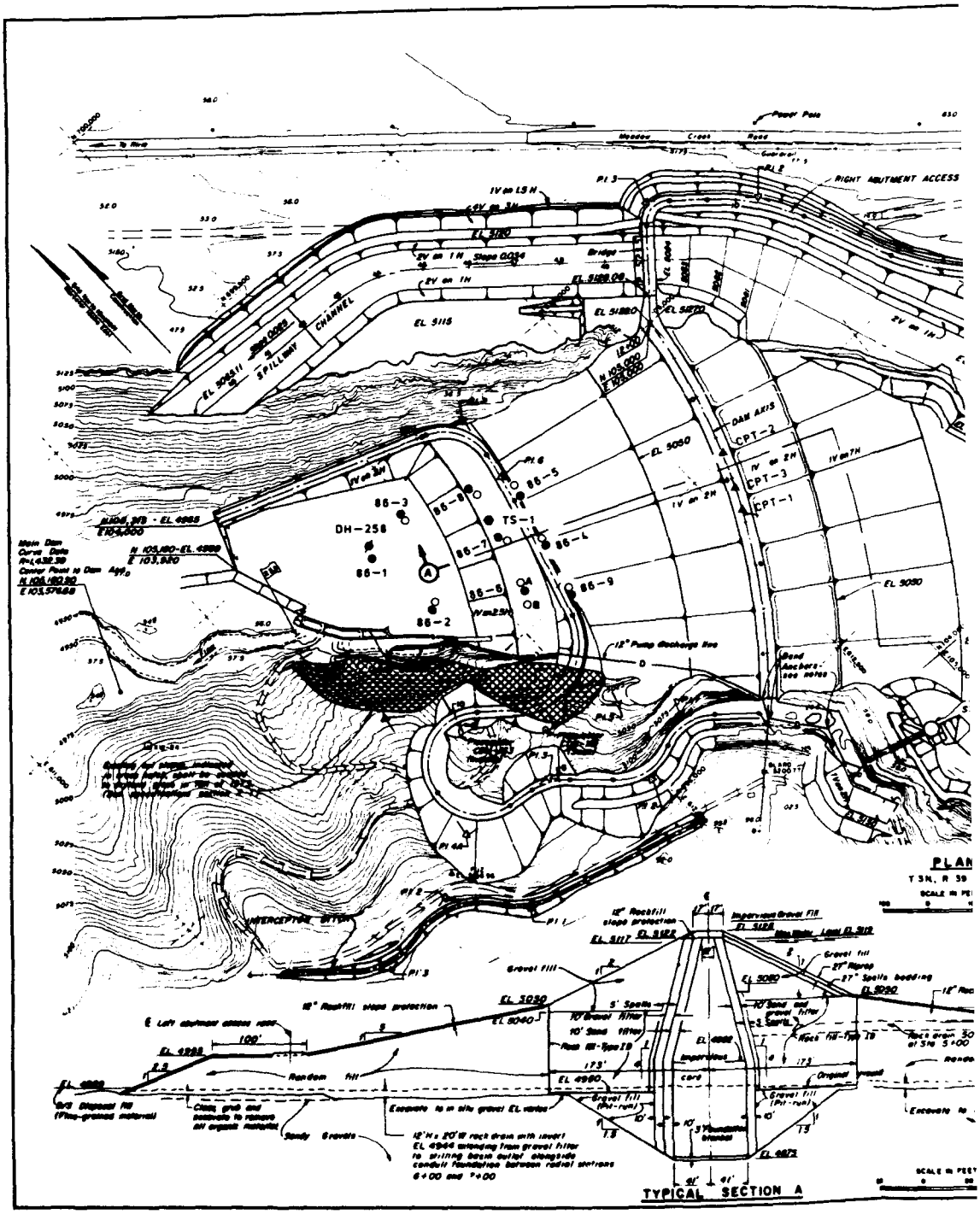

Figure 18. Locations of recent engine

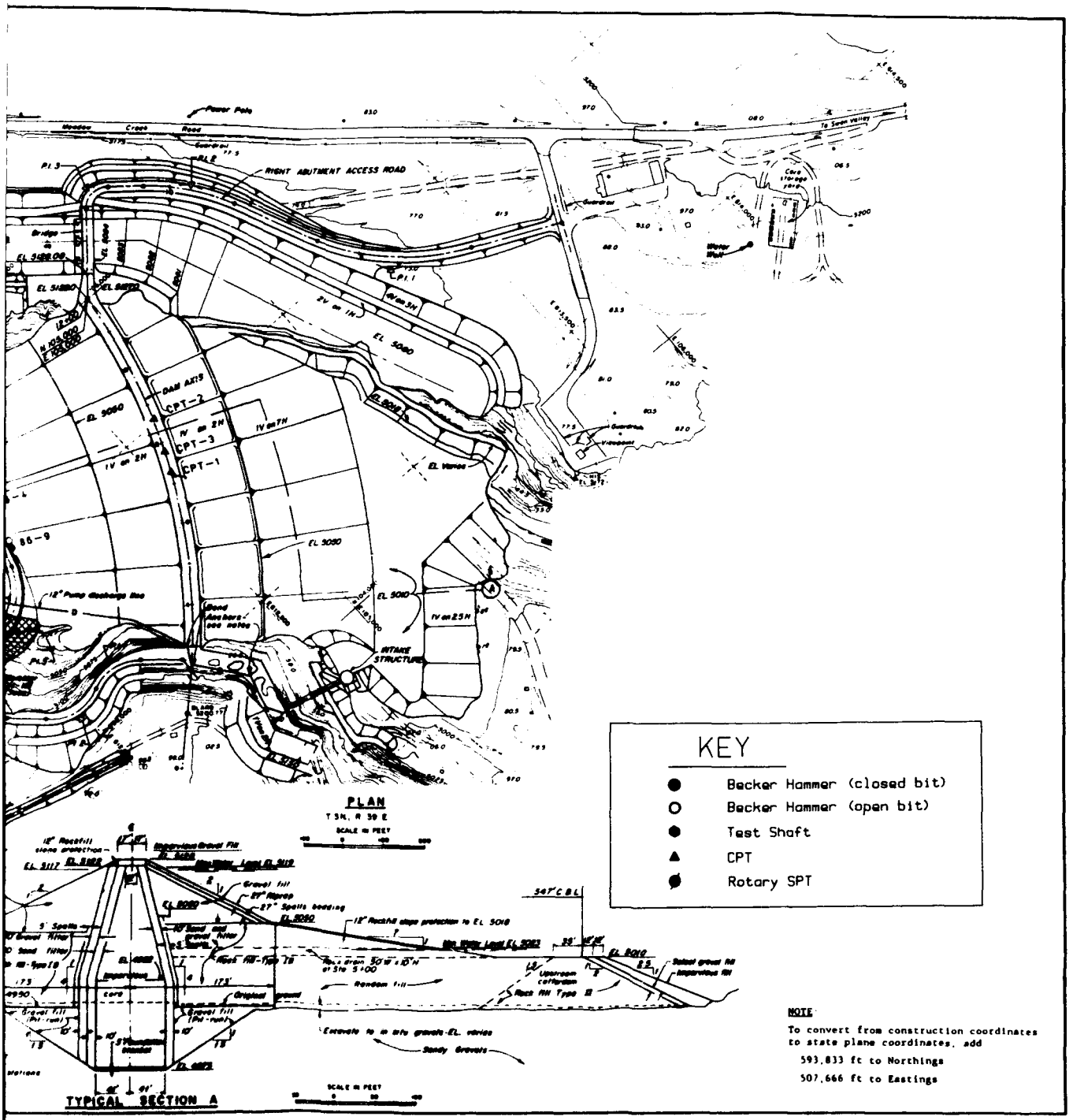

e 18. Locations of recent engineering field studies

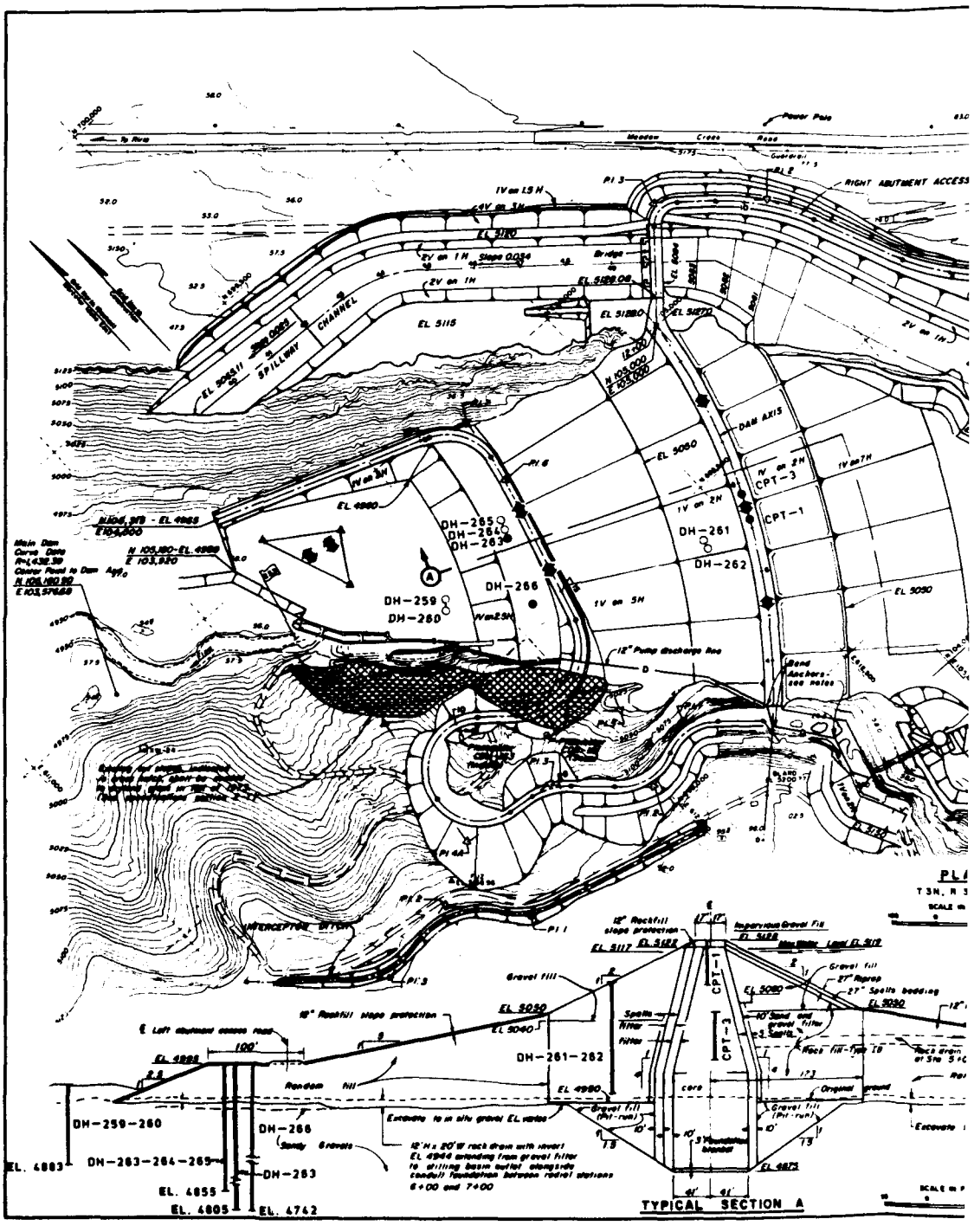

Figure 19. Locations of seismic geop

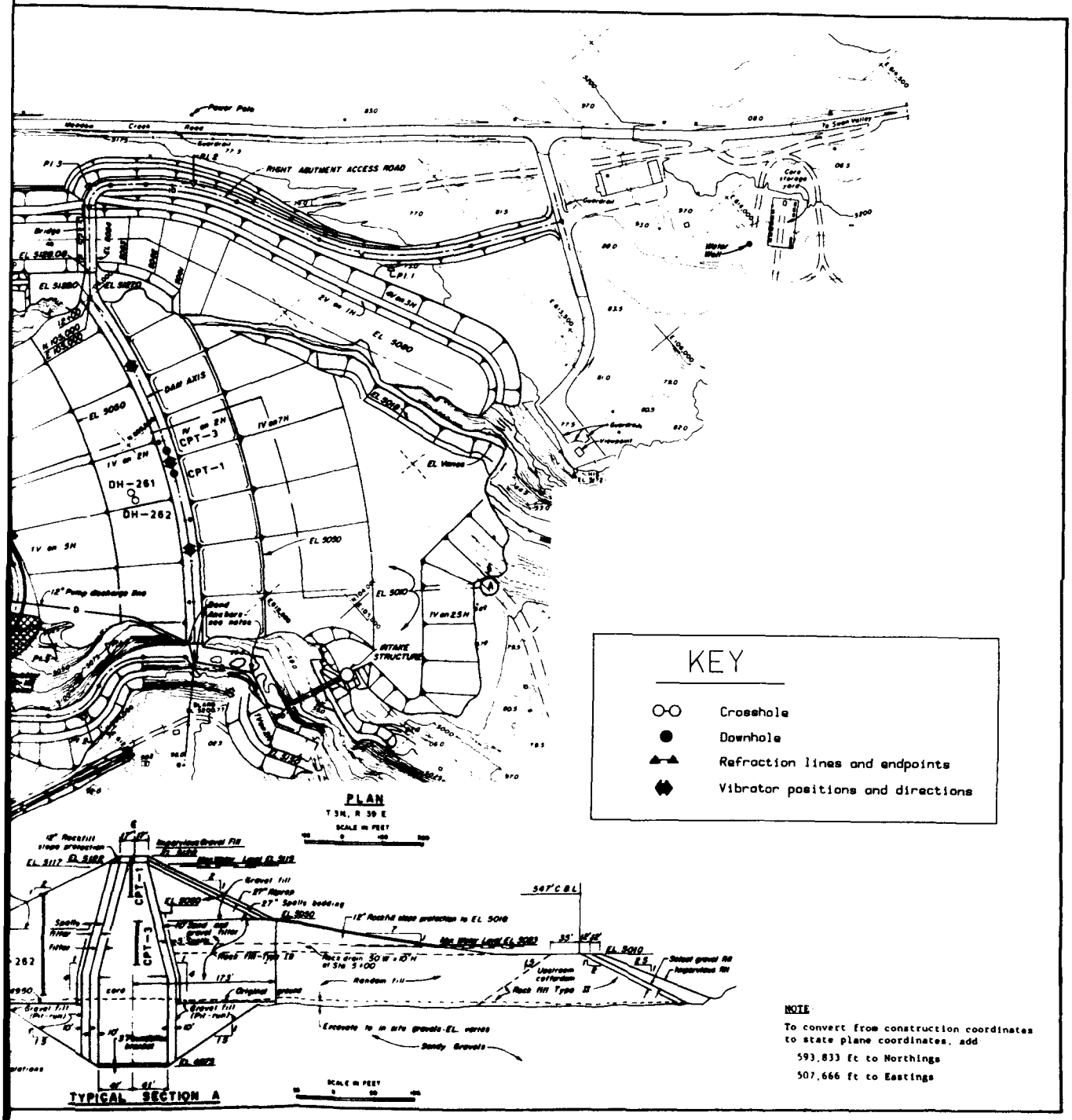

19. Locations of seismic geophysical measurements

tuffaceous sediments. Seismic measurements were used to identify an elevation below which the tuffaceous sediments are more competent and are expected to behave as elastic rock for wave propagation purposes.

Idealizations

43. Idealizations were made to the cross sections used for the seismic stability evaluations. Idealization is the process of generalizing based on: a review of construction records, geologic data (i.e., stratigraphy), and the results of field and laboratory investigations. Some assumptions, interpolations, extrapolations, and simplifications were necessary to analytically or numerically model a complete system within the limitations of the available information. Simplifications were made to the cross section to reduce the computational effort required to solve the problem.

44. The two idealized cross sections used for the seismic stability analysis of Ririe Dam are shown in Figure 20. These two sections were selected to obtain a resulting response that suitably represents the behavior and allow the evaluation of three-dimensional effects. Section AA, the maximum-height section has the lowest frequency. The number of material types in the embankment was reduced from 17 to 4 -- silt core, gravel fill, rock fill, and random fill -- to simplify the numerical modeling process. These four materials comprise about 79 percent of the embankment volume (using data reported in Table 8 of Report 1). This simplification is expected to have little to no effect on the dynamic response and seismic stability analyses. The alluvium was idealized with three zones: loose gravel, medium-dense gravel, and very dense gravel. The location and distribution of the three alluvial zones throughout the valley were selected on the basis of the results of Becker Hammer soundings.

Material Properties

45. The material properties necessary for this study were differentiated into three different categories on the basis of analyses conducted: static stress, dynamic response, and liquefaction potential and stability. Some determinations made during the design and construction of the dam and recently for this study were used to select representative values of unit

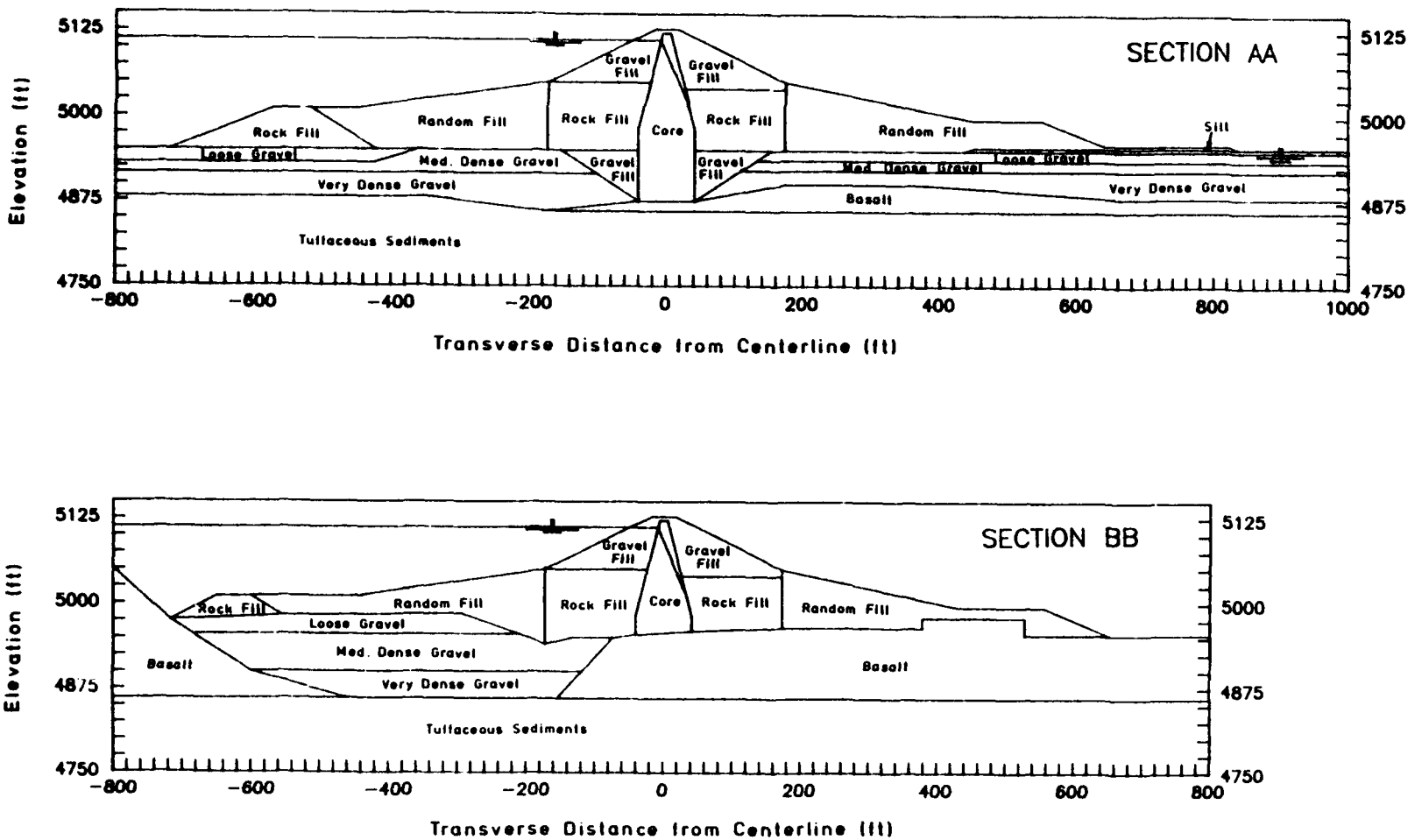

Figure 20. Idealized cross sections for evaluation of seismic stability

weight and static strength parameters. Other parameters such as $(K_2)_{max}$ and τ_{av}/σ_o' , defined and selected as summarized in Report 1, were obtained from the results of recent investigations. The material properties used for each type of analysis are presented in the respective sections.

PART III: PRE-EARTHQUAKE SLOPE STABILITY

Prior Studies

46. The stability of the upstream and downstream slopes of the dam were analyzed during design, and later with as-built parameters, by the sliding wedge method. It was considered that failure would occur in the horizontal plane of the weak clays assumed to completely underlie the gravel alluvium (US Army Engineer District, Walla Walla 1969; 1978). The results of the stability analysis are presented in Table 2. These results are considered to be conservative because a clay foundation was assumed throughout; whereas, the actual zone of alluvium overlying tuffaceous sediments is narrow and very limited in extent (refer to Figure 9). The results of wedge-type slope stability calculations made using these parameters indicated that factors of safety ranged from 1.48 to 2.1 for standard "static" design conditions of: end of construction (upstream and downstream slopes), partial pool (upstream slope), steady-state seepage (downstream slope), and sudden drawdown (upstream slope). The calculations, cross section, and design parameters for each case are shown in Figures 21-24, respectively. The results of pseudo-static analyses conducted to estimate the stability of the dam during an earthquake are also presented in these figures.

Slope Stability Evaluations Performed for This Study

General

47. Conventional slope stability analyses are typically performed assuming two-dimensional limit-equilibrium analyses under assumptions of plane strain (i.e., the failure surface is considered to be infinitely long and transverse geometric or material property variations are not modeled). Ririe Dam is constructed in a relatively narrow canyon, has a curved axis, and its foundation soil deposits are highly variable, all of which led to the decision to consider three-dimensional slope stability analysis methods to realistically model massive translational failure scenarios. Drs. Amr Azzouz and Mohsen Baligh recently developed a three-dimensional slope stability analysis technique at the Massachusetts Institute of Technology (MIT). This technique was used to evaluate the stability of two- and three-dimensional circular and

Table 2

Results of Stability Analysis for As-Built Conditions

(US Army Engineer District, Walla Walla 1978)

Design Condition	Computed Factors of Safety		
		Dynamic	
	Static	0.10 g	0.15 g
End of construction			
- Downstream slope	1.60	1.03	0.87
- Upstream slope	1.71	1.03	0.85
Partial pool			
- Upstream slope	2.07	1.24	1.02
Steady seepage (maximum pool)			
- Downstream slope	1.68	1.09	0.93
Sudden drawdown (maximum pool to minimum pool)			
- Upstream slope	1.48		

noncircular failure surfaces at Ririe Dam. Two reports detailing their stability analyses are provided in Volume II (Azzouz and Baligh 1989a and 1989b). Pertinent features of these reports are adapted and summarized in this section.

Two-dimensional analysis

48. Azzouz and Baligh (1989a) evaluated two-dimensional effective stress slope stability of the idealized cross section depicted in Figure 25 under both gravity loading and gravity-plus-(pseudo-static) earthquake loading conditions. Material properties corresponding to static strengths were used. Their report is provided in Volume II. The curved axis cross section was selected over a straight-lined section to avoid the buttressing effects of the canyon wall upstream of the dam centerline. The use of a curved projection also produced a deeper section roughly following the course of the river. The two-dimensional stability studies provided the framework from which later three-dimensional idealizations were modeled and allowed sensitivity studies on the effects of variations in material properties and other factors. Layer types and material properties corresponding to the labeling used in Figure 25 are given in Table 3. Combined gravity and earthquake loading stability evaluations were also performed for two-dimensional circular and noncircular

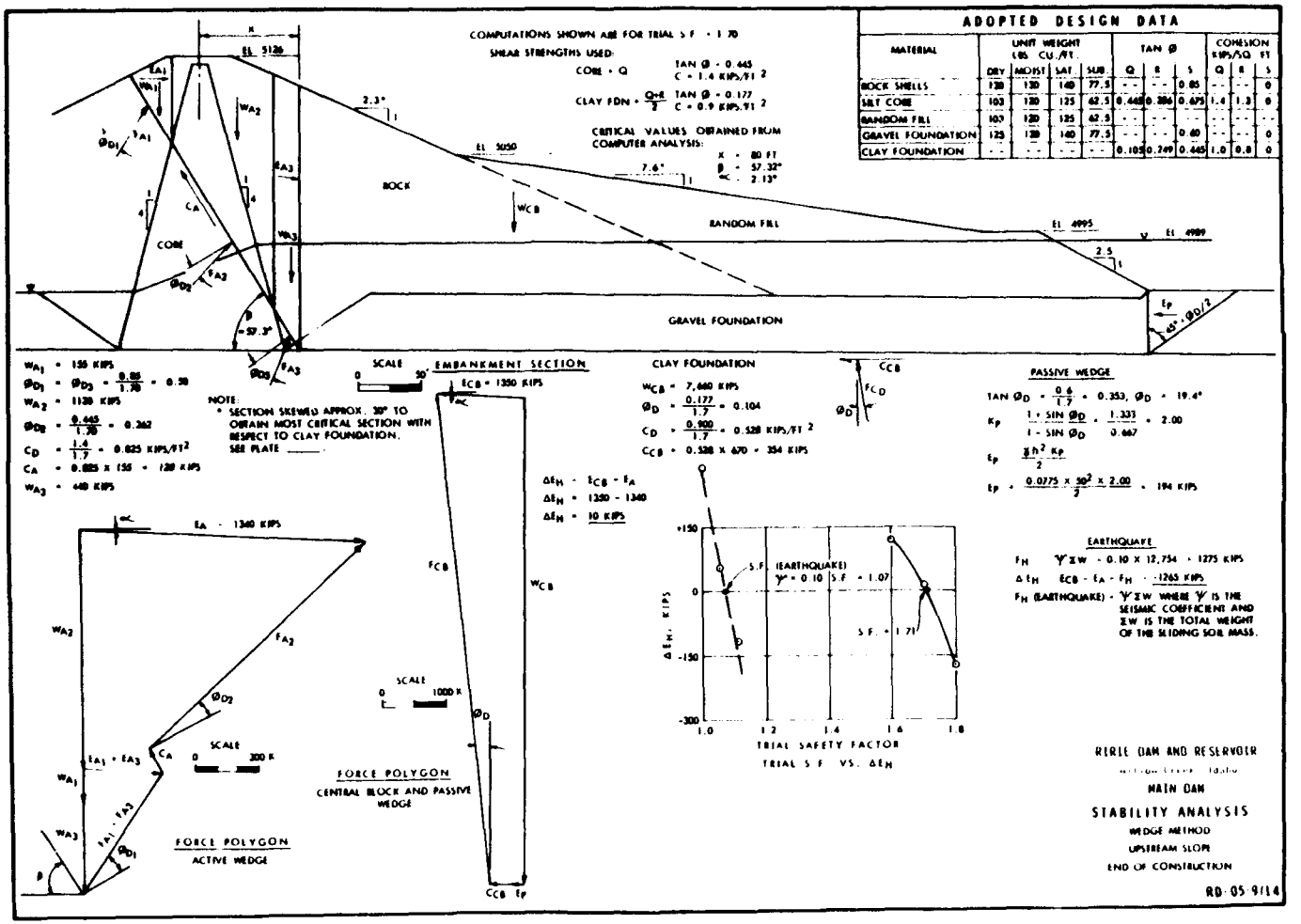

Figure 21. Summary of stability analysis of the upstream slope for the case of end of construction conditions (US Army Engineer District, Walla Walla 1969)

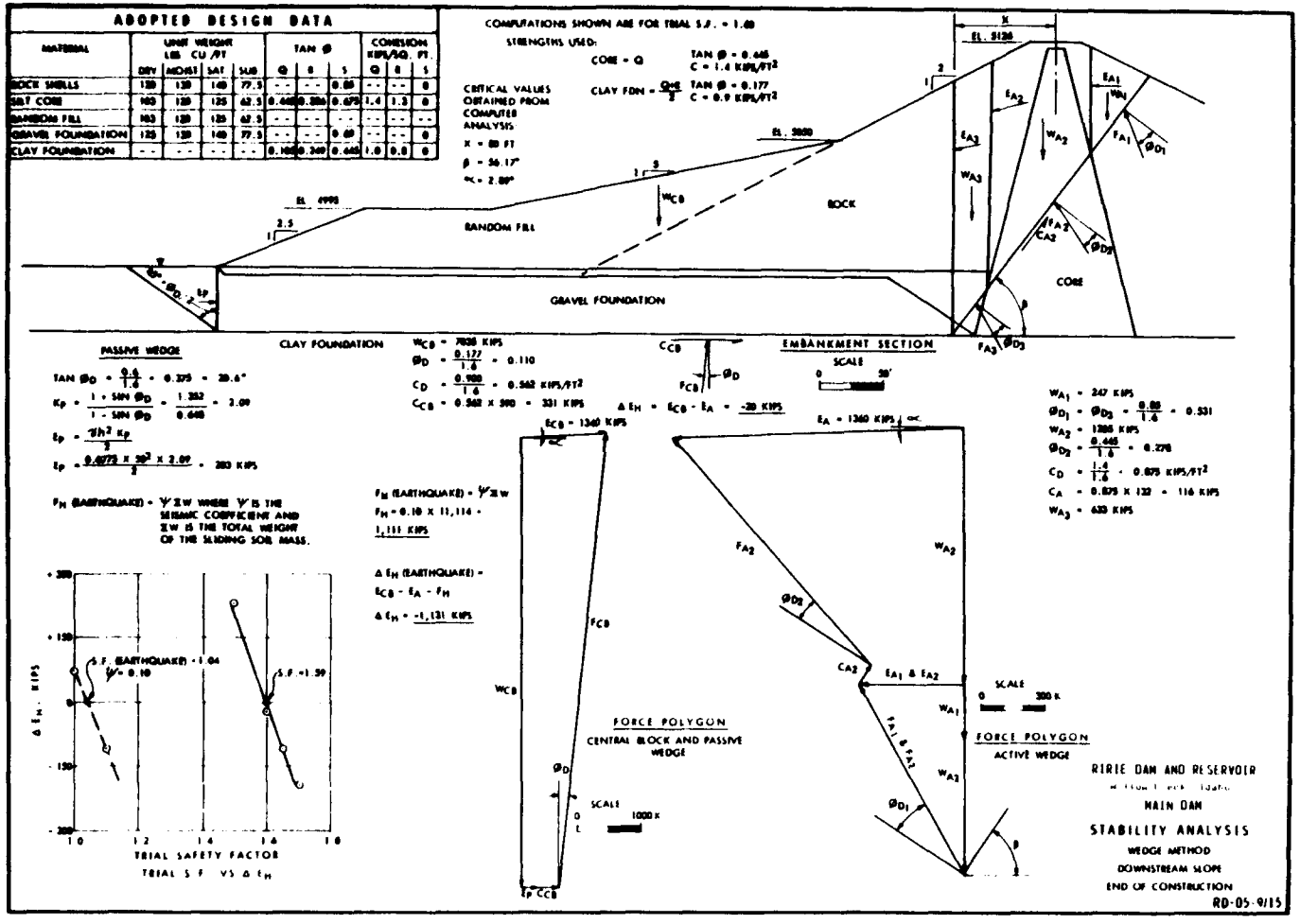

Figure 22. Summary of stability analysis of the downstream slope for the case of end of construction conditions (US Army Engineer District, Walla Walla 1969)

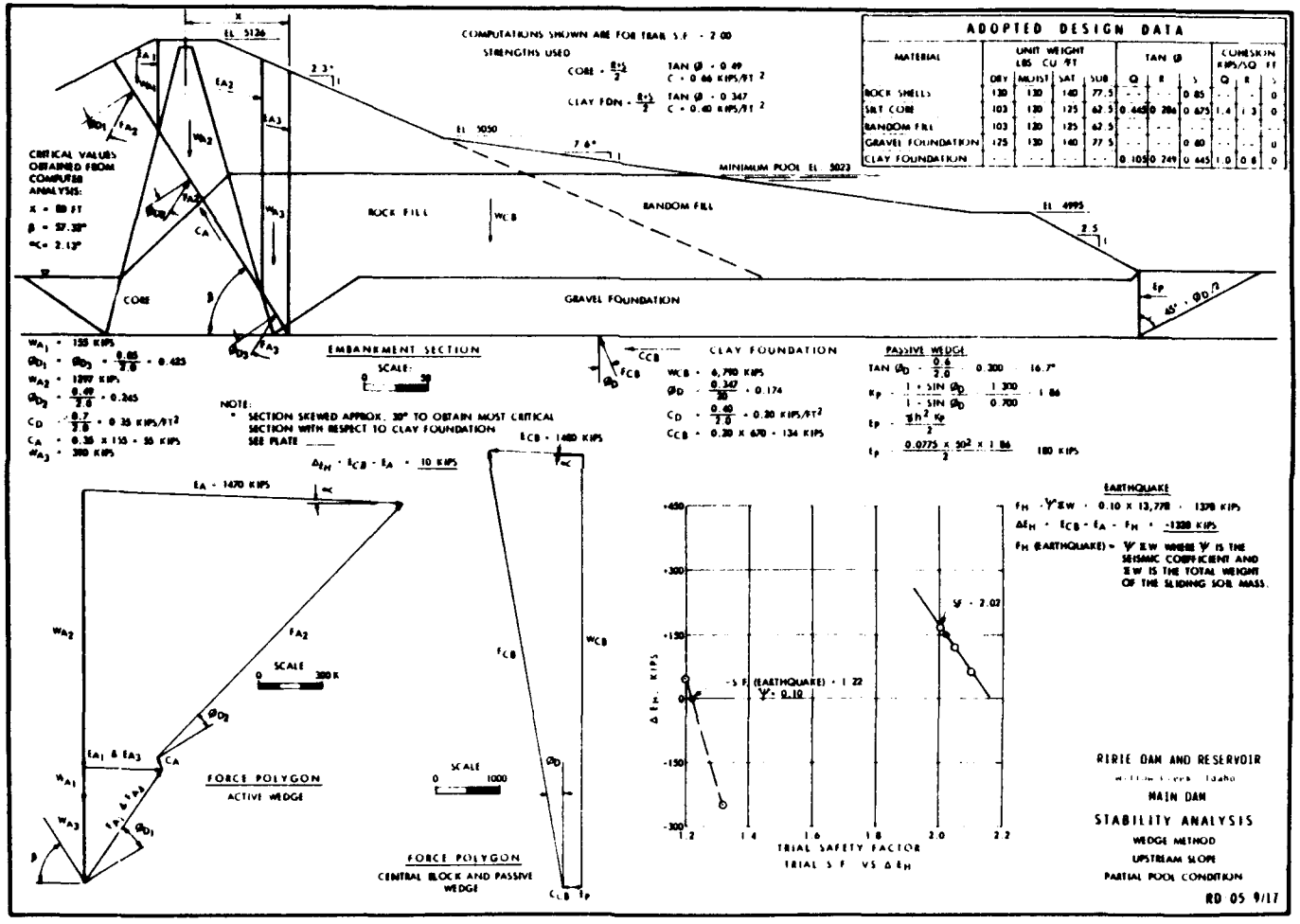

Figure 23. Summary of stability analysis of the upstream slope for the case of partial pool conditions (US Army Engineer District, Walla Walla 1969)

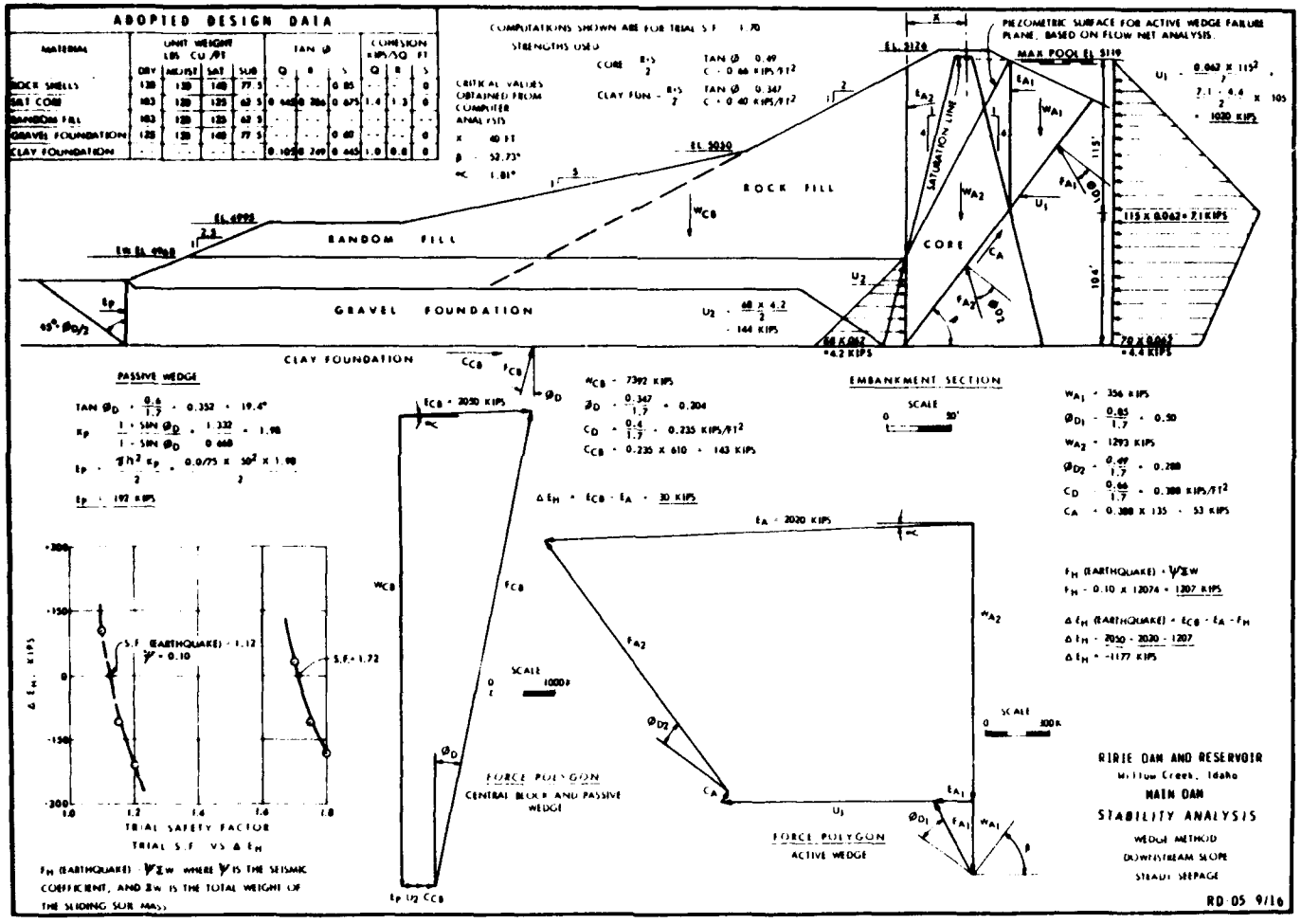

Figure 24. Summary of stability analysis of the downstream slope for the case of steady seepage conditions (US Army Engineer District, Walla Walla 1969)

Table 3

Soil Properties Utilized in Slope Stability Analyses (Azzouz and Baligh 1989a; 1989b)

Layer No.	Material	Saturated Unit Weight pcf	Moist Unit Weight pcf	Effective Friction Angle, ϕ' deg
1	Impervious silt core	125.0	120.0	30-38
2	Gravel fill	145.0	135.0	48
3	Rockfill	145.0	135.0	48
4	Random fill	140.0	130.0	45
5	Weathered basalt/gravel	147.0	147.0	50
6	Basalt	170.0	170.0	50
7	Silt	120.0	112.0	33
8	Tuffaceous sediments	155.0	155.0	45
9	Water	62.4	62.4	0

failure surfaces. The earthquake loading evaluations were intended to compute horizontal yield accelerations for use in permanent displacement analysis, and will be discussed later in this report.

49. Factors of safety were computed for a number of possible circular failure surfaces under gravity loading only using the computer program STAB3D (Azzouz 1977). The STAB3D program allows the user to select any of several accepted slope stability computation schemes, and performs a search to determine the parameters defining the minimum factor of safety for a given geometry and set of engineering properties. The cross section analyzed at Ririe Dam produced minimum factors of safety against gravity-loaded slope failure for shallow failure surfaces. Dr. Azzouz directed the stability computations and elected to report the factors of safety calculated for deeper, more massive and potentially damaging failure surfaces as well, to demonstrate the results of the sensitivity studies. Table 4 lists the cases considered for circular failure surfaces under gravity loading only and

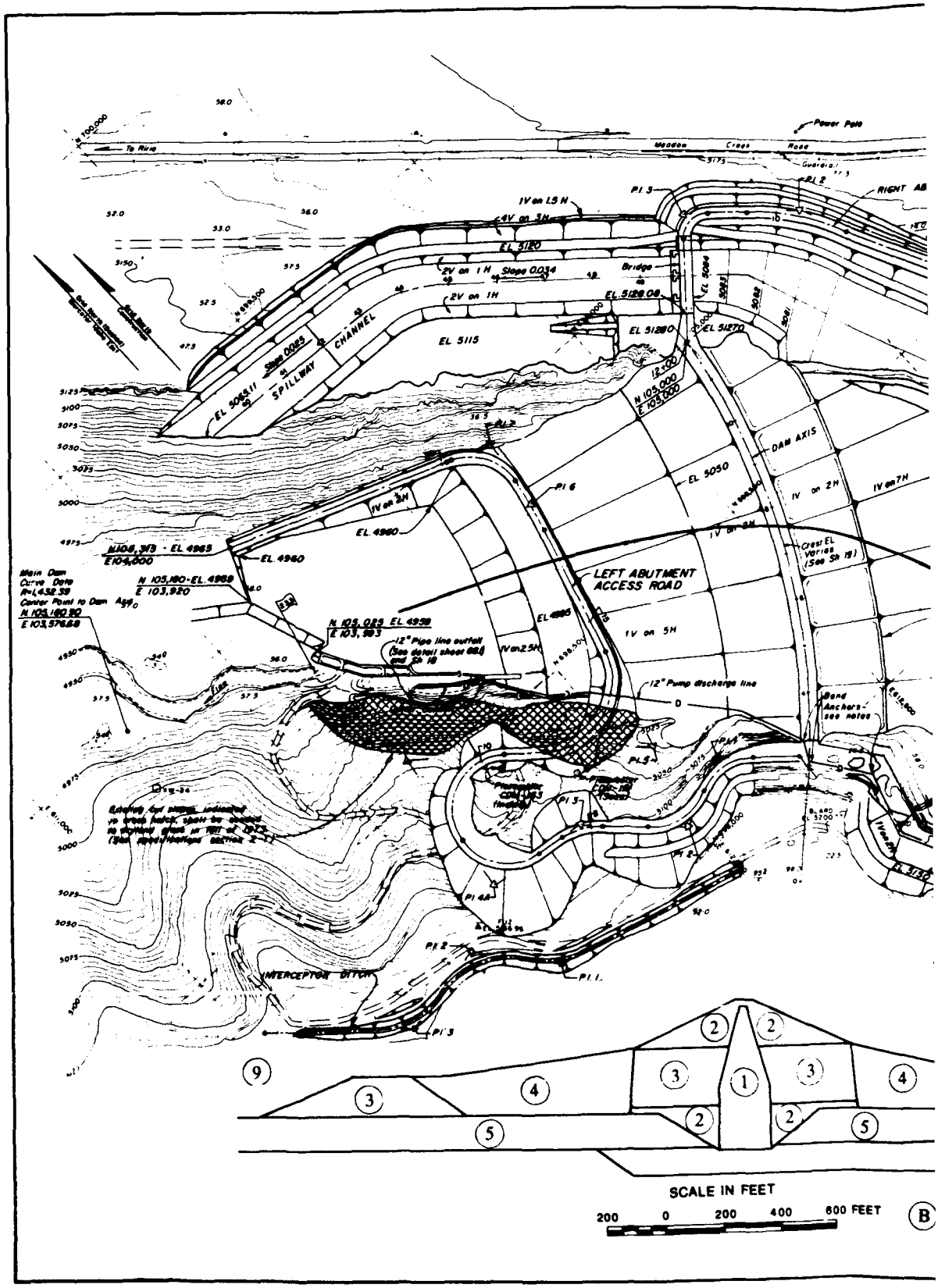

Figure 25. Plan and profile of curved section used for
slope stability analysis (

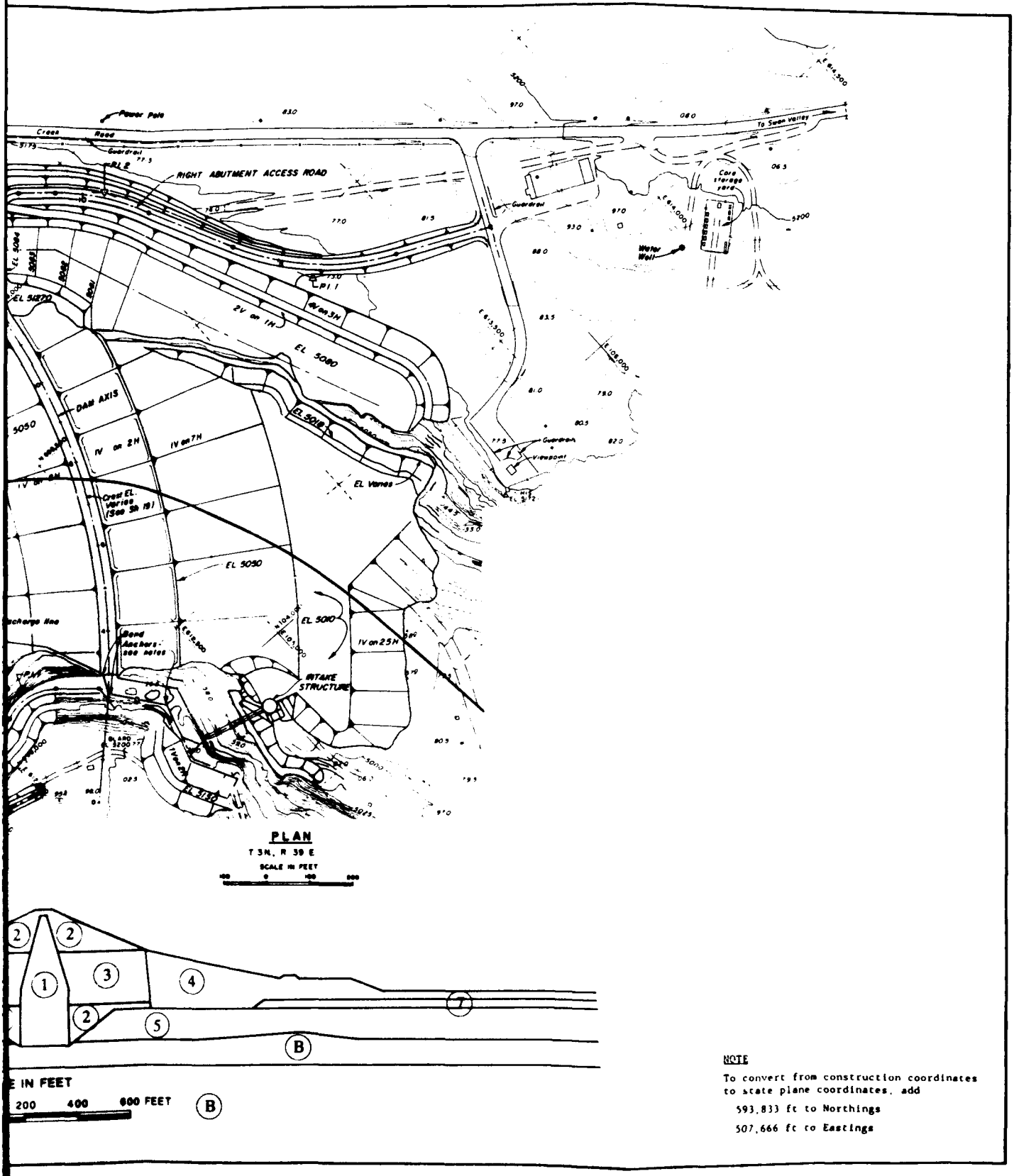

NOTE

To convert from construction coordinates to state plane coordinates, add

593,833 ft to Northings

507,666 ft to Eastings

ed section used for the analysis of two-dimensional and three-dimensional
stability analysis (Azzouz and Baligh 1989a)

Table 4

Results of Two-Dimensional Circular Arc Analysis for Vertical Gravity Loading

(Azzouz and Baligh 1989a)

Case	Method of Analysis	Unit Weight	(ϕ) Core Degrees	Critical Shear Surface OX ft	OY ft	Radius ft	Factor of Safety	Surface Number*
1	Infinite slope	Saturated	30	∞	∞	∞	2.5	
2	Modified Bishop	Saturated	30	2,000	1,300	200	3,168	2
3	Modified Bishop	Saturated	30	2,400	2,100	1,100	3.27	3
4	Modified Bishop	Saturated	30	2,300	1,800	800	3.44	4
5	Modified Bishop	Saturated	34	2,400	2,100	1,100	3.275	3
6	Modified Bishop	Saturated	38	2,400	2,100	1,100	3.281	3
7	MIT	Saturated	30	2,400	2,100	1,100	3.293	3
8	Modified Bishop	Moist	30	2,000	1,300	200	3.168	2
9	Modified Bishop	Moist	30	2,400	2,100	1,100	3.269	3
10	Modified Bishop	Moist	30	2,300	1,800	800	3.438	4

* Refer to Figure 26.

summarizes results obtained from analysis of some 2,000 potential failure surfaces.

50. The lowest factor of safety against sliding, FS_{SL}, determined from two-dimensional, gravity-loading slope stability computations results, as is expected in the case of cohesionless soils, from the so-called "infinite slope" mode of failure in the gravel fill that forms the shells of the central portion of the embankment. The FS_{SL} of a thin zone of gravel along the slope free surface is given by the following expression:

$$FS_{SL} = \frac{\tan \phi'}{\tan i} \tag{2}$$

where

ϕ' = the effective friction angle of the gravel

i = the inclination angle of the slope surface

For this case, ϕ' is about 48 deg and i is about 24 deg. Thus, the FS_{SL} against shallow surficial sliding of the gravel fill at Ririe Dam calculated using these values and Equation 2 is about 2.5.

51. Figure 26 summarizes minimum factors of safety for the downstream slope determined for three circular failure surfaces under gravity loading only. The FS_{SL} ranged from about 3.2 to about 3.4. Upstream failure surfaces were analyzed, but the computations are not specifically reported.

52. The FS_{SL} against slope failure along several prescribed noncircular slip surfaces were calculated using the computer program TSLOPE (TAGA Engineering Software Services 1984) with Spencer's method (Spencer 1967). Cross section geometry and material properties used were identical to those used for circular slip surfaces. The TSLOPE program does not search for the noncircular slip surface that produces the minimum FS_{SL}, rather, the user must prescribe the shape and location of the slip surface. The FS_{SL} were computed under gravity loading for 19 slip surfaces (26 cases in all with parameter variations for sensitivity studies). Figure 27 depicts the non-circular slip surfaces for which pertinent data and results are given in Table 5. The lowest FS_{SL}, 2.4, was computed for a downstream noncircular slip surface that mobilized the shearing resistance of the alluvial silt found beneath the downstream berm.

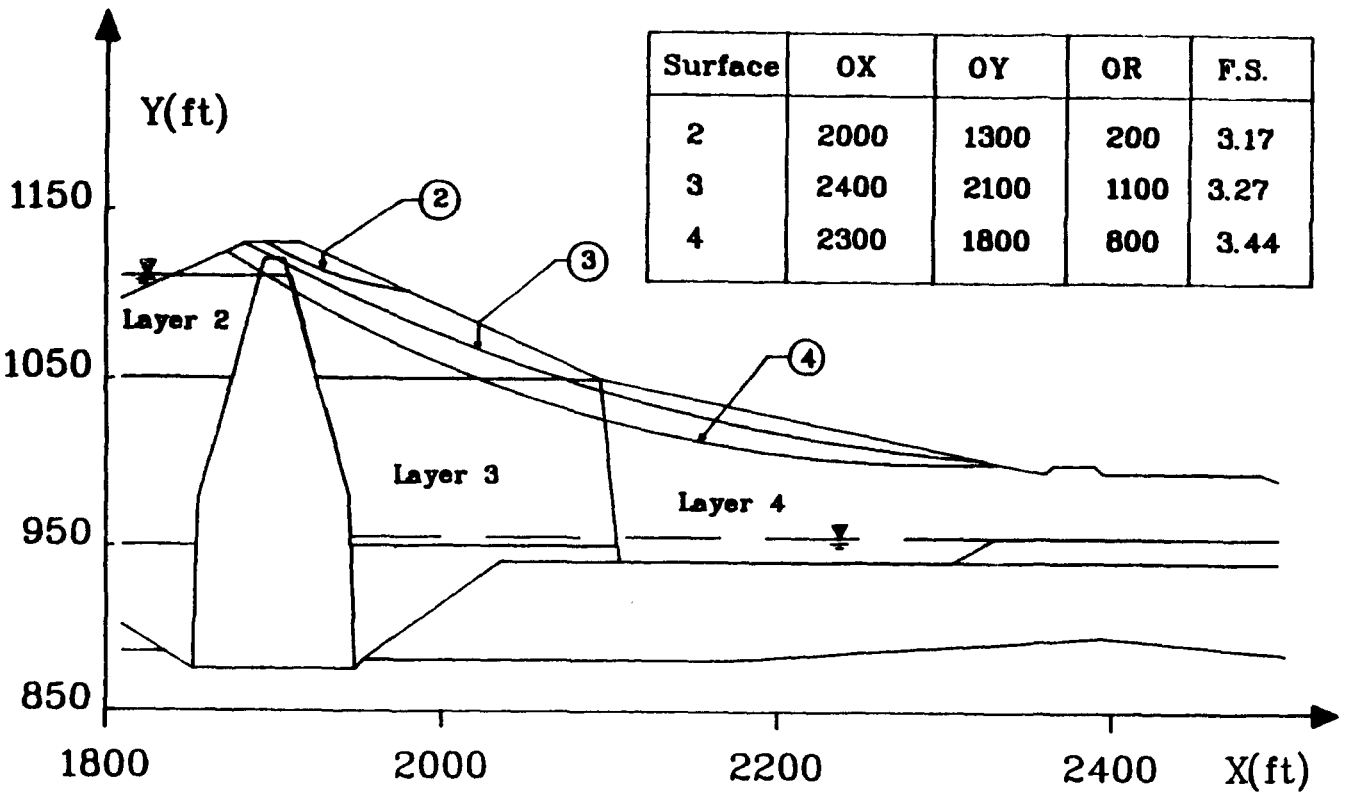

Figure 26. Results of two-dimensional circular arc analysis for gravity loading (Azzouz and Baligh 1989a)

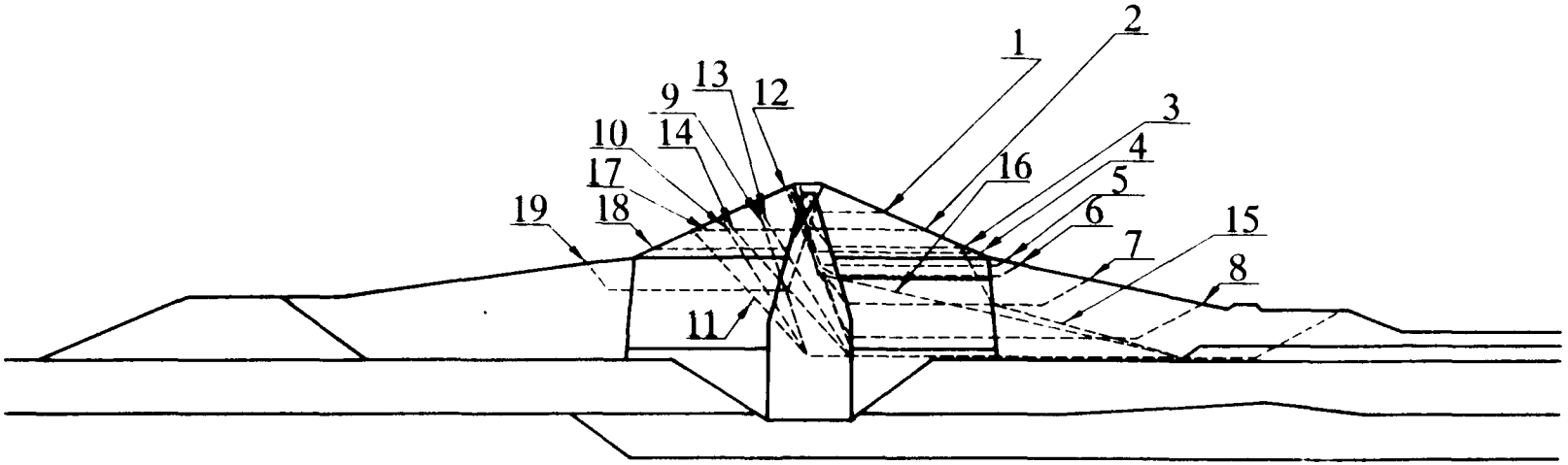

Figure 27. Failure surfaces for two-dimensional and three-dimensional slip surfaces (Azzouz and Baligh 1989a)

Table 5

Results of Two-Dimensional Noncircular Arc Stability Analyses for Gravity Loading (Azzouz and Baligh 1989a)

Case	Shear Surface No.*	FS_{SL}	Comments
1	1	5.426	Saturated unit weights
2	2	5.343	"
3	3	5.063	"
4	4	5.744	"
5	5	4.916	"
6	6	5.28	"
7	7	5.545	"
8	8	8.00	"
9	9	6.785	"
10	10	6.326	"
11	11	5.662	"
12	12	6.553	"
13	13	5.473	"
14	14	5.273	"
15	15	3.806	"
16	16**	2.378	"
17	17	3.848	"
18	18	3.679	"
19	19	5.026	"
20	5	4.835	Moist unit weights
21	15	3.796	"
22	16**	2.373	"
23	5	4.771	Moist unit weights above phreatic surface and saturated below it
24	15	3.533	
25	16**	2.371	
26	16	2.519	Saturated unit weights and assuming the silt layer (layer 7) not to exist

* Refer to Figure 27.
** Critical shear surface.

Three-dimensional analyses

53. Azzouz and Baligh (1989b) performed three-dimensional effective stress gravity loading slope stability analyses on three circular slip surfaces through Ririe Dam using the computer program STAB3D. The three surfaces had maximum circular arcs that were identical to those determined to have the lowest FS_{SL} in two dimensions as described above (Figure 26). Input data were based on the cross section and material properties used in the two-dimensional studies. Details of the analyses are provided in Volume II.

54. Analyses results indicate that a maximum increase in FS_{SL} of about 5 percent could be realized over the two-dimensional factor of safety computed for similar surfaces. Azzouz and Baligh (1989b) report the following relationship to approximately govern the ratio of three-dimensional FS_{SL} to two-dimensional FS_{SL}, $(FS_{SL})_{3D}/(FS_{SL})_{2D}$ (denoted by F/F° in Appendix B), from earlier work:

$$(FS_{SL})_{3D}/(FS_{SL})_{2D} = 1 + 0.7(DR/2L) \qquad (3)$$

where

DR = depth of the shear surface

L = crest length of the dam

The increase produced by the geometry of Ririe Dam is generally small, since the critical surfaces at are generally shallow in relation to the crest length. The crest length of Ririe Dam is 840 ft. For a range in DR of 20 to 100 ft, the corresponding $(FS_{SL})_{3D}/(FS_{SL})_{2D}$ ratios range from 1.01 to 1.04, respectively.

55. It was originally proposed to modify the existing STAB3D computer program to model horizontal earthquake loading effects on three-dimensional circular slip surface stability. The very slight effect of canyon geometry on slope stability observed for gravity loading cases led to the conclusion that the intensive reprogramming effort would be of little use to the seismic stability evaluation. This modification was consequently not undertaken.

PART IV: STATIC STRESS ANALYSIS

Background

56. Most physical systems are continuous, that is, an infinite number of degrees of freedom are requisite to describe the displacements. A dam-foundation-water system such as Ririe Dam, for example, is a continuous system. Means of modeling an infinite system with a discrete number of degrees of freedom are necessary to analyze complex systems for which exact analytical (closed-form) solutions are not available. The Finite Element Method (FEM) is a popular tool to create representative numerical models for engineering analysis, particularly for earthquake engineering applications. Programs used to perform both the static stress and dynamic response calculations for the seismic stability evaluation of Ririe Dam incorporate the FEM. Numerous references exist that describe the FEM; three of these are: Zienkiewicz (1977), Bathe (1982), and Hughes (1987).

57. An extensive effort was made to define idealized two-dimensional cross sections and corresponding material properties for static stress and dynamic response calculations as documented in Report 1. The reliability of results from these calculations are dependent on the ability to adequately define these input values. The accuracy of a FEM analysis is dependent on the number of elements representing the cross section (i.e., degree of discretization). In general, as the element sizes decrease, the accuracy increases. Improved accuracy is oftentimes offset by increased time and expense. The degree of discretization used for the cross sections for Ririe Dam is considered to be suitable for the degree of accuracy necessary for this type of analysis.

Static Finite Element Analysis

General

58. The seismic stability evaluation procedure selected for the Ririe Dam project required the determination of preearthquake vertical effective stresses and the initial static shear stresses on horizontal planes, τ_{xy}, throughout the dam and its foundation. The static stress analysis was used to determine the ratio of initial horizontal shear stress to initial effective

vertical stress, α , throughout the dam and foundation. The parameter α is important for seismic stability evaluation because it is used to select the appropriate cyclic strength. A more detailed discussion of the determination and importance of α is given in Report 1.

59. The computer program FEADAM84, developed by Duncan et al. (1984), was used to calculate initial effective stresses within the Ririe Dam embankment and its foundation. The FEADAM84 program is a two-dimensional, plane strain, finite element method to determine static stresses, strains, and displacements in earth and rock-fill dams and their foundations. The hyperbolic constitutive model developed by Duncan et al. (1980) is used to estimate the nonlinear, stress history dependent, stress-strain behavior of soils. Nine hyperbolic soil parameters, which simulates soil response during layered embankment construction, are required by this model. A technical report describing the static finite element analysis of Ririe Dam by Woodward-Clyde Consultants (1988) is provided in Volume II of this report. The analysis will be summarized in the following paragraphs.

Section idealization and
static finite element inputs

60. The maximum section and one or more smaller sections are typically selected to model the dynamic response of large earth dams. As was the case for the slope stability analyses described in Part III, a section through the midpoint of the Ririe Dam crest appears buttressed upstream by the curved canyon wall. A staggered section, depicted in plan and profile in Figure 4 as section AA, was chosen for static and dynamic analysis as corresponding to the predominant mode of vibration of the dam if subjected to earthquake shaking. The predominant mode of vibration will produce the greatest displacements and stresses which are of importance for this study. The simplified section AA used in the analysis is shown in Figure 28. Section BB, previously shown in plan in Figure 4, is profiled in Figure 29 and corresponds to an approximate quarter section near the left abutment at sta 5+00.

61. The cross sections used for the static stress analysis, shown in Figures 28 and 29, differ somewhat from the idealized sections shown in Figure 20. Minor differences exist in the geometry of rock foundation units to accommodate discretizing with elements. The major difference between cross sections in Figures 28 and 29 and in Figure 20 is the idealization made for gravel alluvium. The idealized sections incorporate a stratigraphy derived

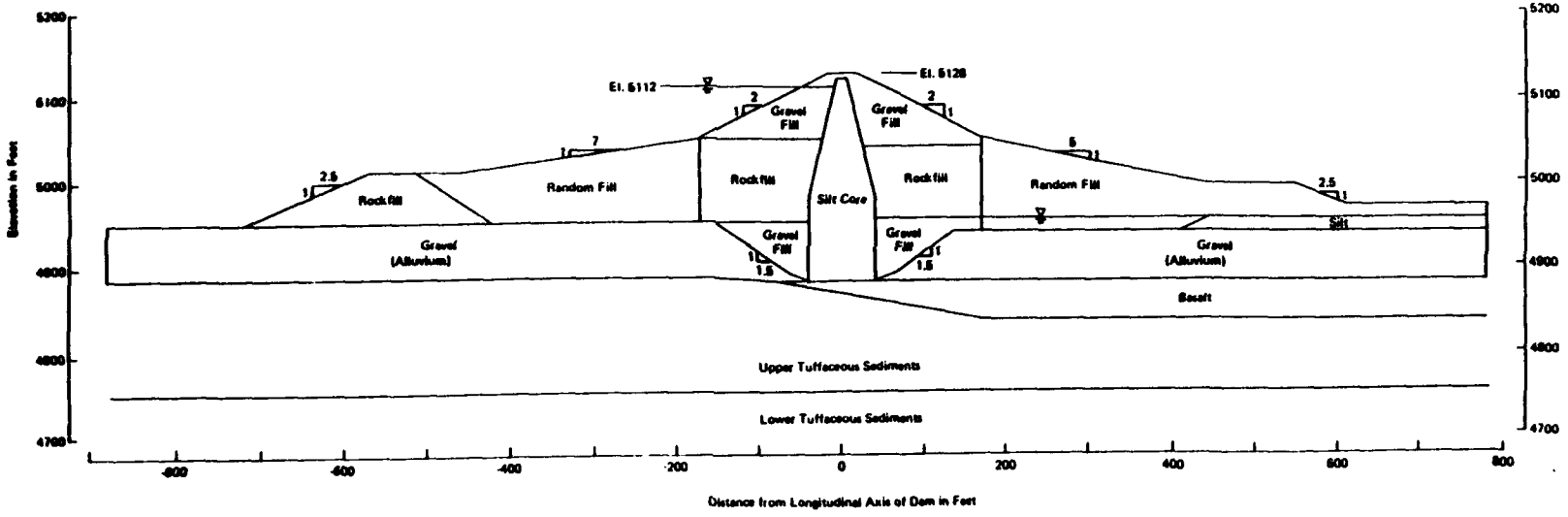

Figure 28. Section AA used for the analysis of seismic stability

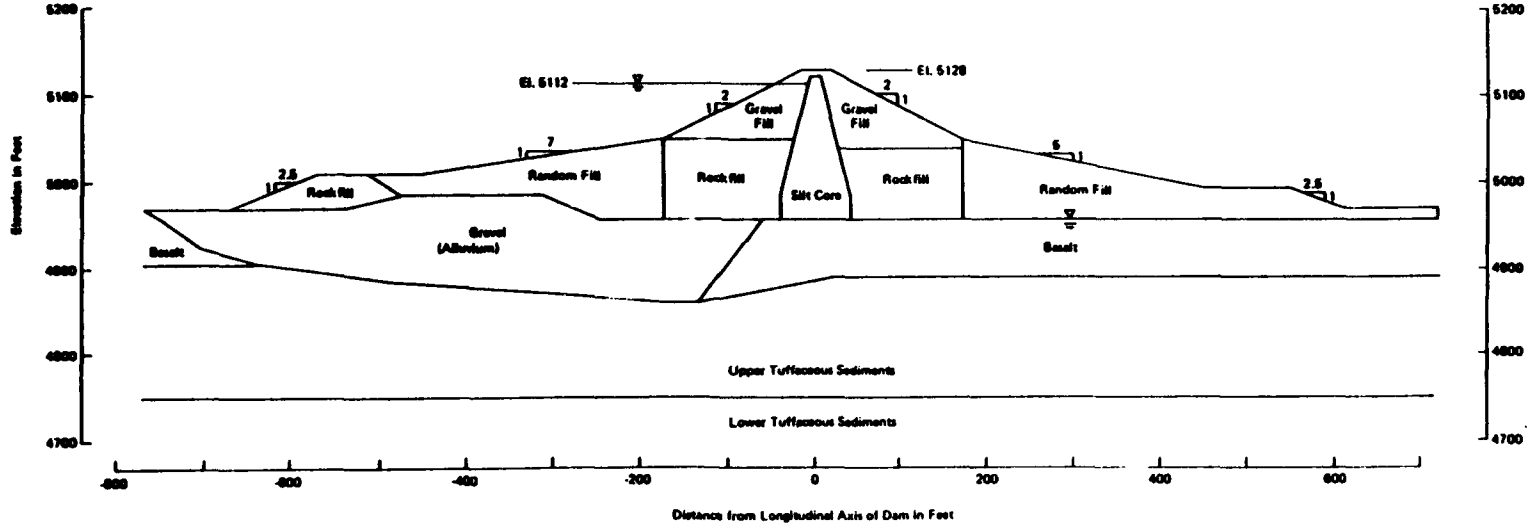

Figure 29. Section BB used for the analysis of seismic stability

from the results of Becker Hammer soundings. The sections used for static stress and dynamic response analyses, however, do not include this stratigraphy because material properties for the latter were selected on the basis of profiles of shear wave velocity.

62. Table 6 lists the engineering properties and hyperbolic constitutive model parameter values of the soils represented in each section as input to FEADAM84. The material properties used in the static stress and stability analyses included unit weights determined by measurements made during construction and more recently in the large diameter test shaft excavated through the downstream berm. Hyperbolic soil model parameters were derived using methods proposed by Duncan et al. (1980). Fundamental characteristics of the soil model are shown in Figure 30. Buoyant unit weights were assumed for materials below the phreatic surface. Static strength values (cohesion and internal friction) for the hyperbolic model represent drained strengths, although strengths for undrained conditions should be about the same for the granular materials. The strengths (internal friction) assigned to rock fill, gravel fill, and dense gravel tend to be quite a bit larger than those used in the design stability analysis calculations. The new values are justified by the types of material they represent and the results of in situ tests. Undrained strength parameters for the silt core and tuffaceous sediments were obtained using the results of undrained triaxial tests performed as part of the design studies. The derivation and selection of material properties is described in Report 1.

63. The finite element meshes developed to model sections AA and BB for static effective stress analysis are shown in Figure 31. The mesh for section AA contains 651 nodes and 624 elements; the mesh for section BB contains of 446 nodes and 414 elements. The discretized portions represent compressible materials (i.e., embankment and alluvium). The meshes used for static analysis of both sections were also used for dynamic finite element analysis, with the exception that more foundation elements were added to model dynamic response of the foundation rock materials. The mesh elements were designed to accommodate the input requirements of both static and dynamic finite element analyses. Element heights conform to the criteria established by Lysmer et al. (1975) for dynamic response analysis discussed in Part V.

Table 6

Static Strength Properties Used for Analysis

Material Location	Unit Weight Saturated/ Buoyant Unit Weight pcf	Unit Weight Moist Unit Weight pcf	Hyperbolic Soil Model Parameters: Young's Modulus Loading/ Unloading ksf	Young's Modulus Exponent, n	Failure Ratio, R_f	Bulk Modulus ksf	Bulk Modulus Exponent, m	Effective Cohesion Intercept, c ksf	Effective Friction Angle, ϕ' deg	Change in ϕ' Per Log Cycle Change in Confining Stress deg	Static Stress Ratio K_o	Static Strength: $\bar{R}$ test c ksf	$\bar{R}$ test ϕ deg	$\bar{S}$ test c' ksf	$\bar{S}$ test ϕ' deg
Impervious silt core	125/63	120	780	0.48	0.8	520	0.3	0	35	5	0.45	1.3	16	0	34
Gravel fill	145/83	135	1400	0.45	0.7	500	0.3	0	48	6	0.4	--	--	--	--
Rock fill	145/83	135	1000	0.45	0.7	500	0.3	0	48	6	0.4	--	--	--	--
Random fill	140/78	130	700	0.45	0.7	255	0.3	0	45	6	0.4	--	--	--	--
Alluvium															
i.) Silt	120/58	112	425	0.5	0.7	205	0.3	0	33	6	0.45	--	--	--	--
ii.) Loose gravel	135/73	135	500	0.5	0.8	255	0.3	0	43	6	0.4	--	--	--	--
iii.) Medium dense gravel	144/82	144	1400	0.5	0.7	1300	0.3	0	48	6	0.4	--	--	--	--
iv.) Dense gravel/ Weathered Basalt	147/85	147	1600	0.5	0.7	1300	0.3	0	50	6	0.4	--	--	--	--
Basalt	180/118	180	2000	0.4	0.7	1400	0.3	0	50	N/A	0.35	--	--	--	--
Upper tuffaceous sediments	140/78	140	1000	0.49	0.9	520	0.3	0	45	N/A	0.45	2.75	26	0.50	34
Lower tuffaceous sediments	140/78	140	1000	0.49	0.9	520	0.3	0	45	N/A	0.45	--	--	--	--

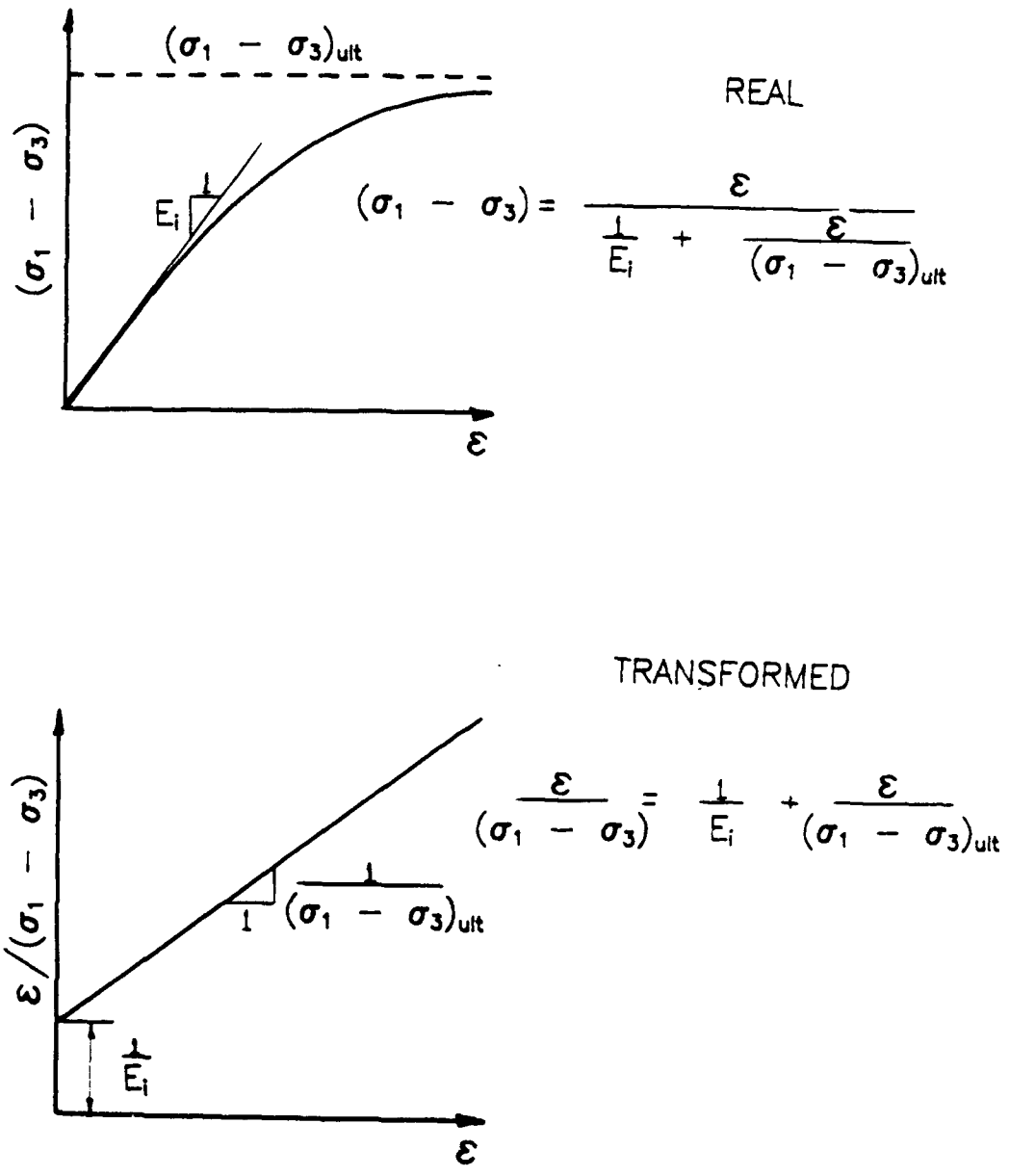

Figure 30. Fundamental characteristics of the hyperbolic soil model proposed by Duncan et al. (1980)

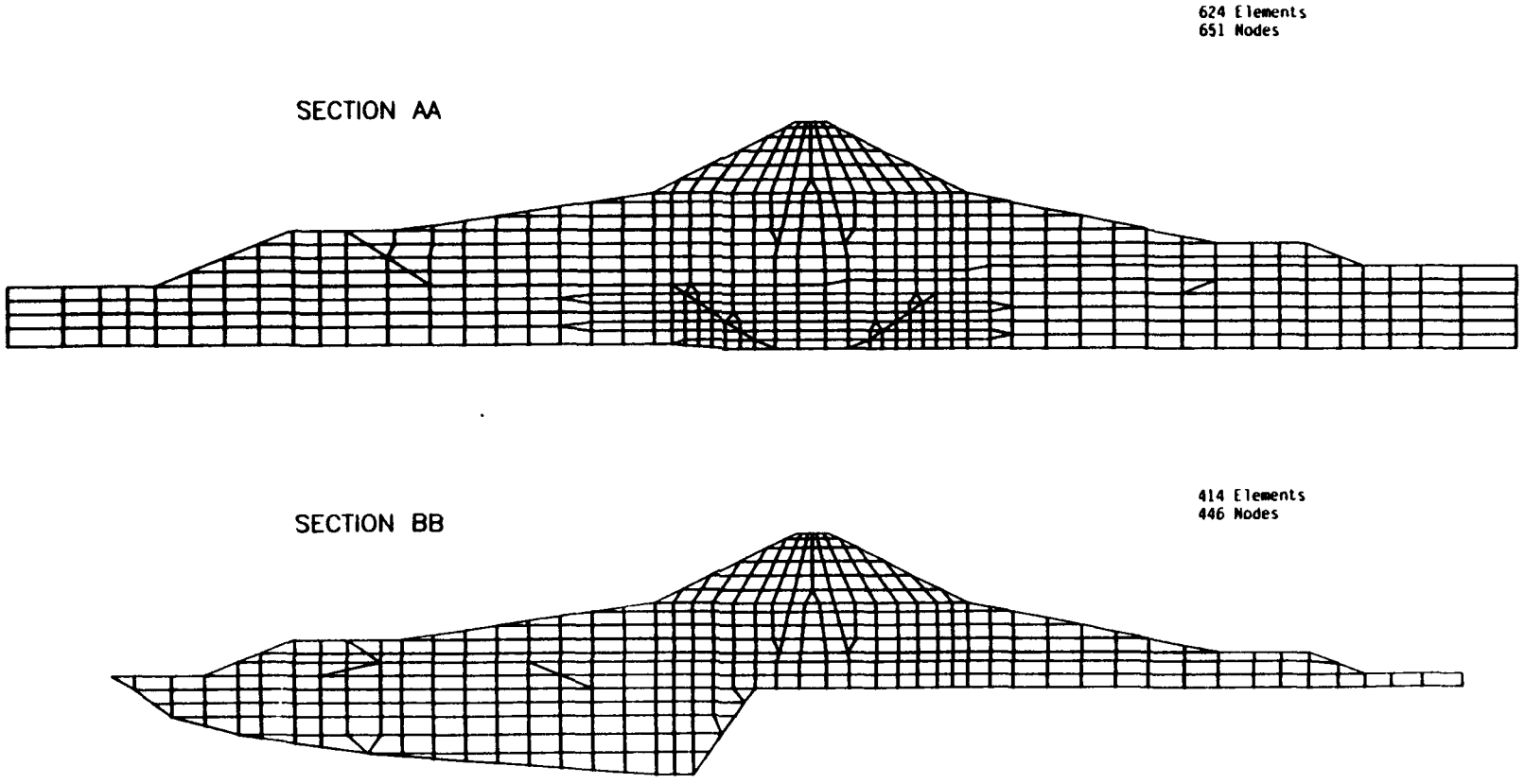

Figure 31. Finite element meshes for sections AA and BB used in the static stress analysis

64. Details of the methodology followed to simulate a logical sequence of construction of the dam are contained in Volume II of this report. Briefly, four main steps were used:

a. Stresses within the alluvial foundation were created by "building up" the foundation on both sides of the ore trench in seven "lifts", as if the trench were preexisting.

b. The construction of the upstream cofferdam was simulated in four lifts.

c. The filling of the core trench and placement of embankment materials were simulated above the foundation materials in 20 increments.

d. Seepage forces due to the reservoir impoundment were applied to the core.

65. Hydraulic head values within the core due to steady state seepage were computed using the finite element computer program SEEP (Wong and Duncan 1985). Seepage forces applied to the nodal points within the core portion of the static meshes for both sections in the final loading step were subsequently computed using another computer program, SFORCE (Chang 1975). A detailed discussion of the process used to assess seepage forces is given in Volume II. All head loss was assumed to occur within the silt core because the shell materials are considered to be highly pervious.

Results of static analysis

66. Static finite element analysis results obtained for the idealized sections are depicted by contour values in Figures 32 through 35. These contour plots were developed using a different contouring program than was used by Woodward-Clyde Consultants (1988) to develop the contour plots shown in Volume II. The contours in Figures 32 through 35 are somewhat smoother, but the values of the stresses represented are not significantly different. Figures 32 and 33 present the values of vertical and horizontal effective stress, in ksf, calculated with FEADAM84 throughout sections AA and BB. Figure 34 gives values of initial horizontal shear stress in both sections, and Figure 35 gives values of α defined earlier. A complete listing of long-term static stress analysis results obtained for every element of both meshes is provided in Volume II of this report.

67. Vertical effective stress values, σ_v' , shown in Figure 32 range up to 25.8 and 19.2 ksf, respectively, for section AA and BB. Values of σ_v' are lower throughout submerged portions of both sections, as are expected

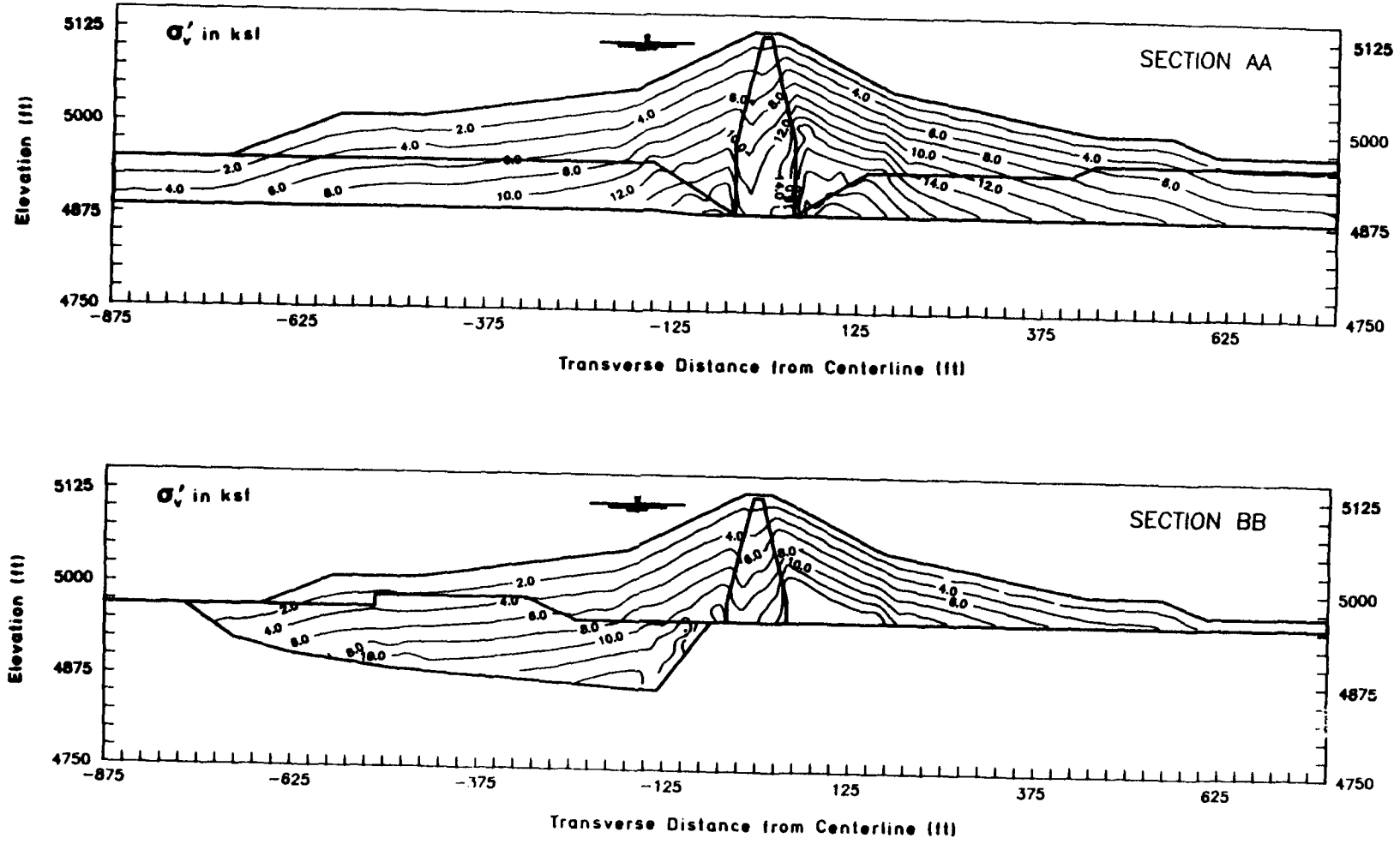

Figure 32. Contours of effective vertical stress calculated using FEADAM84

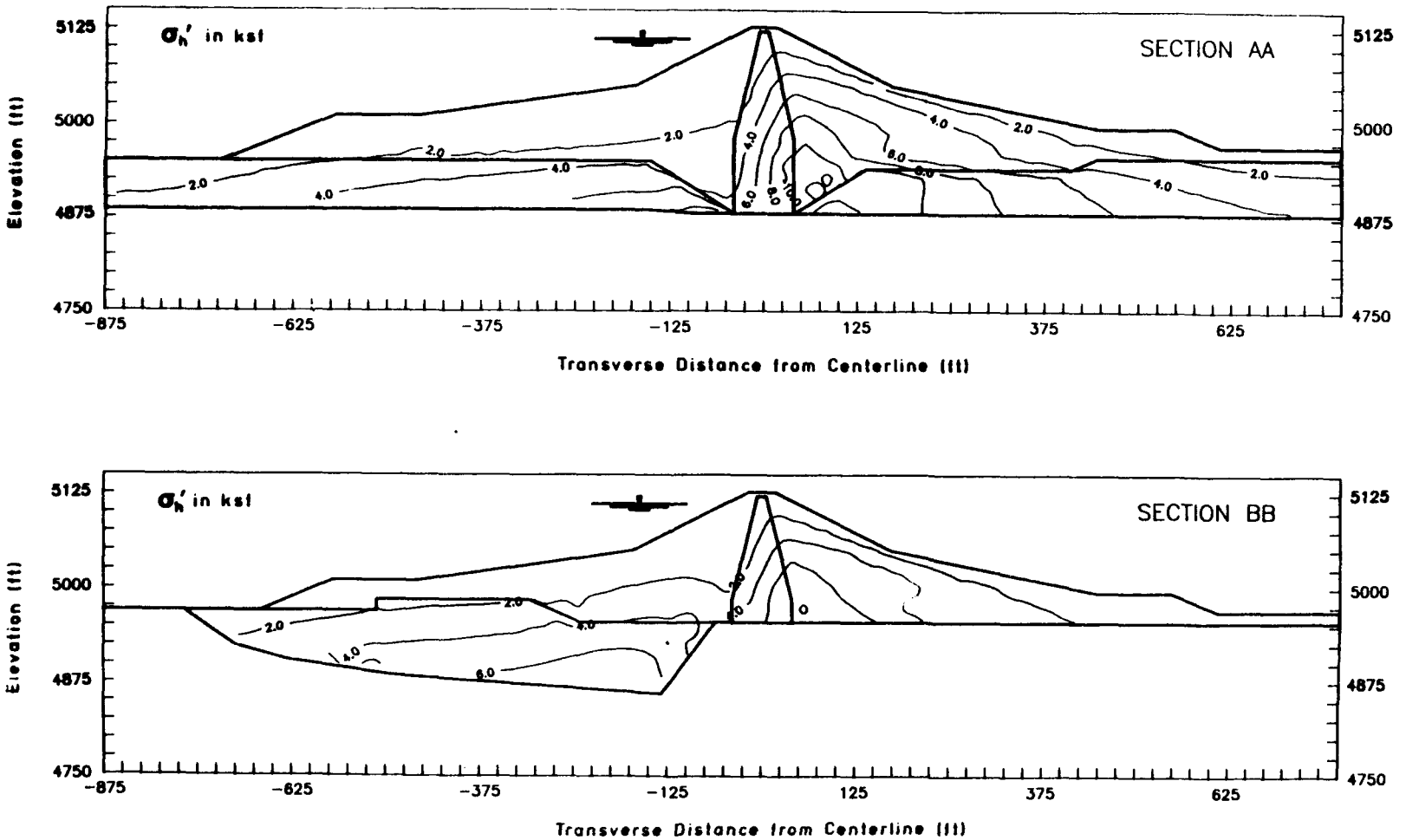

Figure 33. Contours of effective horizontal stress calculated using FEADAM84

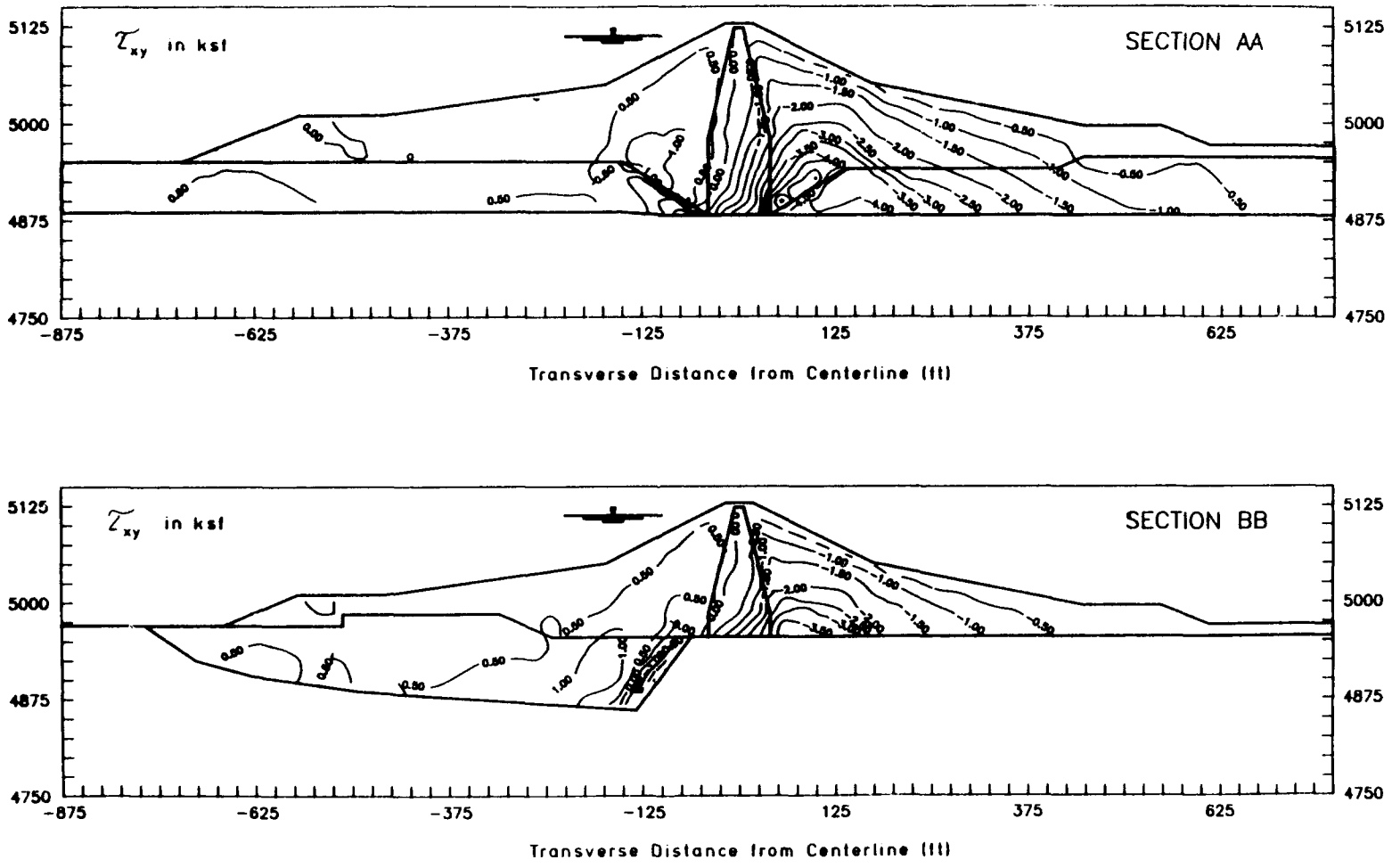

Figure 34. Contours of shear stress on horizontal planes calculated using FEADAM84

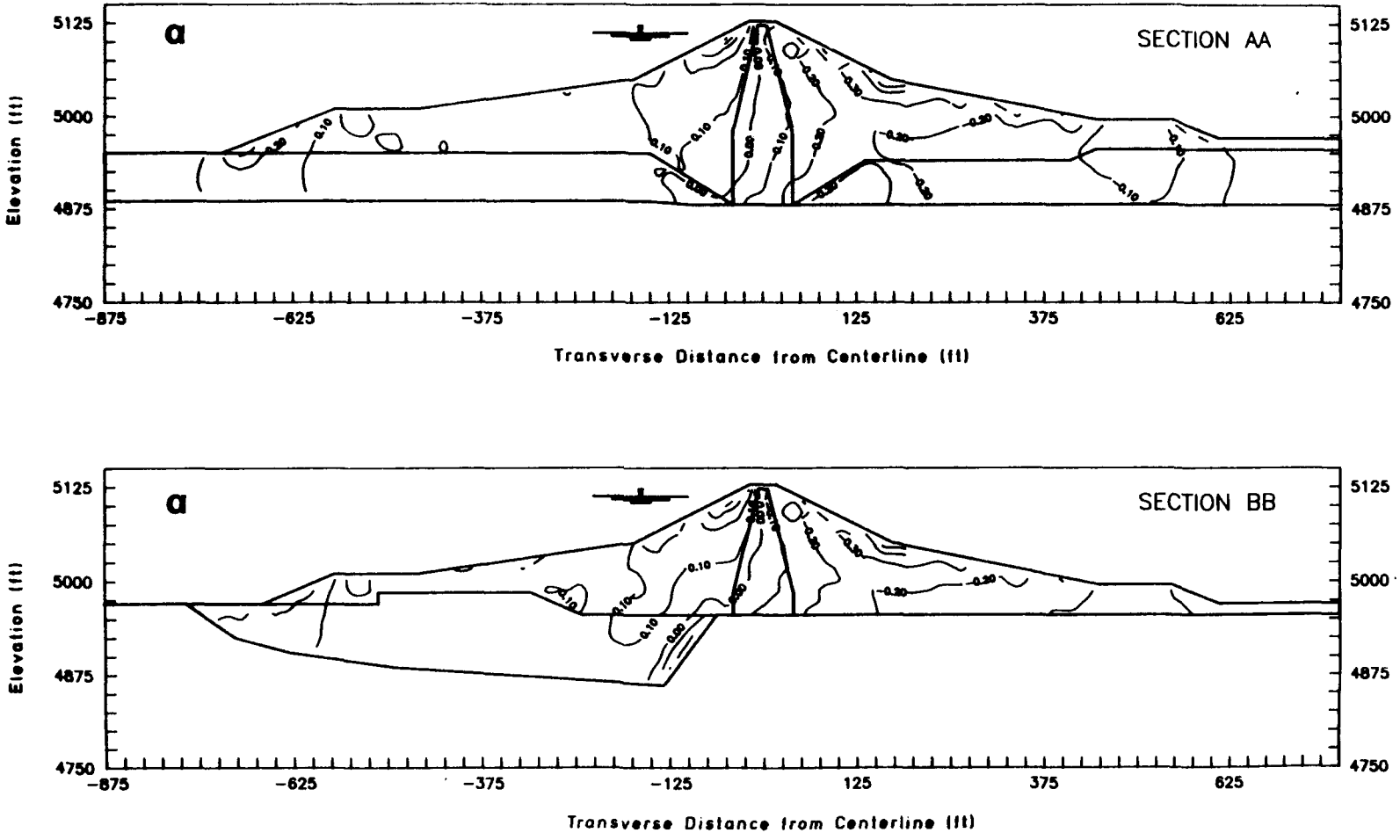

Figure 35. Contours of the ratio of shear stress to effective vertical stress (α)

because of buoyancy effects. Some stress arching (i.e., decrease in rate of vertical stress increase with depth) is indicated in the vicinity of the boundary between gravel fill in the core trench and dense alluvial gravel downstream of the core. This arching effect carries over into horizontal and shear stresses as well, and is typically the result of the contrast between the stiffness of the two materials modeled in this area.

68. Thrust developed by seepage forces within the core acts to reduce horizontal effective stresses, σ_h', in the upstream, submerged portions of the dam and to increase horizontal effective stresses downstream of the core (Figure 33). The largest value of σ_h', 13.6 ksf, occurs downstream of the core near the base of section AA. In addition, during the process of numerical embankment "construction" nodal points in this region may displace downward and away from the core, further reducing horizontal stresses (Hynes et al. 1988). In a few of the rock fill and gravel fill elements just upstream of the core, the reduction in horizontal effective stress causes a high principal stress ratio (i.e., vertical to horizontal in this case) that indicates localized strength mobilization.

69. Contours of static shear stresses on horizontal planes, τ_{xy}, shown in Figure 34 indicate that the upstream portion of the dam has very small shear stresses; whereas, the downstream portion has a concentration of shear stresses downstream of the core. The maximum absolute magnitudes of τ_{xy} are 6.2 and 3.9 ksf for sections AA and BB, respectively. Negative values are a result of the sign convention used in FEADAM84.

70. Contours of α are shown for both sections in Figure 35. Most of the absolute values of α range from 0 to about 0.45, with a localized pocket of higher values occurring in both sections in a very few elements along the 2:1 gravel fill slope of the upper portion of the embankment. Negative values are a result of sign convention in FEADAM84 program and are not indicative of extension stress conditions.

71. Static finite element analysis results were used for several purposes in the Ririe Dam seismic stability evaluation. As was discussed in Report 1, the vertical and horizontal effective stress values were used to calculate mean stress for correction and conversion of Becker Hammer blow-counts to equivalent SPT blowcounts. The vertical effective stress and values were also used to determine appropriate cyclic strengths for each

material type and location, as discussed at the beginning of Part IV and in Report 1.

PART V: DYNAMIC RESPONSE ANALYSES

Introduction

72. A dynamic response analysis is used to evaluate the response of a structure to the specified ground motions. Specifically, the variation of peak ground acceleration with time, the peak values of shear stress and strain, and response spectra (the maximum acceleration, velocity, and displacement as a function of natural frequency to occur at a point in the dam) at both low strain levels and higher earthquake levels are of interest. For the seismic stability study of Ririe Dam, the response of the idealized two-dimensional cross sections was considered. The results of the dynamic response analysis were used to assess the potential for various materials to liquefy and evaluate the slope stability for post-earthquake conditions. The dynamic response analysis is a major step of the process to assess the potential for liquefaction and generally follows the completion of the static stress analysis.

73. Numerical methods are used to perform a dynamic response analysis and calculate the dynamic shear stresses and shear strains produced by the vertical propagation of horizontally polarized shear (SH) waves. The computer program SUPERFLUSH (Earthquake Engineering Technology Corp. 1983), which is a modified version of FLUSH (Lysmer et al. 1975), was used to arrive at solutions by means of the finite element method using main-frame computers. SUPERFLUSH is a two-dimensional program that uses the method of complex response to solve the equations of motion in the frequency domain.

74. Assumptions of plane strain were used to analyze the dynamic response of two cross sections: the "maximum section" (section AA) and a "quarter-section" (section BB). The locations, profiles, and idealizations for these two sections were presented previously in Figures 4, 28, and 29. Two sections were utilized to assess the three-dimensional effects (non-conformance to the assumptions of plane strain) at Ririe Dam. The cost of performing a three-dimensional analysis can be exorbitant and the development of multidimensional motion input highly speculative, so it was decided that, if possible, empirical factors and approximate numerical methods should be applied to the results of two-dimensional SUPERFLUSH analyses to simulate three-dimensional effects.

75. Two other numerical methods of analysis were used to compare and confirm the results of dynamic response analysis using SUPERFLUSH: nonlinear shear beam models (Dakoulas 1989a) and a one-dimensional wave amplification algorithm SHAKE (Woodward-Clyde Consultants 1989). Both of these methods involve one-dimensional (horizontal) motion (like SUPERFLUSH) and were performed on personal computers. The one-dimensional amplification was used to evaluate the free-field response upstream and downstream of the dam. The nonlinear shear beam models were used to estimate the response of the dam using various combinations of assumptions and constitutive models.

Finite Element Analysis

76. The finite element method, in particular SUPERFLUSH, was used to evaluate the dynamic response because it incorporates the following important aspects in its numerical formulation:

a. The variation of soil characteristics with depth.

b. Nonlinear and energy-absorbing characteristics of the soils.

c. The variation of ground motions with depth.

d. A nonrigid lower boundary condition.

Nonlinear soil behavior was approximated with an equivalent linear constitutive model which relates shear modulus and damping ratio to the dynamic strain level developed in the material. As a two-dimensional, total stress, equivalent linear solution, SUPERFLUSH does not account for possible pore water pressure generation and dissipation during the earthquake. Each element in the mesh is assigned properties of unit weight, shear modulus, and strain-dependent modulus degradation and damping ratio curves.

77. The finite element method is considered to be well suited and efficient to evaluate the dynamic response of earth systems. The program FLUSH was established over 15 years ago and has been verified and widely adopted by the geotechnical engineering profession. The dynamic response calculations were performed by Woodward-Clyde Consultants (1989) and are summarized in Volume II.

Finite element mesh

78. The creation of two finite element meshes was described previously in this report. The meshes used for SUPERFLUSH are identical to those used for FEADAM84 except that the meshes for SUPERFLUSH extend into the foundation

rock. More of the foundation was included to allow seismic waves to propagate up from a competent bedrock stratum that extends uniformly beneath the entire site (lower tuffaceous sediments, below el 4,750). The finite element meshes used for the dynamic response analyses are shown in Figure 36. The mesh for section AA contains 781 nodes and 782 elements; the mesh for section BB contains of 632 nodes and 619 elements. Contours of stresses, ratios of stress, and strains determined with SUPERFLUSH were developed using respective values as calculated at the centroids of each element.

79. The boundary conditions for the cross sections were simulated with approximate energy-transmitting boundaries at both ends of the mesh and a compliant base at the contact between the foundation rock and the base rock. Energy-transmitting boundaries are numerical schemes used to represent the physical condition that the soil layers extend to infinity in the horizontal direction. A compliant base stipulates that the material below is elastic (not rigid as assumed with the program FLUSH) and that compatibility of strains must exist.

80. Guidelines are available to size finite elements and ensure that an acceptable level of accuracy exists for dynamic response analyses. Lysmer et al. (1975) recommended that the maximum height of finite elements, h_{max} , be governed by the maximum frequency of interest (cut-off frequency) for the dam:

$$h_{max} = 0.20\left[\frac{V_s}{f_{max}}\right] \tag{4}$$

where

V_s = shear wave velocity (fps) as a function of shear strain

f_{max} = maximum (cut-off) frequency of interest (Hz)

For the shear strains developed in this study, the cutoff frequency was about 6 Hz.

81. Notice that the h_{max} is dependent on the shear wave velocity assigned to the element. The value of h_{max} increases as the shear wave velocity assigned to that element increases. Hence, it is possible to select different heights of elements on the basis of Equation 4 for different materials within the mesh. The horizontal dimension of the element may be much greater than the vertical dimension. It is good practice, however, to

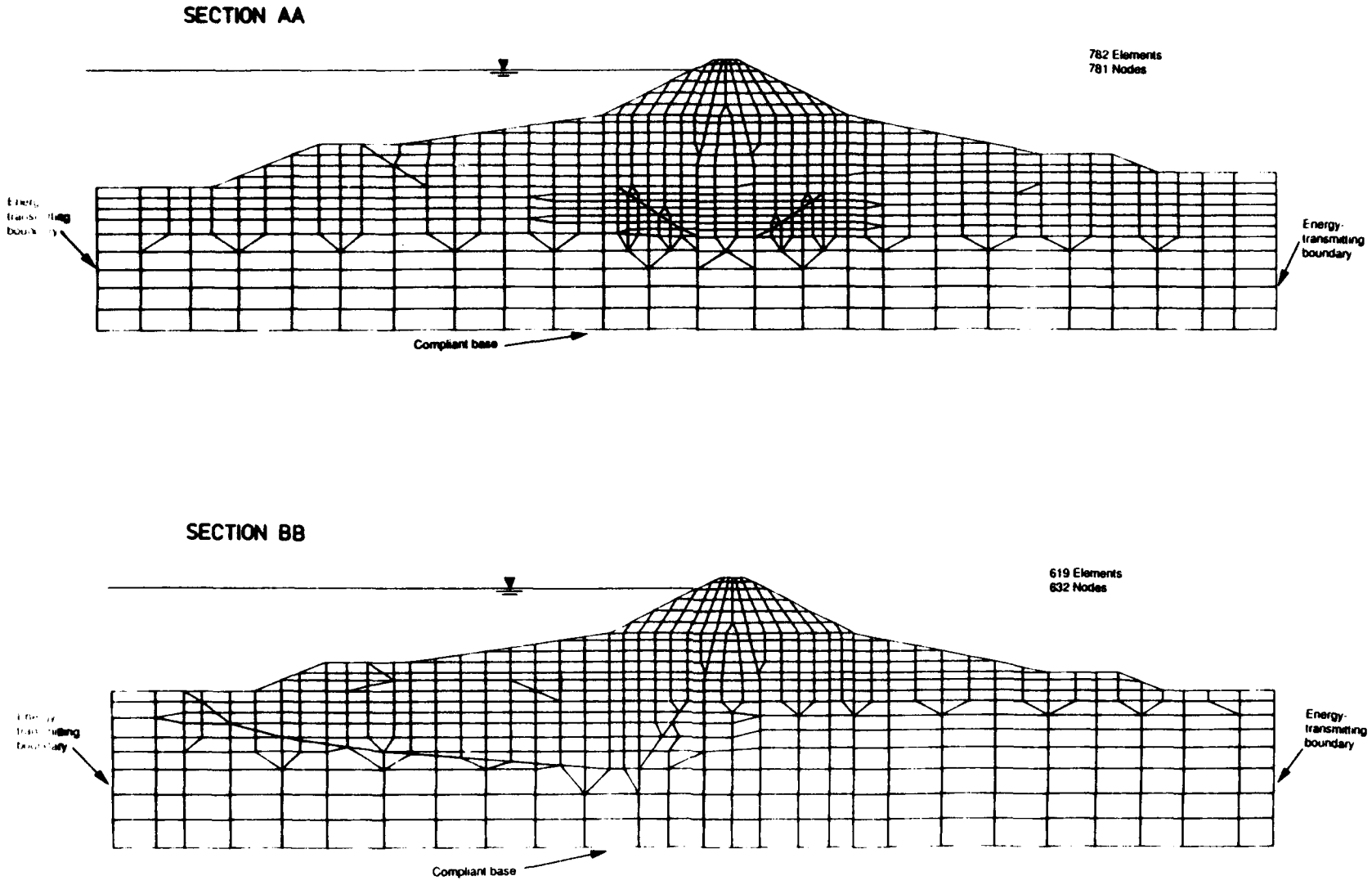

Figure 36. Finite element meshes for sections AA and BB used in the dynamic response analysis

keep the horizontal dimension on the order of four times (or less) the vertical dimension.

Material properties

82. The derivation and selection of material properties is described in detail in Report 1 of this series. The properties selected for dynamic response analyses are presented briefly below. Each element in the mesh is assigned the properties of unit weight, Poisson's ratio, shear modulus at low shear strains (10^{-4} percent), G_{max}, and strain-dependent modulus and damping ratio relations. The material properties used to perform the dynamic response analysis are summarized in Table 7.

83. Values of G_{max} used in dynamic response analysis calculations were calculated using the relationship proposed by Seed et al. (1986) involving the shear modulus parameter $(K_2)_{max}$ and mean effective stress, σ_m':

$$G_{max} = 1000\ (K_2)_{max}\ (\sigma_m')^{1/2} \quad \text{(psf)} \tag{5}$$

where

$\sigma_m' = 1/3\ (\sigma_x' + \sigma_y')\ (1 + \nu)$

σ_x' = effective horizontal stress

σ_y' = effective vertical stress

ν = Poisson's ratio

Values of $(K_2)_{max}$ were derived for each material from in situ seismic geophysical measurements and are listed in Table 7. The mean effective stress was calculated for each element using the results of the static effective stress analysis.

84. The variation of G_{max} throughout sections AA and BB is rather uniform as shown in Figure 37. Dashed lines used for contours represent locations where significant interpretation was required by the computer algorithm. The outline of the core, alluvial foundation, and bedrock are shown for convenience. The values of G_{max} assigned to the upper tuffaceous sediments and basalt were assumed to be independent of confining pressure (and therefore constant throughout since the shear wave velocity and mass density are constant). The G_{max} for the silt core is much lower than that for the remainder of the cross sections. The maximum values of G_{max} for embankment and alluvial foundation materials are 585 and 460 ksf for sections AA and BB, respectively.

Table 7

Material Properties Used for Dynamic Response Calculations

	Unit Weight pcf	$(K_2)_{max}$	Modulus Reduction	Damping	Poisson's Ratio
Core	125	45	Sands*	Sands**	0.48
Gravel fill - Saturated	145	120	Gravels†	Sands	0.40
- Unsaturated	135	120	Gravels	Sands	0.35
Rock fill - Saturated	145	100	Gravels	Sands	0.40
- Unsaturated	135	100	Gravels	Sands	0.35
Random fill - Saturated	140	85	Gravels	Sands	0.45
- Unsaturated	130	85	Gravels	Sands	0.35
Alluvium silt	120	50	Sands	Sands	0.45
Alluvium gravel	144	140	Gravels	Sands	0.40
Tuffaceous sediments	155	Vs=1600 fps	Rock††	Rock‡	0.45
Basalt	170	Vs=3000 fps	Rock	Rock	0.40

Note: * Modulus reduction relationship for sands by Seed and Idriss (1970).
** Damping relationship for sands by Seed and Idriss (1970).
† Modulus reduction relationship for gravels by Seed et al. (1986).
†† Modulus reduction relationship for rock by Schnabel (1973).
‡ Damping relationship for rock by Schnabel (1973).

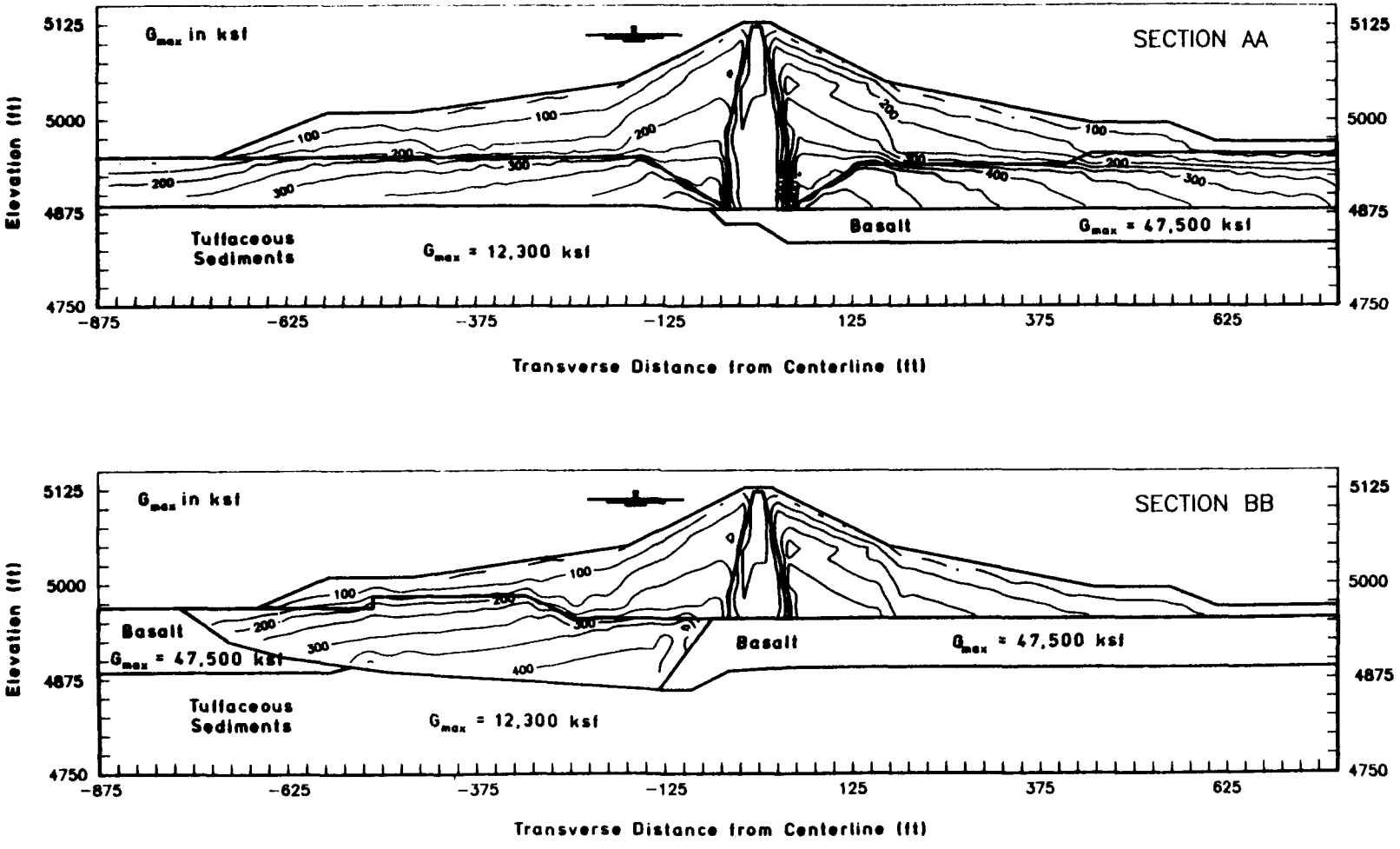

Figure 37. Distribution of G_{max} for sections AA and BB used for dynamic response calculations

85. Variations of shear modulus and damping ratio with shear strain were obtained from standard relationships proposed by Seed and Idriss (1970), Seed et al. (1986), and Schnabel (1973). These relationships have become widely accepted in earthquake engineering studies and are considered appropriate for the analysis of Ririe Dam. The shear modulus and damping degradation curves for the various materials are shown in Figures 38 and 39, respectively. It is interesting to note that gravelly soils have a greater modulus reduction than sandy soils at a given shear strain.

86. A typical cyclic stress-strain relationship measured in the laboratory for soil is nonlinear. The soil will exhibit plastic deformation if the strains are large enough. An example of such behavior is shown in Figure 40a. For each progressive cycle of loading, the plastic deformations ("x" intercept of stress-strain loop) increase in absolute magnitude and the shear modulus (average slope of the cycle loop) decreases.

87. The constitutive model incorporated into SUPERFLUSH is linear with simulated nonlinear effects to account for dependency of moduli on shear strain. This model, called the equivalent-linear method, was proposed by Seed and Idriss (1970) and is widely used in earthquake engineering studies. The model uses secant shear moduli that are adjusted during each iteration. Damping is input by using complex moduli and hysteretic damping (which is independent of frequency). An example of the iterative procedure for the equivalent-linear model is shown in Figure 40b. The model is initiated with an assumed value of shear modulus, G_1 , typically chosen to be less than or equal to G_{max} . For the first cycle of loading, the stress-strain relation is linear up to γ_1 then back through the origin (no plastic deformation) and down to $-\gamma_1$. The new value of shear modulus, G_2 , is determined by taking the maximum shear strain from the previous cycle, γ_1 , and using the modulus degradation curves (Figures 38 and 39) to estimate the percentage of modulus reduction. This process then repeats with G_2 , and so on until the moduli (and damping) for two successive iterations are within a specified tolerance (5 percent for this study). Upon release of the shear stress, the shear strains are always zero using this model regardless of the shear modulus.

Input motion

88. In SUPERFLUSH, it is assumed that the earthquake produces only horizontal shear waves that emanate from directly beneath the earth structure in the form of plane waves. The motion specified for the seismic stability

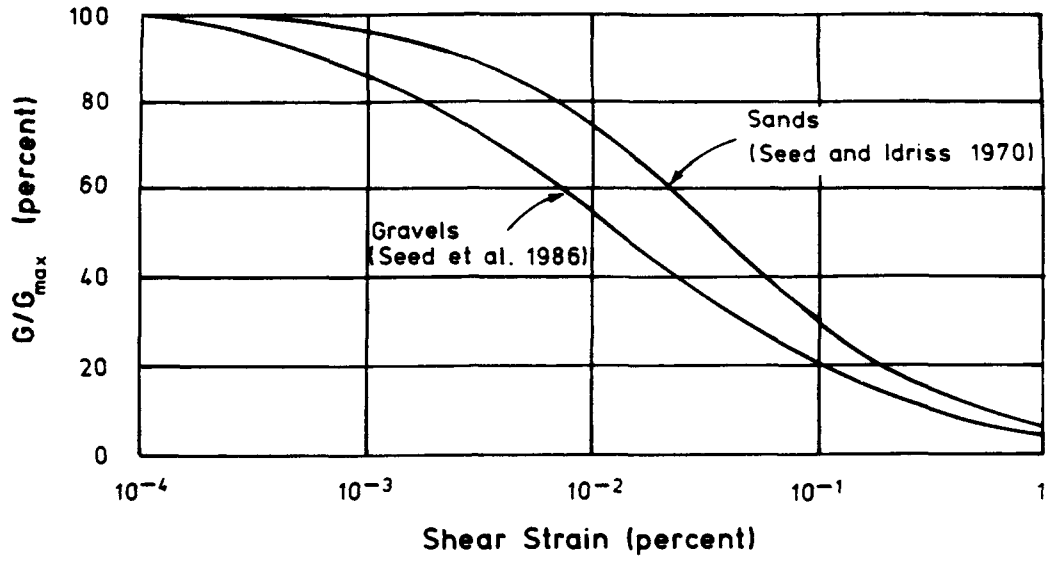

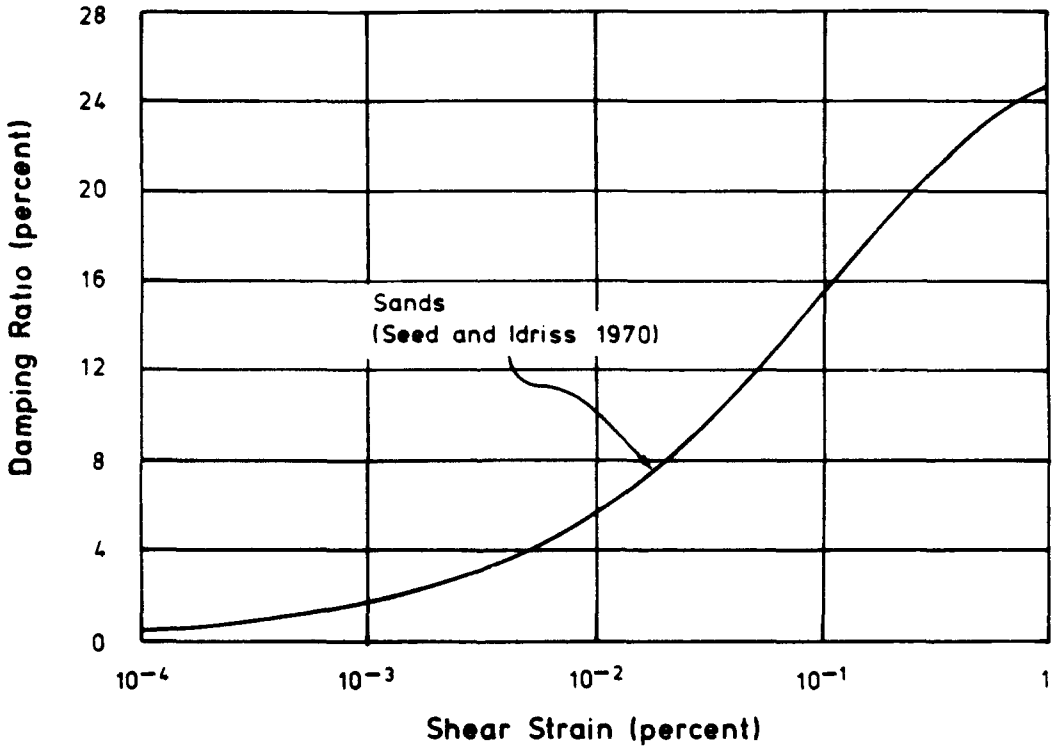

Figure 38. Strain-dependent shear modulus and damping relationships for sands and gravels

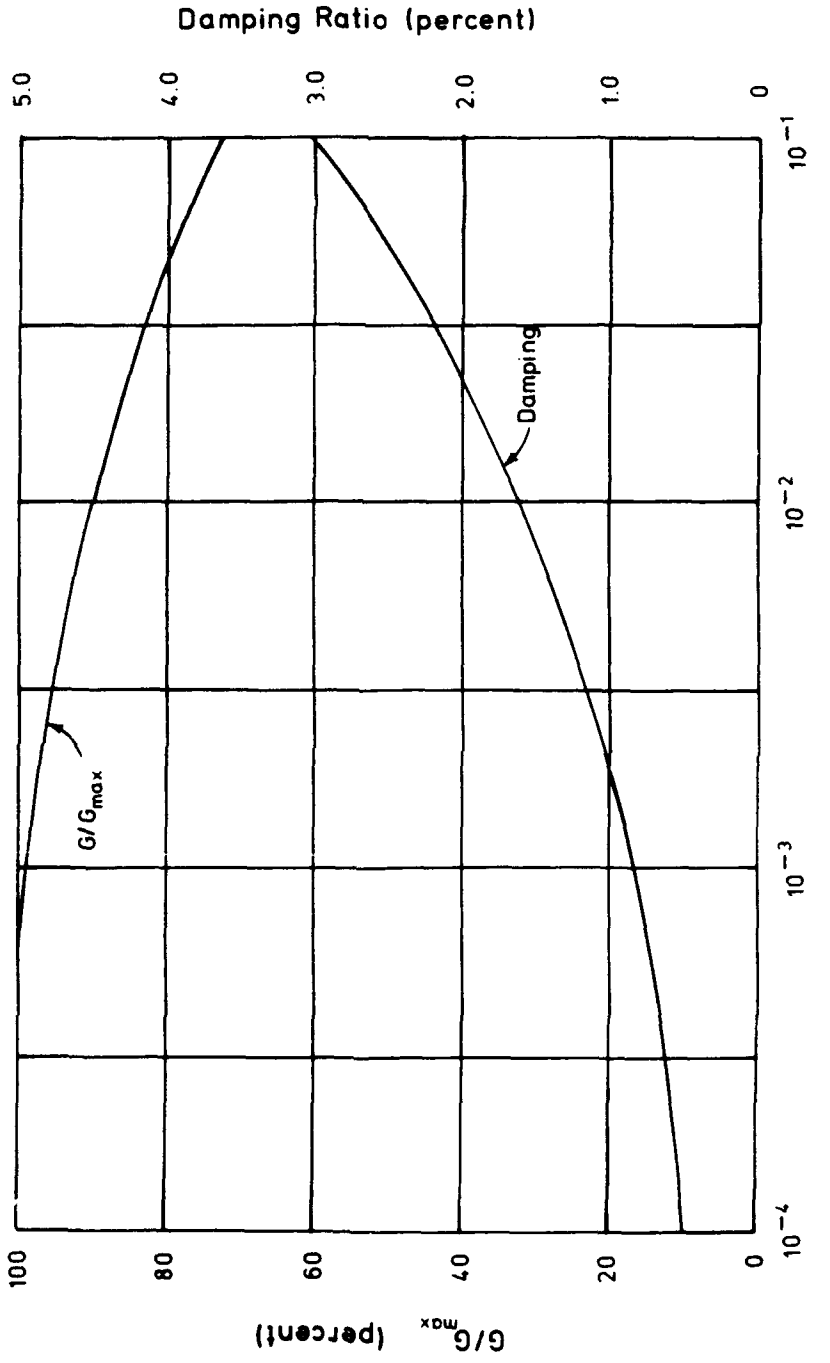

Figure 39. Strain-dependent shear modulus and damping relationships for rock (Schnabel 1973)

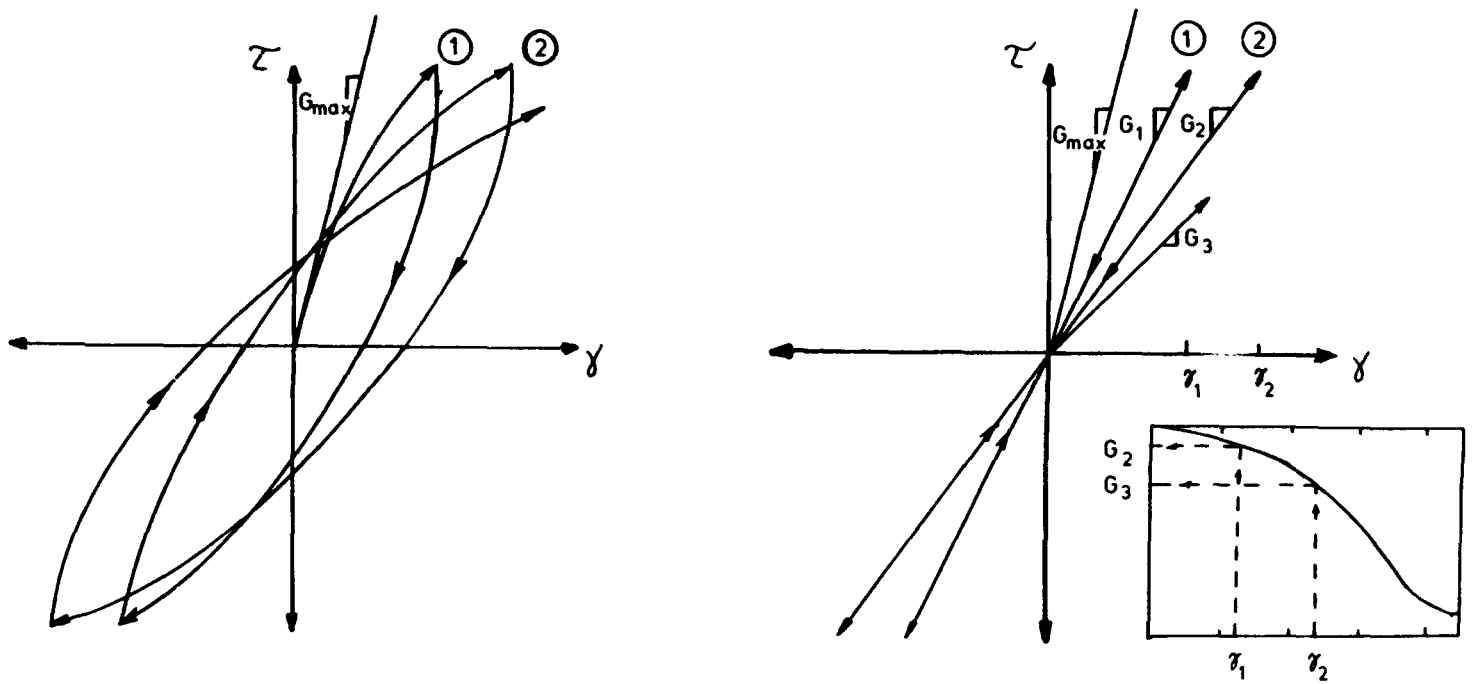

Figure 40. Generalized comparison between hysteretic soil behavior and the equivalent-linear soil model for a constant stress state

analysis by Seed (1987) corresponds to "outcrop rock" meaning all areas of the dam where rock is essentially exposed at the ground surface, regardless of the surface elevation. The ground motion at competent rock in the foundation of the structure is termed "base rock" motion and is specific to the local soil and site conditions. The general locations of these different motions are shown in Figure 41. The ground motions at each of the depicted locations will be different for the same causative earthquake. This includes the base rock motions at two different locations. The dam, alluvium, and upper rock units have an effect on the waves that propagate through the rock thereby creating the difference. Another general category of ground motion location is called "free field" which corresponds to ground surface motions where soil overlies rock. (For a thorough discussion of these concepts, see Wolf (1985).)

89. Ground motions specific to one location can be converted to another location using principles of wave propagation and knowing the dynamic material properties of the media. The process of converting motions from the outcrop to the base rock is performed as an option with SUPERFLUSH. The ground motions specified for this study represent outcrop motions and were converted into base rock motions for dynamic response analyses. Base rock motions were calculated at the contact between the upper and lower units of tuffaceous sediments, designated as the compliant base.

Results of Analysis

90. The results of the dynamic response analysis performed using SUPERFLUSH are presented and described below. The first set of results to be presented involves a comparison of calculated and measured response of Ririe Dam to the Mt. Borah earthquake which occurred in 1983. These results afforded a "fine-tuning" of the input parameters to SUPERFLUSH prior to the application of design motions.

Analysis of Mt. Borah earthquake

91. On 28 October 1983, a major earthquake of Richter Magnitude 6.9 occurred at 8:06 a.m. MDT in central Idaho (US Geologic Survey 1983). The earthquake was centered west of Mt. Borah (el 12,662), near the towns of Mackay and Challis, Idaho. The epicenter of the Mt. Borah earthquake was about 179 km from Ririe Dam (Chang 1985). The ground motions produced at

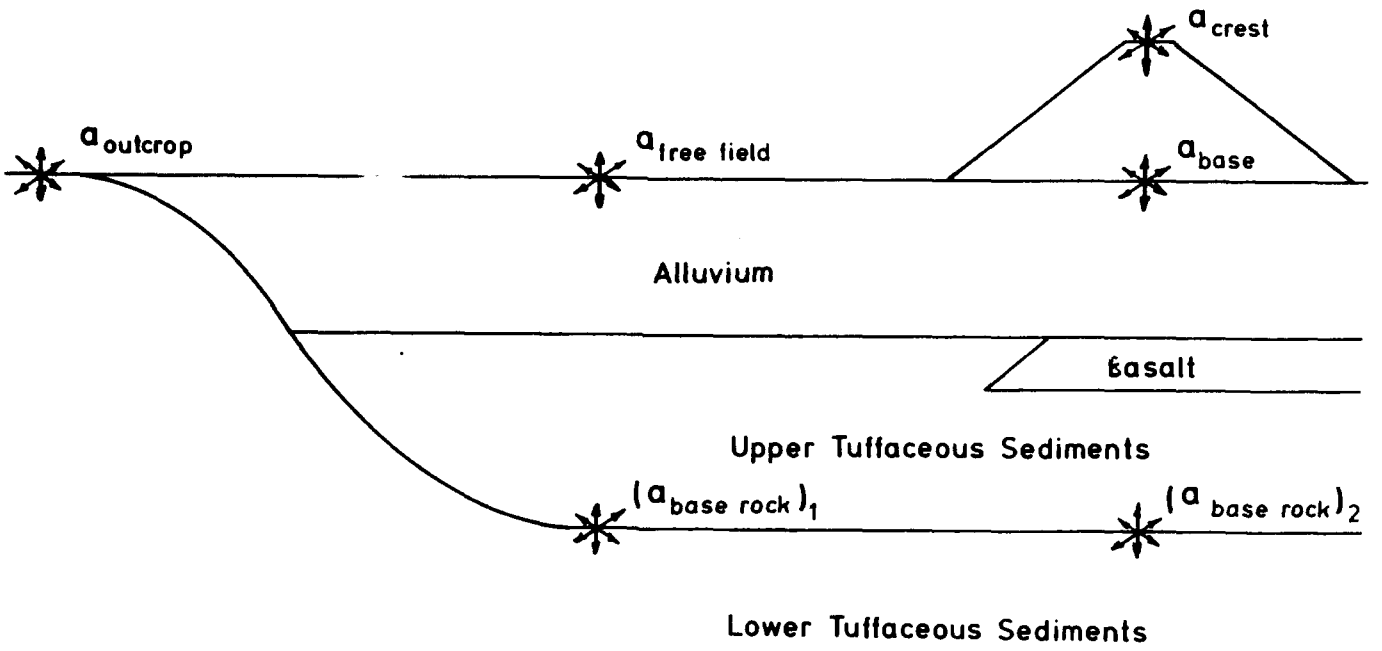

Figure 41. Schematic showing locations of different categories of ground motion

Ririe Dam were recorded by five strong motion accelerographs (Kinemetrics, Inc. Model SMA-1) installed at Ririe Dam by NPW during construction. The locations of these and other instrumentation devices are shown in Figure 42. Seismographs (accelerographs) S1 and S2 are located at the intake tower. Seismograph (accelerograph) S3 is on the crest near sta 7+00. Seismographs (accelerographs) S4 and S5 are on the left abutment, the former at el 5,150 upstream of the centerline, the latter at el 5,000 near the downstream berm. These recorded acceleration data were used as a basis of validation for the simplifications, idealizations, and material properties selected to conduct the dynamic response analysis.

92. The original set of material properties was evaluated and adjusted slightly based on a comparison between a computed response for the Mt. Borah earthquake motions and the recorded motions. First, the two-dimensional dynamic response (SUPERFLUSH) of the dam using the original material properties was conducted. In Figure 43a, the computed and measured responses at the crest are shown for the original set of material properties. The two response spectra are similar, especially at frequencies of less than about 1.5 Hz. At frequencies between 1.5 and 6 Hz, the computed response matches the general shape of the measured response although it underestimates the amplification by about 10 to 15 percent. At frequencies greater than 6 Hz, the two spectra are less similar.

93. The material properties for rock fill, alluvial gravel, and the silt core were then changed slightly. Specifically, values of $(K_2)_{max}$ were changed from 120 to 100 for rock fill, 100 to 140 for alluvial gravel, and 55 to 45 for the silt core. (The presentation of material properties for dynamic response analyses reported previously represents the modified values.) The two-dimensional dynamic response analysis was then recomputed. The comparison between computed and measured amplification spectra is shown in Figure 43b. In general, a better match exists at frequencies less than 1.5 Hz. At frequencies greater than 1.5 Hz, the computed spectra tend to match the general shape of the measured spectra, although the amplification ratios are still about 50 to 70 percent of the measured values.

94. The general agreement between measured and computed amplification spectra indicates that the model used to represent Ririe Dam is suitable to assess the dynamic response to the design earthquake. The remaining differences between amplification spectra are assumed to exist, at least in part,

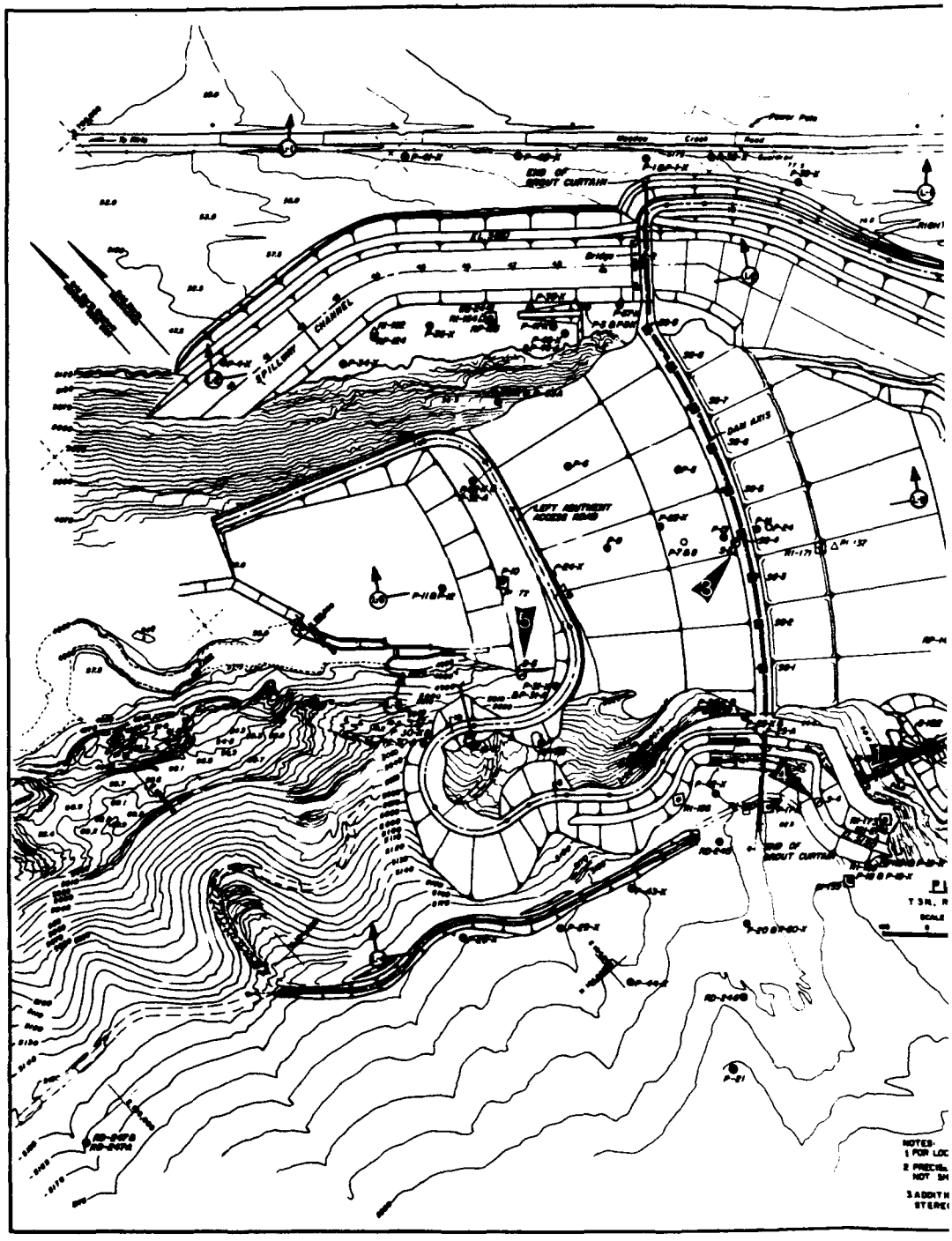

Figure 42. Location of strong motion in

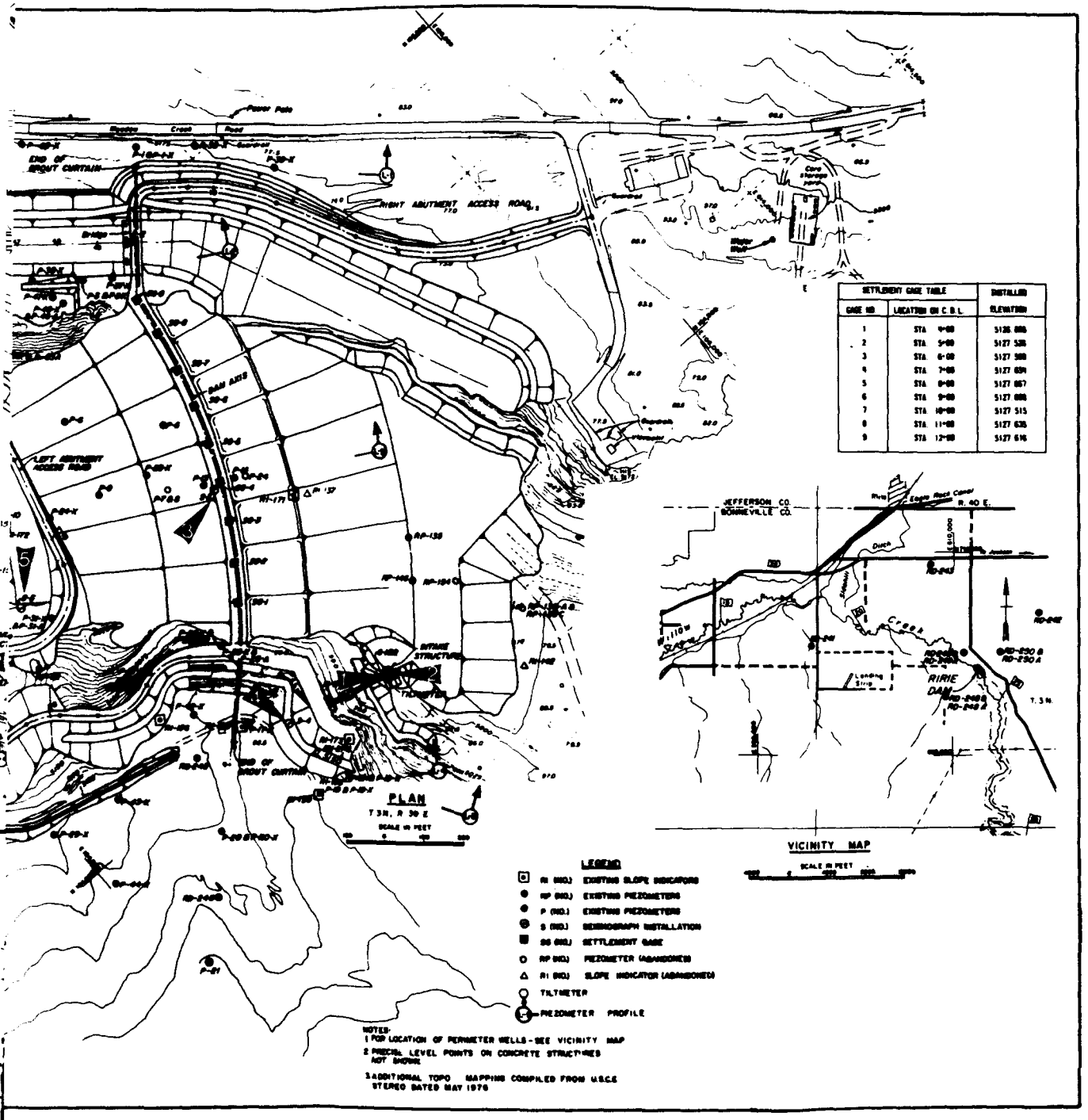

42. Location of strong motion instrumentation of Ririe Dam

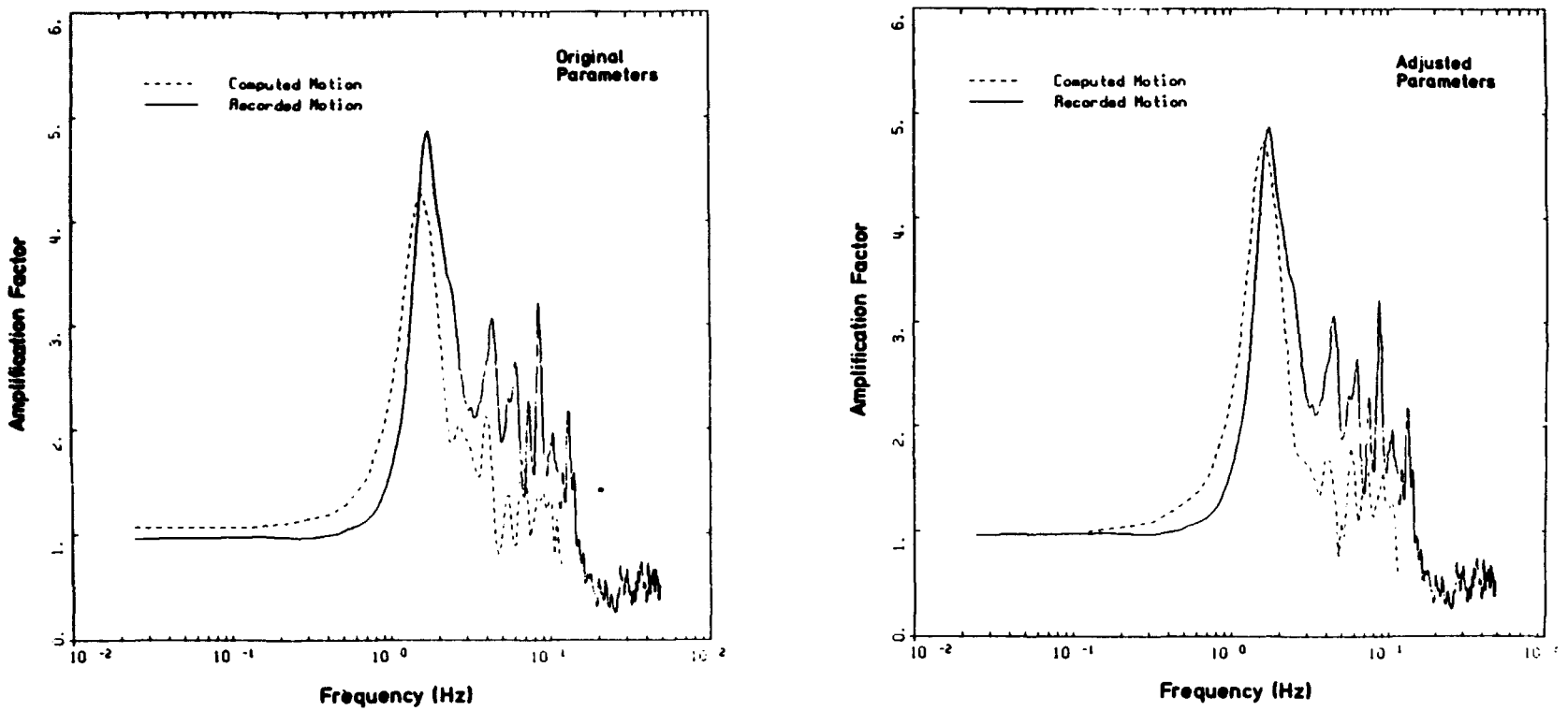

Figure 43. Computed and recorded amplification ratios during the Mt. Borah earthquake at crest of Ririe Dam

because of the three-dimensional nature of the problem. The measured response was three-dimensional; the computed response was two-dimensional with empirical adjustments to include some effects of 3-D behavior. At lower frequencies, the effects of three-dimensional conditions would tend to have a lesser effect because the wavelengths are greater.

Accelerations

95. The peak horizontal accelerations induced by the design earthquake were computed at select nodes of the meshes for sections AA and BB using the results of the two-dimensional dynamic response analysis (SUPERFLUSH). These peak accelerations are shown in Figure 44 and the interpolated contours are shown in Figure 45. The maximum base rock accelerations, $a_{base\ rock}$, for section AA are in the range of 0.53 to 0.59 g, or about one-half the outcrop motion (1.17 g). Very large accelerations occur at the ground surface and the contact between rock and soil units because of the additive nature of reflected waves traveling through a stiffer material and reflected off a softer material or free surface. The maximum acceleration of the selected nodes is about 1.0 g at the upstream profile but, in general, the accelerations throughout the embankment and foundation alluvium are in the range of 0.3 to 0.8 g. The peak horizontal acceleration at the crest, a_{crest}, is 0.77g, well below the peak outcrop acceleration, $a_{outcrop}$, of 1.17 g. It is apparent from the distribution of peak accelerations that significant amplification of base rock motions occurs. Localized concentrations of contours evident in Figure 45 result from a large separation distance between points of known acceleration. The computed acceleration records for design earthquake motions at section AA and section BB at the crest are shown in Figure 46. A number of other acceleration records are presented in Volume II.

96. The base rock accelerations for section BB are larger than those for section AA. The accelerations throughout the foundation and embankment tend to be quite a bit larger in section BB than section AA, generally between 0.4 to 0.9 g. The reason for these higher levels of acceleration is directly attributable to the greater base rock accelerations and it being a stiffer system. Section BB is also a stiffer structure because of its shorter height and, therefore, is able to transmit larger accelerations. The maximum acceleration is 1.17 g at the downstream surface free field (which only coincidently matches the peak outcrop acceleration). The peak horizontal acceleration at the crest is 0.92 g.

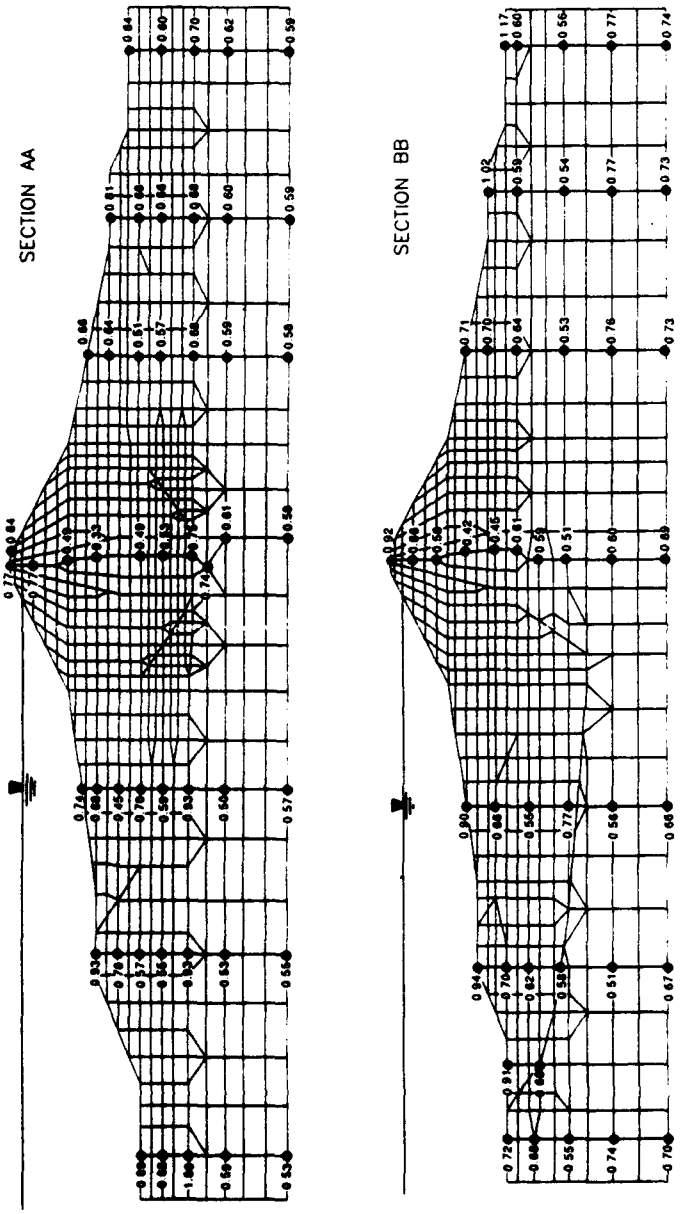

Figure 44. Peak horizontal accelerations induced by the design ground motions as computed using SUPERFLUSH

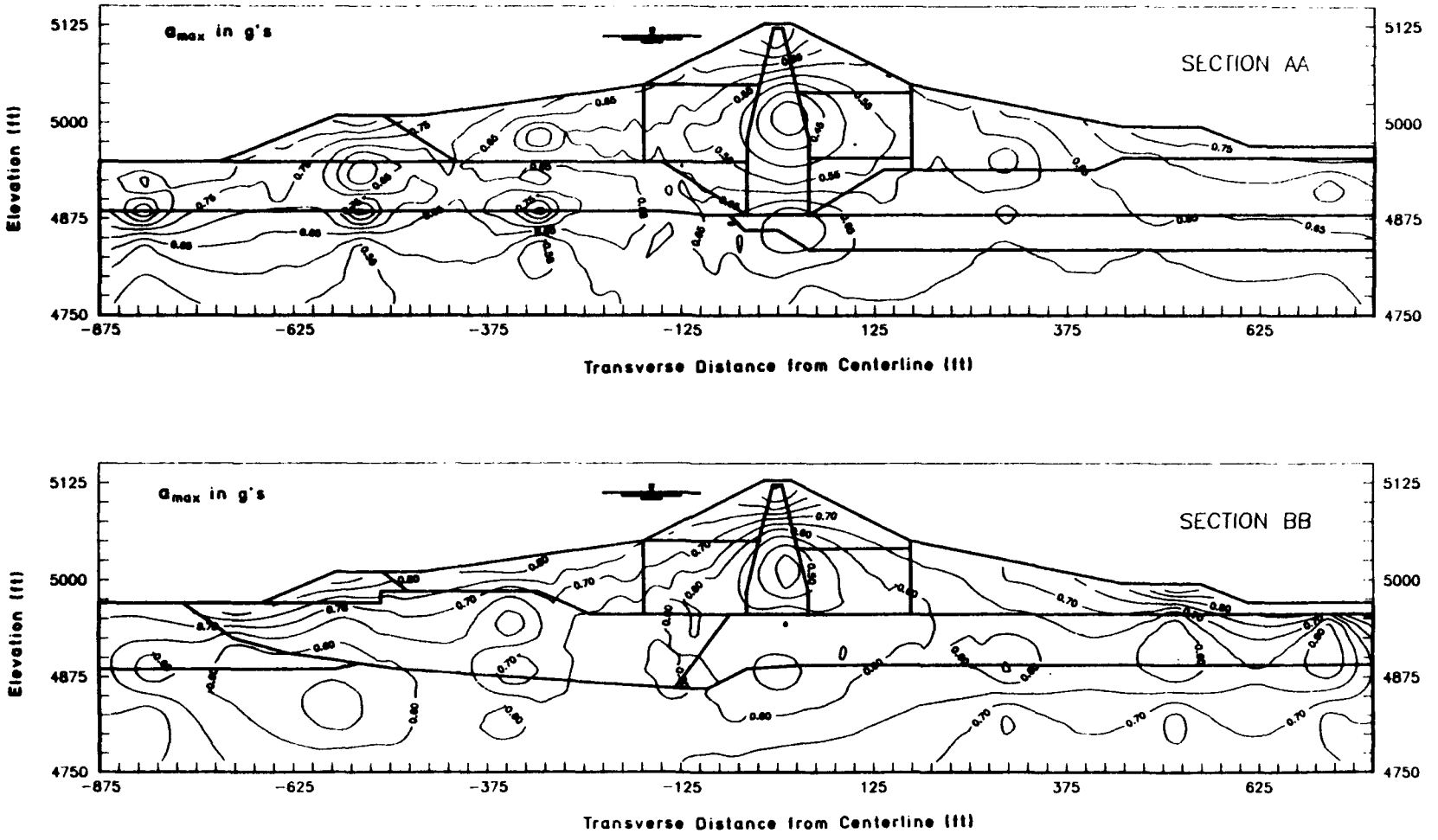

Figure 45. Distribution of peak horizontal acceleration for sections AA and BB for design ground motions as computed using SUPERFLUSH

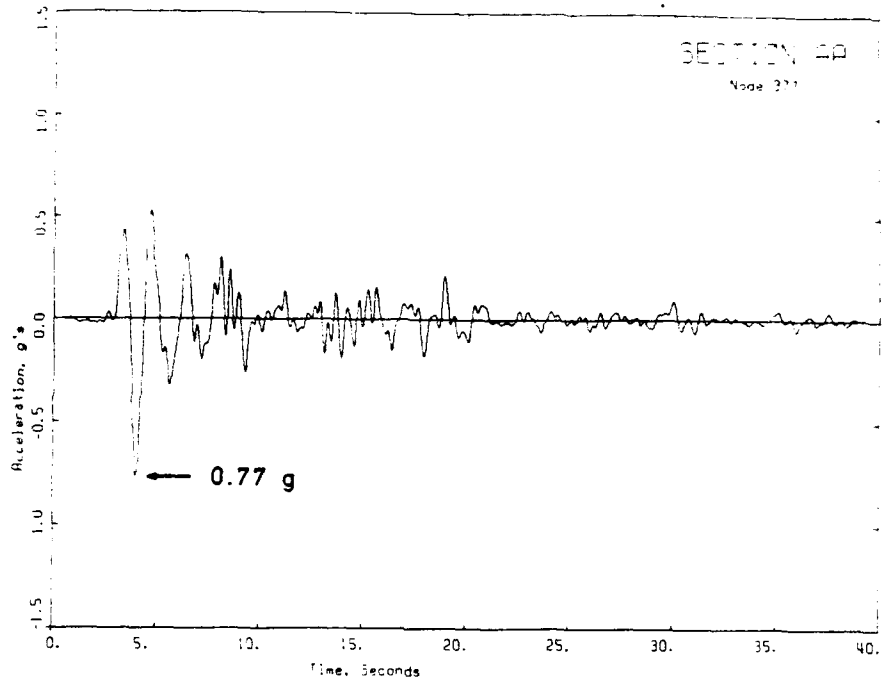

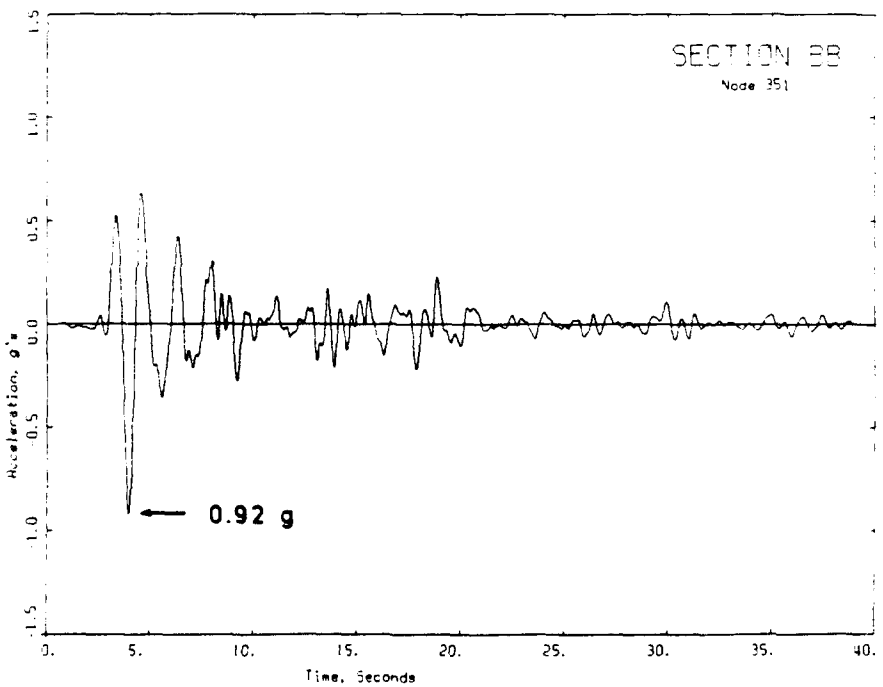

Figure 46. Acceleration records at crest for sections AA and BB as computed using SUPERFLUSH

Shear strains

97. The effective shear strain induced by the design earthquake, $\gamma_{.65}$, was computed for each element of the meshes for sections AA and BB using SUPERFLUSH. The distribution of effective shear strain, defined as 65 percent of the maximum shear strains, are shown for sections AA and BB in Figure 47. The factor of 65 percent best represents the level of shear strains occurring throughout the duration of earthquake motions that control the seismic behavior of the soil.

98. The magnitude of shear strains for a given seismic excitation is strongly dependent on the type of material. This is quite evident from the distribution of contours shown in Figure 47. The effective shear strains in the basalt and tuffaceous sediments are relatively low (generally 0.1 percent or less). The effective shear strains in the moderately stiff granular alluvium and shells which are moderately high (0.2 to 1 percent). The effective shear strains in the alluvial silt in the downstream portion of section AA and the core are very high (0.8 to 2.0 percent). For a range in shear strains of 0.1 to 1.0 percent, the shear modulus is generally between only 20 and 6 percent of G_{max}, respectively (refer to Figure 38). This represents a tremendous amount of modulus degradation. The magnitude and distribution of effective shear strains for sections AA and BB shown in Figure 47 are very similar. Most differences that exist are the result of differences in the materials present and the geometry of the cross section. The effective shear strains in the core material are slightly greater for section BB which is consistent with the conclusions drawn from a comparison of peak accelerations for the two sections.

99. The magnitude of effective shear strains can be compared with empirical thresholds to evaluate the potential for development of excess pore water pressures in granular materials. For gravels, a threshold strain of 0.05 percent is often used (Hynes 1988). It is quite evident from Figure 47 that all of the foundation and embankment will experience effective shear strains above this threshold. Therefore, it can be generally concluded that the design earthquake will generate excess pore water pressures in the embankment and foundation materials.

Shear stresses

100. The maximum shear stress on horizontal planes induced by the design earthquake, $(\tau_{xy})_{max}$, was computed for each element of sections AA

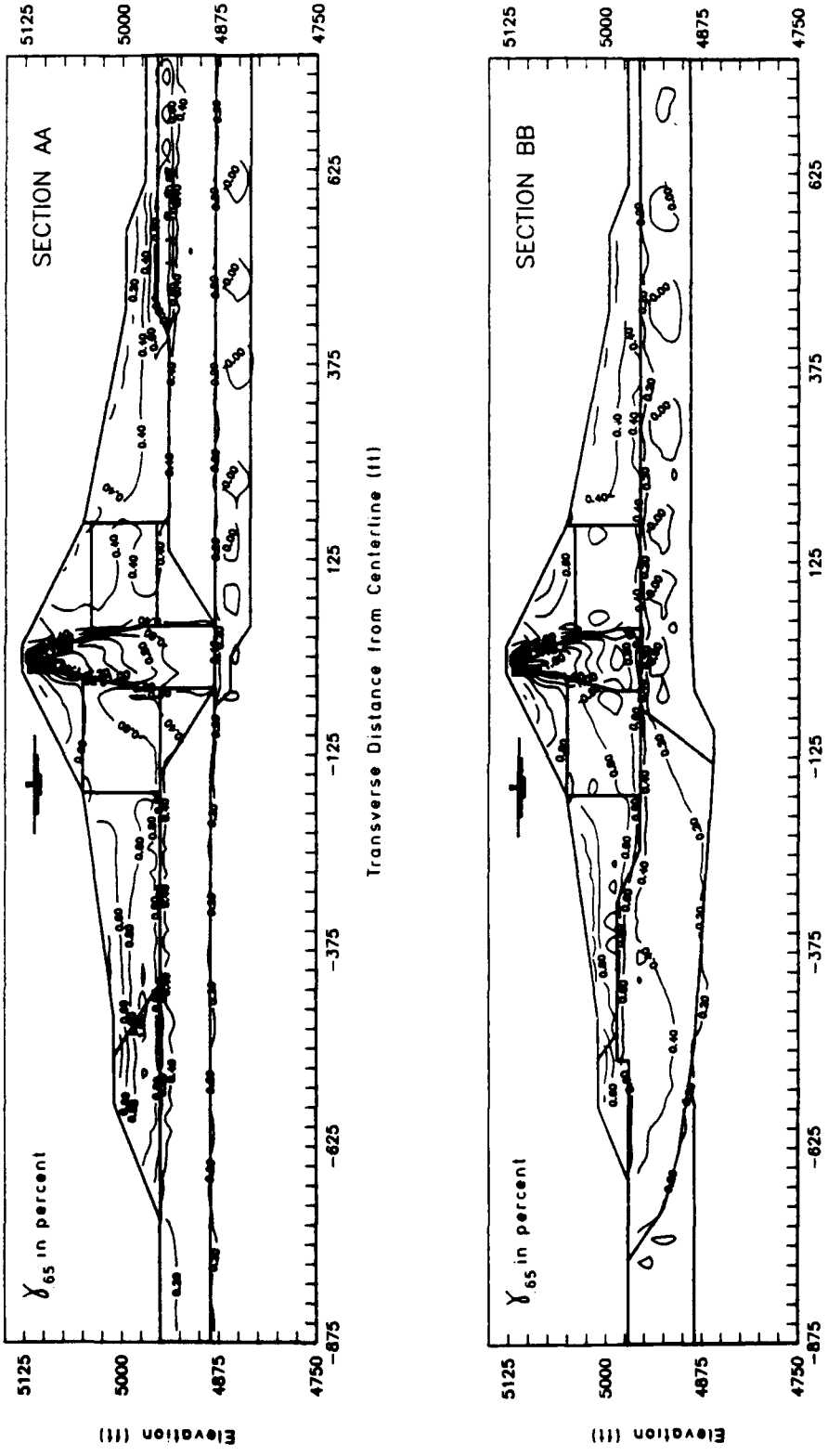

Figure 47. Distribution of effective shear strain for sections AA and BB for the design ground motions as computed using SUPERFLUSH

and BB using the results of SUPERFLUSH. The distribution of shear stresses is represented by contours of equal shear stress shown in Figure 48. The magnitude of shear stresses is very high, which is apparent when the contours shown in Figure 48 are compared with the contours of static shear stress shown in Figure 35. Peak shear stresses of 18.6 and 22.6 ksf were computed for sections AA and BB, respectively. The larger shear stresses associated with section BB result from it being a stiffer system (lower natural period of vibration). The variation of $(\tau_{xy})_{max}$ is relatively uniform except where foundation rock is discontinuous. A zone of concentrated high shear stresses exists at the termination of the basalt stratum beneath the core. Stress concentrations are not unusual at locations where a discontinuity exists for two materials with very different material properties.

Natural frequency

101. The natural (damped) frequency, f_d, represents the frequency of excitation at which a damped system experiences the greatest amplification for a given forcing function. The natural frequency at earthquake strain levels can be determined from the amplification spectra, that is, a plot of amplification versus frequency. The amplification spectra at the crest corresponding to a damping ratio of 5 percent were calculated using SUPERFLUSH for sections AA and BB and are shown in Figure 49. The natural frequencies of sections AA and BB for the design earthquake are 0.52 and 0.59 Hz, respectively.

102. The natural frequencies calculated for the design earthquake are much lower than those determined using the accelerograph records made during the Mt. Borah earthquake (1.76 Hz). The Fourier amplification spectra for that event are shown in Figure 50. This difference is attributed to the significant reductions in soil shear modulus caused by the large shear strains. As the stiffness (shear modulus) of a system decreases, the natural frequency decreases.

103. The computed natural periods (inverse of frequency) are compared with the response period spectra of the outcrop motion in Figure 51. The periods corresponding to peak spectral accelerations occur are 0.22 and 0.39 sec. The natural period of Ririe Dam at low shear strains (for the Mt. Borah event) was measured with accelerographs to be 0.57 sec. The spectral acceleration at 0.57 sec is much lower than the nearest peak at 0.39 sec. Furthermore, as the dam is subjected to larger strains (design earthquake event), the natural period moves farther away from the two peaks.

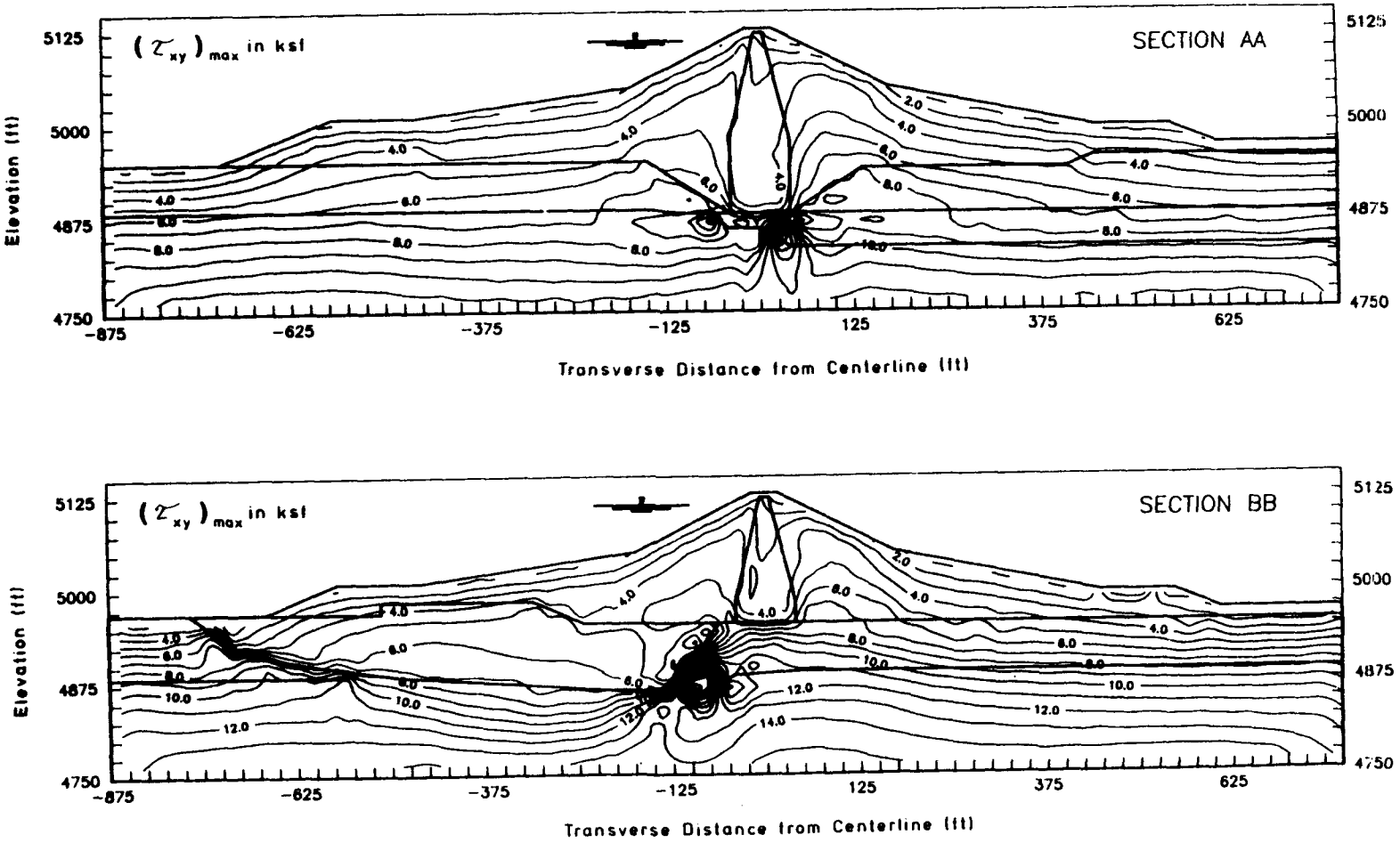

Figure 48. Distribution of maximum shear stresses on horizontal planes for sections AA and BB as computed using SUPERFLUSH

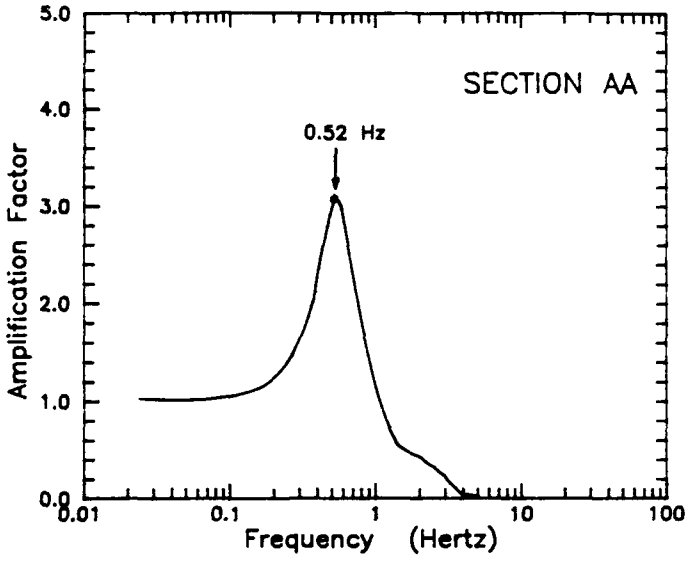

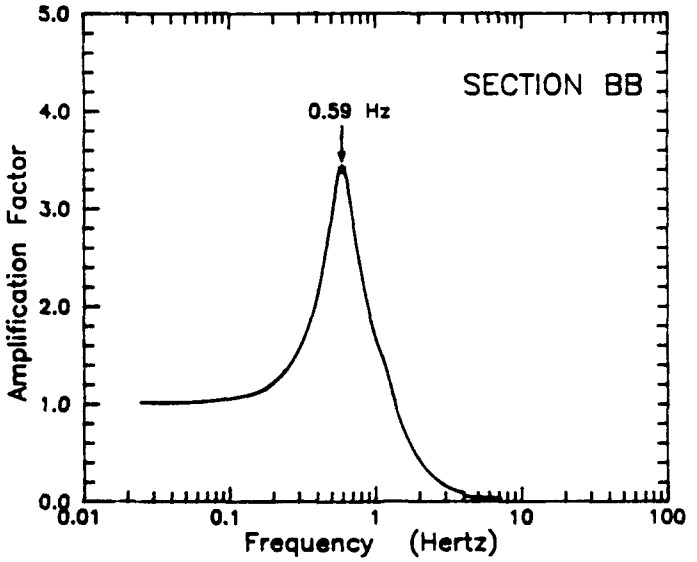

Figure 49. Amplification spectra for sections AA and BB using a damping ratio of 5 percent

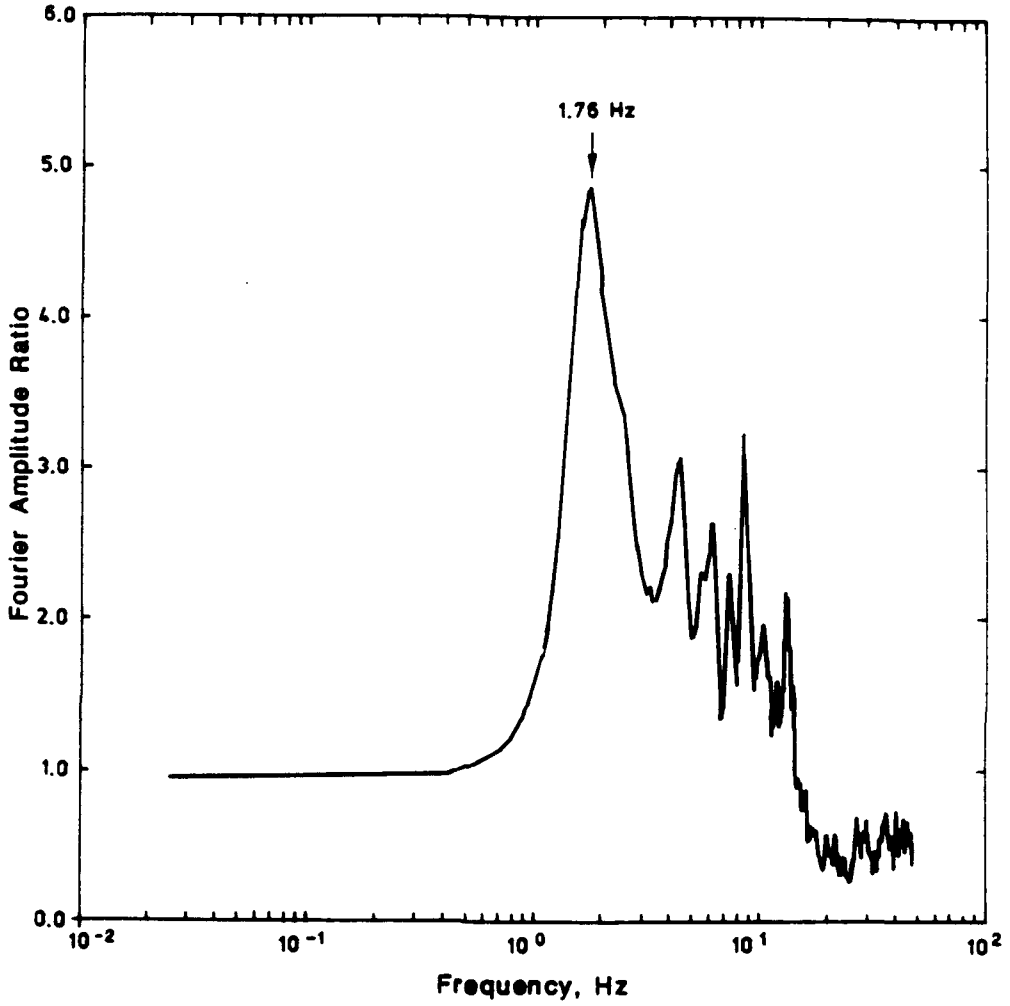

Figure 50. Fourier amplitude ratio between crest and abutment records during the Mt. Borah earthquake computed using SUPERFLUSH

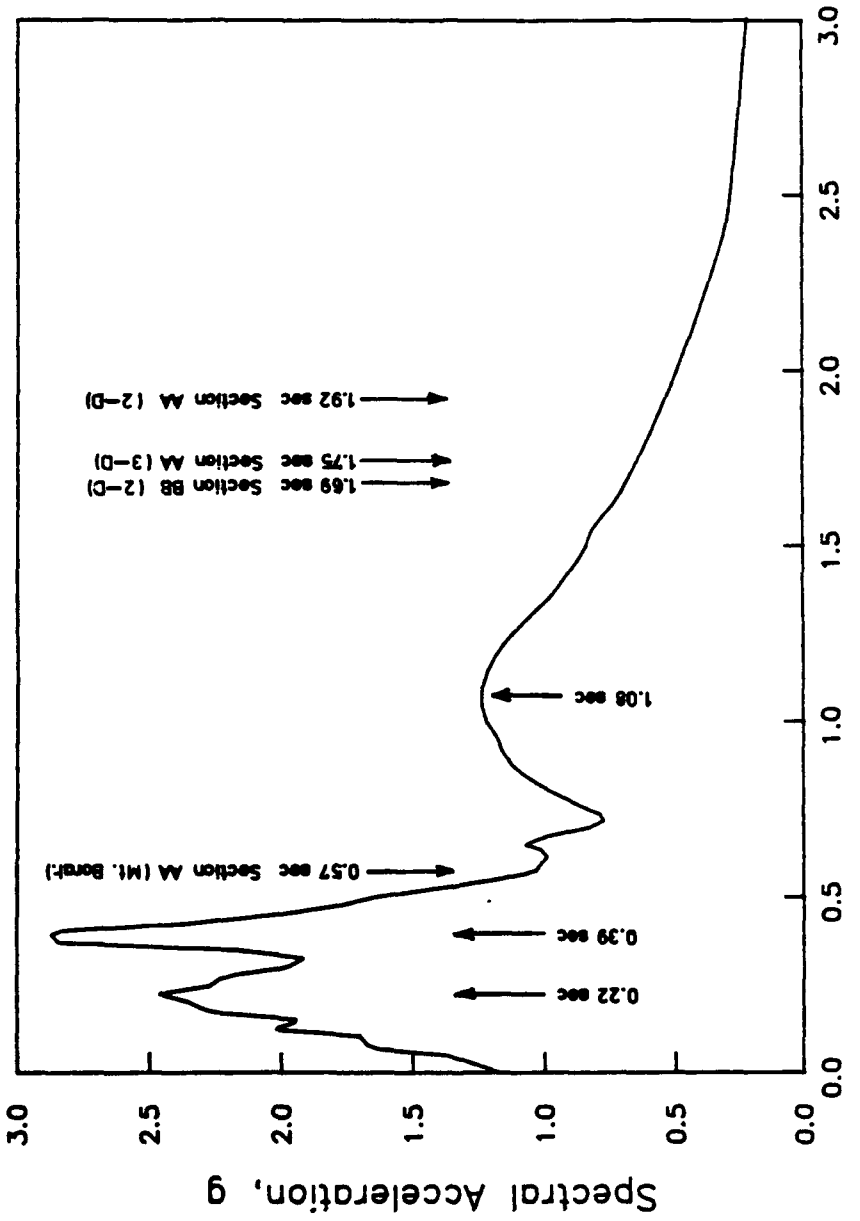

Figure 51. Response period spectra of design earthquake showing natural periods computed with SUPERFLUSH

A more severe response would result if the peak spectral acceleration of the design ground motion were to occur at a frequency nearer the natural frequency of the dam.

One-Dimensional Amplification

104. The computer program SHAKE was used to compare the results of peak ground accelerations and peak shear stresses obtained using the two-dimensional routine in SUPERFLUSH. As described by Schnabel et al. (1972):

> Program SHAKE computes the responses in a system of homogeneous, visco-elastic layers of infinite horizontal extent subjected to vertically travelling shear waves. The program is based on the continuous solution to the wave equation (Kanai 1951) adapted for use with transient motions through the Fast Fourier Transform algorithm (Cooley and Tukey 1965).

The input to SHAKE includes the free field profile, dynamic material properties (utilizing the equivalent-linear model described previously), the outcrop ground motion, and the maximum (cutoff) frequency of interest. Two cutoff frequencies were considered: 12 Hz and 25 Hz.

105. Comparisons of shear stresses and accelerations are shown in Figure 52. The shear stresses are almost exactly the same for the three conditions considered. The accelerations differ somewhat, but are still considered to be reasonably close. The accelerations calculated with SUPERFLUSH tend to be median values of the three. From this comparison, it can be concluded that the height of the finite elements used in SUPERFLUSH are short enough to propagate the range of frequencies which predominantly affect the dynamic response of the dam.

Effects of Canyon

106. The effect of the narrow and curved canyon on the dynamic response of the dam and foundation, generally termed three-dimensional effects, was evaluated using means established by Mejia and Seed (1983). The three-dimensional effects at Ririe Dam were determined to be large enough to have an effect on the natural frequency of the system and the shear stresses and peak accelerations induced by the earthquake, but not enough to warrant conducting a three-dimensional finite element analysis. Two-dimensional shear stresses

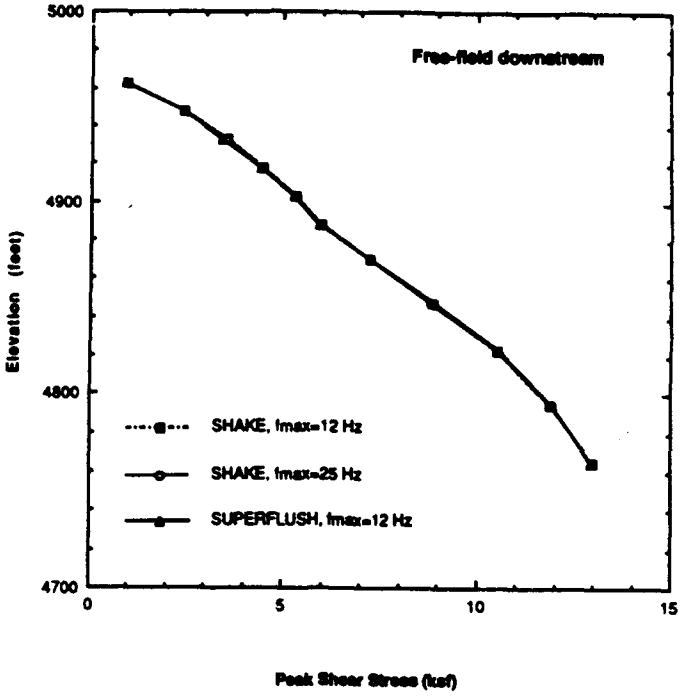

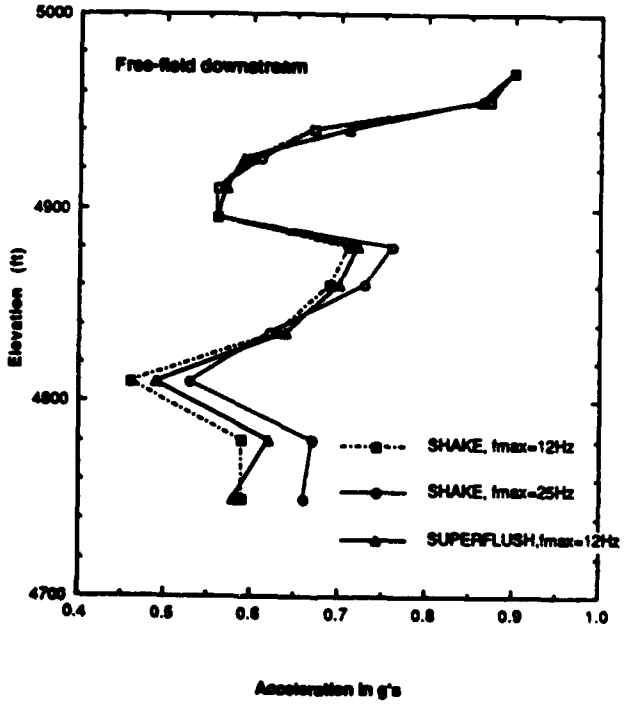

Figure 52. Comparisons of results obtained using computer programs SUPERFLUSH AND SHAKE

are decreased and peak accelerations and the natural frequency are increased by the three-dimensional effects as described below.

107. Mejia and Seed (1983) compared the results of three-dimensional and two-dimensional dynamic response analyses for two different dams with different canyon geometries. The results of other studies reported in the literature (Ambraseys 1960, Makdisi 1976, and Severn et al. 1979) were also presented and compared. Based on these comparisons, Mejia and Seed (1983) concluded that for one dam (Oroville Dam located in California) the values of shear stresses were within 20 percent of those computed from a three-dimensional analysis. Empirical correction factors could be applied appropriately for such cases. For dams in steeper canyons, it was found that a three-dimensional analysis is required to obtain satisfactory results.

108. Following the evaluation of the two-dimensional dynamic response analysis, Dr. Mejia (Woodward-Clyde Consultants 1989) concluded that it is reasonable to assume that adjustment factors are adequate to analyze Ririe Dam. The natural frequency for the three-dimensional case was estimated using the results of Mejia and Seed (1983) plotted in Figure 53. The ratio of natural frequency for the three-dimensional case to the two-dimensional case is about 1.15. Therefore, the natural frequency for the three-dimensional system is estimated to be about 0.57 Hz for section AA. The natural period for section AA including three-dimensional effects is also plotted in Figure 51. The peak ground acceleration at the crest is likely to increase because of this increase in frequency. The estimated three-dimensional crest acceleration at section AA is 1.05 g. At sta 5+00 (section BB), the crest acceleration is not likely to be much higher than that computed using the two-dimensional analysis.

109. The dynamic shear stresses for a three-dimensional dynamic response were estimated again using the results of Mejia and Seed (1983) and accounting qualitatively for the geometry of the river canyon, the internal zoning of the dam, the difference in stiffness between the upstream and downstream shells, and the intensity of the ground motions. A shear stress adjustment factor was derived as a function of normalized depth as shown in Figure 54. At any given point within the embankment, the adjustment factor depends on the ratio of the height of the point above the base of the foundation to the total height of the embankment and foundation at that station of the cross section. The adjustment factor varies from 1.0 (no adjustment) for

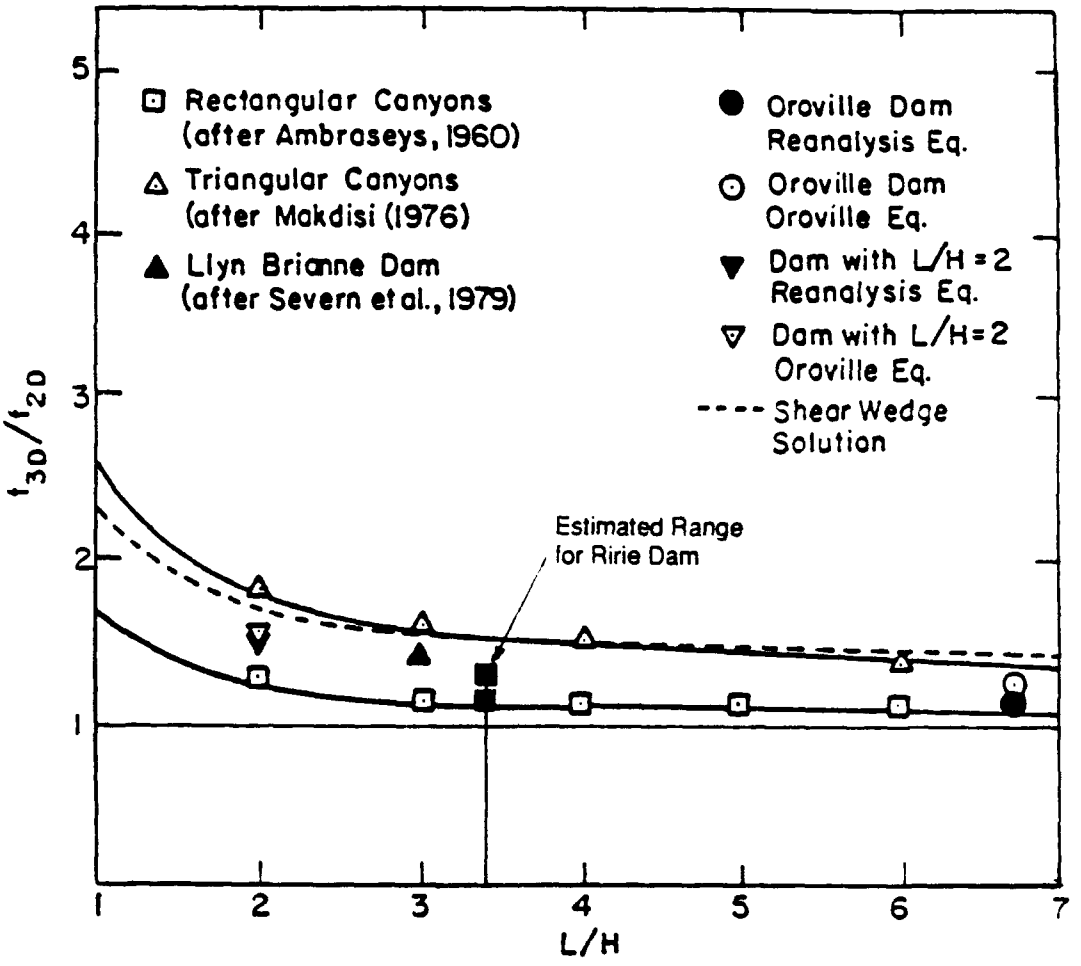

Figure 53. Comparison between natural frequencies computed from two-dimensional and three-dimensional analyses of dams in triangular and rectangular canyons (Mejia and Seed 1983)

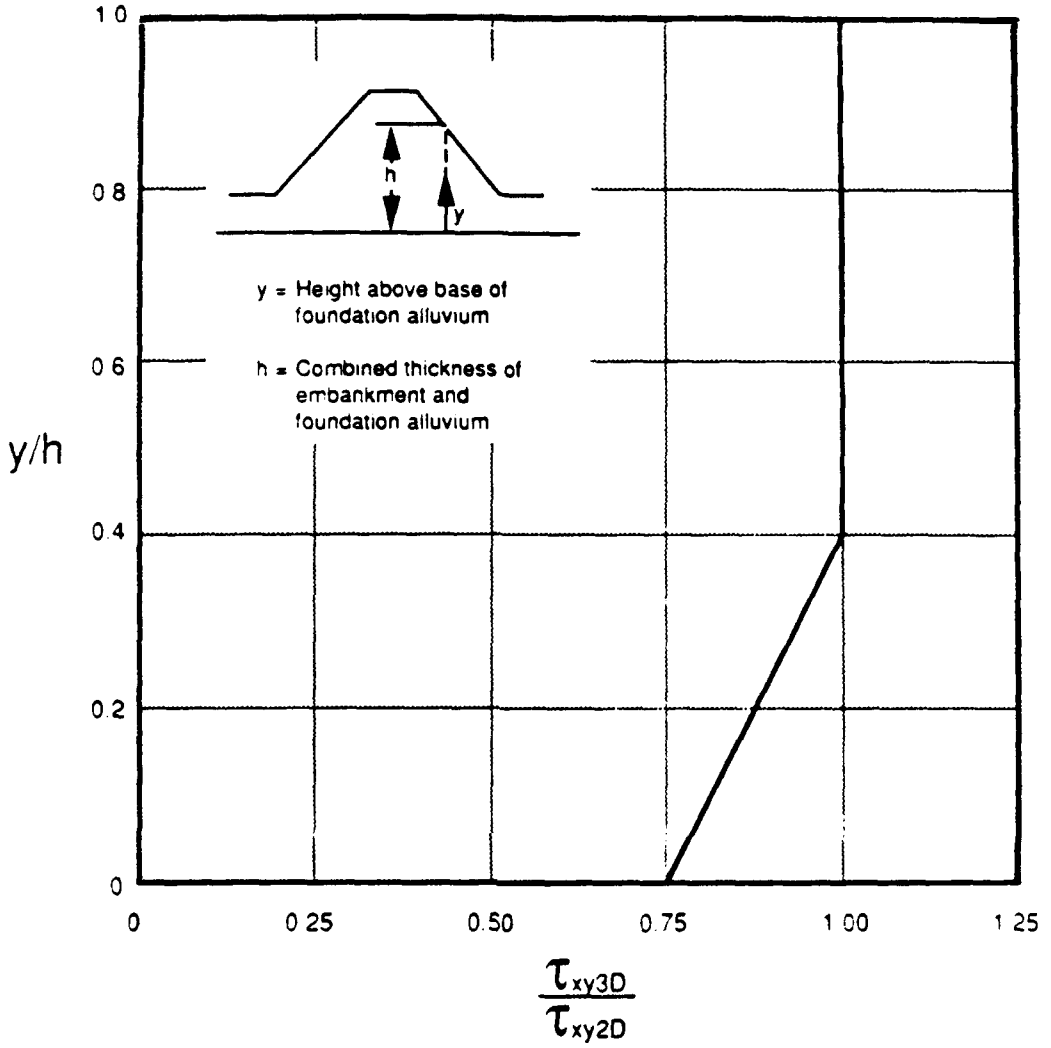

Figure 54. Adjustment factor to estimate three-dimensional horizontal shear stresses from computed two-dimensional horizontal shear stresses (Woodward-Clyde Consultants 1989)

the upper three-fifths of the embankment and foundation height to 0.75 for the lower two-fifths of the embankment and foundation height.

110. It is important to note that the variation of the adjustment factor in Figure 54 applies to shear stresses on horizontal planes, τ_{xy} , or the maximum shear stress on the horizontal plane, $(\tau_{xy})_{max}$. The maximum shear stress, τ_{max}, may not occur on a horizontal plane because of the effects of complementary horizontal shear stress on vertical planes and multi-dimensional shaking. Woodward-Clyde Consultants (1989) estimated the range of $(\tau_{xy})_{max}$ to be:

$$0.85\ \tau_{max} \leq (\tau_{xy})_{max} \leq \tau_{max} \qquad (6)$$

using the results of a study by Mejia and Seed (1981). Typical two-dimensional conditions have the lower bound at 0.9 τ_{max} . Dynamic shear stresses calculated using SUPERFLUSH were assumed to be maximum values ($(\tau_{xy})_{max} = \tau_{max}$) which is a realistic assumption.

111. Shear stresses used for the evaluation of liquefaction potential are not peak values but rather "effective" values corresponding to 65 percent of the peak values. The distribution of maximum shear stresses for sections AA and BB was presented previously in Figure 48. In addition, the effects of the three-dimensional geometry were applied to reduce the stresses. The resulting distribution of three-dimensional-adjusted maximum shear stresses, $(\tau_{.65\ xy3D})_{max}$, for sections AA and BB used for the evaluation of liquefaction potential are presented in Figure 55. Only the embankment and alluvial zones are considered. The shape of contours in the upper portions of the embankment cross sections are very similar to those shown in Figure 48, only the magnitudes differ (by a factor of 0.65). This was expected because the three-dimensional adjustment factor was only administered throughout the bottom two-fifths of the localized height. In the lower two-fifths of the localized height, the distribution of $(\tau_{.65\ xy3D})_{max}$ is similar to the distribution of τ_{max} except the localized stress concentrations are reduced.

Shear Beam Analogy

112. Dakoulas (1989a) reported the results of a comprehensive evaluation of the dynamic response of a shear beam representing Ririe Dam (contained

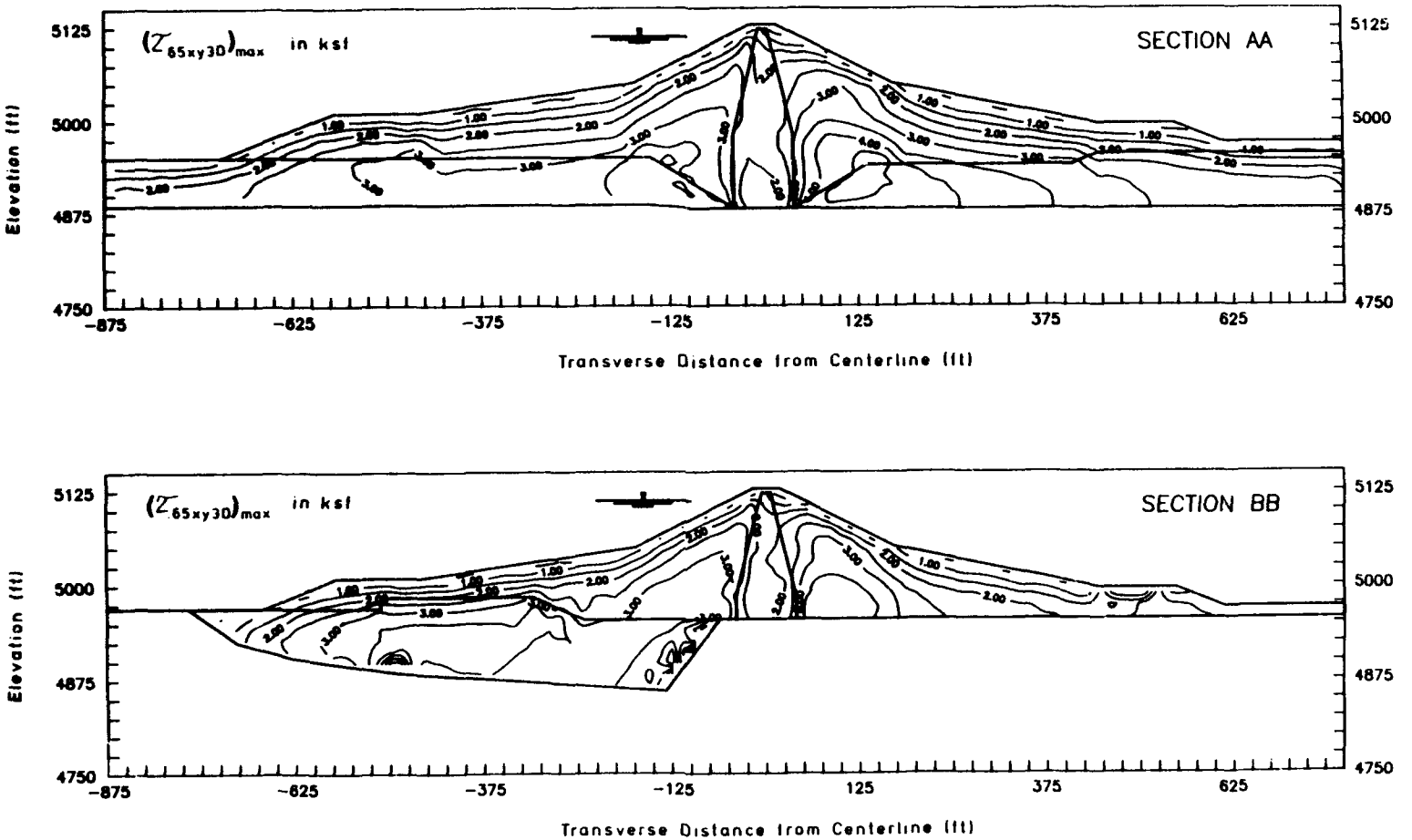

Figure 55. Distribution of effective shear stresses adjusted to account for three-dimensional effects at sections AA and BB for the design ground motions as computed using SUPERFLUSH

in full in Volume II). A shear beam is a continuous system that deforms due to (pure) shear. Motion in the beam can only be in a direction perpendicular to the beam. A shear beam is a mathematical idealization. However, a natural soil deposit is a physical system that may be well represented with a shear beam. When applied to dams, lateral shear deformations are considered to be uniformly distributed across the width of the dam.

113. Three different types of shear beam models were used to account for the most important parameters influencing the response. Combinations of shear beam models, soil models (mostly nonlinear), input motions, thicknesses of the dam and foundation and profiles of shear wave velocity were varied to evaluate a range of potential effects. Each of the three models is described below and the results of the calculations presented.

Model 1

114. Model 1 represents the canyon with an equivalent rectangular shape and the dam as a triangular wedge lying on a soil foundation layer at the bottom of the canyon as shown in Figure 56. This model is coded in the computer program DLC as described by Dakoulas (1989b). The embankment materials are assumed to be hysteretic (dependent on strain history) with a single (constant) mass density, ρ_1 , and a profile of shear modulus defined by the relation:

$$G(z) = G_b \, (z/H)^m \tag{7}$$

where

G_b = shear modulus at the base of the dam

m = inhomogeneity parameter

H = height of the dam (and foundation)

z = depth from the crest

which is uniform across the width of the valley. The foundation layer consists of a uniform layer with constant mass density, ρ_2, hysteretic damping ratio, β_2 , and shear modulus, G_2 . The seismic excitation consists of horizontally polarized shear waves propagating in the vertical direction and oriented with maximum accelerations in the direction of the valley, similar to the dynamic response analyses. The base can be either rigid or flexible.

115. These assumptions constitute the basis for classic shear beam models and seem to realistically represent conditions at Ririe Dam.

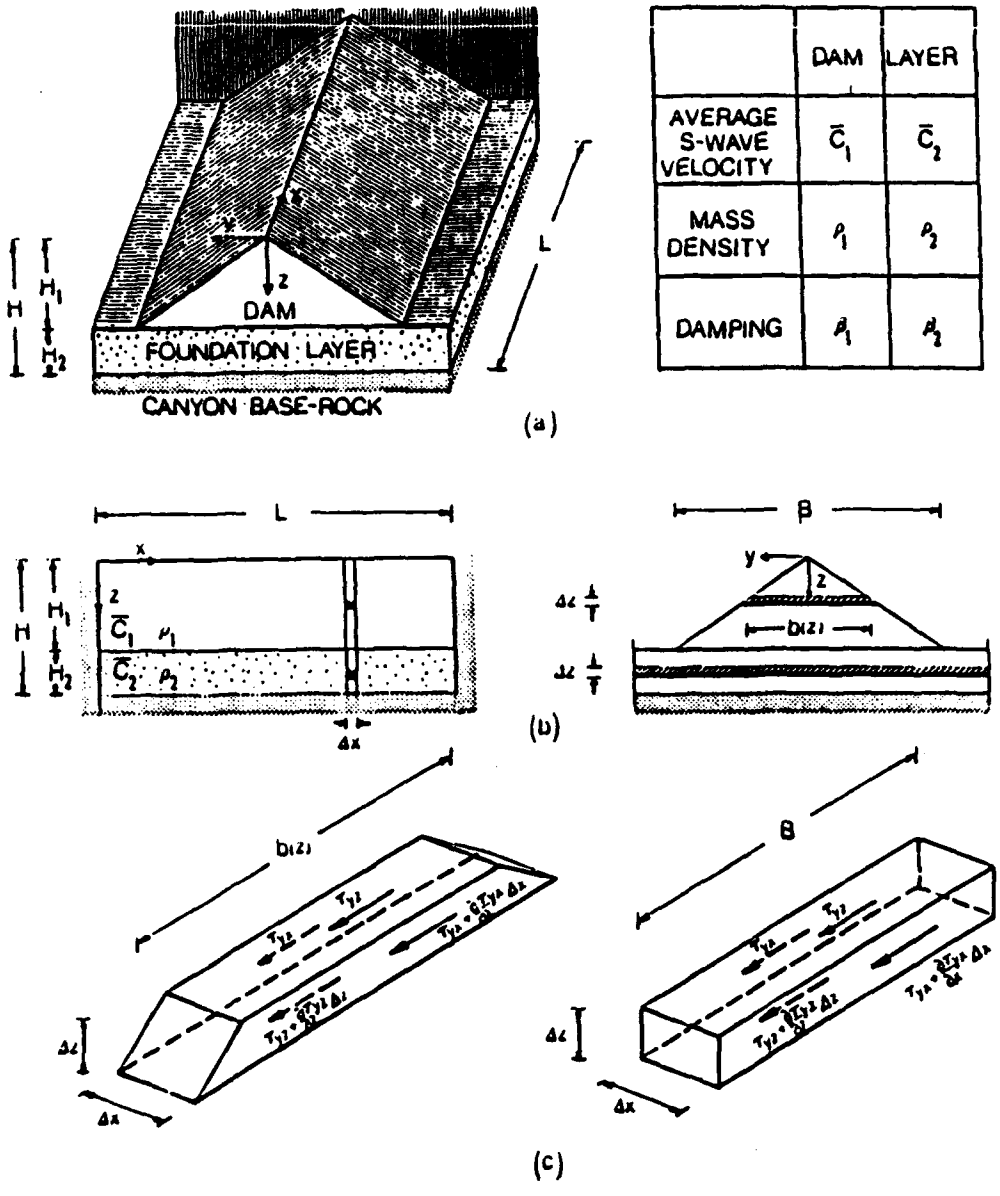

	DAM	LAYER
AVERAGE S-WAVE VELOCITY	$\bar{C}_1$	$\bar{C}_2$
MASS DENSITY	ρ_1	ρ_2
DAMPING	β_1	β_2

Figure 56. Shear beam model 1 used by Dakoulas (1989a)

Comparisons of results on seismic response obtained from detailed analyses of earth dams have confirmed the validity of the above assumptions (Dakoulas and Gazetas 1985; Dakoulas and Gazetas 1986; and Gazetas 1987).

Model 2

116. Model 2 idealizes the dam as an infinitely long truncated triangular shear beam as shown in Figure 57. This model is coded in the computer program NISB as described by Dakoulas (1989b). This model was derived under the assumption that nonlinearity of material properties has a greater effect than the geometry (narrowness) of the canyon. The distribution of shear modulus within the embankment is the same as that defined in Equation 7 and used in model 2. The (average) shear wave velocity of the embankment was 1,245 fps. The height of the dam was assumed to be 200 ft. No other parameters were necessary.

Model 3

117. Model 3 idealizes the dam as a triangular, homogeneous shear wedge in a semicylindrical canyon as shown in Figure 58. The model is coded in the computer program DCYL as described by Dakoulas (1989b). Although the canyon geometry at Ririe Dam is not semicylindrical, it was considered to be useful to examine the response of this model simulating embankment conditions at Ririe Dam.

Presentation of results

118. A total of eight cases were evaluated using the three shear beam models representing various combinations of input parameters. Three cases were considered for each of models 1 and 2; two cases were considered for model 3. Combinations of input parameters and the corresponding results are presented in Table 8.

119. The natural frequencies calculated for the eight cases range from 2.17 to 2.5 Hz (corresponding to natural periods of 0.46 and 0.4 sec, respectively). This range has frequencies much larger than those determined for the three-dimensional response (about 0.57 Hz) and measured for the Mt. Borah earthquake (1.76 Hz). These higher frequencies indicate that the shear beam models are much stiffer systems than desired and coincidently correspond to a range of larger spectral accelerations of the design earthquake (refer to Figure 51).

120. The peak horizontal accelerations calculated for the eight cases range from 1.23 g to 1.97 g. Again, the magnitude of accelerations using the

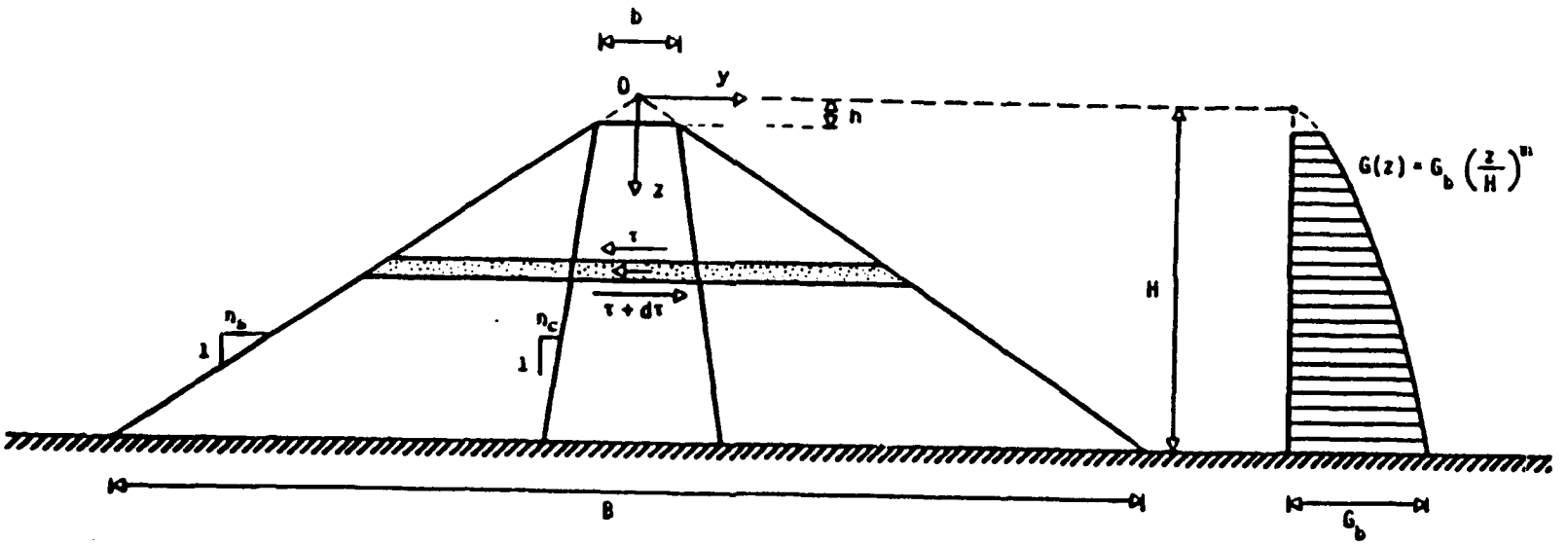

Figure 57. Shear beam model 2 used by Dakoulas (1989a)

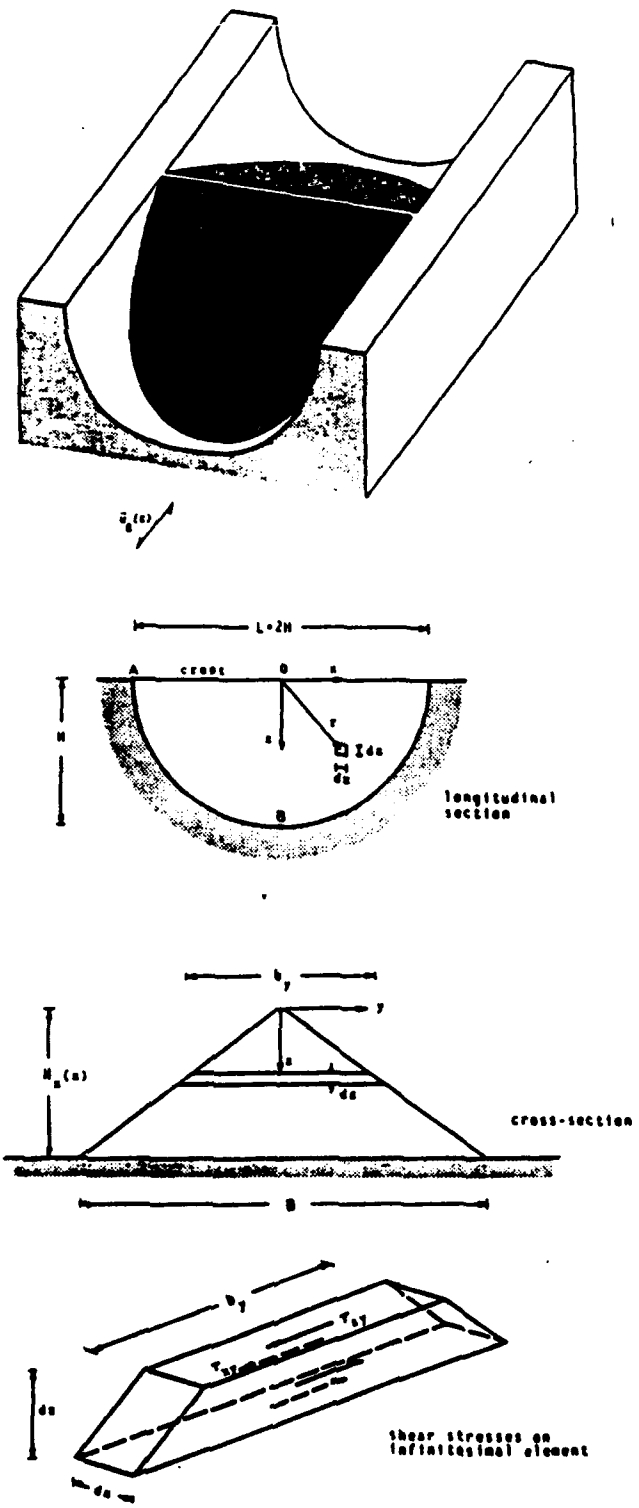

Figure 58. Shear beam model 3 used by Dakoulas (1989a)

Table 8

Various Cases Used for Shear Beam Analysis (Dakoulas 1989a)

Case	Model	Foundation Stiffness	Soil Idealization	Input Motion	Thickness, ft		Shear Wave Velocity, fps			Natural Frequency Hz	Peak Acceleration g's	Peak Strain percent	Peak Displacement ft
					Dam	Foundation	Dam	Foundation	Rock				
1	1	Rigid	Nonlinear (piecewise)	Seed (1987)	78	122	1,050	1,300	--	2.17	1.49	1.08	1.60
2	1	Flexible	Nonlinear (piecewise)	Deconv.	78	122	1,050	1,300	3,000	2.17	1.52	0.85	1.21
3	1	Flexible	Nonlinear (piecewise)	Deconv.	118	82	1,102	1,330	3,000	2.33	1.53	0.77	0.86
4	2	Rigid	Nonlinear (piecewise)	Seed (1987)	200	--	1,245	--	--	2.27	1.23	0.69	1.11
5	2	Flexible	Nonlinear (piecewise)	Deconv.	200	--	1,245	--	3,000	2.27	1.33	0.52	0.83
6	2	Flexible	Nonlinear (piecewise)	Deconv.	200	--	1,245	--	3,000	2.33	1.32	0.53	0.89
7	3	Flexible	Nonlinear (piecewise)	Deconv.	178	--	1,210	--	3,000	2.5	1.41	0.44	0.60
8	3	Flexible	Equivalent linear	Deconv.	262	--	1,210	--	3,000	2.33	1.97	0.69	1.30

shear beam models are considerably larger than the three-dimensional crest acceleration of 1.05 g estimated using adjusted SUPERFLUSH results. The higher accelerations are also indicative of a stiffer system and reflect the close proximity of the frequency to the frequency at which peak spectral accelerations occur. The profiles of peak horizontal accelerations for each case are presented in Figure 59. The range of data is moderately wide, tending to converge to a common value at the base. The results using model 1, in general, tend to produce the greatest accelerations. Model 2, in general, tends to produce the lowest peak accelerations.

121. The peak shear strains calculated for the eight cases range from 0.44 to 1.08 percent. These strains must be converted to effective shear strains in order to compare with the distribution of shear strains shown previously in Figure 47. Accordingly, the range is 0.29 to 0.70 percent. The peak shear strain determined using SUPERFLUSH was about 2.0 percent, much larger than the shear beam results. This difference is consistent with the shear beam representing a stiffer system which would incur lower shear strains. The profiles of peak shear strains for the eight cases are shown in Figure 60. The shear strain at the ground surface is zero. Again, the range of data is moderately wide. Some discontinuities are evident for cases 2 and 3 which result from the use of two materials (dam and foundation).

122. The maximum displacements (relative to the base) calculated for the eight cases range from 0.60 to 1.60 ft. The profiles of displacements for each case are presented in Figure 61. The greatest displacements tend to be produced using model 1. The smallest displacements tend to be produced using model 2. The results of SUPERFLUSH were used in the seismic stability evaluation since they were determined from a more representative numerical model of the in situ problem.

Conclusions

123. The dynamic response of Ririe Dam to the design earthquake has been calculated using the finite element program SUPERFLUSH for two-dimensional cross sections. The results of SUPERFLUSH indicate that large dynamic shear stresses will be induced and amplification of ground motions will occur by the embankment. The natural period of the dam is considerably greater than the period corresponding to peak spectral accelerations of the

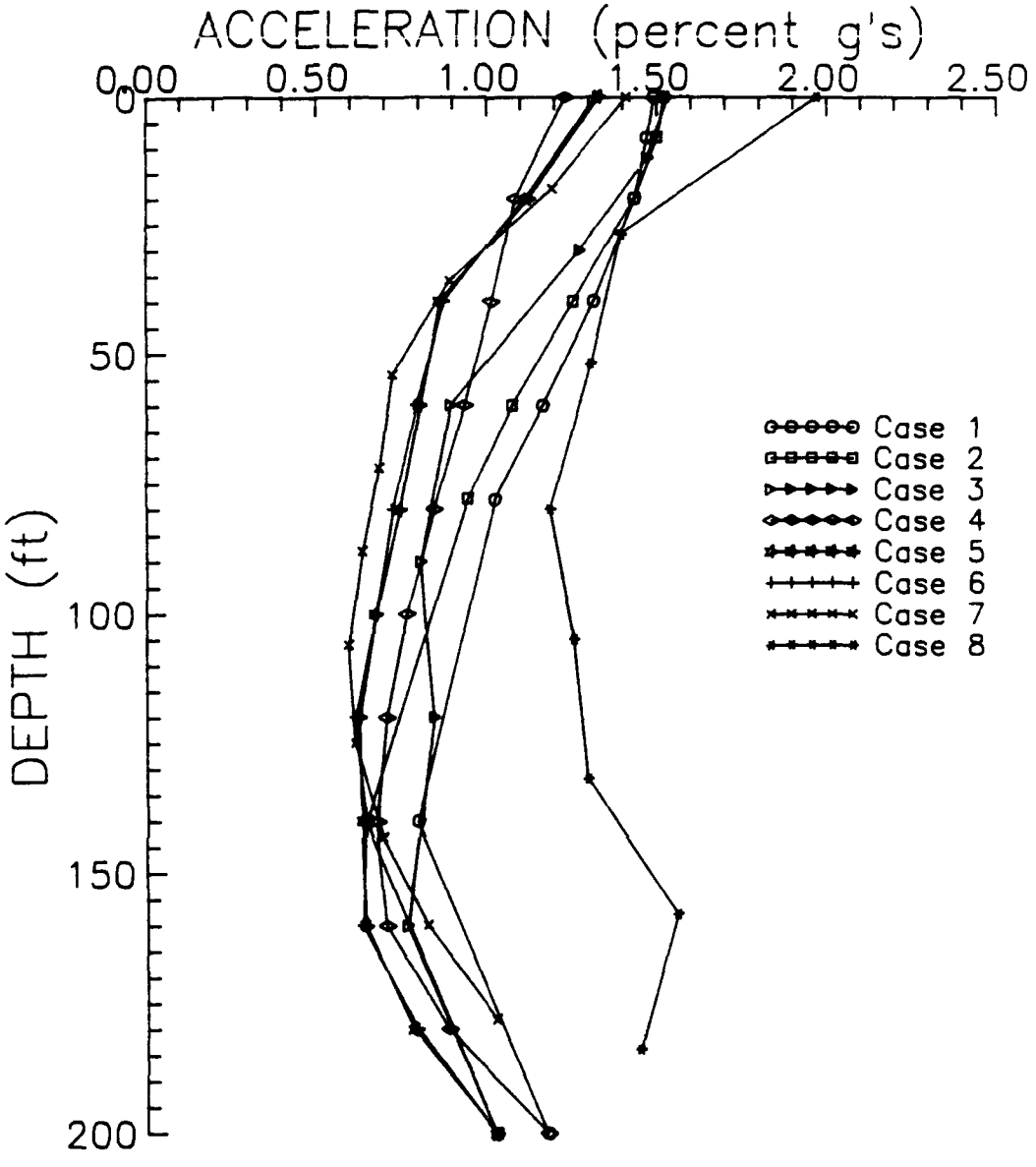

Figure 59. Comparison of profiles of maximum acceleration for the various cases considered using shear beam analyses

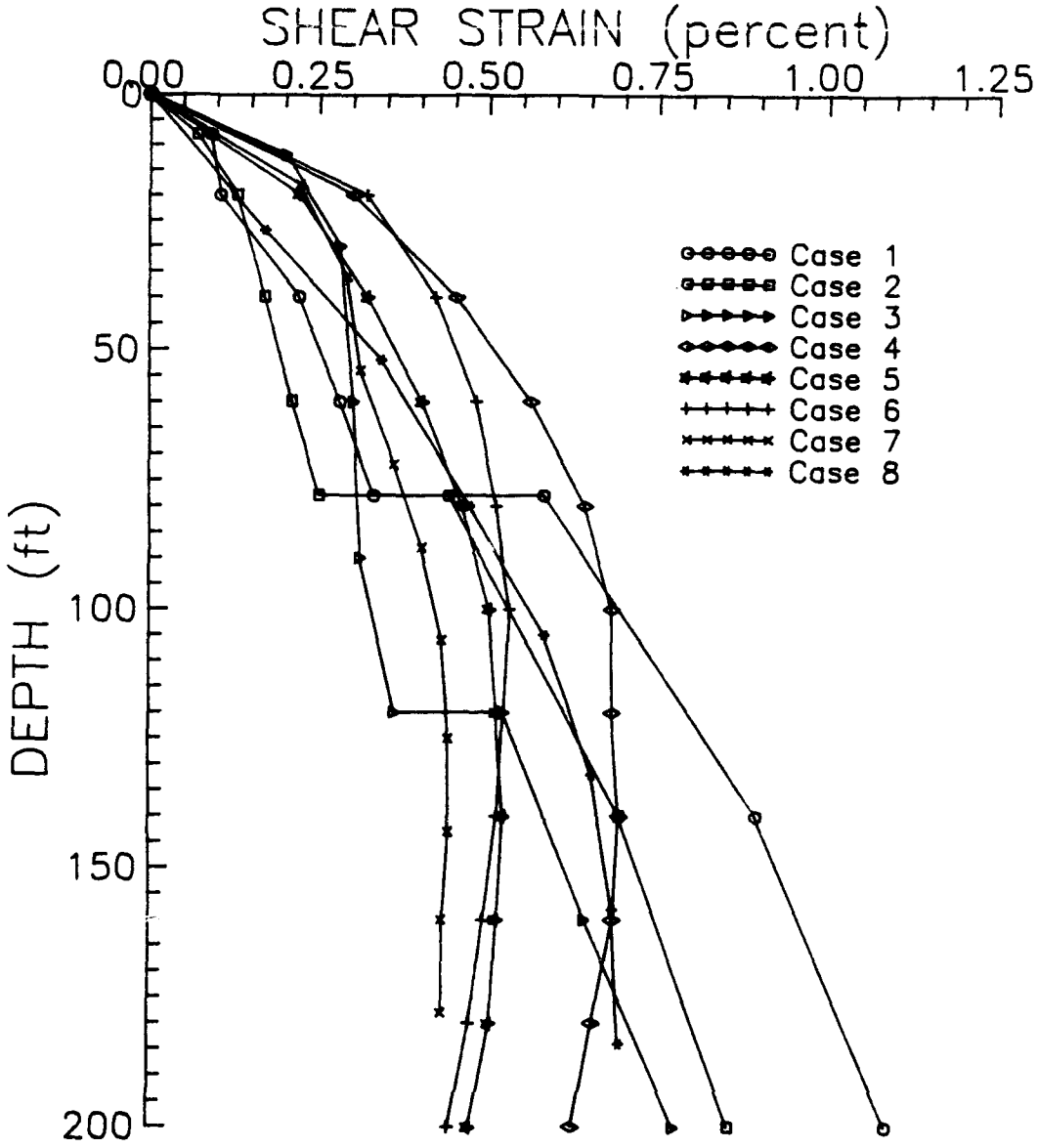

Figure 60. Comparison of profiles of maximum shear strain for the various cases considered using shear beam analyses

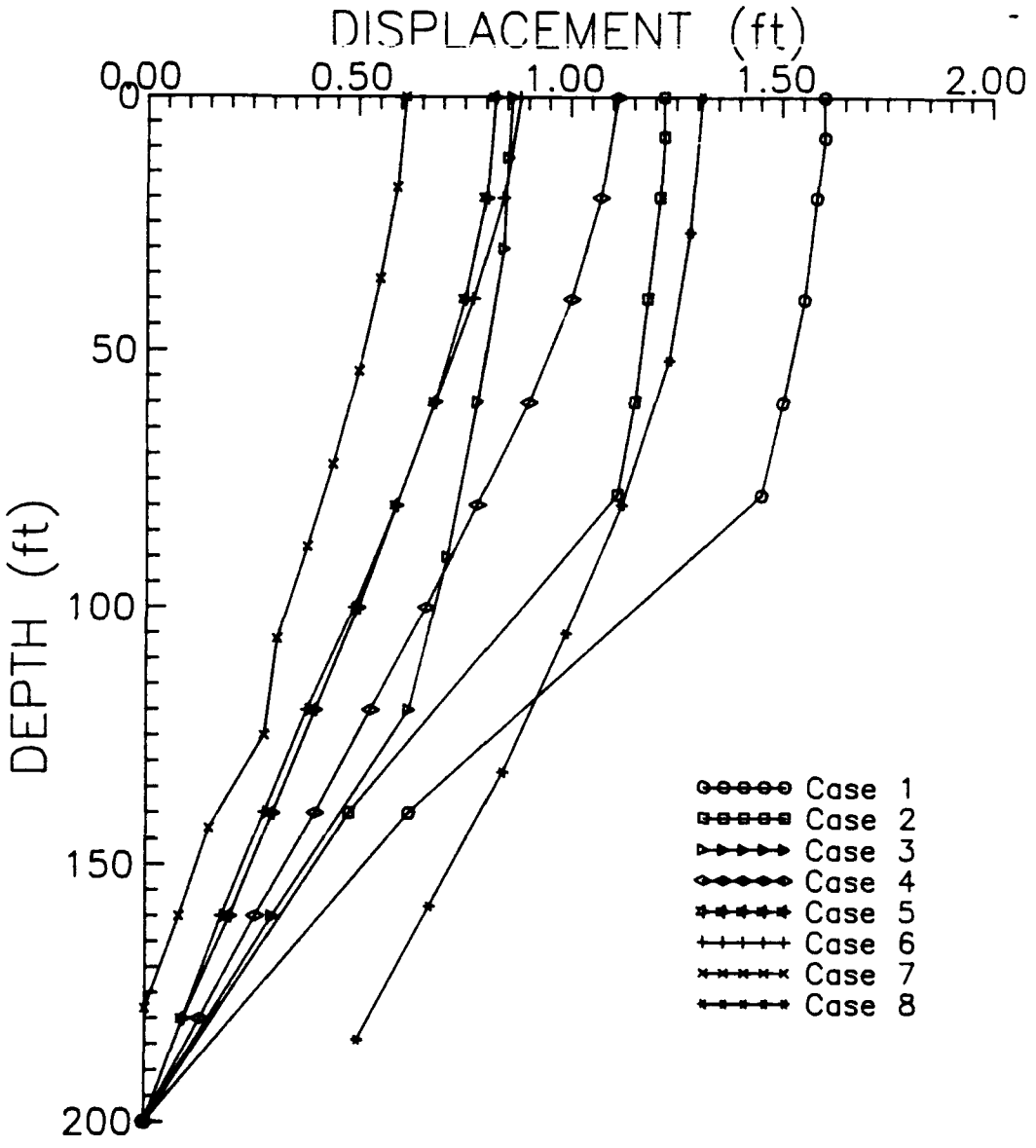

Figure 61. Comparison of profiles of maximum displacement for the various cases considered using shear beam analyses

design earthquake. The results of the two-dimensional calculations and the experience gained from previous studies indicate that three-dimensional response can be adequately predicted with empirical and analytically derived adjustment factors applied to the two-dimensional results.

124. A one-dimensional wave amplification algorithm was used to confirm the magnitude of accelerations and computed shear stresses. In general, there was good agreement between the two methods. A shear beam analogy was used to apply three different shear beam models to compare with various aspects of dynamic response. In general, these models produced different results than those obtained with SUPERFLUSH. The SUPERFLUSH results are used in the remaining chapters since they were derived from a more realistic numerical representation of the field problem.

PART VI. LIQUEFACTION POTENTIAL EVALUATION

Introduction

125. Slope or foundation instability consequent to the reduction in shear strengths due to the generation of excess pore water pressures was considered to assess the potential for loss of freeboard. Excess pore water pressures reduce the strength of a material because of the reduction in effective confining stress. Furthermore, if excess pore water pressures reach 100 percent (of the corresponding vertical effective stress), liquefaction is expected to occur in these zones. Liquefied materials exhibit a very low strength compared with the strength of the same material with no excess pore water pressure. The shear stresses estimated for the three-dimensional dynamic response of Ririe Dam were used to evaluate the susceptibility to liquefaction.

Performance-Based Approach

126. The performance-based approach was introduced at the outset of this report. The procedure described by Seed (1983) specific to evaluation of the potential for liquefaction involves:

a. Selecting the design earthquake motions.

b. Evaluating the long-term static stresses in the dam and its foundation prior to the earthquake.

c. Computing the dynamic stresses induced in the dam and its foundation by the selected design earthquake.

d. Estimating the cyclic strength of embankment and foundation materials using relations derived from empirical data.

e. Evaluating the pore pressure generation and postcyclic strength of the dam and foundation materials.

f. Based on the results of steps c and d, evaluating the overall stability of the dam.

The components of the design earthquake (step a) were previously shown in Figures 15 through 17. The static stress analysis and dynamic response (stress) analysis (steps b and c) were presented in previous chapters of this report. The pore pressure generation and cyclic strength characteristics of the embankment and foundation materials (step e) were evaluated and summarized in Report 1. The remaining step to the evaluation of liquefaction potential

involves the comparison of earthquake-induced dynamic stresses to available dynamic shear strength.

Material properties

127. The derivation and selection of material properties and various laboratory relations necessary to conduct the liquefaction potential analysis, presented in Report 1, are described briefly below for convenience. The cyclic stress ratio, τ_{av}/σ_o' , is the primary parameter used for liquefaction potential analysis. The cyclic stress ratio has been found to be a convenient parameter for expressing the cyclic liquefaction characteristics of a material (Seed and Idriss 1981). The cyclic stress ratio is the ratio of the average cyclic shear stress developed on horizontal surfaces as a result of the earthquake loading to the vertical effective stress before the dynamic stresses are applied, σ_o' and represents the cyclic strength at an effective vertical stress of 1 tsf and with no shear stress on horizontal planes ($\alpha = 0$). The cyclic strength ratio has the advantage of accounting for the depth of the soil, location of the water table, and the intensity of earthquake shaking.

128. Values of the cyclic stress ratio were derived from equivalent values of $(N_1)_{60cs}$ using recent data reported by Seed et al. (1985) as described in Report 1. A summary of cyclic stress ratios is presented in Table 9. Values of cyclic stress ratio were not assigned to materials considered to be not susceptible to liquefaction. The locations of zones within the dam and foundation for sections AA and BB that are and are not potentially susceptible to liquefaction are shown in Figure 62. Materials considered to be susceptible to liquefaction are loose and medium-dense gravel alluvium and submerged random fill. All other materials are assumed to be capable of producing only limited excess pore pressures (generally less than 20 percent of the vertical effective stress).

129. Laboratory studies were performed to determine the pore water generation characteristics of the various materials. Cyclic triaxial undrained shear tests were conducted on samples of gravel alluvium as summarized in Report 1. Relations for other potentially liquefiable materials were estimated based on physical properties and using the results of tests on similar samples. Two relations used for each material account for the influence of effective stress and shear stresses on horizontal planes in situ.

Table 9

Cyclic Stress Ratios Used for Liquefaction Analysis

Material Type	Average $(N_1)_{60cs}$	Percentage of Fines	τ_{av}/σ_o'
Random fill	25	7	0.31
Alluvial silt	11	45-50	N.L.*
Loose gravel	16	4	0.18
Medium dense gravel	26	4-5	0.31
Very dense gravel	51	7	N.L.

* N.L. = Nonliquefiable.

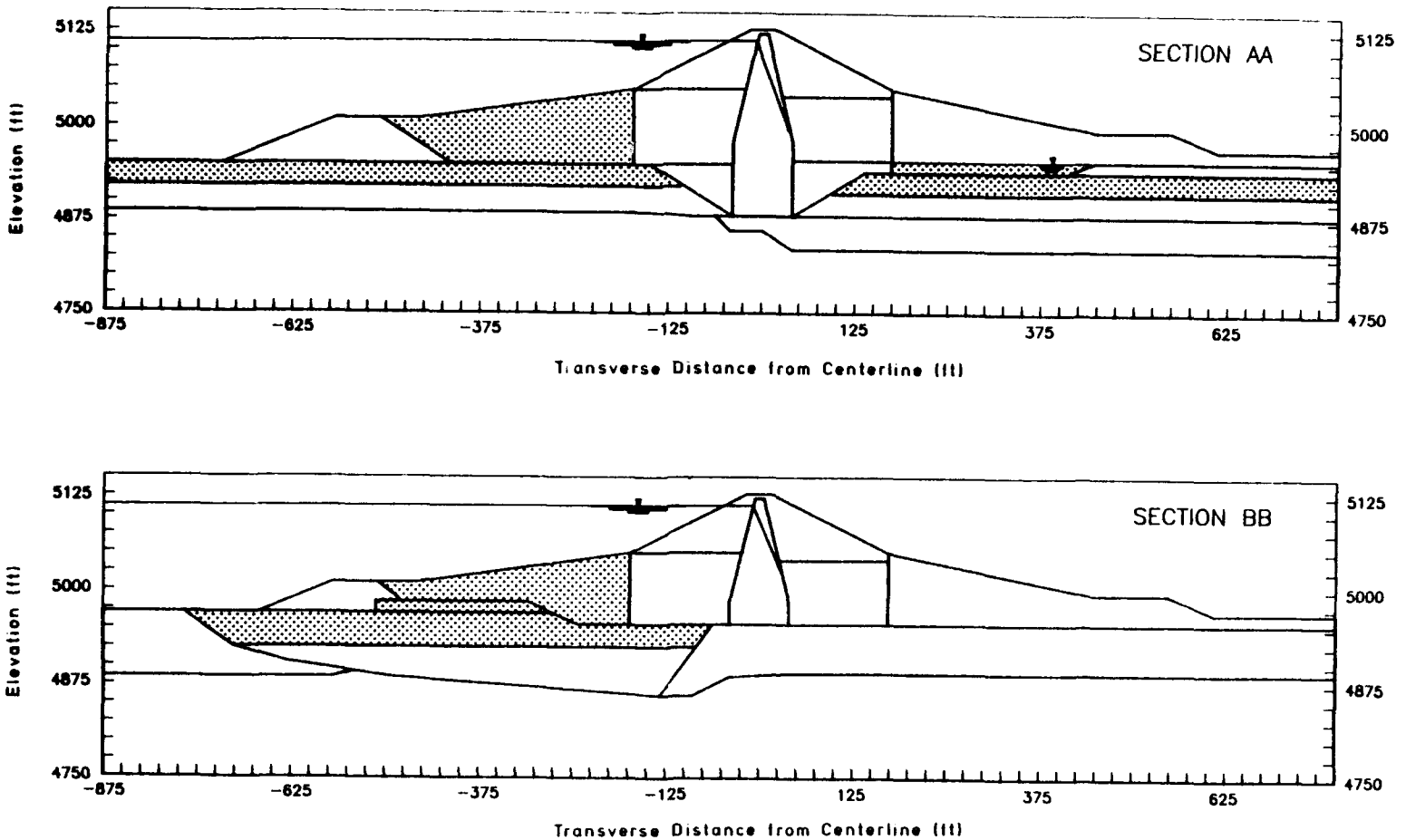

Figure 62. Cross sections used to evaluate liquefaction potential showing the locations of zones susceptible to liquefaction

A third relation allows the determination of the pore pressure ratio, R_u:

$$R_u = \frac{\Delta u}{\sigma_v'} \tag{8}$$

where Δu equal the change in residual excess pore water pressure knowing the factor of safety against liquefaction, FS_L . The use of each of these relations is described in the following sub-sections.

Available cyclic strength

130. The cyclic stress ratio, τ_{av}/σ_o' , for each material corresponds to an effective vertical stress of 1.0 tsf and $\alpha = 0$ (i.e., no shear stresses on a horizontal plane). The adjusted cyclic stress ratio, CSR, calculated for each element reflects the effects of nonlevel ground and effective stress and is calculated using the following equation:

$$CSR = (\tau_{av}/\sigma_o')\ K_\sigma\ K_\alpha \tag{9}$$

where

K_σ = adjustment factor to account for effective vertical stress

K_α = adjustment factor to account for variation of α

The relations used to derive K_σ and K_α were presented in Report 1 and are shown in Figures 63 and 64.

Dynamic shear stresses

131. The dynamic shear stresses were determined by applying the empirical factor of 0.65 to the peak shear stresses calculated in the two-dimensional dynamic response analysis. The stresses were then adjusted to account for the three-dimensional effects, $(\tau_{.65\ xy3D})_{max}$, according to the adjustment factor shown previously in Figure 54. The distribution of $(\tau_{.65\ xy3D})_{max}$ throughout sections AA and BB were shown previously in Figure 48.

Comparison of stresses

132. The factor of safety against liquefaction, FS_L, is defined as:

$$FS_L = CSR/((\tau_{.65\ xy3D})_{max}/\sigma_v')) \tag{10}$$

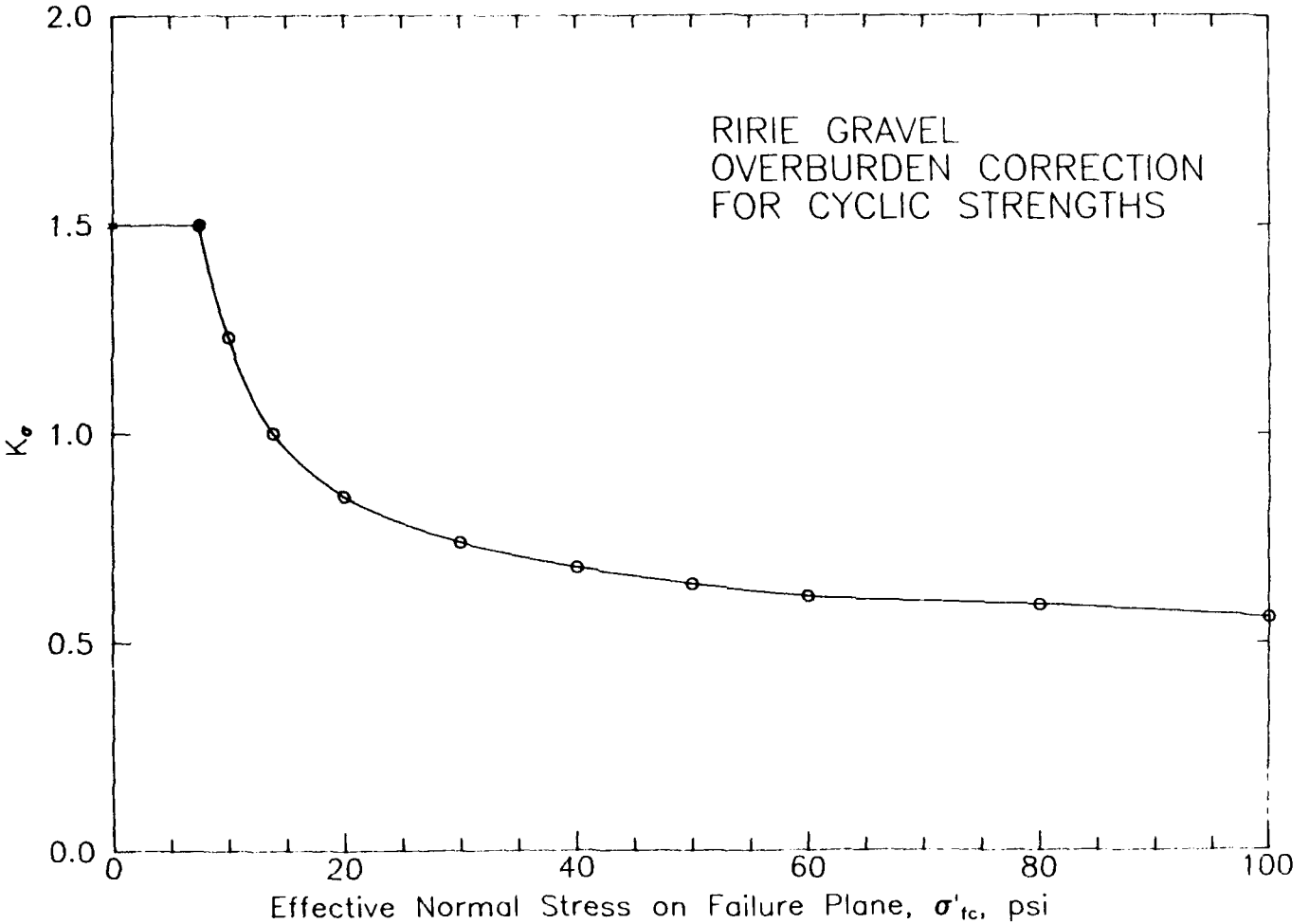

Figure 63. Effective overburden stress correction factors determined from *laboratory cyclic* triaxial tests on loose Ririe Dam gravel specimens

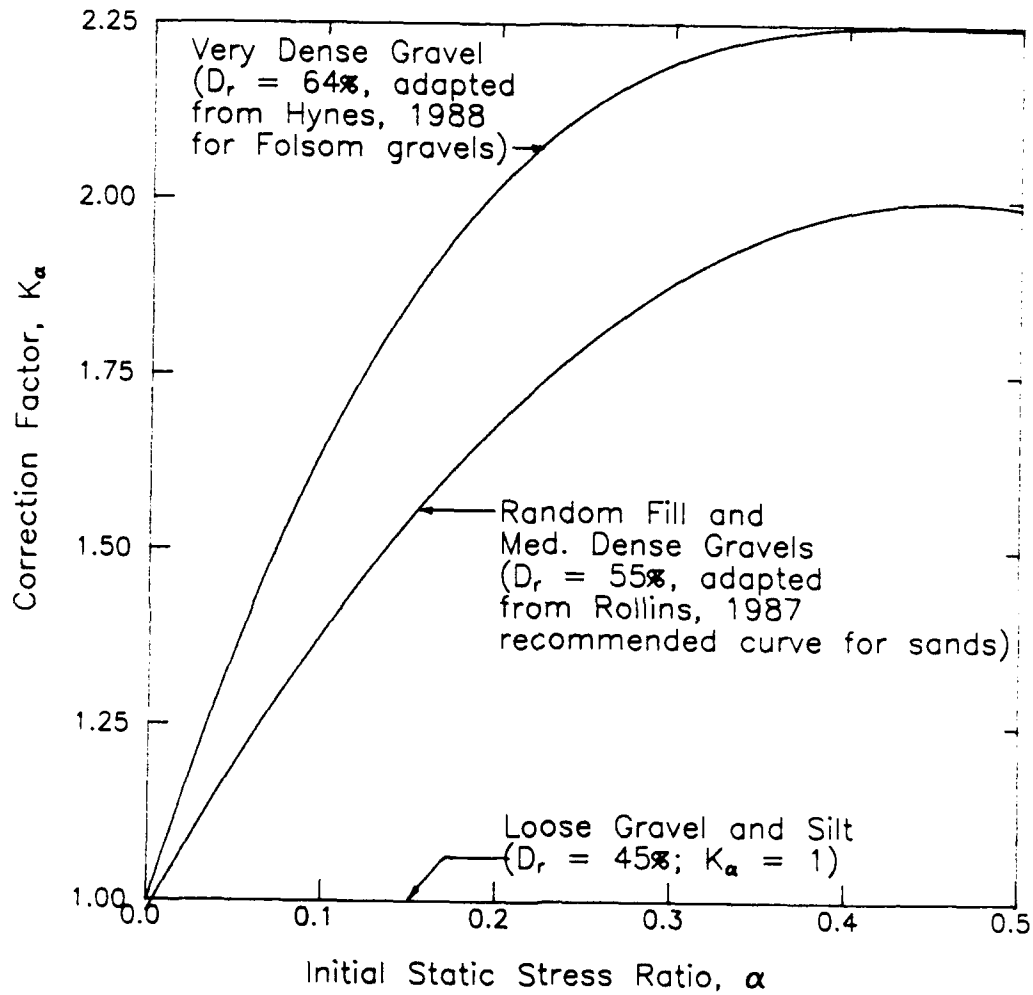

Figure 64. Initial shear stress correction factors for Ririe Dam alluvial foundation soils

The material element under consideration is said to liquefy if $FS_L < 1.0$. If the material element does not liquefy ($FS_L \geq 1.0$), the excess pore water pressure expected to develop can be analyzed using Figure 65. So, FS_L and R_u may be determined for each finite element in the cross sections.

Presentation of Results

133. The results of the performance-based approach indicate that all of the submerged random fill (downstream and upstream) and most of the upper alluvium (downstream and upstream) will liquefy (R_u = 100 percent). Rock and gravel fill, the core material, downstream random fill, the lower portion of the gravel alluvium, and alluvial silt downstream were shown earlier not to have a potential to liquefy. The elements which were determined to liquefy ($FS_L < 1$) are indicated in Figure 66 for section AA and BB. Only a small portion of the upper alluvium are not expected to liquefy. The pore water pressures in the zones of potentially liquefiable material that did not liquefy are quite large. The values of FS_L for potentially liquefiable materials were as low as 0.23 and 0.16 for sections AA and BB, respectively.

Conclusions

134. The results of a performance-based liquefaction analysis using the results of a two-dimensional dynamic response analysis including three-dimensional effects indicate that submerged random fill and large portions of the upper alluvium will liquefy as a consequence of the design earthquake. The actual extent of zones of alluvium that will liquefy are confined to upper layers of loose gravel and medium dense gravel that were idealized to exist in the upper portion of alluvium. The excess pore water pressures developed in the remaining portions of the alluvium are very high. The rock fill, gravel fill, core, very dense gravel alluvium (at depth) and silt alluvium Xarenot expected to develop significant excess pore water pressures when subjected to the design earthquake.

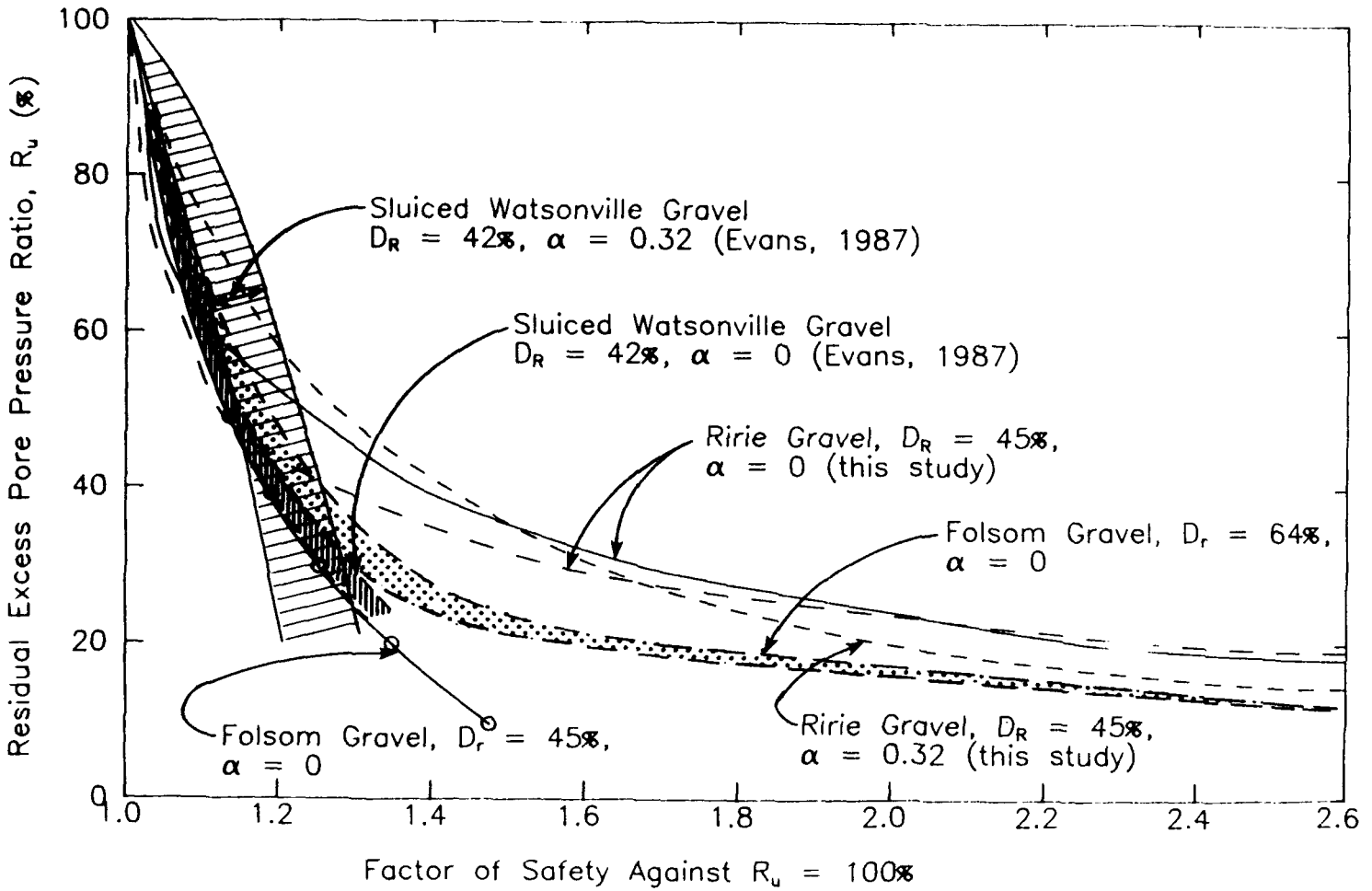

Figure 65. Comparison of laboratory determined R_u versus safety factor against R_u = 100 percent for Ririe Dam gravels with other data from tests on gravels

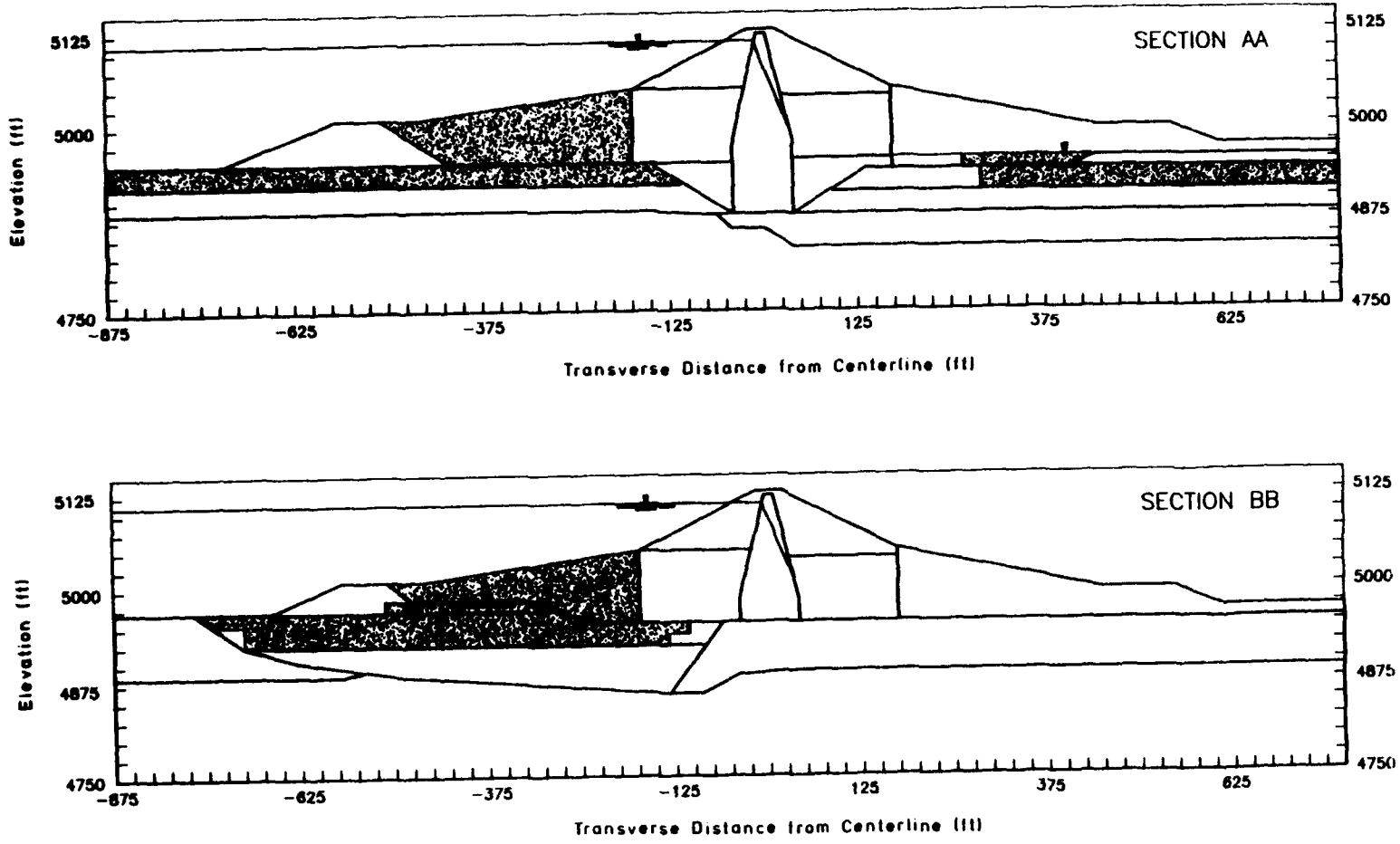

Figure 66. Results of liquefaction analysis showing the locations of elements that are expected to liquefy as a consequence of the design ground motions

PART VII: POSTEARTHQUAKE SLOPE STABILITY ANALYSIS

Introduction

135. The potential for sliding of the dam on weakened foundation materials causing a loss of freeboard was evaluated following the determination of zones that would liquefy and the distribution of excess pore water pressures in other regions. This slope stability evaluation involved (static) limit equilibrium calculations of upstream and downstream slopes using the computer program UTEXAS2 (Edris and Wright 1987). UTEXAS2 is a versatile two-dimensional slope stability program that has been implemented on a personal computer. The program allows automatic searching of both circular and non-circular critical slip surfaces. Factors of safety against sliding may be determined using any of several procedures. The factor of safety against sliding is the ratio along the slip surface of shearing strength (stress) required for just-stable equilibrium to shear stresses. A method proposed by Spencer (1967) was used to calculate factor of safety for this study because it satisfies complete static equilibrium (force and moment) for each slice (i.e., it is statically complete). Either total stress or effective stress analysis is possible; a combined approach was selected for this study.

Definition of Input Parameters

136. The computer program UTEXAS2 requires details about the cross section including: locations and distributions of various material zones (defined by "profile" lines), unit weights and material strengths, location(s) of piezometric surface(s), distribution of any excess pore water pressures, surface pressures (if any), coordinates defining the initial trial surface, and details of search procedures. Some of the many options include: means of defining material strength, inclusion of tension cracks, reinforcement, and seismic coefficient, and limiting various parameters of the search iterations and force imbalance. The process of deriving all of the input parameters is described in the following subsections.

Representative cross sections

137. Two cross sections were desired for postearthquake stability analysis corresponding to general section locations used for the dynamic

response calculations. Although a staggered section was used to best represent the dynamic response of a maximum-height section, a curved cross section was selected for postearthquake stability because it better represents the conditions acting on failure surfaces in the curved valley. This procedure is similar to that used by Azzouz and Baligh (1989a). Specifically, a circular arc was used through the embankment, then becoming straight at the upstream and downstream sides, coinciding with the valley axis. The effect of using a curved section is to lengthen horizontal distances and flatten slopes; vertical distances are unaffected. The curved section, in plan called section CC, and corresponding profile are shown in Figure 67. The cross section representing the "quarter section" was again derived using a straight-line projection located transverse at sta 5+00 and is referred to as section DD. Cross sections CC and DD used for the postearthquake stability analysis are shown in Figure 68. Thin zones of material considered to have a negligible effect on the analysis were not included. Cross section CC incorporates 20 different continuous material layers, the maximum allowed in UTEXAS2. Section DD is very similar to section BB shown in Figure 20 with minor modifications made to accommodate use of UTEXAS2.

138. The contact between the embankment and foundation materials was carefully analyzed using available information to derive the representative sections. Material profiles from drill holes along the profiles were used to locate the depth to bedrock. The downstream alluvial silt (see Figure 20) was combined with the liquefied loose alluvial gravel because of the limitation of the number of material zones allowed. This is considered to be a conservative simplification given that alluvium was found to liquefy and alluvial silt was found to be nonliquefiable.

Material strengths

139. The specific material properties used for postearthquake stability calculations are listed in Table 10. Some of these parameters were taken from Table 6 while others were derived specifically for the stability calculations from these values or by other means. Additionally, material properties were varied to evaluate the sensitivity of the results to material strengths. Mohr-Coulomb parameters (c and ϕ) were used to represent the shear strength of all materials in which R_u < 100 percent. Residual strengths (cohesion term only) were used to represent the shear strength of all materials in

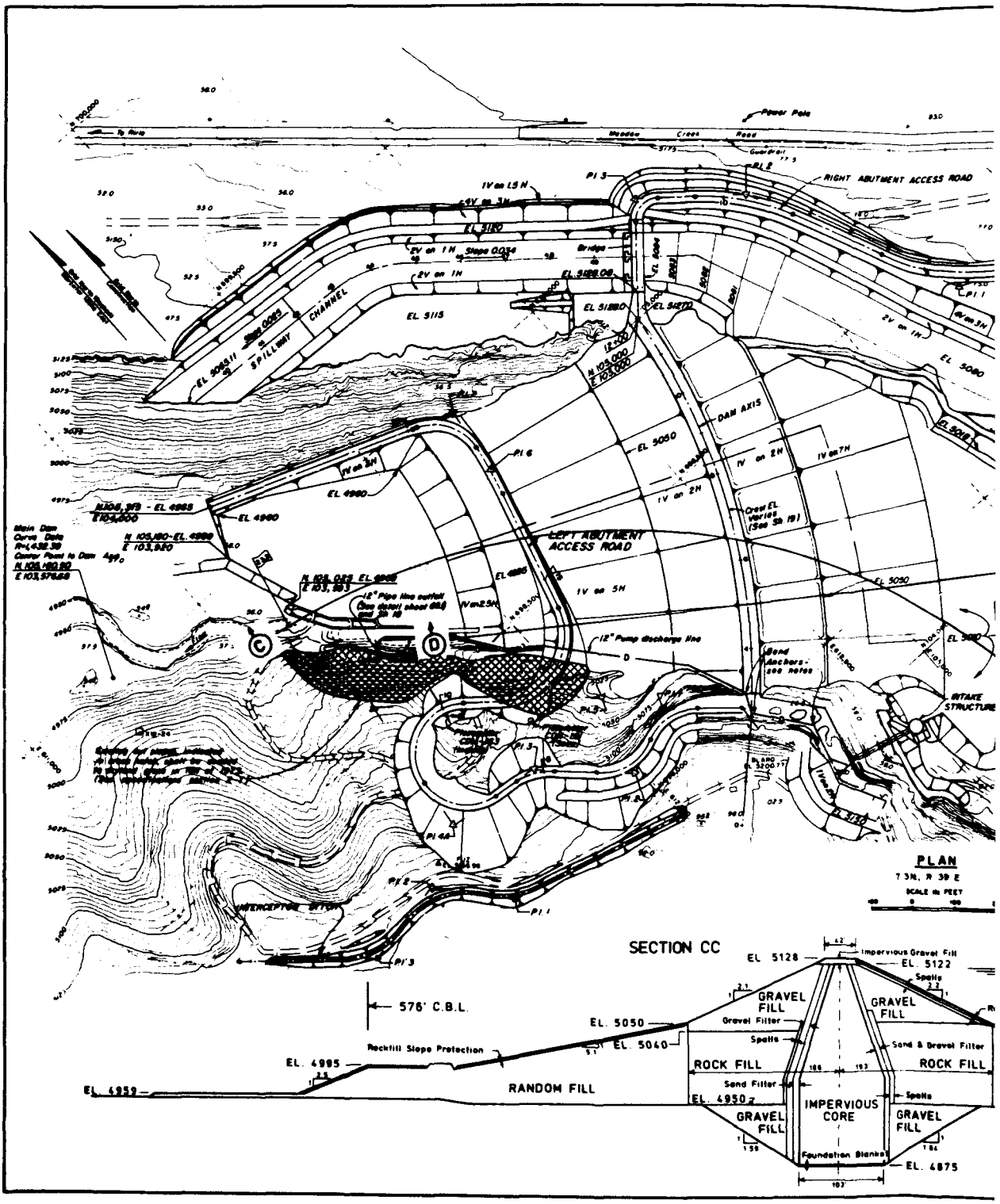

Figure 67. Plan view of project area showing the locations of section

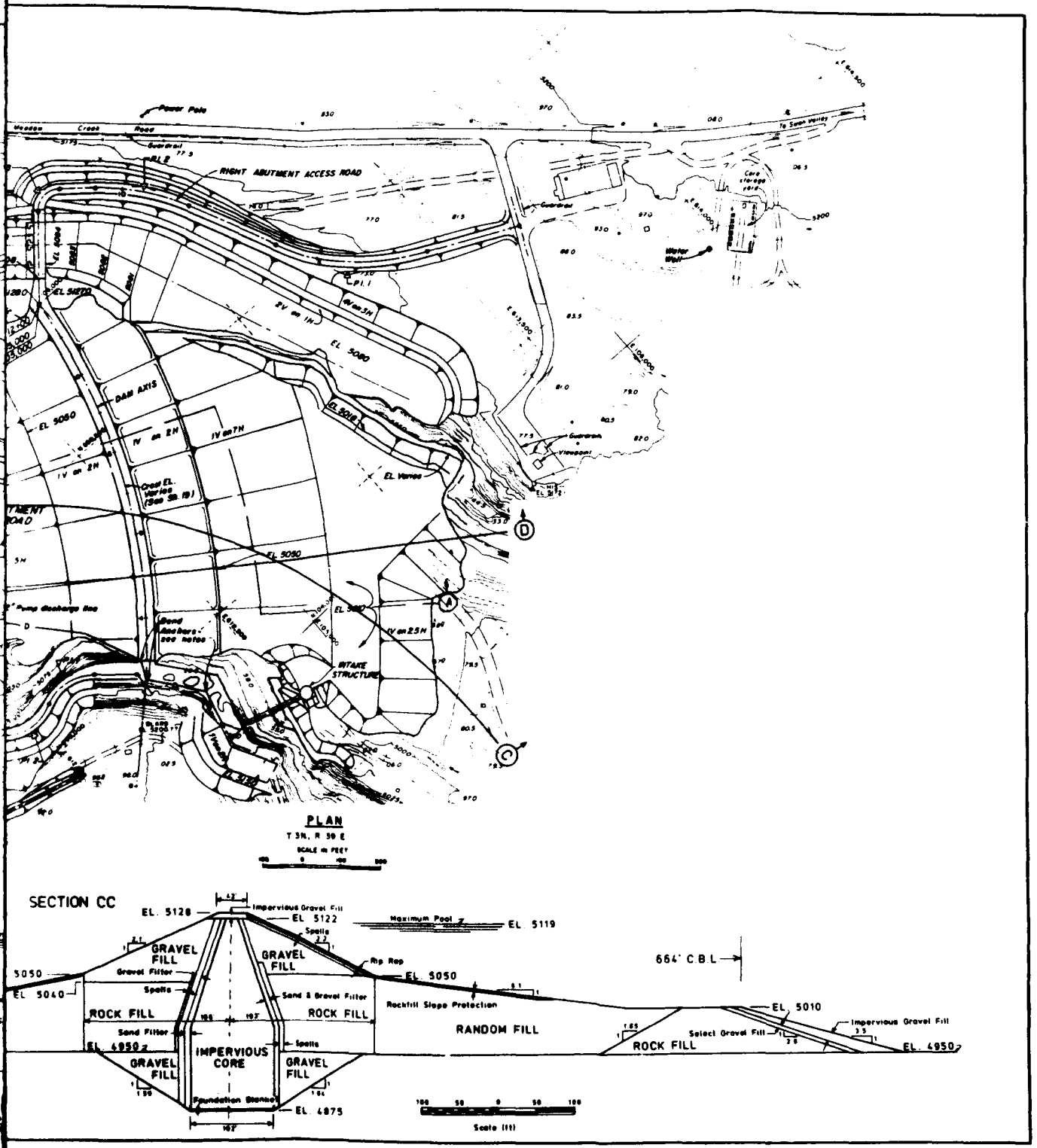

showing the locations of sections used for postearthquake stability analyses

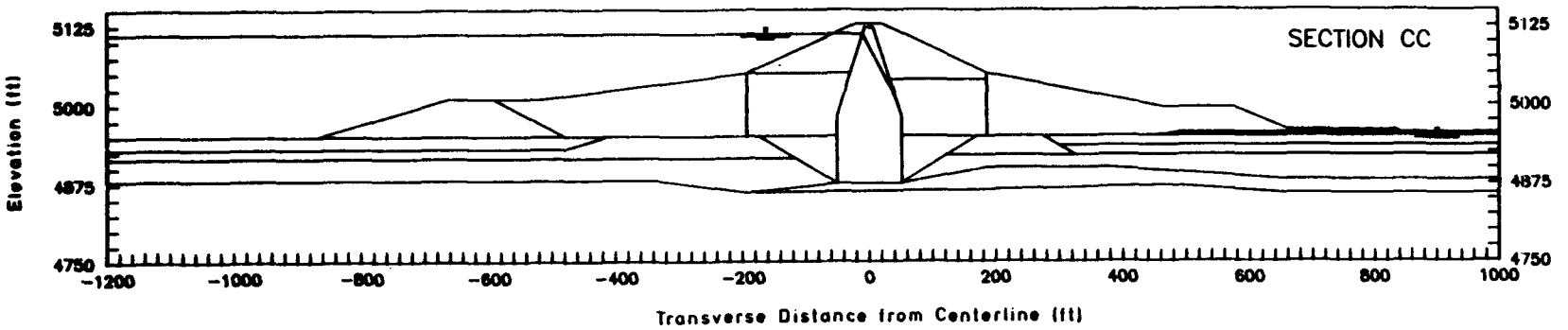

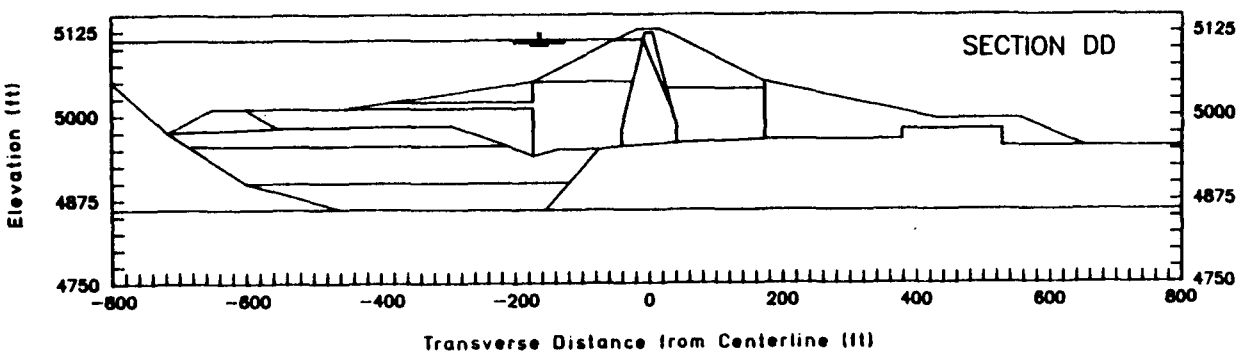

Figure 68. Cross sections CC and DD used to evaluate postearthquake stability

Table 10

Material Properties Used for Postearthquake Slope Stability Calculations

Material	Condition	Total Unit Weight pcf	Mohr-Coulomb ϕ', deg	Mohr-Coulomb c', psf	Residual Strength* psf
Gravel Fill	Unsubmerged	135	48	0	--
	Submerged	145	48	0	--
Silt Core	Unsubmerged	120	35	0	--
	Submerged	125	35	0	--
Rock Fill	Unsubmerged	135	48	0	--
	Submerged	145	48	0	--
Random Fill	Unsubmerged	130	45	0	--
	Submerged	140	--	--	1,200
Loose gravel alluvium**	Submerged	135	--	--	500
Medium-dense gravel alluvium	Submerged	144	48	0	1,200
Very dense gravel alluvium	Submerged	147	50	0	--
Tuffaceous sediments	Submerged	155	30	1,500	--
Basalt	Submerged	150	33	5,000	--

* Liquefied zones only.
** Silt alluvium combined with loose gravel stratum.

which R_u = 100 percent. The selection of material properties is described below.

140. Static shear strengths. Static shear strengths were assumed to be isotropic (shear strength is independent of the orientation of the failure plane) and were defined using the Mohr-Coulomb failure criterion involving the parameters: cohesion, c , and angle of internal friction, ϕ . An effective stress analysis was chosen, so effective stress parameters (c' and ϕ') were evaluated based on an average of consolidated-drained and consolidated-undrained (with pore pressure measurements) triaxial shear compression tests. Representative values of drained, c'_d and ϕ'_d , and undrained, c'_{cu} and ϕ'_{cu} , strength parameters (presented in Table 3) were averaged for the upper tuffaceous sediments to obtain c'_{avg} and ϕ'_{avg} for slope stability calculations. The average strengths for tuffaceous sediments determined from laboratory tests during construction and the strengths used in the analysis are compared in Figure 69a. A strength criterion for the core material was assumed to be purely frictional, very similar to the internal friction measured in the laboratory during construction. The strength envelope used for the analysis and the those for consolidated-drained and consolidated-undrained tests for core material are shown in Figure 69b. The collection of material strength envelopes are shown in Figure 70.

141. Residual strengths. Residual strength refers to the strength that a material retains following liquefaction. This inherent resistance consists purely of a cohesion term (independent of effective stress). Few studies have been possible to analyze appropriate residual strengths for various materials. One such study which focused on the slide resulting from the liquefaction of hydraulic-fill sand at the Lower San Fernando Dam was reported by Seed et al. (1989). The residual strengths were back-calculated from slope stability calculations and correlated with the SPT N-value corrected for effective overburden stress, energy efficiency, and percentage of fines, $(N_1)_{60}$ (described in Report 1). The resulting correlation is shown in Figure 71 along with a data point for gravel from Whiskey Springs, Idaho (Harder 1988).

142. Most of the data shown in Figure 71 have low values of $(N_1)_{60}$ (less than 15 blows per ft); whereas, the liquefiable materials at Ririe Dam have average values of $(N_1)_{60}$ ranging between 16 and 26. Therefore, some extrapolation of the correlation is necessary. Professor H. B. Seed recommended the use of the lower bound of the range shown in Figure 71

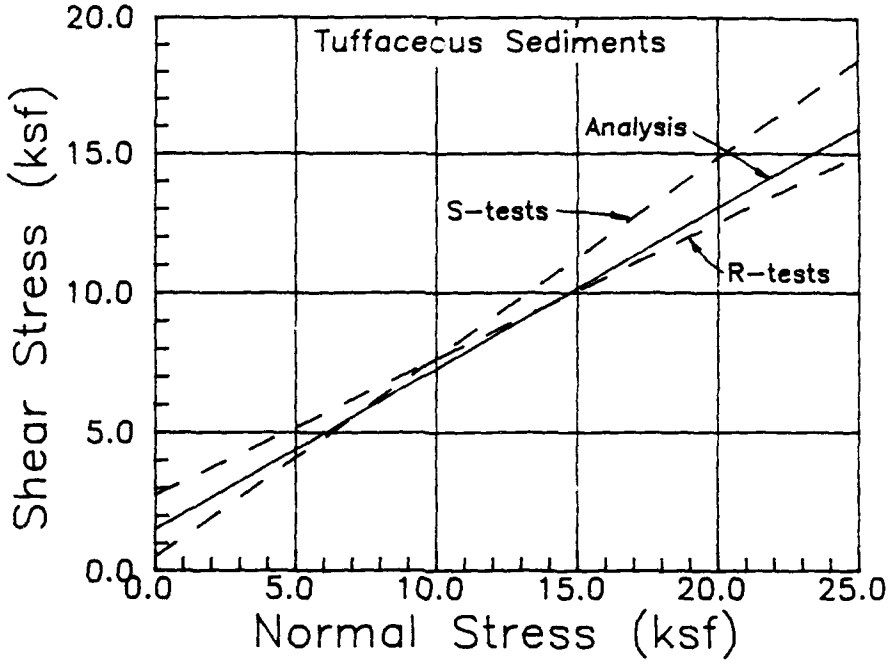

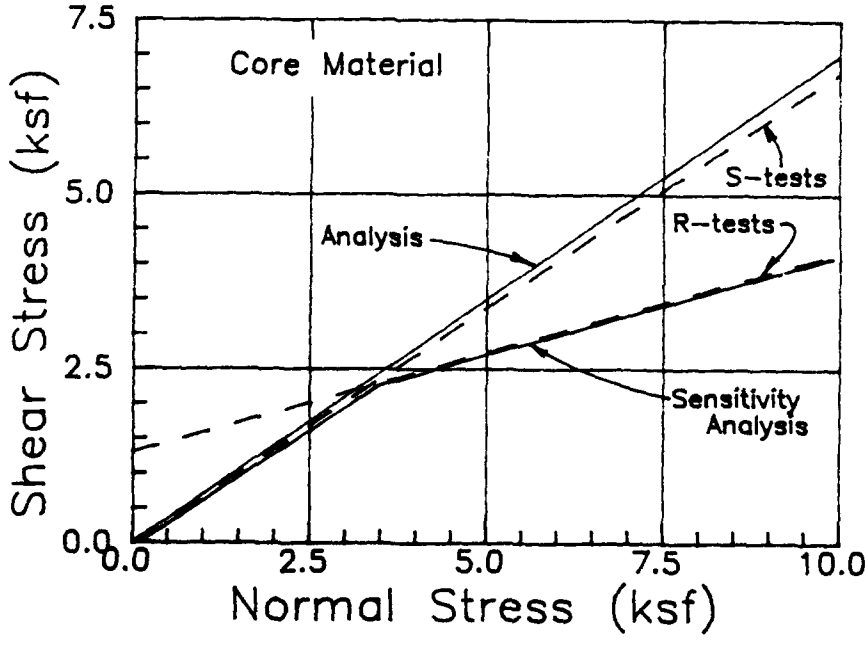

Figure 69. Derivation of Mohr-Coulomb failure envelopes for core material and tuffaceous sediments

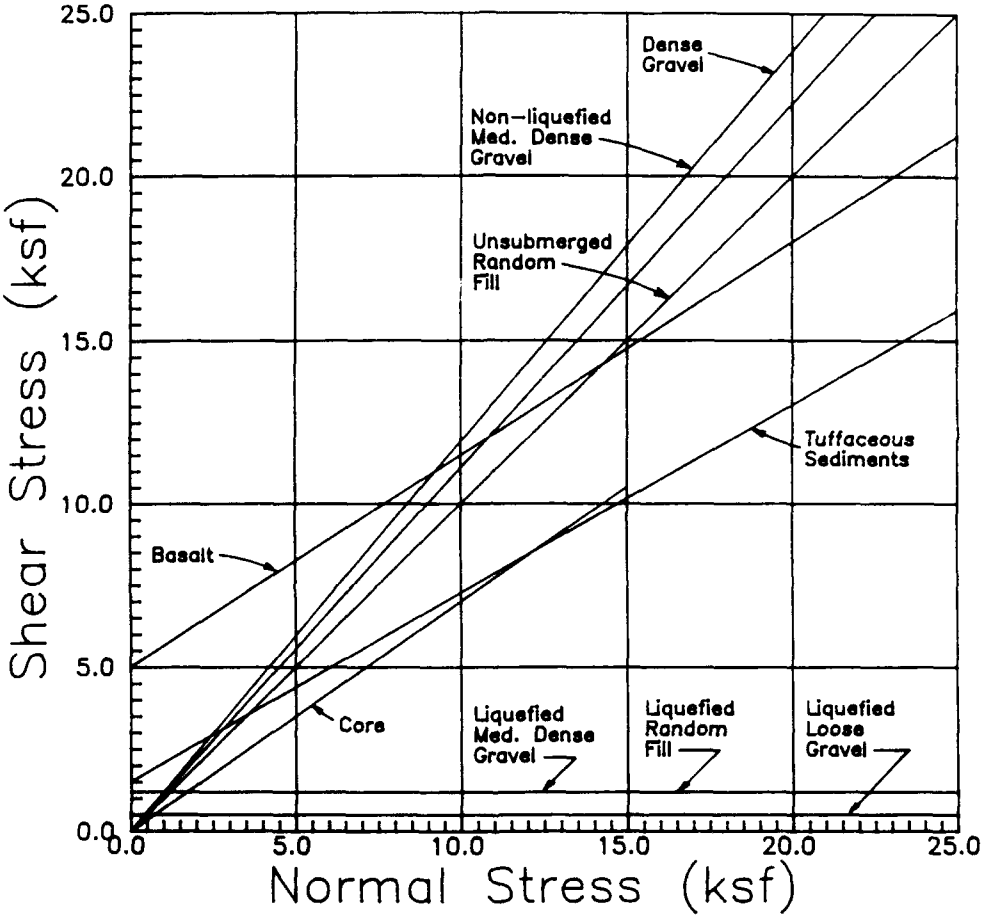

Figure 70. Mohr-Coulomb failure envelopes used for postearthquake stability studies

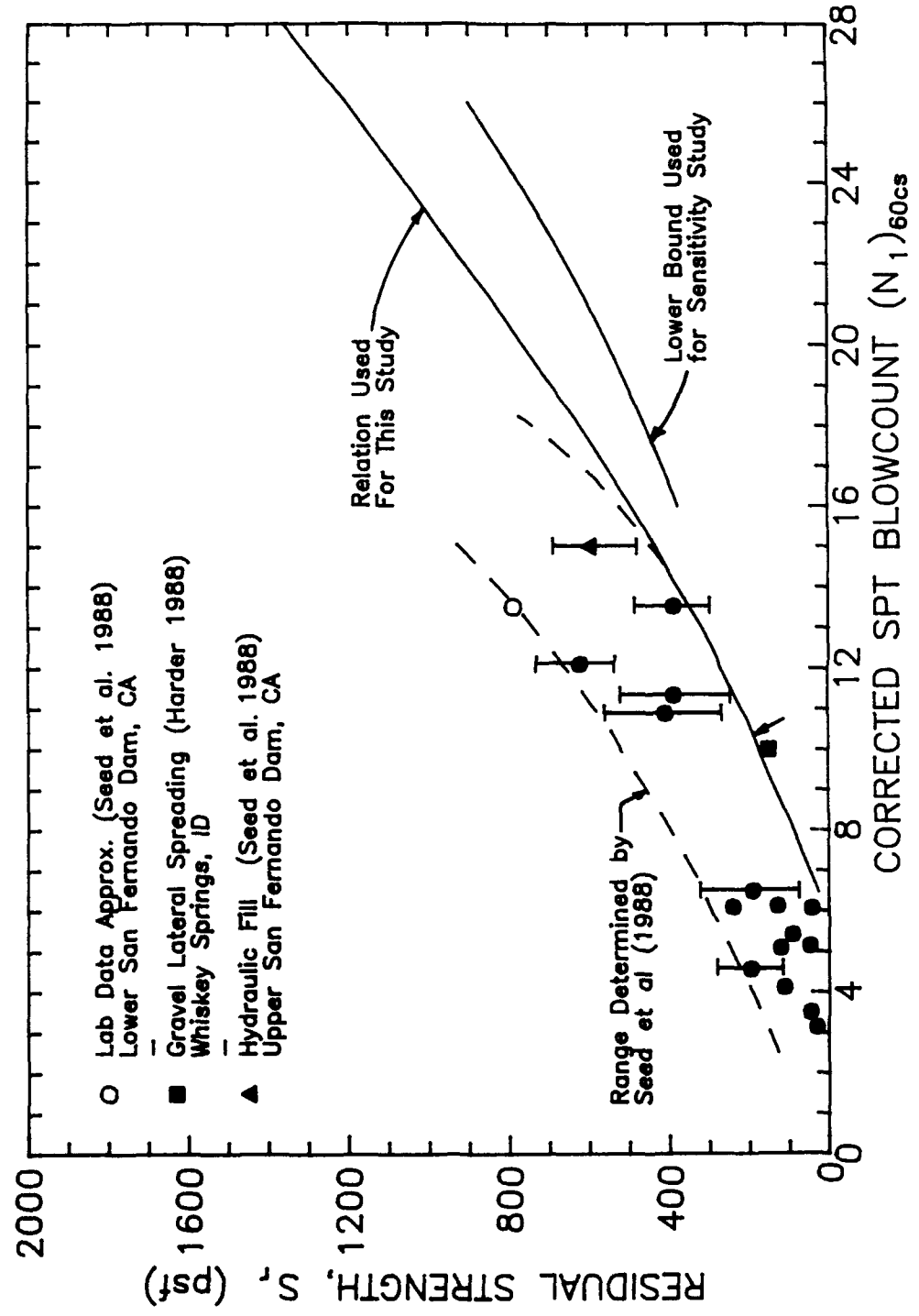

Figure 71. Empirical relation used to derive residual strengths (Seed et al. 1989)

for this study. The data point for gravel falls on this lower bound. A mobilized shear strain of 15 percent was assumed for purposes of this study.

Pore water pressures

143. A single piezometric surface was used to allow calculation of pore water pressures and the effective stress at any point in the cross section. The piezometric surface selected based on piezometric data was shown previously in Figure 10.

144. Excess pore water pressures were also used in the postearthquake stability analysis. Excess pore water pressures that did not reach 100 percent of the effective overburden stress (liquefy) were produced in only small portions of potentially liquefiable materials for sections CC and DD. The liquefaction potential evaluation determined an excess pore water pressure for each element of potentially liquefiable material. UTEXAS2 can interpolate excess pore water pressures given a grid of known values. Therefore, the excess pore water pressures for each element in the nonliquefied zones of potentially liquefiable materials were input directly to UTEXAS2.

Surface pressures

145. The procedure recommended by Edris and Wright (1987) to conduct effective stress slope stability calculations for submerged slopes (upstream slope at Ririe Dam) is to use total unit weights of materials, piezometric surfaces, and surface pressures acting on the submerged slope. This procedure was followed for this study. Surface pressures exerted by a reservoir act normal to the slope with a magnitude that equals the product of the unit weight of the fluid (water) and the height of the column of fluid at the point of interest.

Tension cracks

146. Tension cracks were not assumed to exist for this study primarily because the embankment materials derive purely frictional resistance. This characteristic lessens the effect of tension cracks.

Results of Slope Stability Calculations

147. Numerous combinations of input values were used to calculate factors of safety against sliding and determine the most critical (minimum) values. Eight cases were considered for all combinations of circular and noncircular surfaces on the downstream and upstream slopes for

sections CC and DD. For each case, a number of initial surfaces were input to the program to evaluate the convergence to the most critical surface. For each initial surface, the computer generated between 75 and 600 trial surfaces. Over 47 initial surfaces were used (not including sensitivity studies). In addition, the sensitivity of computed factors of safety to variations in static shear strengths was examined. The results of slope stability calculations for sections CC and DD are discussed separately below.

148. Circular and noncircular search methods were used to determine minimum values of factor of safety for failure surfaces on the upstream and downstream slopes of section CC. Only failure surfaces that were believed to affect the stability of the overall structure were considered in the analysis. That is, shallow slip surfaces on the slopes were ignored.

149. The critical factors of safety calculated for postearthquake conditions in this study are generally higher than the critical factors of safety calculated by the design engineers. This difference is attributed to the difference in the cross sections used. The cross sections used for the design study incorporated a continuous clay foundation beneath the gravel alluvium.

Section CC

150. Upstream slope. The minimum factors of safety against sliding for the upstream slope of section CC were 1.64 and 1.48 for the critical circle and noncircular surface, respectively. The locations of these surfaces are shown in Figure 72. The factor of safety for the critical non-circular surface is the lower of the two values but is greater than unity, representing safe slope conditions. The location of the critical surface suggests that even if this failure plane were to develop, slope failure would not affect the stability of the dam since it is restricted to the upstream slope.

151. Downstream slope. The minimum factors of safety against sliding for the downstream slope of section CC were 2.01 and 1.33 for the critical circle and noncircular surface, respectively. The locations of these surfaces are shown in Figure 72. The factor of safety for the critical noncircular surface is the lower of the two values and is greater than unity representing safe slope conditions. The factor of safety of 1.33 represents a reasonably safe postearthquake condition.

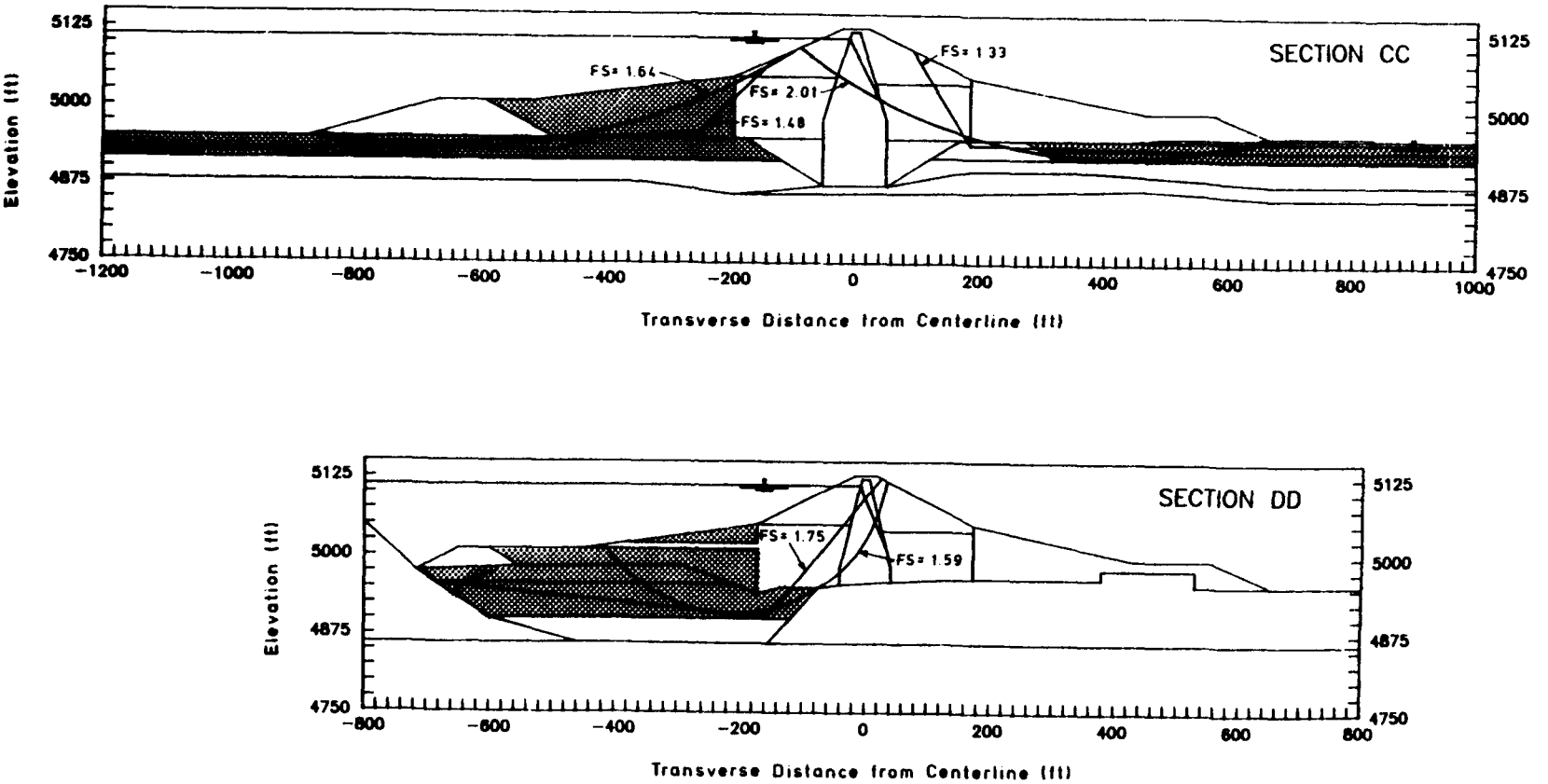

Figure 72. Locations of critical surfaces determined from postearthquake slope stability analysis

Section DD

152. Upstream slope. The minimum factors of safety against sliding for the upstream slope of section DD were 1.59 and 1.75 for the critical circle and noncircular surface, respectively. The locations of these surfaces are shown in Figure 72. The factor of safety for the critical circular surface is the lower of the two values and is greater than unity representing slope stability. Both failure surfaces extend to points near the bottom of the liquefied gravel alluvium. It is apparent by comparing these results with those for the upstream slope of section CC that the absence of a continuous layer of tuffaceous sediments in the foundation provides for safe upstream slope conditions.

153. Downstream slope. The minimum factor of safety against sliding for the downstream slope of section DD was 2.22 for the critical circle. This magnitude of factor of safety represents very safe slope conditions. Notice that only engineered materials exist on the downstream portion of section DD. Noncircular surfaces were not analyzed.

Sensitivity of Results to Shear Strengths

154. The effect of varying some of the material properties on the calculated factors of safety was considered for this study. This sensitivity analysis was conducted to assist in the evaluation of postearthquake stability. (Note, however, that changes in material properties would also affect the dynamic response and liquefaction potential analyses. This sensitivity study, then, is only approximate.)

Residual strengths

155. The factors of safety for critical slip surfaces was found to be moderately sensitive to the magnitude of residual strengths for liquefied materials. This sensitivity was found for the slope stability of the upstream portion of sections CC and DD but not the downstream portion of section CC. The sensitivity of factor of safety to residual strength is expected because of the large percentage of cross-sectional area which liquefied materials comprise.

156. A 25 percent reduction of residual strengths was used to evaluate the sensitivity of residual strengths assigned to liquefied layers. The location of these strengths with respect to the relationship used to derive

the original values is also shown in Figure 71. The range between original and reduced residual strengths bracket projections of the lower bound proposed by Seed et al. (1989). The factors of safety for the affected slopes of sections CC and DD were reduced by about 18 percent for a corresponding reduction of 25 percent in residual strengths.

Nonliquefied zones of
potentially liquefiable materials

157. The factor of safety for critical slip surfaces was found to be insensitive to the status of zones of potentially liquefiable material that did not liquefy. Specifically, the zone of medium-dense gravel alluvium located downstream of the centerline was considered to have liquefied rather than having the excess pore water pressures used in the baseline analysis. The factor of safety for this case was essentially equal to the factor of safety for the baseline case for the critical circular surface which passed through this zone.

Reduced strength of other
foundation and embankment materials

158. Residual excess pore pressure ratios, R_u, in saturated zones of embankment gravels and those foundation zones not considered susceptible to liquefaction may still develop to about 10 percent, based on laboratory test data on dense gravels in other studies (Hynes-Griffin et al. 1988). The effect of these earthquake-induced excess pore pressures was modeled as causing a reduction in available frictional strength (by means of a reduced effective angle of internal friction, ϕ') for input to UTEXAS2. An artificially reduced ϕ' was calculated for materials that are not susceptible to liquefaction using the following expression (after Hynes 1990):

$$(\sin \phi')_{Ru \neq 0} = ((1 - R_u)\sin \phi')_{Ru=0} \qquad (11)$$

Minimum factors of safety calculated using UTEXAS2 were reduced by less than 5 percent for critical circles as a consequence of this artificial strength reduction.

Strength envelope of core material

159. The strength parameters assigned to the core material adhered to drained strengths established from laboratory tests. The use of these strength parameters may be unconservative for postearthquake stability

analysis at large values of normal stress. A bilinear envelope, defined by the drained parameters (ϕ' = 35°, c' = 0) up to a normal stress of 3.0 ksf and then defined by consolidated-undrained parameters (ϕ' = 16°), was used to determine the effect on calculated factors of safety and the location of critical circles (refer to Figure 69). The analysis was performed for the upstream slope of sections CC and DD and the downstream slope of section CC.

160. In general, the effect of reducing the failure envelope for core material by using a bilinear relationship had little effect on the calculated factors of safety or the locations of critical circles. The factors of safety for the three conditions previously stated were reduced by only 2-7 percent. This minimal effect is attributed to the low normal stresses that act on the base of slices located within the core, below the threshold for use of the second failure criterion.

Conclusions

161. The results of limit-equilibrium, slope stability analysis using the computer program UTEXAS2 indicate that the upstream and downstream slopes at sections CC and DD are safe against sliding for postearthquake conditions. Sensitivity analyses indicate that the results are moderately sensitive to the residual strengths of liquefied materials. The results appear to be insensitive to minor changes in the properties of the tuffaceous sediments and failure envelope for core material, and whether all potentially liquefiable zones were assumed to liquefy. The sensitivity study did not include reanalysis of the dynamic response and considered a limited range of stresses and strengths. It can be concluded using the performance-based approach that the mode of failure corresponding to loss of freeboard due to slope failure is not a potential threat to Ririe Dam for the design earthquake.

PART VIII: PERMANENT DISPLACEMENT ANALYSIS

Introduction

162. A permanent displacement analysis was conducted to evaluate the potential for slope failures under the inertial loads induced by ground motions which would cause a loss of freeboard. The potential for this mode of failure is intrinsically high at Ririe Dam because of the small freeboard and short height of core material above the analysis pool level (16 and 10 ft, respectively). Permanent displacement refers to the amount of differential movement along a potential slip surface resulting from inertial effects during an earthquake. These permanent displacements are estimated by analyzing the forces acting on bodies defined by slip surfaces tangent to arbitrary elevations. A permanent displacement analysis is a criterion for performance as opposed to a stability calculation based on principles of limit equilibrium (Makdisi and Seed 1978). One cross section was used for the analysis of permanent displacements. The curved, maximum-height section (section CC) was selected because it best represents conditions affecting earthquake-induced slides at Ririe Dam.

163. The magnitude of permanent displacements is difficult to assess accurately because of the simplifying assumptions made with current techniques, the narrow canyon at Ririe Dam, and the large variability in data used to predict permanent displacements. Most procedures available to estimate permanent displacements are two-dimensional and based on the principles of a sliding block analogy. For this study, the evaluation of magnitude of permanent displacements involved three phases: use of three separate studies to obtain a best estimate of displacements, use of five separate studies to obtain an upper-bound of displacements associated with respective data bases of earthquakes, and a comparison of associated crest settlement with empirical data.

164. The procedures for predicting permanent displacement were derived assuming that the material properties did not change during excitation. Typically, static strength parameters are used for a permanent deformation analysis. In reality, the material properties do change with increased cycling from modulus degradation and increases in pore water pressures. Seismic shear waves attenuate rapidly when propagating through materials with

high pore water pressures. Adequate methods of analyzing the attenuation of seismic waves traveling through liquiefied soils were not available for this analysis. Since some foundation materials at Ririe Dam are expected to liquefy, it is difficult to select material strengths to calculate realistic values of permanent displacement. For this study, it was assumed that materials expected to liquefy had only residual strengths. This assumption was expected to allow the best assessment of the deformed shape following the earthquake.

Simplified Analyses for Best Estimate of Permanent Displacement

165. Simplified procedures considered for this study are adaptations of the sliding block analogy reported by Newmark (1965). The sliding block analogy considers the forces that act on a rigid block or wedge. Sliding is postulated to occur if gravity and inertia forces acting on a potential sliding mass exceed the resisting forces along the base of the slip surface. Only horizontal accelerations are considered which can be unconservative.

166. Various studies have examined permanent displacement analysis for earth- and rock-fill dams. Five such studies were used to predict permanent displacements for Ririe Dam: Ambraseys (1972), Makdisi and Seed (1978), Sarma (1979), Hynes-Griffin and Franklin (1984), and Ambraseys and Menu (1988). Studies by Makdisi and Seed (1978), Sarma (1979), and Hynes-Griffin and Franklin (1984) were used to obtain best estimates of permanent displacement. All five procedures were used to obtain an upper bound of displacements corresponding to maximum sliding block displacement calculations.

167. Simplified procedures may best be represented by three phases: pseudo-static slope stability analysis, embankment response analysis, and a sliding block analysis. The slope stability analysis is used to determine the magnitude of accelerations required to initiate displacements. The embankment response analysis is used to evaluate the accelerations that act on the sliding block. The sliding block analysis produces relationships between displacement and a normalized acceleration from accelerations measured during earthquakes. The pseudo-static slope stability analysis is unique to the conditions at the dam so that the results are applicable to all five methods of analysis. In general, simplified procedures involve the use of empirical charts and simple calculations.

168. Yield accelerations for selected failure surfaces are required for all the above simplified analysis procedures. A yield acceleration coefficient, k_y (in g's), is the pseudo-static acceleration applied at the center of gravity of a sliding mass which will reduce the safety factor against sliding to unity. Each peak acceleration with a magnitude greater than k_y will produce permanent displacements.

169. The yield accelerations were determined iteratively using the results of limit equilibrium calculations performed using UTEXAS2 (Edris and Wright 1987). UTEXAS2 allows for the input of a (horizontal) seismic coefficient to each slice for the analysis. A trial value of acceleration was chosen for each initial slip surface and the factor of safety against sliding was calculated using critical surface search routines. The trial value of acceleration was then adjusted to force the factor of safety near or equal to unity. Several sets of data comprising acceleration and the corresponding factor of safety were used to determine the yield acceleration at each tangent elevation.

170. Initial potential slip surfaces were selected to be wedges or deeper circles that were tangent to five distributed elevations on the downstream and upstream slopes. Potential slip surfaces were selected from section CC that would intersect the core below the phreatic surface thus creating the potential for dam failure and overtopping. Slope failures in purely granular materials typically have shallow surfaces. For the cross section at Ririe Dam, most shallow surfaces would not intersect the phreatic surface. Therefore, final slip surfaces at each tangent elevation were also resolved to intersect the core below the phreatic surface. The locations of the final slip surfaces and tangent elevations used for all simplified methods are shown for the downstream and upstream slopes in Figures 73 and 74, respectively. The profiles of yield accelerations for the downstream and upstream slopes are presented in Figure 75. Data labeled as residual correspond to accelerations derived for postearthquake study. Data labeled as static correspond to accelerations calculated by Azzouz and Baligh (1989b) using static strengths for all material types as will be discussed later in this section.

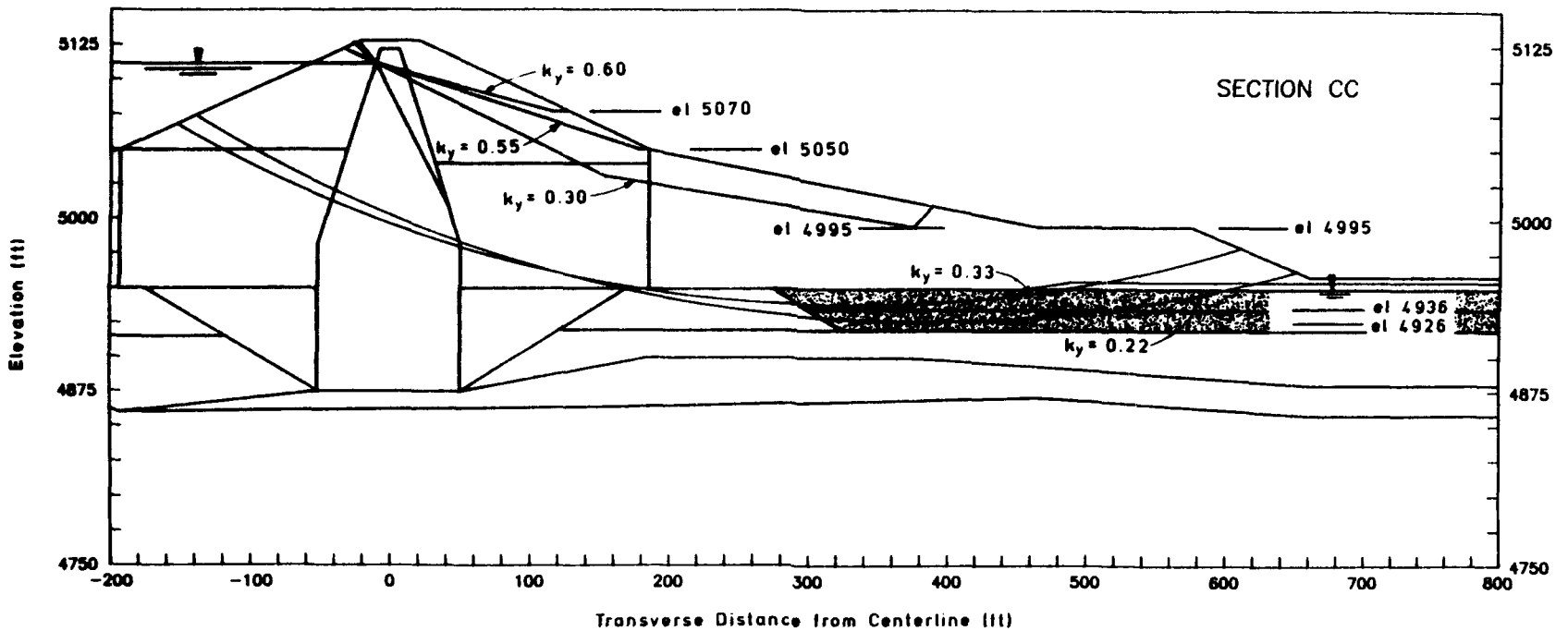

Figure 73. Locations of potential failure surfaces on downstream side used for permanent displacement analysis

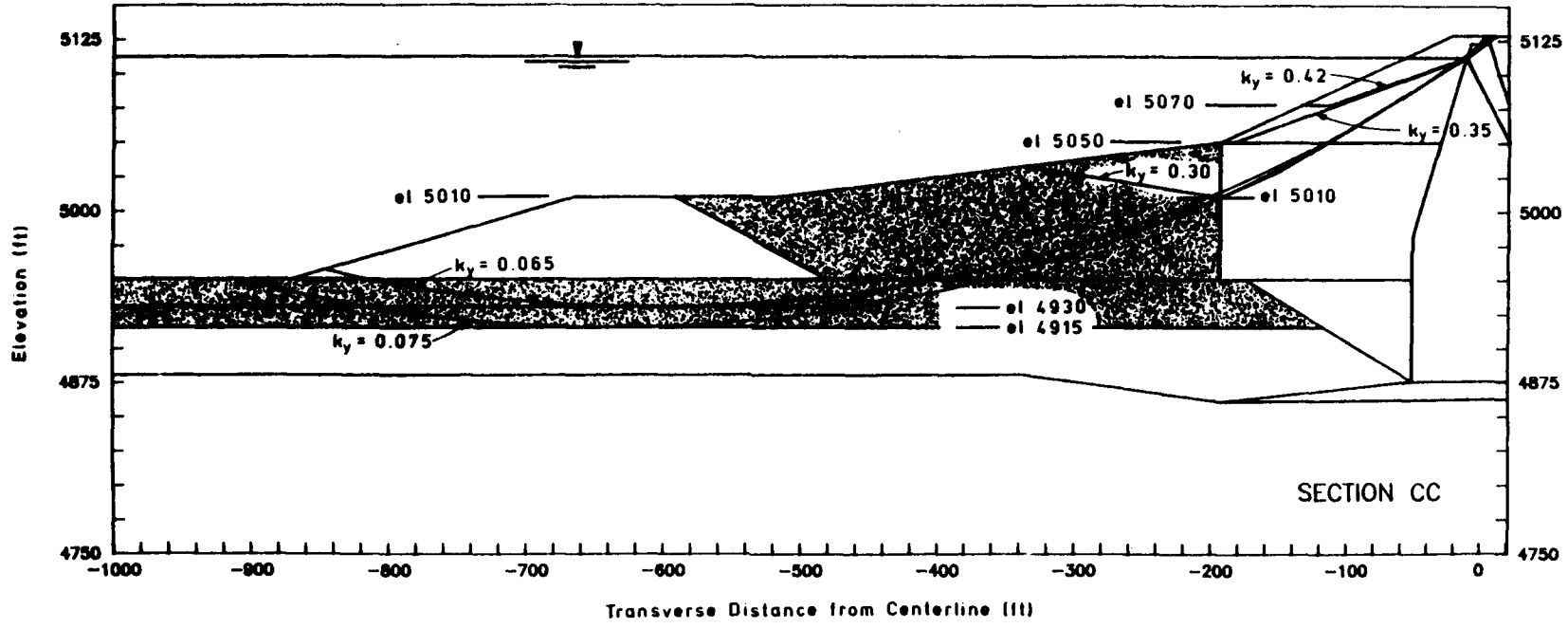

Figure 74. Locations of potential failure surfaces on upstream side used for permanent displacement analysis

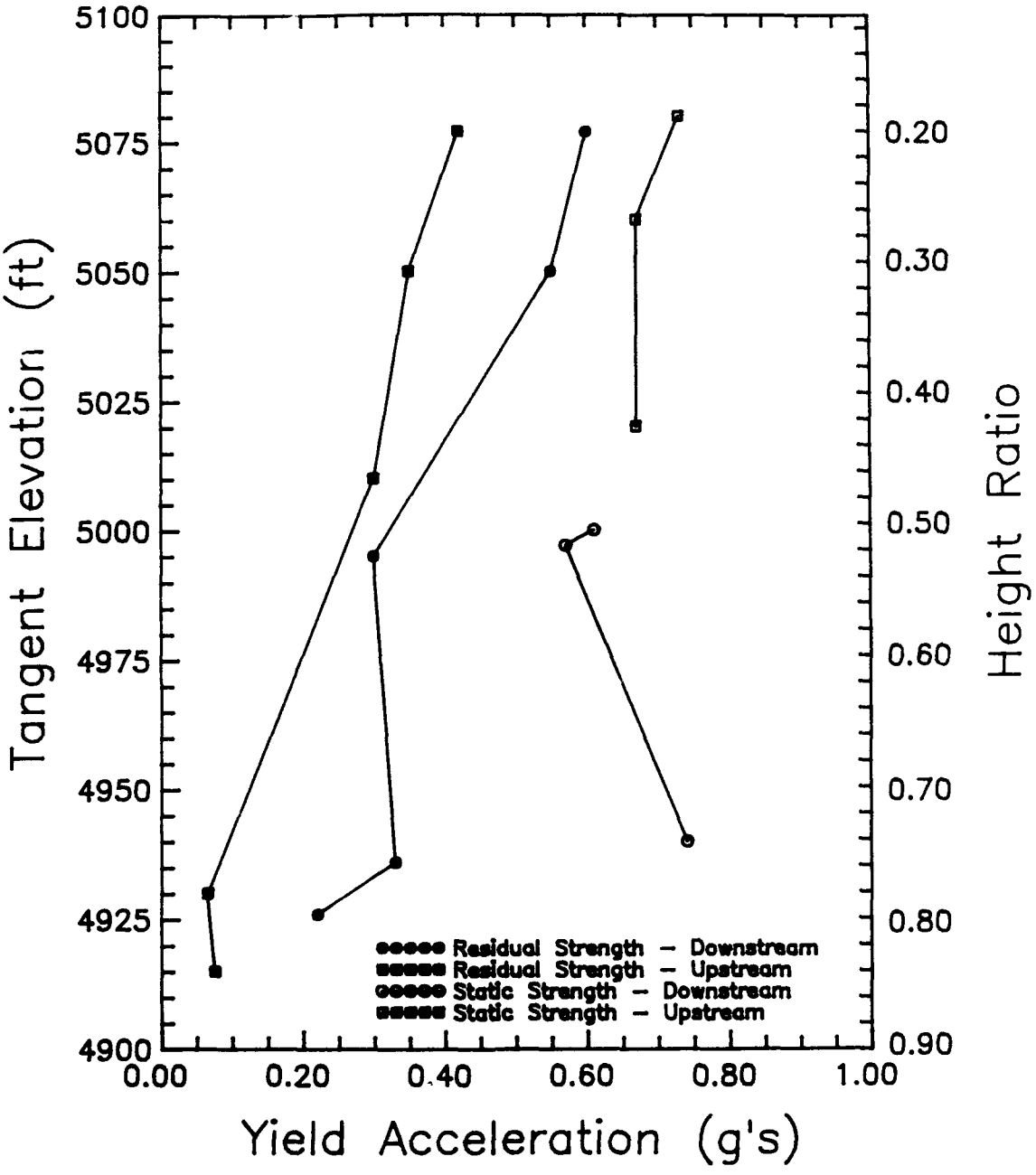

Figure 75. Distribution of yield accelerations for upstream and downstream slopes

171. The height ratio (y/h) used in Figure 75 is different from that used in Figure 54. The ratio of y/h for the permanent displacement analysis refers to the ratio of distance below the crest, y, to the total height of the dam, h. The value of h, therefore, was constant for the analysis and chosen to be the height from the base of the core trench to the crest (253 ft). This convention is depicted in Figure 76.

172. The yield accelerations were computed using the same material properties used for postearthquake stability analysis. The slope materials were assumed to behave as an elastic material at levels of stress below the failure criterion and as a perfectly plastic material at levels of stress above the failure criterion. Excess pore water pressures and residual strengths were used and follow from the conservative assumption that pore pressures will build up to their maximum values at the onset of shaking and will be maintained throughout the duration of shaking. Undrained strengths were not reduced for this analysis as recommended by Makdisi and Seed (1978) because all embankment and alluvial foundation materials were assumed to be purely frictional materials.

173. Yield accelerations were also calculated by Azzouz and Baligh (1989b) using the computer program TSLOPE (TAGA Engineering Software Services 1984). The results of this study are contained in Appendix B and presented in Figure 75 as "static strength". These accelerations, however, were determined using static material strengths without considering excess pore water pressure. Therefore, they are expected to be quite a bit larger than those determined for materials with excess pore water pressure (and liquefied materials). Azzouz and Baligh (1987b) concluded on the basis of results of gravity loading studies that three-dimensional geometric and material property effects did not significantly influence the calculation of yield acceleration.

174. The variation of yield acceleration with height shown in Figure 75 is rather uniform, decreasing moderately with depth. Lower yield accelerations are generally associated with large permanent displacements. The yield accelerations indicate that the maximum displacements are generally associated with deeper failure surfaces. As expected for a rock-fill dam, the yield accelerations generally are quite high for surfaces contained primarily in the rock fill. Also expected are the consistently lower yield accelerations for

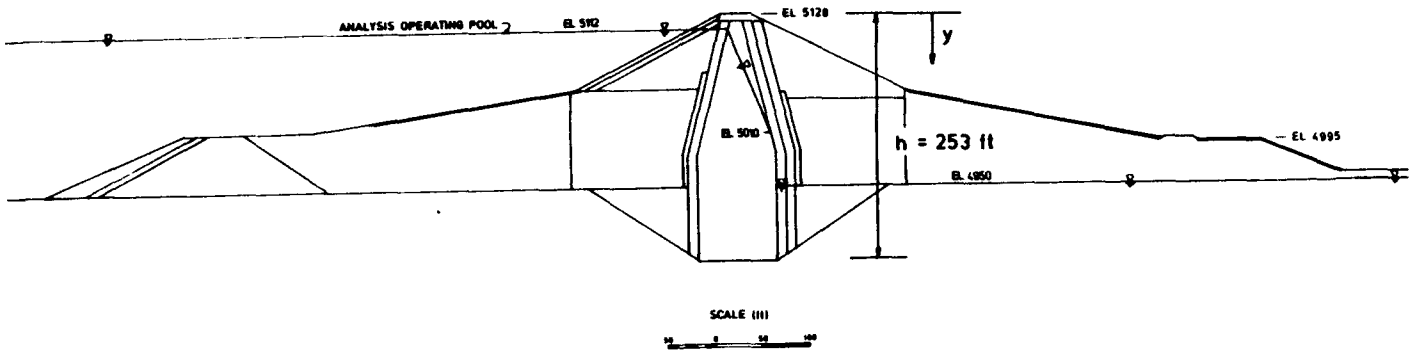

Figure 76. Convention for height ratio used for permanent displacement analysis

the upstream side which result from lower confining effective stresses caused by the lower (buoyant) weight of the materials.

Makdisi-Seed method

175. The procedure proposed by Makdisi and Seed (1978) was derived from a two-dimensional analysis assuming that the dam is founded on rock. The conditions at Ririe Dam do not exactly fit this condition because of the thick layer of alluvium overlying bedrock. Nevertheless, the results of this procedure are valuable because this procedure is widely used. Parameters required for the calculations include the maximum (horizontal) acceleration coefficient at the crest, k_c , the natural period of the dam, T_o , the earthquake magnitude, and an empirical correction factor for displacement. The parameters necessary to conduct the permanent displacement analysis were readily available or easily calculated. The earthquake magnitude is 7.5. The natural period and peak horizontal acceleration at the crest, k_c , were found from the results of the two-dimensional dynamic response analysis (1.92 sec and 0.77 g, respectively).

176. Makdisi and Seed (1978) used the results of dynamic response analyses to develop an average relationship to quantify amplification of accelerations within an embankment. The maximum average acceleration coefficient, k_{max} , was defined to be the maximum acceleration determined by the following (force) averaging equation:

$$k_{max} = \frac{\text{MAX } \Sigma \sigma_{hi}(t)\, d_i + \tau_{hvi}(t)\, L_i}{\text{Weight of Wedge}} \qquad (12)$$

where

σ_{hi} = increment of horizontal stress acting on infinitesimal element i at time t

d_i = infinitesimal height of element i

τ_{hvi} = increment of shear stress acting on horizontal plane of infinitesimal element i at time t

L_i = infinitesimal width of element i

Notice that k_{max} is determined at an instant in time. Values of k_{max} can be estimated using the average relationship proposed by Makdisi and Seed shown in Figure 77a which involves the maximum-to-crest acceleration ratio, k_{max}/k_c (called maximum acceleration ratio by Makdisi and Seed).

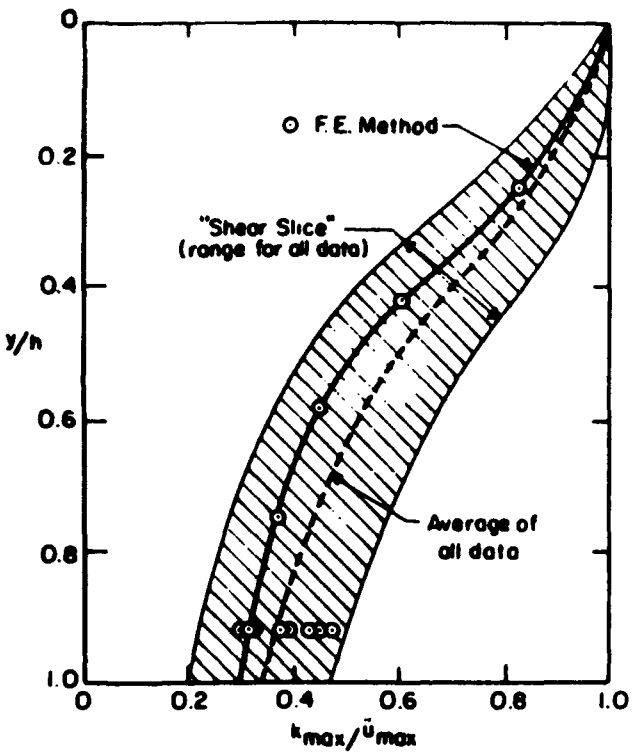

a. Variation of maximum acceleration ratio with depth

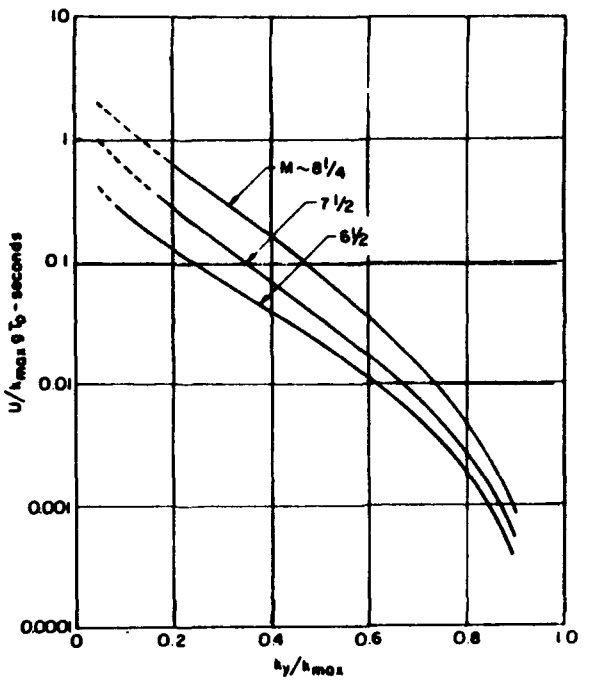

b. Variation of averaged normalized displacement with yield acceleration

Figure 77. Empirical charts to predict permanent displacement using the Makdisi-Seed method

177. The permanent displacement, U, is obtained using the results of sliding block analyses. Relations proposed by Makdisi and Seed for earthquakes of various magnitudes are shown in Figure 77b. The maximum-to-crest acceleration ratio and the relation for the appropriate earthquake (for Ririe Dam, M=7.5) are used to extract the Makdisi-Seed displacement factor, U_{ms}, defined as:

$$U_{ms} = U/(k_{max}\ T_o\ g) \tag{13}$$

where

U = uncorrected permanent displacement (same length units as acceleration)

T_o = natural period of dam (sec)

Knowing k_{max}, T_o, and the gravitational acceleration of the earth, g (32.2 ft/sec^2), U is calculated.

178. One adjustment should be made to permanent displacements to account for the direction of the resultant shearing resistance force (Sarma 1979, and Hynes-Griffin and Franklin 1984). This adjustment is based on the solution to the equation of motion for a sliding block on a plane. The factor α is calculated by:

$$\alpha = \frac{\cos\ (\beta - \theta - \phi)}{\cos\ \phi} \tag{14}$$

where

β = direction of the resultant shear force and displacement, and the inclination of the plane

θ = direction of the acceleration, measured from the horizontal

ϕ = friction angle between the block and the plane

Values of β were estimated based on the slope and location of the failure surfaces and ranged from 27 deg for a mid-height, shallow slip surface to 7 deg for a deep slip surface. A value for θ of zero was used since horizontal accelerations were assumed. The friction angles for the various materials were obtained from the drained values listed in Table 6. Estimated permanent displacements, U_c were then calculated by:

$$U_c = \alpha U \tag{15}$$

The calculations made to obtain best estimates of the permanent displacements using the Makdisi-Seed method are summarized in Table 11. The maximum

Table 11

Permanent Displacement Calculations Using the Makdisi-Seed Method and Average Values of Acceleration (Makdisi and Seed 1978)

Location	Tangent Elevation ft	y/h	k_{max}/k_c*	k_{max}	k_y	k_y/k_{max}	U_{ms}**	U, ft	α	U_c, ft
Downstream	5,077	0.20	0.90	0.69	0.60	0.87	0.00086	0.04	1.24	0.05
Downstream	5,050	0.31	0.80	0.62	0.55	0.89	0.00059	0.02	1.29	0.03
Downstream	4,995	0.53	0.58	0.45	0.30	0.67	0.01	0.28	1.32	0.37
Downstream	4,936	0.76	0.43	0.33	0.33	1.00	--	<.01	1.02	<.01
Downstream	4,926	0.80	0.42	0.32	0.22	0.69	0.008	0.16	1.02	0.16
Upstream	5,077	0.20	0.90	0.69	0.42	0.61	0.015	0.64	1.21	0.84
Upstream	5,050	0.31	0.80	0.62	0.35	0.56	0.023	0.88	1.32	1.16
Upstream	5,010	0.47	0.625	0.48	0.30	0.63	0.014	0.42	1.09	0.45
Upstream	4,930	0.78	0.42	0.32	0.065	0.20	0.28	5.5	1.03	5.7
Upstream	4,915	0.84	0.40	0.31	0.075	0.24	0.21	4.0	1.03	4.1

* Referred to as u_{max} by Makdisi and Seed (1978). k_c = 0.77 g (two-dimensional analysis).

** $U_{ms} = \frac{U}{k_{max} T_o g}$.

where

T_o = natural period (1.92 sec for two-dimensional analysis).

g = 32.2 ft/sec^2.

best-estimate of permanent displacements for the downstream and upstream slopes are 0.37 and 5.7 ft, respectively.

Sarma method

179. Sarma (1979) proposed a method similar to the Makdisi-Seed method. The difference is that Sarma suggests using the average horizontal acceleration acting on the wedge at any instant in time. For this study, a simplified and more conservative average acceleration, defined as the peak average acceleration, k_{pav} , was used:

$$k_{pav} = MAX \int_{A} \frac{k_p}{A} dA \qquad (16)$$

where

k_p = distribution of maximum acceleration coefficients within section

A = area of wedge

The use of k_{pav} is conservative because the overall peak accelerations of the slip surface are used rather than accelerations at an instant in time. The results of the two-dimensional dynamic response analysis (SUPERFLUSH) were used to evaluate the distribution of peak acceleration over the cross section (refer to Figure 45). Note that maximum accelerations may occur at different times for any number of points within the dam. The variation of the yield-to-peak acceleration ratio with height for the downstream and upstream slopes is shown in Figure 78. Best-fit relations are also interpreted which show that independent relations exist for each slope. Although some scatter exists about the best-fit relations, the variation of k_y/k_{pav} with height is fairly consistent, decreasing rapidly with decreasing elevation.

180. The sliding block analysis was performed using the acceleration record at the abutment of Pacoima Dam during the 1971 San Fernando Earthquake (specified as the design earthquake for this study). Sarma (1979) provides the data for this earthquake in the form of a displacement factor, U_S, defined as:

$$U_S = \frac{4\, U_c}{k_{pav}\, T^2\, g} \qquad (17)$$

and k_y/k_{pav} which is shown in Figure 79. A summary of the calculations is contained in Table 12. The maximum best-estimate of permanent displacements for the downstream and upstream slopes are 0.61 and 4.3 ft, respectively.

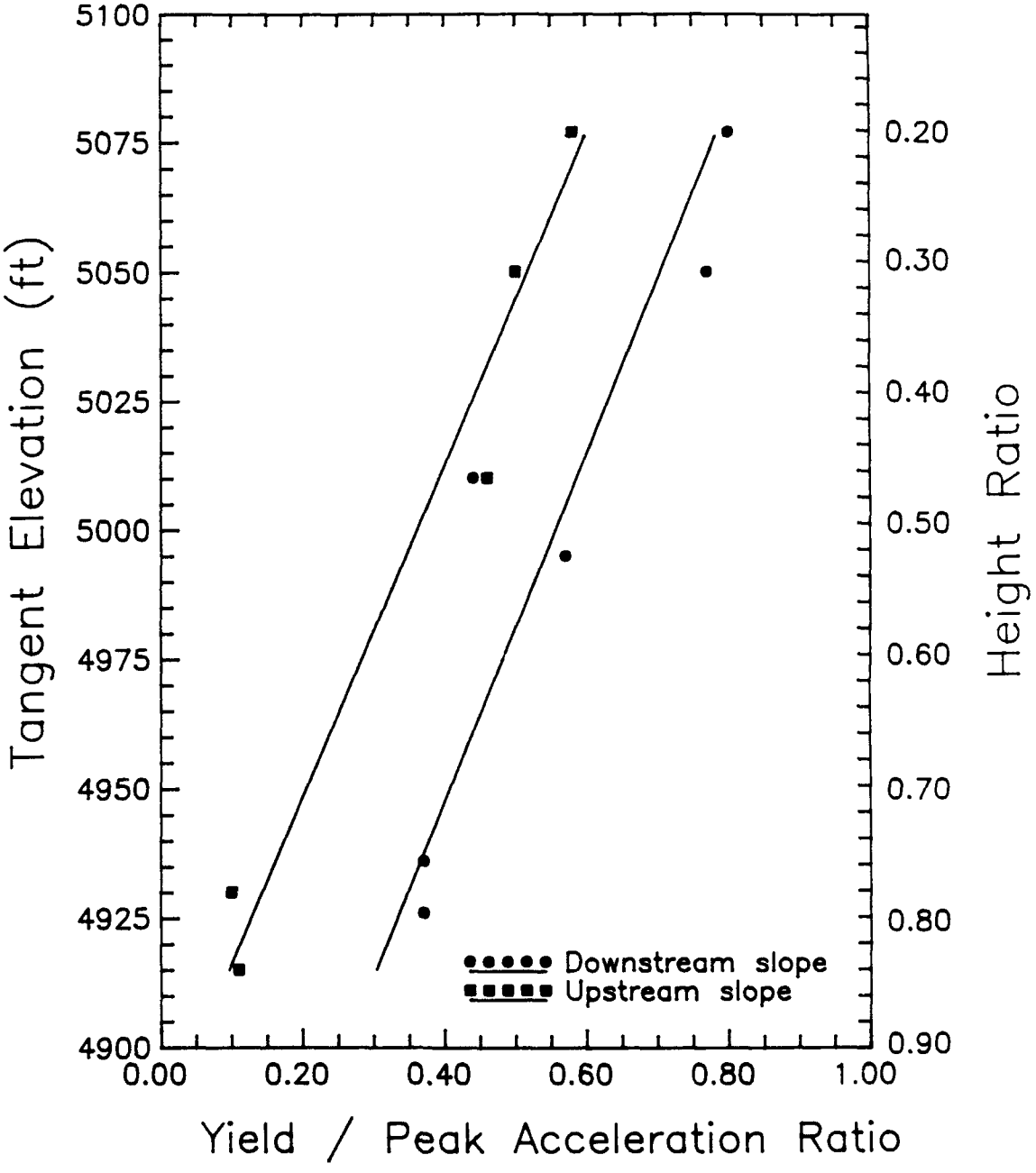

Figure 78. Variation of yield/peak acceleration ratio with height ratio for Ririe Dam

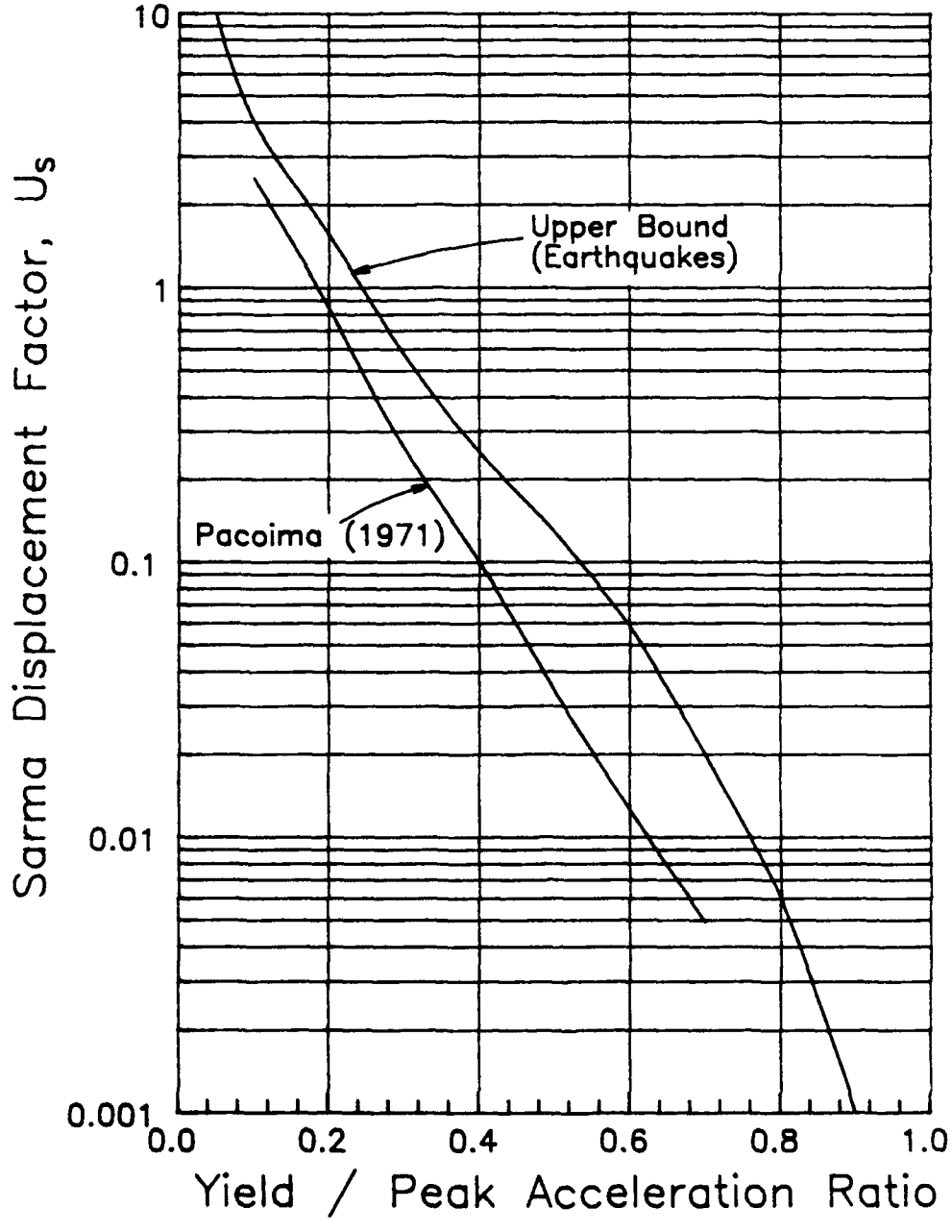

Figure 79. Relations between yield/peak acceleration ratio and permanent displacement factor (from Sarma 1979)

Table 12

Permanent Displacement Calculations Using the Sarma Method and Design Earthquake (Sarma 1979)

Location	Tangent Elevation ft	k_{avg}	k_y	k_y/k_{avg}	U_s*	α	U_c, ft
Downstream	5,077	0.75	0.60	0.80	<0.005	1.24	<0.1
Downstream	5,050	0.71	0.55	0.77	<0.005	1.29	<0.1
Downstream	4,995	0.68	0.30	0.44	0.069	1.32	0.61
Downstream	4,936	0.58	0.33	0.57	0.017	1.02	0.02
Downstream	4,926	0.60	0.22	0.37	0.13	1.03	0.20
Upstream	5,077	0.73	0.42	0.58	0.015	1.31	0.04
Upstream	5,050	0.70	0.35	0.50	0.032	1.32	0.07
Upstream	5,010	0.65	0.30	0.46	0.054	1.09	0.09
Upstream	4,930	0.66	0.065	0.10	2.2	1.03	3.70
Upstream	4,915	0.68	0.075	0.11	2.5	1.03	4.33

* $U_s = \frac{1}{\alpha} \frac{4\,U_c}{k_{avg} T_o^2 g}$ (inches).

where

T_o = natural period (1.92 sec for two-dimensional analysis).

$g = 32.2$ ft/sec^2.

181. The ratio of k_{pav}/k_c as a function of height ratio was plotted to evaluate the consistency and to qualitatively compare it with a similar relation used by Makdisi and Seed (1978). These data are plotted in Figure 80 and indicate that data for upstream and downstream slopes may be adequately represented by the same best-fit relation (the data suggest that the acceleration ratios for the upstream slope are slightly lower, however). The best-fit relation is somewhat higher from the range shown in Figure 77a. Values of k_{pav} are as large as 100 percent greater than k_{max} at consistent height ratios (greater differences being associated with larger height ratios). This is attributed to the difference between peak and maximum acceleration described previously.

WES method

182. Franklin and Chang (1977), Franklin and Hynes (1981), and Hynes and Franklin (1984) propose another procedure similar to the Sarma method with an expanded data base of earthquake records. The ratio of yield acceleration to peak acceleration, k_y/k_{pav} (called N/A by Hynes and Franklin 1984) is again used to determine permanent displacements using relationships from sliding block analyses. This ratio is a measure of the sliding resistance of an embankment. The higher the ratio, the lower the displacement. The natural period is reflected in the dynamic response ratio, k_y/k_{pav} .

183. The sliding block analysis was performed using the displacements associated with the Pacoima record. This relation is shown in Figure 81. Uncorrected permanent displacements, U , are determined using Figure 82 and the appropriate values of yield/peak acceleration. Then, the permanent displacements, U_c , are corrected using Equation 15. The calculations made to estimate permanent displacements using the WES method are summarized in Table 13. The maximum permanent displacements for the downstream and upstream slopes are 0.16 and 2.9 ft, respectively.

Simplified Analyses for Upper Bound Estimates for Permanent Displacement

Makdisi-Seed method

184. The Makdisi-Seed method was also used to obtain upper-bound estimates of permanent displacement by using the upper bound of the range in

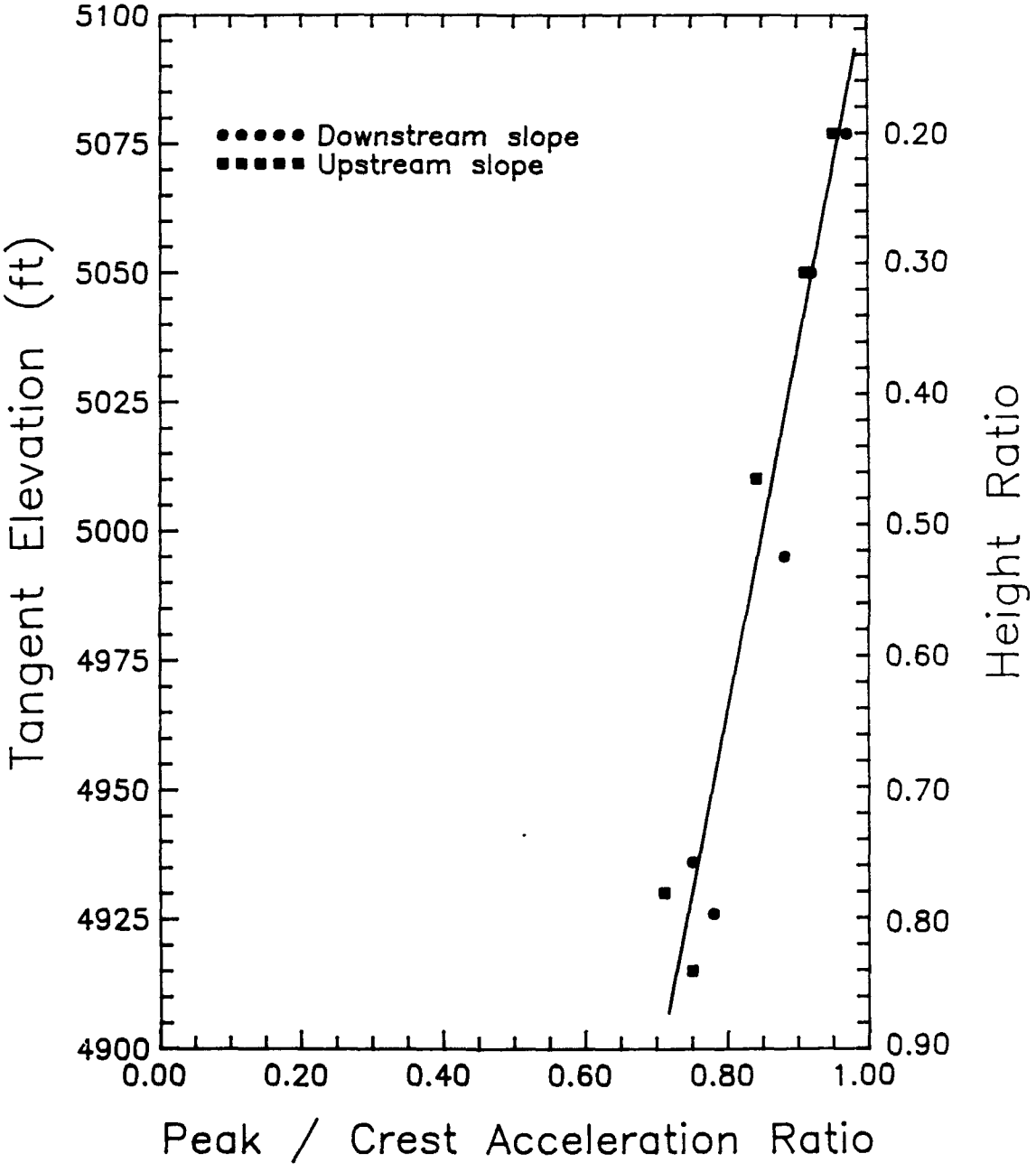

Figure 80. Variation of peak/crest acceleration ratio with height ratio for Ririe Dam

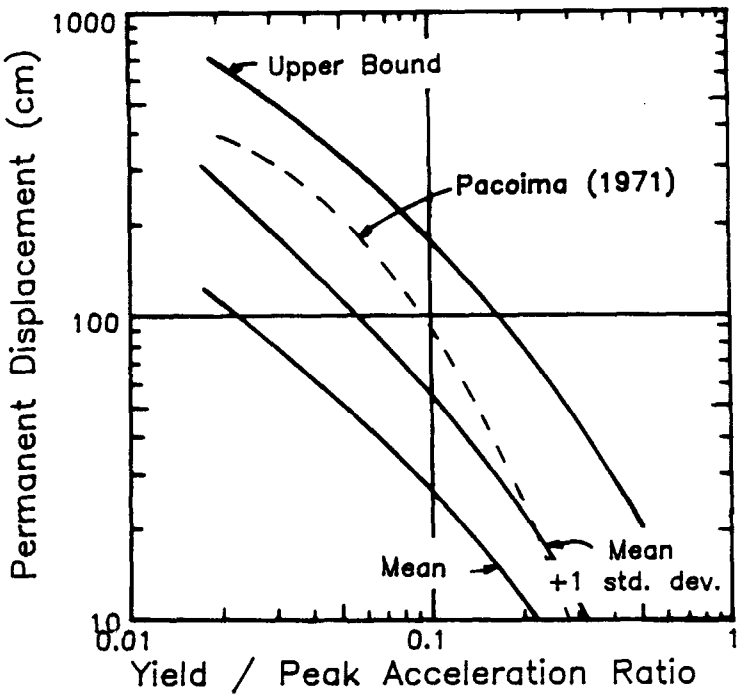

Figure 81. Relationships between normalized acceleration and permanent displacement for Pacoima record and 348 horizontal earthquake components and six synthetic records (Hynes and Franklin 1984)

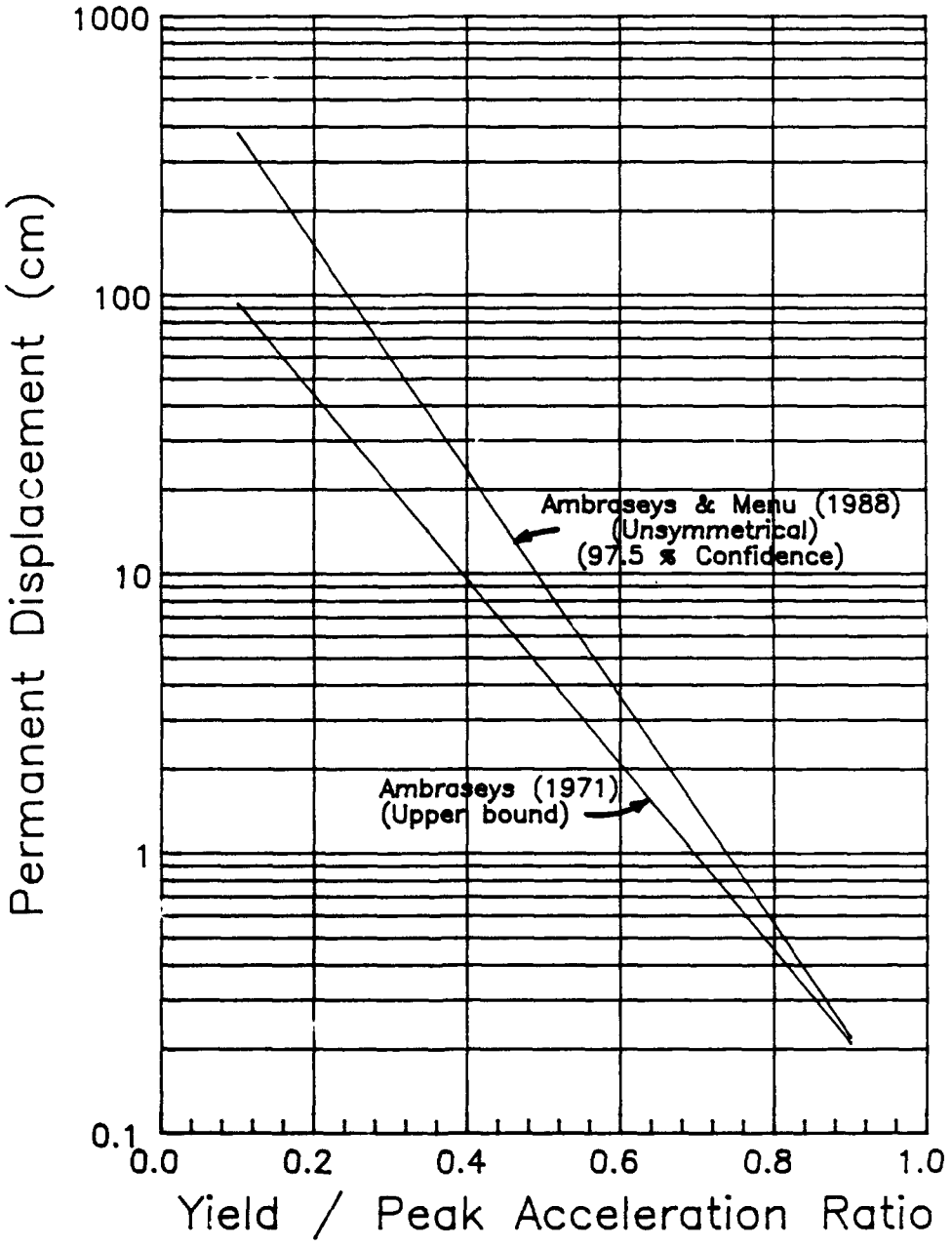

Figure 82. Relations between yield/peak acceleration ratio and permanent displacement for Ambrasey's method

Table 13

Permanent Displacement Calculations Using the WES Method and Design Earthquake (Hynes-Griffin and Franklin 1984)

Location	Tangent Elevation ft	y/h	k_{avg}	k_y	k_y/k_{avg}	U, cm	α	U_c cm	U_c ft
Downstream	5,077	0.20	0.75	0.60	0.80	<1	1.24	<1.2	<0.04
Downstream	5,050	0.31	0.71	0.55	0.77	<1	1.29	<1.3	<0.04
Downstream	4,995	0.53	0.68	0.30	0.44	2.5	1.32	3.30	0.11
Downstream	4,936	0.76	0.58	0.33	0.57	1.4	1.02	1.43	0.05
Downstream	4,926	0.80	0.60	0.22	0.37	4.6	1.03	4.76	0.16
Upstream	5,077	0.20	0.73	0.42	0.58	1.4	1.31	1.83	0.06
Upstream	5,050	0.31	0.70	0.35	0.50	1.5	1.32	1.98	0.06
Upstream	5,010	0.47	0.65	0.30	0.46	2.4	1.09	2.62	0.09
Upstream	4,930	0.78	0.66	0.065	0.10	87.0	1.03	89.6	2.9
Upstream	4,915	0.84	0.68	0.075	0.11	78.0	1.03	80.3	2.6

acceleration ratio (k_{max}/k_c) shown in Figure 77a. The remaining steps in the procedure used are the same as those used previously. A summary of the calculations made is contained in Table 14. The maximum permanent displacements for the downstream and upstream slopes are 0.8 and 12 ft, respectively.

Sarma method

185. The Sarma method was also used to obtain upper-bound estimates of permanent displacement by using the upper bound of displacements from four different earthquakes. (Sarma (1979) had also included ground motions from underground nuclear blasts which were not included for this study.) The upper-bound relation is shown in Figure 79 and the calculations made are summarized in Table 15. The maximum permanent displacements for the downstream and upstream slopes are 2.2 and 8.3 ft, respectively.

WES method

186. The WES method was also used to obtain upper-bound estimates of permanent displacement by using the upper bound of displacements for 348 horizontal earthquakes components and six synthetic records. Relationships for the upper bound, mean, and mean plus one standard deviation of displacements are shown in Figure 80 and the calculations made are summarized in Table 16. The maximum displacements for the downstream and upstream slopes are 1.2 and 6.0 ft, respectively.

Ambraseys method

187. Ambraseys (1972) and Ambraseys and Menu (1988) suggested a method which is similar to the WES method. Ambraseys (1972) used a variety of earthquake motions recorded before 1972 for the sliding block analysis. Ground motions used by Ambraseys and Menu (1988) were selected from near-field data generated by shallow earthquakes including more recent earthquake records. Twenty-six strong-motion records obtained from eleven earthquakes with peak accelerations ranging between 0.06 and 1.15 g were used representing a range in surface wave magnitudes, M_s, of 6.4 to 7.7. The design ground motion specified for Ririe Dam ($M = 7.5$, $a_{max} = 1.17$) should be well represented by this data base.

188. The ratio of acceleration used by Ambraseys (1972) and Ambraseys and Menu (1988) to predict permanent displacements is the yield acceleration divided by the maximum horizontal ground acceleration coefficient, k_g. The acceleration ratio, k_y/k_g, is then used with different charts representing different modes of displacement to determine the permanent displacement. The

Table 14

Permanent Displacement Calculations Using the Makdisi-Seed Method and Maximum Values of Acceleration (Makdisi and Seed 1978)

Location	Tangent Elevation ft	y/h	k_{max}/k_c *	k_{max}	k_y	k_y/k_{max}	U_{ms} **	U, ft	α	U_c, ft
Downstream	5,077	0.20	0.97	0.75	0.60	0.80	0.0025	0.12	1.24	0.14
Downstream	5,050	0.31	0.91	0.70	0.55	0.79	0.003	0.13	1.29	0.17
Downstream	4,995	0.53	0.72	0.55	0.30	0.55	0.025	0.85	1.32	0.12
Downstream	4,936	0.76	0.58	0.45	0.33	0.73	0.0055	0.15	1.02	0.16
Downstream	4,926	0.80	0.55	0.42	0.22	0.52	0.03	0.78	1.02	0.80
Upstream	5,077	0.20	0.97	0.75	0.42	0.56	0.023	1.1	1.31	1.4
Upstream	5,050	0.31	0.91	0.70	0.35	0.50	0.035	1.5	1.32	2.0
Upstream	5,010	0.47	0.77	0.59	0.30	0.51	0.033	1.2	1.09	1.3
Upstream	4,930	0.78	0.56	0.43	0.065	0.15	0.44	11.7	1.03	12.0
Upstream	4,915	0.84	0.53	0.41	0.075	0.18	0.35	8.9	1.03	9.1

* Referred to as u_{max} by Makdisi and Seed (1978). k_c = 0.77 g (two-dimensional analysis).

** $U_{ms} = \frac{U}{k_{max} T_o g}$

where

T_o = natural period (1.92 sec for two-dimensional analysis).

g = 32.2 ft/sec^2.

Table 15

Permanent Displacement Calculations Using the WES Method and Upper Bound for Acceleration (Sarma 1979)

Location	Tangent Elevation ft	k_{avg}	k_y	k_y/k_{avg}	U_s*	α	U_c, ft
Downstream	5,077	0.75	0.60	0.80	0.006	1.24	0.01
Downstream	5,050	0.71	0.55	0 77	0.009	1.29	0.02
Downstream	4,995	0.68	0.30	0.44	0.19	1.32	0.42
Downstream	4,936	0.58	0.33	0.57	0.072	1.02	0.11
Downstream	4,926	0.60	0.22	0.37	0.325	1.03	0.50
Upstream	5,077	0.73	0.42	0.58	0.07	1.31	0.17
Upstream	5,050	0.70	0.35	0.50	0.13	1.32	0.30
Upstream	5,010	0.65	0.30	0.46	0.165	1.09	0.29
Upstream	4,930	0.66	0.065	0.10	4.0	1.03	6.73
Upstream	4,915	0.68	0.075	0.11	3.6	1.03	6.23

* $U_s = \frac{1}{\alpha} \frac{4 U_c}{k_{avg} T_o^2 g}$ (inches).

where

T_o = natural period (1.92 sec for two-dimensional analysis).

g = 32.2 ft/sec^2.

Table 16

Permanent Displacement Calculations Using the WES Method and Upper Bound for Acceleration (Hynes-Griffin and Franklin 1984)

Location	Tangent Elevation ft	y/h	k_{avg}	k_y	k_y/k_{avg}	U, cm	α	U_c cm	U_c ft
Downstream	5,077	0.20	0.75	0.60	0.80	9.0	1.24	11.2	0.37
Downstream	5,050	0.31	0.71	0.55	0.77	10.0	1.29	12.9	0.42
Downstream	4,995	0.53	0.68	0.30	0.44	26.0	1.32	34.3	1.1
Downstream	4,936	0.76	0.58	0.33	0.57	17.0	1.02	17.3	0.57
Downstream	4,926	0.80	0.60	0.22	0.37	34.0	1.03	35.0	1.1
Upstream	5,077	0.20	0.73	0.42	0.58	16.0	1.31	21.0	0.69
Upstream	5,050	0.31	0.70	0.35	0.50	20.5	1.32	27.1	0.89
Upstream	5,010	0.47	0.65	0.30	0.46	24.0	1.09	26.2	0.86
Upstream	4,930	0.78	0.66	0.065	0.10	177.0	1.03	182.0	6.0
Upstream	4,915	0.84	0.68	0.075	0.11	145.0	1.03	149.0	4.9

definition of ground acceleration used by Ambraseys is rather ambiguous. As shown in Figure 41, the outcrop ground motion and the free-field ground motion can be significantly different. Furthermore, the effects of imposition of an embankment on the ground surface will alter the motions at the previous ground surface as discussed previously (analogous to base rock motions if the ground surface is rock). Therefore, some judgment was required to implement this method. The most judicious interpretation of ground acceleration is the area-average acceleration coefficient, k_{pav} . Permanent displacement analysis using the Ambraseys method for this study, then, uses the same yield-peak acceleration ratio (k_y/k_{pav}) described previously by Hynes-Griffin and Franklin (1984) and shown in Figure 78.

189. The upper-bound relation derived from the sliding block analysis by Ambraseys (1972) was used to predict permanent displacements on the downstream and upstream slopes. The upper-bound relation is shown in Figure 81. Permanent displacements were corrected using Equation 13. The maximum displacements for the downstream and upstream slopes are 0.42 and 3.2 ft, respectively.

190. Ambraseys and Menu (1988) offer two modes of displacement: symmetric and unsymmetric. Symmetrical displacements are produced when the sliding block moves in opposite directions when the accelerations reverse. Symmetrical displacements can be expected for level-ground conditions and slopes for which the base of the sliding block is near horizontal. Unsymmetrical displacements are produced when the block essentially only moves in one direction. Unsymmetrical displacements are expected for blocks resting on a steep base. The relation for unsymmetrical permanent displacements with a confidence interval of 97.5 percent was assumed for potential slip surfaces used for this study and is shown in Figure 82. The maximum displacements for the downstream and upstream slopes are 1.1 and 13 ft, respectively.

Presentation of results

191. The best estimates of permanent displacement obtained using simplified approaches are plotted as a function of tangent elevation and normalized height in Figures 83 and 84, for the downstream and upstream slopes, respectively. Some scatter exists among data for each method but, in general, the methods produced similar results. The maximum permanent displacements for the downstream and upstream slopes are about 0.6 and 6 ft, respectively. The downstream displacement corresponds to a shallow circle at

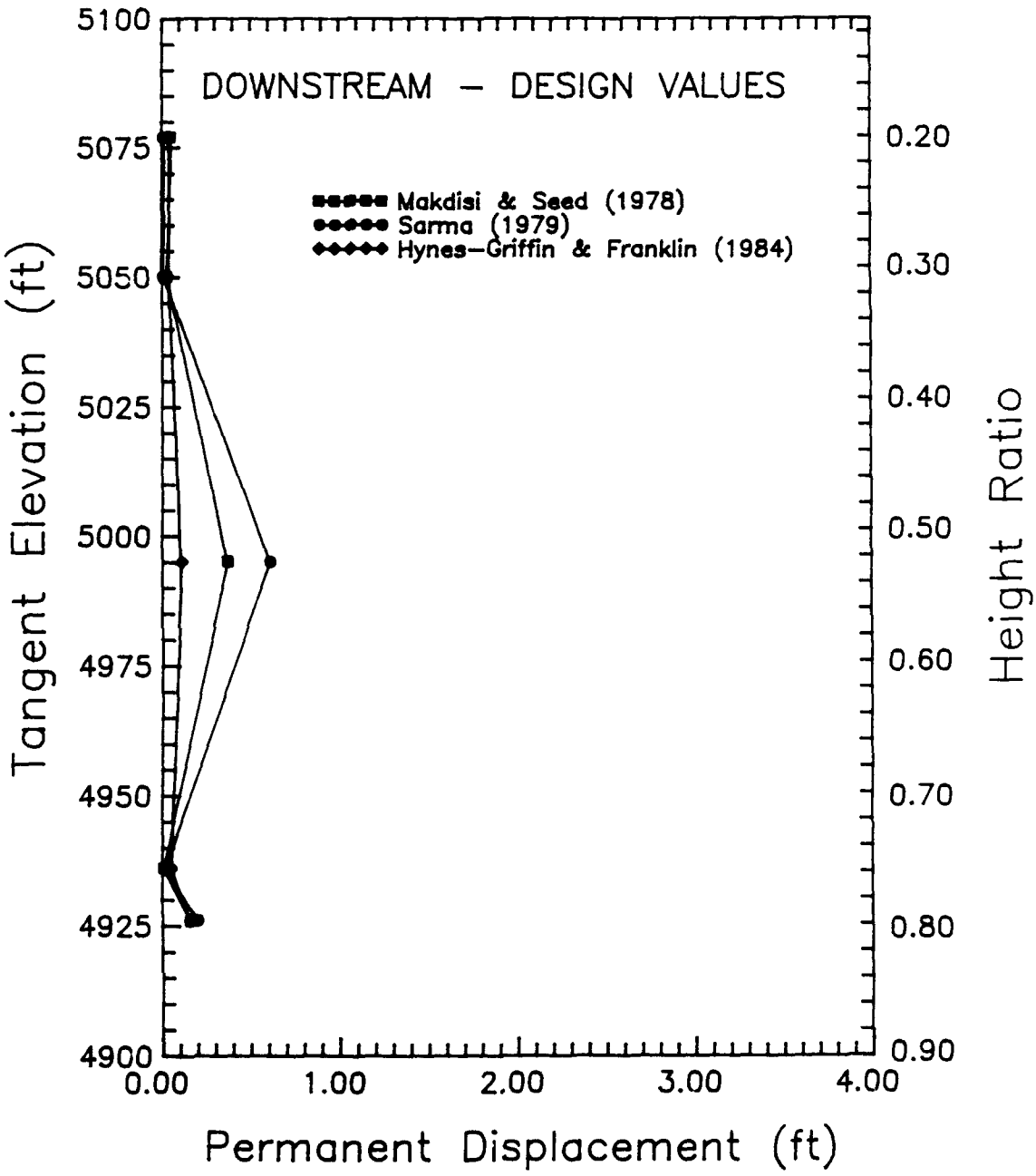

Figure 83. Comparison of best estimates of permanent displacements for downstream slope estimated using simplified analysis techniques

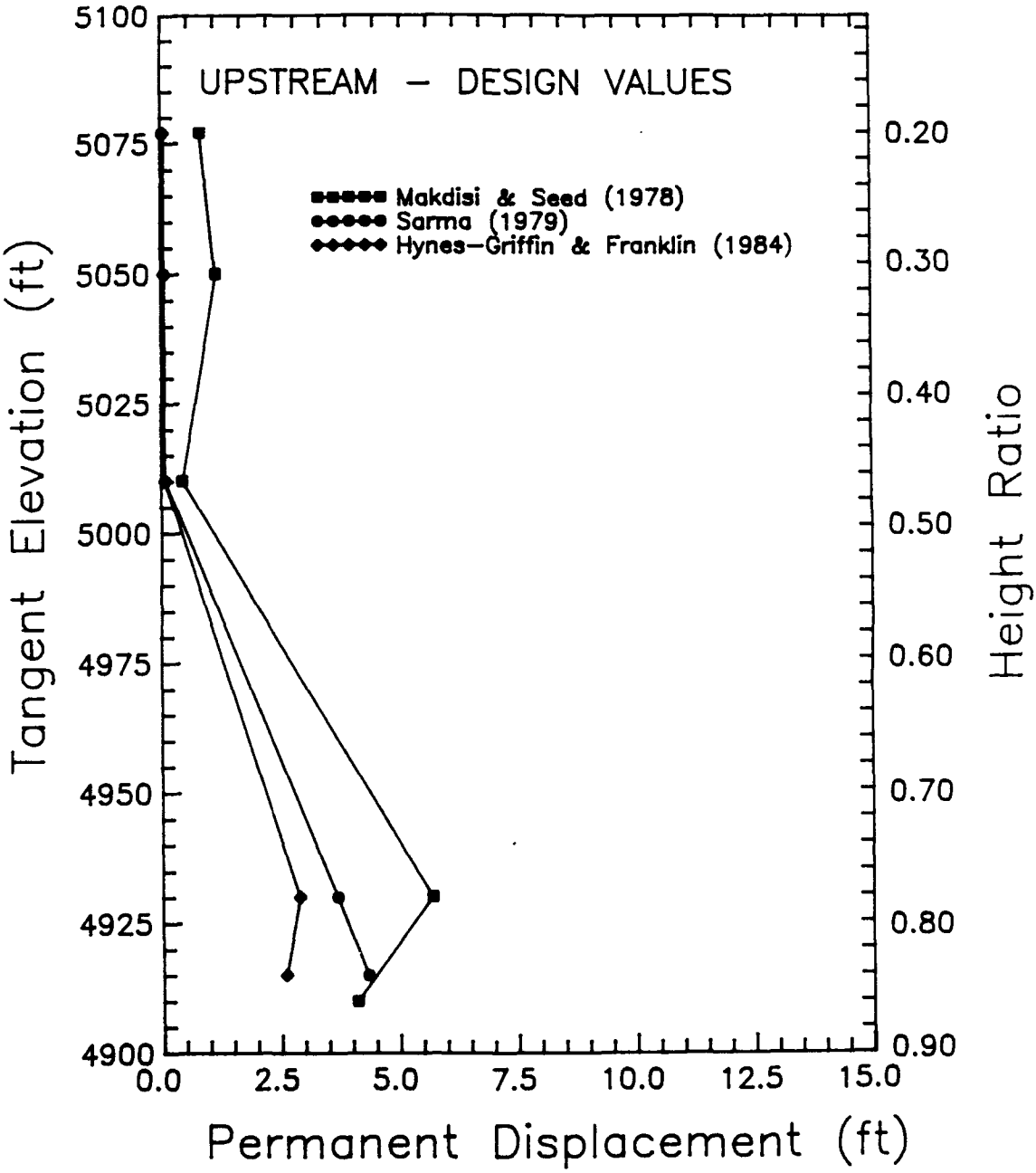

Figure 84. Comparison of best estimates of permanent displacements for upstream slope estimated using simplified analysis techniques

a tangent elevation of 4,995 ft; whereas, the upstream displacement corresponds to a deep circle passing through the liquefied alluvium (el 4,930).

192. The permanent displacements obtained using upper-bound relations for displacements are plotted in Figures 85 and 86. The five relations produced a moderately-wide range of values. The maximum permanent displacements for the downstream and upstream slopes are about 2.2 and 13 ft, respectively. Both downstream and upstream displacements correspond to deep slip surfaces (el 4,926 and el 4,930, respectively).

Estimated Displaced Shape

193. The displaced shape of the embankment and the vertical crest movements were estimated using the results of maximum permanent displacements from best estimate analyses. A failure surface on each side of the embankment was assumed to displace independent of the surface on the other side. Also superimposed to the permanent displacement along each surface was a displacement corresponding to a mobilized shear strain of 15 percent estimated to be the value necessary to mobilize the full residual strengths of liquefied materials.

194. The failure surface for each slope was selected on the basis of minimum yield accelerations. The slip surface corresponding to the minimum yield acceleration is expected to move first during an earthquake. For the upstream slope, the minimum yield acceleration was 0.065 at a tangent elevation of 4,930 ft. For the downstream slope, the minimum yield acceleration was 0.22 g at a tangent elevation of 4,926 ft.

195. The resultant magnitude and direction of assumed mobilized shear strain is dependent on the thickness and location of liquefied materials. For both the upstream and downstream sides, the height of liquefied alluvium is about 35 ft. At the assumed strain of 15 percent, the mobilized shear strain is about 5 ft. For the downstream slope, this movement is primarily horizontal because the slip surface is horizontal, on the average, in regions where it passes through liquefied layers. For the upstream slope, the movement is essentially along the slip surface because the slip surface passes through predominantly liquefied materials. The interpretation of the postearthquake, two-dimensional displaced shape is subjective. Permanent displacements correspond to the center of mass of the sliding mass and occur in a direction

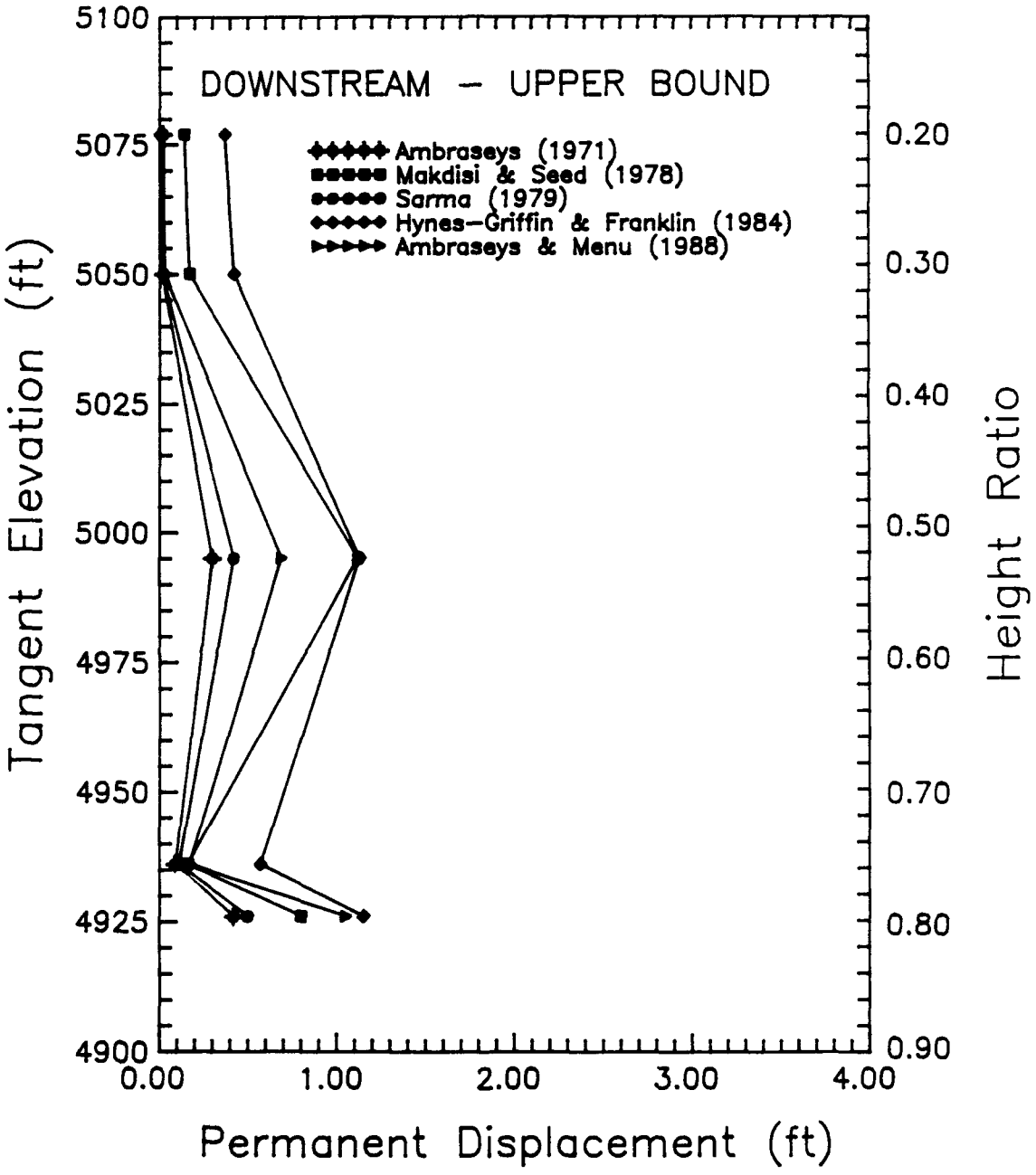

Figure 85. Comparison of upper bound of permanent displacements for downstream slope estimated using simplified analysis techniques

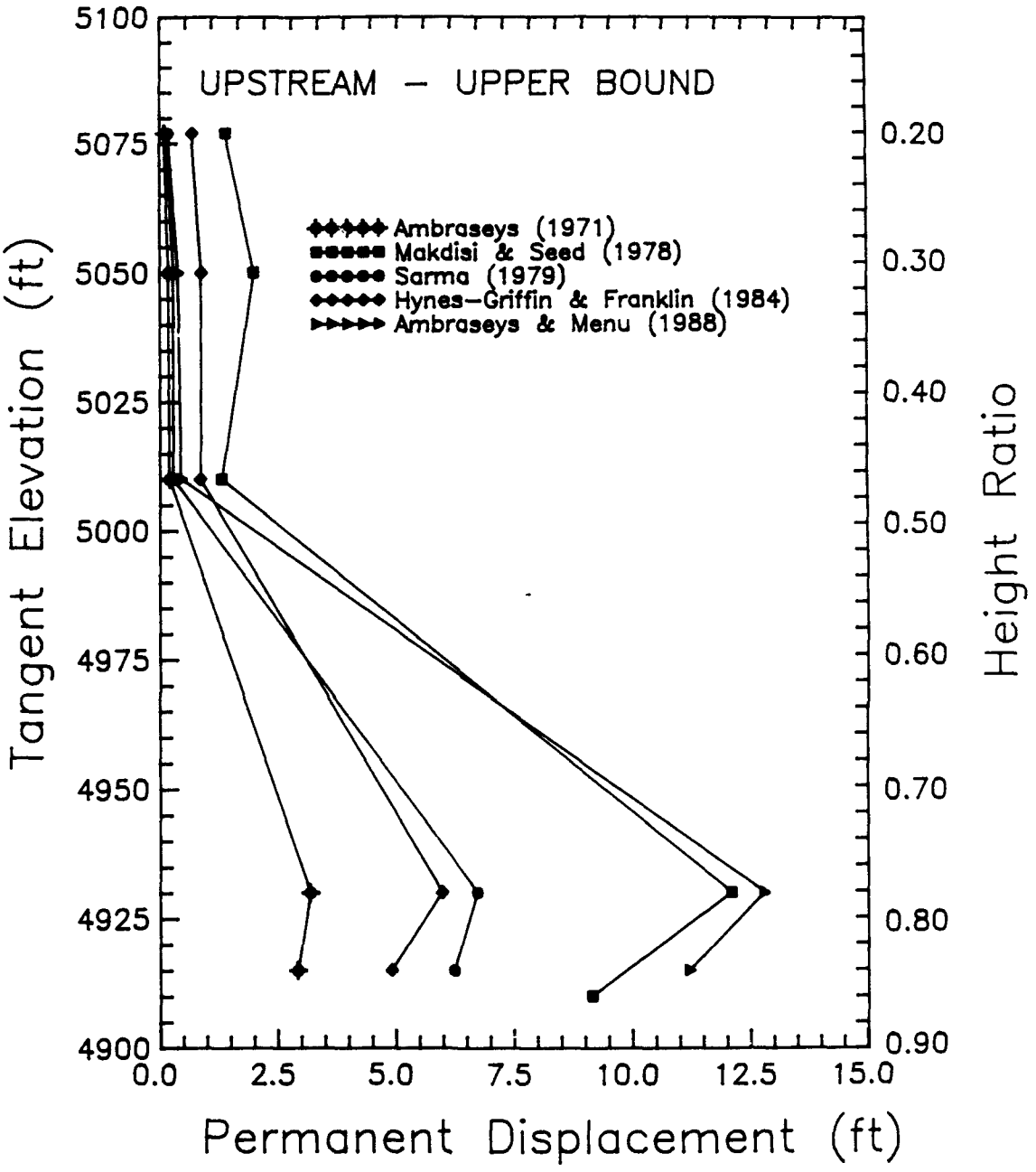

Figure 86. Comparison of upper bound of permanent displacements for upstream slope estimated using simplified analysis techniques

parallel to the resultant shear force acting on the base of the surface and away from the slope. For example, the best estimate of permanent displacement for the upstream slope (6 ft) acts at an angle of about 10 deg down from the horizontal and away from the slope. The horizontal component of this displacement (6 cos 10°) is about 6 ft. Because the most critical failure surfaces are circular, rotations are likely to be a primary mode of motion, too. The estimated displaced shape of the two-dimensional cross section at Ririe Dam was derived by a combination of translations and rotations. The displacement component from inertial effects, as described above, was applied as a rigid-body translation of the failure wedge at a point on the failure curve where the tangent of the curve is parallel to the resultant shear force. Because the bodies are suppose to be rigid and pure translation would require additional movement of mass downstream of the failure wedge, the failure wedge was then rotated about the same tangent point until the failure surface of the wedge mapped onto the failure surface of the dam. A similar process was used for the effect of mobilized shear strains although the point of rigid translation and rotation was assumed to correspond to the point on the failure surface with a tangent equal to the average slope of the failure surface through liquefied material. The displaced shape corresponding to the best estimate of permanent displacement and mobilized shear strain in liquefied zones is shown in Figure 87.

196. The displaced shape derived from best estimates of permanent displacement has a crest settlement of 6 ft. This pattern provides a remaining freeboard of 10 ft and a height of core above the pool of 4 ft with the cap of impervious gravel unaffected. The calculated design wave heights are 1.8 ft for 55 mph wind sustained over 1-hr with 1 percent of the waves reaching 3 ft and 2.3 ft for a 70 mph wind lasting 10 min with 1 percent of the waves reaching 3.8 ft (US Army Engineer District, Walla Walla 1966). These waves most likely will not breech the core. The impervious gravel is expected to serve as a barrier to water from waves. The function of the core and filter zones probably will not be affected by the magnitude of displacements expected.

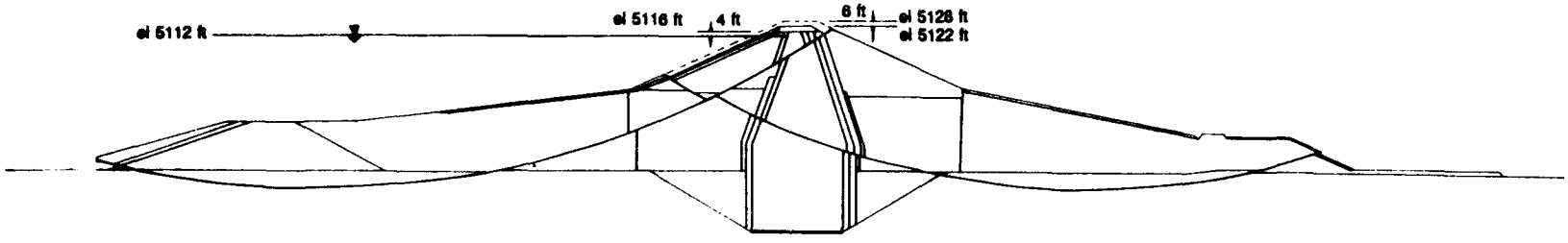

Figure 87. Estimated displaced shape of Ririe Dam using best estimates of permanent displacements upstream and downstream

Empirical Relation

197. Bureau et al. (1985) performed a survey of the performance and analyses of twelve large rock fill dams located throughout the world. The heights of these dams range from 50 to 240 m. Measured earthquake-induced crest settlements were available from seven dams. The range of accelerations was 0.08 to 0.41 g and the range of settlements was 9 to 381 mm. The intensity of ground motions transmitted to these dams, to date, generally were less than modern earthquake-resistant levels. Relative settlements ranged from 0.004 to 0.45 percent. Estimated earthquake-induced settlements were available from eight dams. The range of accelerations was 0.02 to 0.85 g and the range of calculated settlements was 7 to 4,450 mm. Relative settlements ranged from 0.01 to 1.2 percent. A summary of the seismic performance for fourteen dams is presented in Table 17.

198. Bureau et al. (1985) developed a correlation between a proposed index of earthquake shaking, the Earthquake Severity Index (ESI), and the consequent relative vertical settlement of the crest. The proposed relation is:

$$ESI = a_{max} \ (M - 4.5)^3 \qquad (18)$$

where

a_{max} = peak ground acceleration near base of dam, g's

The correlation was based on both the observed performance of dams and also the estimated (computed) settlement. Estimates of vertical crest settlement apparently were made by the different analysis groups responsible for the analysis of each dam using variations of the sliding block analogy. The dams used for the correlation are summarized in Table 18. The proposed correlation is shown in Figure 88.

199. The a_{max} used by Bureau et al. (1985) was intended to be at or near the base of the dam. For their analysis, both accelerations at the base and in the free field were used. Four of eight accelerations used for observed data were estimated. As indicated in Figure 41 and observed in Figure 44 for Ririe Dam, the acceleration at the base of the dam can be considerably less than the acceleration at the ground surface. For that reason, both

Table 17

Seismic Performance of Existing Rockfill Dams (from Bureau et al. 1985)

Rock-Fill Dam [Year Completed]	Height ft	Slope (Horizontal/ Vertical) Upstream	Slope (Horizontal/ Vertical) Downstream	Earthquake	Magnitude	Epicentral Distance km	Peak Ground Acceleration g	Peak Crest Acceleration	Crest Movement Vert in.	Crest Movement Horiz in.
MALPASSO (Peru) [1936]	255	0.5	1.33	10 Oct 1938	VI (1)	--	0.10 (2)	--	3.0	2.0
MORENA (Calif.) [1895]	177	0.5-0.9	1.3	04 Jun 1940	IV (1)	--	0.02 (2)	--	--	--
COGOTI (Chile) [1939]	275	1.6	1.8	07 Apr 1943 (Illapel)	8.3	16	0.20 (2)	--	15.0	--
PINZANES (Chile) [1956]	220	2.1	1.3	28 Jul 1957	7.5	--	0.05 (2)	--	--	--
MIBORO (Japan) [1960]	430	2.5	1.75	19 Aug 1961 (Kitamino)	7.0	16	0.20 (2)	--	1.2	2.0
MINASE (Japan) [1964]	220	1.35	2.0	16 Jun 1964 (Nigata)	7.5	16	0.08 (2)	--	2.4	1.6
LA CALERA (Mexico) [- -]	92	1.5	--	-- -- 1964	VIII (1)	--	--	--	--	--
KUZURYU (Japan) [- -]	419	2.6	1.8	09 Sep 1969 (Gifu)	6.6	40	0.02 (3)	0.04 (3)	--	--
KISENYAMA (Japan) [- -]	312	2.5	2.2	09 Sep 1969	6.8	--	--	0.10	--	--
OROVILLE (Calif.) (4) [1968]	770	2.75	2.0	01 Aug 1975 (Oroville)	5.7 (5)	6.9	0.10 (3)	0.12 (3)	0.4	--
TARUMIZU (Japan) [1976]	141	3.7	2.4	12 Jun 1978 (Miyagi)	7.4	100	0.24 (3)	0.36 (3)	--	--
EL INFIERNILLO (Mexico) [1964]	485	1.75	1.75	14 Mar 1979	7.6	110	0.12 (3)	0.35 (3)	5.1	1.8
LA VILLITA (Mexico) [1967]	197	2.5	2.5	14 Mar 1979	7.6	110	0.10 (2)	0.36 (3)	1.8	1.2
LEROY ANDERSON [1950]	235	2.0	2.0	24 Apr 1984 (Morgan Hill)	6.2	16	0.41 (3)	0.63 (3)	0.6	0.4

Notes:
(1) Modified Mercalli Intensity at Dam Site.
(2) Estimated.
(3) Recorded.
(4) Earthfill dam with coarse pervious shell.
(5) Magnitude 5.7 (Berkeley), 5.9 (USGS), 6.1 (Pasadena).

Table 18

Relative Settlement and Earthquake Severity Data (Bureau et al. 1985)

Dam Name (Location)	Height m	Change in Height mm*	Relative Settlement percent	Peak Ground Acceleration g's	Earthquake Magnitude	Earthquake Severity Index
COGOTI (Chile)	84	381(o)	0.45	0.20	8.3	11.0
MIBORO (Japan)	131	30(o)	0.023	0.20	7.0	3.1
MINASE (Japan)	67	7(e)	0.010	0.02	6.9	0.3
		61(o)	0.091	0.08	7.5	2.2
OROVILLE (CA)	235	9(o)	0.004	0.10	5.7	0.2
EL INFIERNILLO (Mexico)	148	130(o)	0.088	0.12	7.6	3.6
LA VILLITA (Mexico)	60	45(o)	0.075	0.10	7.6	3.0
LEROY ANDERSON (CA)	72	15(o)	0.021	0.41	6.2	2.0
TERROR LAKE (AK)	50	600(e)	1.2	0.35	8.5	22.4
TERROR LAKE (AK)	50	300(e)	0.60	0.50	6.5	4.0
CIRRATA (Indonesia)	125	300(e)	0.24	0.35	6.5	2.8
PUEBLO VIEJO (Guatemala)	133	4450(e)	3.3	0.65	8.25	34.3

(Continued)

* (o) observed settlement.
(e) estimated settlement.

Table 18 (Concluded)

Dam Name (Location)	Height m	Change in Height mm*	Relative Settlement percent	Peak Ground Acceleration g's	Earthquake Magnitude	Earthquake Severity Index
CHICOASEN (Mexico)	240	1000(e)	0.42	0.85	7.0	13.3
FORTUNA (Panama) (Raised)	104	800(e)	0.77	0.40	7.5	13.3
USBR (Example Dam)	213	700(e)	0.33	0.43	6.5	3.5
Dames & Moore (Example Dam)	100	487(e)	0.49	0.70	7.1	12.3

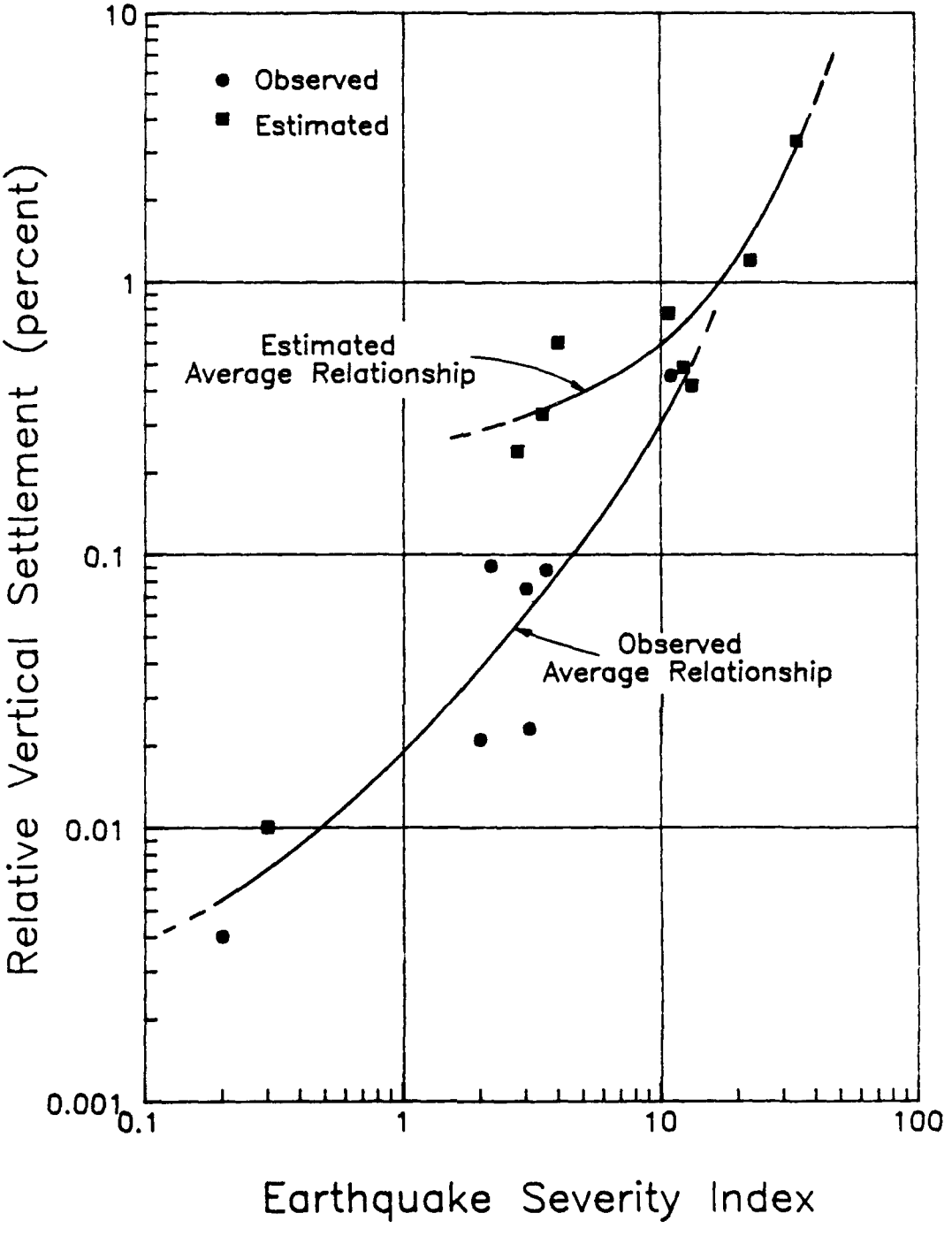

Figure 88. Correlations between Earthquake Severity Index and vertical settlement of dam crest for observed and calculated data (Bureau et al. 1985)

the base and outcrop accelerations at Ririe Dam (0.58 g and 1.22 g, respectively) were considered to estimate crest settlement.

200. The data plotted in Figure 88 indicate that two distinct relations correspond to observed and estimated behavior. The range in ESI for observed behavior is 0.2 to 11.0. The range in ESI for estimated behavior is 2.8 to 34. It is apparent from the relations shown in Figure 88 that for values of ESI greater than 10, the relations representing estimated and observed behavior tend to converge. Only one datum of observed behavior exists above an ESI of 3.6, however.

201. The correlation proposed by Bureau et al. (1985) was used to evaluate the potential vertical settlement at Ririe Dam as a consequence of the design earthquake. A potential range of settlement was determined using the base acceleration for the lower bound and the outcrop acceleration for the upper bound. Using a magnitude of 7.5 and a peak ground acceleration at the base of the dam of 0.58 g, an ESI of 16 was calculated. Using Figure 88, the relative vertical settlement was determined to be about 0.65 percent for observed behavior. Using the full height of the dam (253 ft), the vertical crest movement was calculated to be about 1.6 ft. Similarly, for an acceleration of 1.22 g, a vertical crest settlement of 8.8 ft was obtained. The vertical movement of the majority of the crest determined using the results of the combined simplified procedures is in fairly good agreement with the relationship proposed by Bureau et al. (1985).

Conclusions and Recommendation

202. The results of simplified sliding-block analyses suggest that maximum permanent displacements of about 6 ft on the upstream slope and 0.6 ft on the downstream slope can be expected. In addition, the mobilization of shear strain in liquefied materials will produce up to 5 ft of displacement along the slip surface. The magnitude of permanent displacement on the upstream slope indicates that significant deformations will occur in the dam. A projection of the displaced shape, however, suggests that the dam will not fail as a consequence of expected permanent displacements.

203. A review of observations and analyses for other rock-fill dams by Bureau (1985) confirms that very large settlements may be expected at the crest as a consequence of slope failures cause by large ground motions. A

relation they proposed suggests that vertical settlements will be between 1.6 and 8.8 ft. The settlement estimated for Ririe Dam of 6 ft is well within this range.

204. It is recommended that a controlled water dumping procedure and release policy for earthquake damage situations be formulated. Assessment of earthquake damage to outlet works is beyond the scope of this study.

PART IX: SUMMARY AND CONCLUSIONS

205. A seismic stability analysis has been conducted to evaluate the performance of Ririe Dam during and immediately after the design earthquake (M = 7.5, a_{max} = 1.17 g). The scope of this study included a quantitative assessment of all embankment and foundation materials and a qualitative assessment of abutment slopes. A methodology for analysis was carefully selected which focused on the performance-based approach developed by the late Professor Seed and his coworkers at the University of California at Berkeley. The potential mode of failure considered was the loss of freeboard caused by slope failure induced by ground motion or sliding failures on weakened foundation materials. In our judgment, based on the results of the present seismic stability analysis, Ririe Dam will perform its primary function by retaining the reservoir during and immediately after the design earthquake. However, the embankment is expected to be damaged.

206. The methods of analysis to evaluate the seismic stability for the two means of failure are different and were considered separately. The evaluation of loss of freeboard caused by slope or sliding failures on weakened foundation materials was analyzed in four steps: static stress analysis, dynamic response analysis, liquefaction potential analysis, and postearthquake stability analysis. The evaluation of loss of freeboard caused by slope failures induced by ground motion was conducted using Newmark sliding-block and empirical methods.

207. The overall seismic stability analysis was conducted in three phases: characterization studies, numerical analysis, and engineering performance evaluation. Specific tasks and end products are associated with each phase in accordance with the methodology adopted for the study.

208. The characterization studies phase began with a review of construction records and previous geotechnical investigative work in the region. From that, field and laboratory studies were selected to provide information necessary to evaluate potential modes of failure by qualitative and quantitative analyses. The end product of characterization studies were: the design ground motions (reported by Krinitzsky and Dunbar 1991), idealized cross sections, and material properties to be used in the subsequent two phases.

209. The next phase of the seismic stability analysis was the numerical analysis phase which was used to accomplish two steps in the procedure to

evaluate the slope failure mode. In this phase, the finite element method was used to calculate static effective stresses within the dam and foundation resulting from the construction sequence. The finite element method was also used to evaluate the dynamic response of the embankment and foundation system. Two-dimensional, plane-strain analyses were assumed for both static stress and dynamic response calculations. Two representative cross sections were utilized--a maximum section and a "quarter" section. Three-dimensional effects were estimated for the dynamic response using the results of numerical analysis and empirical relations.

210. The final phase of the analysis used the parameters and results derived from the other two phases to evaluate the potential for the two postulated modes of failure to occur. The mode corresponding to sliding failure on weakened foundation materials was analyzed using a liquefaction analysis and postearthquake stability analysis in this phase. The liquefaction analysis used the cyclic strengths of the various materials to compare with soils that have liquefied in the past during earthquakes to determine if liquefaction will occur and predict excess pore water pressures. The postearthquake stability analysis used the excess pore water pressures developed during the earthquake to evaluate slope stability. The minimum factor of safety using limit equilibrium analysis for postearthquake conditions was determined to be 1.33 on the downstream slope at the maximum cross section. This factor of safety is well above unity which indicates that the slopes are safe for this potential means of failure.

211. The results of investigation of the potential means of failure pertaining to slope failures induced by ground motion (inertial effects) indicate that the embankment will be moderately damaged downstream and severely damaged upstream, on the basis of results of simplified sliding block analyses and empirical studies. However, it is likely that these deformations will not result in immediate, uncontrolled loss of the pool. The permanent displacement expected for the downstream slope is 0.6 ft. The permanent displacement for the upstream slope was estimated to be about 6 ft. Analytical upper-bound estimates of displacement were 1 ft downstream and 14 ft upstream. Sliding-block methods of analysis are approximate and are considered to have a level of accuracy of about a factor of three times the best estimate.

212. An estimated displaced shape of the cross section from average inertial displacements and 15 percent shear strains in liquefied zones suggests that the crest will subside about 6 ft leaving a freeboard of 10 ft. The postdisplaced configuration is expected to retain the pool although measures should be taken to lower the pool level after deformations have occurred. Emergency lowering of the reservoir should be carefully analyzed to prevent slope failures resulting from rapid drawdown conditions.

213. Liquefaction of embankment and foundation materials will likely cause significant deformations in the upstream portion of the embankment. Noticeable deformations in the downstream portion of the embankment are also likely. Estimation of magnitude or shape of the deformed cross sections was not attempted.

214. An appropriate degree of realism has been maintained throughout the course of this seismic stability study. Some conservatism was used to offset inherent variability in input parameters such as material properties and variability that exists when relations were derived for the various types of analysis. Over-conservatism was avoided for this study because the severe ground motions that were specified are considered to involve a fair amount of conservatism inthemselves. It is concluded that Ririe Dam will be marginally safe if subjected to the design earthquake.

REFERENCES

Ambraseys, N. N. 1960. "On the Shear Response of a Two-Dimensional Wedge Subjected to an Arbitrary Disturbance," Bulletin of the Seismological Society of America, Vol 50, No. 1, pp 45-56.

Ambraseys, N. N. 1972. "Earthquake Resistance of Earth and Rock-Fill Dams, Report 3: Feasibility of Simulating Earthquake Effects on Earth Dams Using Underground Nuclear Events," Appendix A, Miscellaneous Paper S-71-17, US Army Engineers Waterways Experiment Station, Vicksburg, MS.

Ambraseys, N. N., and Menu, J. M. 1988. "Earthquake-Induced Ground Displacements," Earthquake Engineering and Structural Dynamics, Vol 16, pp 985-1006.

Andrus, R. D. 1986. "Subsurface Investigations of a Liquefaction Induced Lateral Spread, Thousand Springs Valley, Idaho: Liquefaction Recurrence and a Case History in Gravel," M.S. in Engineering Thesis, Brigham Young University, Provo, UT.

Azzouz, A. S. 1977. "Three-Dimensional Analysis of Slopes," DcS thesis, MIT, p 383.

Azzouz, A. S., and Baligh, M. M. 1989a. "Stability Analyses of Ririe Dam," Report to US Army Engineer Waterways Experiment Station, under purchase order agreement DACW39-86-P-0607, Vicksburg, MS.

Azzouz, A. S. , and Baligh, M. M. 1989b. "Three Dimensional Stability Analysis of Ririe Dam," Report to US Army Engineer Waterways Experiment Station, under purchase order agreement DACW39-86-P-0607, Vicksburg, MS.

Bathe, K. J. 1982. Finite Element Procedures in Engineering Analysis, Prentice-Hall, Inc., Englewood Cliffs, NJ.

Bureau, G., Volpe, R. L., Roth, W. H., and Udaka, T. 1985. "Seismic Analysis of Concrete Face Rockfill Dams," Proceedings of the International Symposium on Concrete Face Rockfill Dams, ASCE, Detroit, MI.

Castro, G., Keller, T. O., and Boynton, S. S. 1989. "Re-evaluation of the Lower San Fernando Dam, Report 1: An Investigation of the February 9, 1971 Slide Contract Report, GL-82-2, Vol 2, US Army Engineer Waterways Experiment Station, Vicksburg, MS.

Chang, C. S. 1975. "User's Guide for Program SFORCE," Department of Civil Engineering, University of California, Berkeley, CA.

Chang, F. K. 1985. "Analysis of Strong-Motion Data from the Mount Borah, Idaho, Earthquake of 28 October 1983," Miscellaneous Paper, GL-85-12, US Army Engineer Waterways Experiment Station, Vicksburg, MS, p 25.

Christiansen, R. L. 1982. "Late Cenozoic Volcanism of the Island Park Area, Eastern Idaho," Cenozoic Geology of Idaho, Bulletin 26, Idaho Bureau of Mines and Geology, eds. Bonnichsen and Breckenridge, Boise, ID, pp 345-368.

Cooley, J. W. and Tukey, J. W. 1965. "An Algorithm for the Machine Calculation of Complex Fourier Series," Mathematics of Computation, Vol 19, No. 90, pp 297-301.

Dakoulas, P. C. 1989a. "Prediction of the Seismic Response of the Ririe Dam Using Simplified Nonlinear Shear Beam Models," Report to US Army Engineer Waterways Experiment Station, Vicksurg, MS.

Dakoulas, P. C. 1989b. "Three Computer Programs for Seismic Analysis of Earth Dams Using Nonlinear Shear Beam Models," Dept. of Civil Engineering, Rice University, Houston, TX.

Dakoulas, P. and Gazetas, G. 1985. "A Class of Inhomogeneous Shear Models for Seismic Response of Dams and Embankments," Journal of Soil Dynamics and Earthquake Engineering, Vol 4, No. 4, pp 166-182.

_____ 1986. "Shear Strains and Seismic Coefficients for Dams and Embankments," Journal of Soil Dynamics and Earthquake Engineering, Vol 5, No. 2, pp 75-83.

Department of the Army 1983. "Earthquake Design and Analysis for Corps of Engineers Projects," Engineering Regulation 1110-2-1806, USACE, Washington, DC.

Duncan, J. M., Byrne, P., Wong, K. S., and Mabry, P. 1980. "Strength, Stess-Strain and Bulk Modulus Parameters for Finite Element Analysis of Stresses and Movements in Soil Masses," Report UCB/GT/80-01, University of California, Berkeley, CA.

Duncan, J. M., Seed, R. B., Wong, K. S., and Ozawa, Y. 1984. "FEADAM84: A Computer Program for Finite Element Analysis of Dams," Research Report SU/GT/84-03, Stanford University, Stanford, CA.

Earthquake Engineering Technology Corporation. 1983. "SUPERFLUSH: User's Manual," Vols 1-3.

Edris, E. V., Jr., and Wright, S. G. 1987. "User's Guide: UTEXAS2 Slope Stability Package," Technical Report GL-81-1, Vol 1, US Army Engineer Waterways Experiment Station, Vicksburg, MS.

Embree, G. F., McBroome, L. A., and Doherty, D. J. 1982. "Preliminary Stratigraphic Framework of the Pliocene and Miocene Rhyolite, Eastern Snake River Plain, Idaho," Cenozoic Geology of Idaho, Bulletin 26, Idaho Bureau of Mines and Geology, ed. Bonnichsen and Breckenridge, Boise, ID, pp 333-343.

Evans, M. 1987. "Undrained Cyclic Triaxial Testing of Gravels--The Effect of Membrane Compliance," Ph.D Dissertation, University of California, Berkeley, CA.

Finn, W. D. L. 1982. "Soil Liquefaction Studies in the People's Republic of China," Soil Mechanics - Transient and Cyclic Loads, John Wiley and Sons, Ltd., New York, NY.

Franklin, A. G., and Chang, F. K. 1977. "Earthquake Resistance of Earth and Rock-Fill Dams; Permanent Displacements of Earth Embankments by Newmark Sliding Block Analysis," Miscellaneous Paper S-71-17, Report 5, US Army Engineer Waterways Experiment Station, Vicksburg, MS.

Franklin, A. G., and Hynes, M. E. 1981. "Dynamic Analysis of Embankment Sections, Richard B. Russel Dam," Proceedings, Earthquakes and Earthquake Engineering - The Eastern US Conference, Knoxville, TN.

Gazetas, G. 1987. "Seismic Response of Earth Dams: Some Recent Developments," Journal of Soil Dynamics and Earthquake Engineering, Vol 6, No. 1, pp 2-47.

Harder, L. F., Jr. 1988. "Use of Penetration Tests to Determine the Liquefaction Potential of Soils During Earthquake Shaking," PhD Thesis, University of California, Berkeley, CA.

Hughes, T. J. R. 1987. The Finite Element Method, Prentice-Hall, Inc., Englewood Cliffs, NJ.

Hynes, M. E. 1988. "Pore Pressure Generation Characteristics of Gravels Under Undrained Cyclic Loading," PhD Thesis, University of California, Berkeley, CA.

Hynes, M. E. 1990. "Seismic Stability Evaluation of Folsom Dam and Reservoir Project, Report 1: Summary Report," Technical Report GL-87-14, US Army Engineer Waterways Experiment Station, Vicksburg, MS.

Hynes, M. E. and Franklin, A. G. 1984. "Rationalizing the Seismic Coefficient Method," Miscellaneous Paper GL-84-13, US Army Engineer Waterways Experiment Station, Vicksburg, MS.

Hynes, M. E., Wahl, R. E., Donaghe, R. T., and Takashi, T. 1988. "Seismic Stability Evaluation of Folsom Dam and Reservoir Project -- Report 4: Mormon Island Auxiliary Dam - Phase I," Technical Report GL-87-14, US Army Engineer Waterways Experiment Station, Vicksburg, MS.

Idriss, I. M., and Seed, H. B. 1968. "Seismic Response of Horizontal Soil Layers," Journal of the Soil Mechanics and Foundation Engineering Division, ASCE, Vol 94, No. SM 4, pp 1003-1031.

Ishihara, K. 1985. "Stability of Natural Deposits During Earthquakes," Proceedings of the Eleventh International Conference on Soil Mechanics and Foundation Engineering, Balkema Publishers, Rotterdam, The Netherlands.

Kanai, K. 1951. "Relation Between the Nature of Surface Layer and the Amplitude of Earthquake Motions," Bulletin of the Tokyo Earthquake Research Institute, Tokyo, Japan.

Krinitzsky, E. L. and Dunbar J. B. 1991. "Geological and Seismological Evaluation of Earthquake Hazards at Ririe Dam, Idaho," Technical Report GL-91-11, US Army Engineer Waterways Experiment Station, Vicksburg, MS.

Lysmer, J., Udaka, T., Tsai, C. F., and Seed, H. B. 1975. "FLUSH: A Computer Program for Approximate 3-D Analysis of Soil-Structure Interaction Problems," Report UCB/EERC 75-30, University of California, Berkeley, CA.

Makdisi, F. I. 1976. "Performance and Analysis of Earth Dams During Strong Earthquakes," PhD Thesis, University of California, Berkeley, CA.

Makdisi, F. I., and Seed, H. B. 1978. "Simplified Procedure for Estimating Dam and Embankment Deformations," Journal of the Geotechnical Engineering Division, ASCE, Vol 104, No. 7, pp 849-867.

Mejia, L. H., and Seed, H. B. 1981. "Three-Dimensional Dynamic Response Analysis of Earth Dams," Report UCB-EERC-81/15, University of California, Berkeley, CA.

Mejia, L. H., and Seed, H. B. 1983. "Comparison of 2-D and 3-D Dynamic Analyses of Earth Dams," Journal of the Geotechnical Engineering Division, ASCE, Vol 109, No. GT4, pp 1383-1398.

National Research Council 1985. "Liquefaction of Soils During Earthquakes," National Academy Press, Washington, DC.

Newmark, N. M. 1965. "Effects of Earthquakes on Dams and Embankments," Geotechnique, Vol 15, No. 2, pp 139-160.

Patrick, D. M., and Whitten, C. B. 1981. "Geological and Seismological Investigations at Ririe Dam, Idaho," Miscellaneous Paper GL-81-7, US Army Engineer Waterways Experiment Station, Vicksburg, MS.

Pierce, K. L., and Scott, W. E. 1982. "Pleistocene Episodes of Alluvial-Gravel Deposition, Southeastern Idaho," Cenozoic Geology of Idaho, Bulletin 26, Idaho Bureau of Mines and Geology, eds. Bonnichsen and Breckenridge, Boise, ID, pp 685-702.

Protska, H. J., and Embree, G. F. 1978. "Geology and Geothermal Potential of the Rexburg Area, Southeastern Idaho," Open File Report 78-1009, US Geological Survey, Denver, CO, p 14.

Sarma, S. K. 1979. "Response and Stability of Earth Dams During Strong Earthquakes," Miscellaneous Paper, GL-79-13, US Army Engineer Waterways Experiment Station, Vicksburg, MS.

Schnabel, P. B. 1973. "Effects of Local Geology and Distance from Source on Earthquake Ground Motions," PhD Thesis, University of California, Berkeley, CA.

Schnabel, P. B., Lysmer, J., and Seed, H. B. 1972. "SHAKE, A Computer Program for Earthquake Response Analysis of Horizontally Layered Sites," Report EERC 72-12, Earthquake Engineering Research Center, University of California, Berkeley, CA.

Seed, H. B. 1979. "Considerations in the Earthquake-Resistant Design of Earth and Rockfill Dams," Nineteenth Rankine Lecture, Geotechnique, Vol 29, No. 3, pp 215-263.

_____ 1983. "Earthquake-Resistant Design of Earth Dams," Presented at the ASCE Spring Convention, Philadelphia, PA, May.

Seed, H. B. 1985. Discussion to: "A Note on Earthquake-Induced Liquefaction," by D. V. Morris, Geotechnique, Vol 35, No. 3, pp 369-370.

_____ 1987. "Hypothetical Ground Motion Accelerogram for Ririe Dam," Letter report dated 5 August.

Seed, H. B. and Idriss, I. M. 1970. "Soil Moduli and Damping Factors for Dynamic Response Analysis," Report EERC-70/10, University of California, Berkeley, CA.

_____ 1971. "," Journal of the Soil Mechanics and Foundation Engineering Division, ASCE, Vol 97, No. SM9, pp 1249-1273.

_____ 1981. "Evaluation of Liquefaction Potential of Sand Deposits Based on Observations of Performance in Previous Earthquakes," Insitu Testing to Evaluate Liquefaction Susceptibility, ASCE Preprint 81-544, p 21.

Seed, H. B., Idriss, I. M., Arango, J. 1983. "Evaluation of Liquefaction Potential Using Field Performance Data," Journal of the Geotechnical Engineering Division, ASCE, Vol 109, No. GT3, pp 458-482.

Seed, H. B., and Lee, K. L. 1966. "," Journal of the Soil Mechanics and Foundation Engineering Division, ASCE, Vol 92, No. SM6, pp 105-136.

Seed, H. B., Lee, K. L., Idriss, I. M., and Makdisi, F. I. 1973. "Analysis of the Slides in the San Fernando Dams During the Earthquake of February 9, 1971," Report EERC 73-2, Earthquake Engineering Research Center, Berkeley, CA, p 150.

Seed, H. B., Seed, R. B., Harder, L. F., and Jong. H. J. 1989. "Reevaluation of the Lower San Fernando Dam, Report 2: Examination of the Post-Earthquake Slide of February 9, 1971," Contract Report GL-89-2, US Army Engineer Waterways Experiment Station, Vicksburg, MS.

Seed, H. B., Tokimatsu, K., Harder, L. F., Jr., and Chung, R. M. 1985. "Influence of SPT Procedures in Soil Liquefaction Resistance Evaluation," Journal of the Geotechnical Engineering Division, ASCE, Vol 111, No. 11, pp 1425-1445.

Seed, H. B., Wong, R., Idriss, I. M., and Tokimatsu, K. 1986. "Moduli and Damping Factors for Dynamic Analysis of Cohesionless Soils," Journal of the Geotechnical Engineering Division, Vol 112, No. 11, pp 1016-1032.

Severn, R. T., Jeary, A. P., Ellis, B. R., and Dungar, R. 1979. "Prototype Dynamic Studies on a Rockfill Dam and on a Buttress Dam," Proceedings of the Thirteenth International Congress on Large Dams, Q. 51, R. 16, New Delhi, India.

Spencer, E. 1967. "A Method of Analysis of the Stability of Embankments Assuming Parallel Inter-Slice Forces," Geotechnique, Vol 17, No. 1, pp 11-26.

TAGA Engineering Software Services 1984. "TSLOPE/TSTAB User's Manual," Berkeley, CA.

US Army Engineer District, Walla Walla. 1966. "Ririe Dam and Reservoir: General Design Memorandum," Design Memorandum No. 3, Walla Walla, WA.

_____. 1969. "Ririe Dam and Reservoir: Main Dam, Spillway, Diversion Facilities, and Outlet Works," Design Memorandum No. 5, Walla Walla District, Walla Walla, WA.

_____ 1972a. "Ririe Dam and Lake, Willow Creek, Idaho: Environmental Statement," Walla Walla, WA.

_____ 1972b. "Ririe Lake, Idaho: Historical Report on Construction," Walla Walla District, Walla Walla, WA.

_____ 1977. "Ririe Lake, Willow Creek, Idaho: Foundation Report-Volume 2," Walla Walla, WA.

_____ 1978. "Ririe Dam, Willow Creek, Idaho: Embankment Criteria and Performance Report," Walla Walla, WA.

_____ 1979. "Ririe Lake, Willow Creek, Idaho: After-Action Pool Raise Report," Walla Walla, WA.

US Department of Interior, Bureau of Reclamation. 1982. "Emergency Preparedness Brief with Inundation Map from Standing Operating Procedures, Ririe Dam, Idaho," Pacific Northwest Regional Office, Boise, ID.

US Geologic Survey 1983. "Preliminary Determination of Epicenters, Monthly Listing," No. 43-83, National Earthquake Information Service, Golden, CO.

Vasquez-Herera, A. and Dobry, R. 1989. "Re-evaluation of the Lower San Fernando Dam; Report 3: The Behavior of Undrained Contractive Sand and Its Effect on Seismic Liquefaction Flow Failures of Earth Structures," Contract Report GL-89-2, US Army Engineer Waterways Experiment Station, Vicksburg, MS.

Wolf, J. P. 1985. Dynamic Soil-Structure Interaction, Prentice-Hall, Inc., Englewood Cliffs, NJ.

Wong, K. S., and Duncan, J. M. 1985. "SEEP: A Computer Program for Seepage Analysis of Saturated Free Surface or Confined Steady Flow," Department of Civil Engineering, Virginia Polytechnic Institute, Blacksburg, VA.

Woodward-Clyde Consultants 1988. "Static Analysis of Ririe Dam," report submitted to USACE-WES under contract DAEW 39-87-0083, Oakland, CA.

Woodward-Clyde Consultants 1989. "Dynamic Response Analysis of Ririe Dam," report submitted to USACE-WES under contract DACW-39-87-C-0083, Oakland, CA.

Youd, T. L., Harp, E. L., Keefer, D. K., and Wilson, R. C. 1985. "The Borah Peak, Idaho Earthquake of October 28, 1983 - Liquefaction," Earthquake Spectra, Earthquake Engineering Research Institute, Vol 2, No. 1.

Youd, T. L., and Perkins, M. 1978. "Liquefaction and Secondary Ground Failure," Journal of the Geotechnical Engineering Division, ASCE, Vol 104, No. GT4, pp 443-446.

Zienkiewicz, O. C. 1977. The Finite Element Method, McGraw-Hill, London.